DEVELOPMENT OF A PHYSIOLOGICAL-PARAMETER-BASED THERMAL SENSATION MODEL FOR OUTDOOR MICROCLIMATE ASSESSMENT

YING JIANG

PhD

The Hong Kong Polytechnic University

2025

The Hong Kong Polytechnic University

Department of Building Environment and Energy Engineering

Development of a physiological-parameter-based thermal sensation model for outdoor microclimate assessment

Ying Jiang

A thesis submitted in partial fulfillment of the requirements for the degree of Doctor of Philosophy

July, 2025

CERTIFICATE OF ORIGINALITY

I hereby declare that this thesis is my own work and that, to the best of my knowledge and belief, it reproduces no material previously published or written, nor material that has been accepted for the award of any other degree or diploma, except where due acknowledgement has been made in the text.

_____ (Signed)

Ying Jiang

_____ (Name of student)

Abstract

Abstract of thesis entitled: Development of a physiological-parameter-based thermal sensation model for outdoor microclimate assessment

Submitted by : Ying Jiang

For the degree of : Doctor of Philosophy

In the context of climate change, outdoor thermal comfort models serve as useful tools for evaluating thermal environment conditions and advanced active cooling strategies for outdoor users. Currently, no applicable and accurate model can provide a reliable prediction of thermal perception across diverse outdoor environments. There are several key limitations: 1) Most existing classical indices were developed based on indoor chamber studies, and many emerging outdoor thermal comfort models did not fully consider various outdoor thermal environments. 2) The developing outdoor thermal comfort models only considered overall thermal sensation prediction and did not provide the prediction of thermal sensation for local body parts, which are important in asymmetric outdoor conditions. 3) Few studies explored the combined psycho-physiological effect of thermal alliesthesia and adaptation phenomena on dynamic thermal perceptions in real-life environments.

This study aims to build a thermal sensation model that correlates the subjective thermal sensation votes (TSV) with the human-body thermo-physiological responses in warm-biased outdoor conditions, in order to improve the assessment of outdoor thermal comfort in urban spaces during the design and renovation stages. The study includes the steady-state model, the

step-up phase, and the step-down phase of the dynamic model, as well as an exploratory investigation into thermal alliesthesia and short-term adaptation phenomenon.

The steady-state part involves the local TSV model for 11 body parts when the human body is in a steady state, as well as an overall TSV model. A series of semi-controlled experiments were conducted, with a total of 86 human subject tests under varying wind speeds and solar radiation levels using an adjustable windshield and shading device in real outdoor settings. Questionnaire survey data on local and overall TSV and simultaneously measured data of environmental parameters and physiological responses in terms of local skin temperatures of 18 body parts, core temperature, and sweat rate of 3 body parts, were collected. Results show a strong correlation between local sweat rate and local skin temperature, leading to the selection of local skin temperature as the sole variable for the local TSV model. Individual differences and thermal sensation overshoot outdoors were observed, and a new parameter accounting for the neutral skin temperature variation was introduced into the local TSV model to provide three prediction values, i.e., the mean, the 10th, and 90th percentiles. The overall TSV model, which calculates overall TSV as a weighted average of local TSVs, demonstrated a high fit with actual overall TSV ($R^2 = 0.96$).

The step-up phase of dynamic model provides thermal sensation prediction when the human body experiences positive changes in skin temperatures. This model uses the dynamic-state dataset collected from the semi-controlled experiment when subjects transitioned from indoors to outdoors. To address naturally occurring thermal fluctuations outdoors, two fluctuation modes are defined, namely, the highly-dynamic mode and the weakly-dynamic mode. A classification method was developed based on the empirical critical values of the derivative of local skin temperature ($dT_{sk,i}/dt$), categorizing data according to the percentage of values exceeding the critical threshold within a 30 s window. The step-up phase of the dynamic model was developed via linear regression, utilizing the derivative of mean skin temperature

($dT_{sk,m}/dt$) as the independent variable for the weakly-dynamic mode, while both $dT_{sk,i}/dt$ and $dT_{sk,m}/dt$ were used for the highly-dynamic mode. The dynamic model exhibits a satisfactory performance, with an average $Accuracy$ of 74.2% for the highly-dynamic mode, and 73.8% for the weakly-dynamic mode.

The step-down phase of dynamic model provides thermal sensation prediction when the human body experiences negative changes in skin temperatures. This model is developed based on experiments involving 142 human subjects who experienced step-change thermal environments, during which both environmental parameters including skin temperatures of 12 body parts and subjective votes via questionnaire survey, in terms of TSV, thermal comfort vote (TCV), thermal acceptability (TA), thermal pleasure (TP), and thermal stay willingness (TSW), were collected. Around 700 subjective surveys were used in the step-down phase model development. The steady-state part prediction of the abdomen, foot, and neck has been updated in this study. Furthermore, a combined sun and wind condition index (SWI) correction term was added to quantify different effects of wind and solar radiation on TSV. Skin temperature data were classified into the highly-dynamic and weakly-dynamic modes. Lower correlations were found between $dT_{sk,i}/dt$ and dynamic local TSV and between the derivative of Physiology Equivalent Temperature ($dPET/dt$) and $dT_{sk,i}/dt$ in the weakly-dynamic mode than those in the highly-dynamic mode. Comparing the two phases, higher associations between dPETs and dTSVs in the step-up phase were observed than those in the step-down phase. The step-down phase model was developed using linear regression, utilizing $dT_{sk,i}/dt$ as the independent variable in both the highly-dynamic and weakly-dynamic modes. For most body parts, the model exhibits satisfactory results. The average *Accuracy* for the highly-dynamic model is 62.1%, and 69.0% for the weakly-dynamic mode. In addition, among all the subjective thermal environment assessment scales TSV, TA, TP and TSW, TSW illustrates the largest r_s with PET during both the transition period (exposure time ≤ 120s) and the prolonged

exposure period (exposure time > 120s). TSW appears to be more suitable for the assessment of outdoor thermal conditions.

Finally, as an extension of the previous findings, thermal alliesthesia and short-term adaptation phenomenon in outdoor conditions are explored. This study examined the dynamic thermal perceptions and physiological responses of 50 subjects exposed to transient outdoor environments, including underneath an elevated building (UEB) and sunlit areas. Results show that when thermal environment changed, overshoot in thermal sensation persisted for at least 5 mins, and its influence on thermal comfort increased and then diminished at around 5 min, at which point thermal adaptation began to occur. The current thermal comfort was affected by the preceding thermal status: in the strong alliesthesia zone, a 1.00 scale decrease in changes in thermal sensation vote (dTSV) resulted in a 0.44 scale increase in changes in thermal comfort vote (dTCV); whereas in the moderate alliesthesia zone, a slight dTSV within 1.00 scale could positively affect dTCV. Skin temperature of exposed segments correlated better with TSV than that of unexposed ones. Skin temperatures had lower correlations with TSV compared with experiments at static conditions conducted by other researchers. Besides thermal alliesthesia and adaptation effects, sweat accumulation and evaporation are possible reasons for the low correlations.

For the outdoor thermal sensation model developed in this study, there are four main differences from other mainstream models. Firstly, this study employed a series of semi-controlled experiments and field experiments to cover various outdoor settings for model development. Secondly, the model accounts for individual differences and thermal sensation overshoot effect outdoors. It predicts thermal sensation using three values - mean, 10th percentile, and 90th percentile - covering about 80% of individuals. Thirdly, in contrast to indoor models, the dynamic part of this model captures natural environmental fluctuations in outdoor settings by classifying data into two fluctuation modes, highly-dynamic and weakly-

dynamic modes. Lastly, the complete model provides three sets of local TSV predictions for 11 body parts, as well as three values of overall TSV predictions based on local skin temperatures and the derivatives of local and/or mean skin temperatures. It is designed to be integrated with a multi-nodal human thermoregulation model to numerically assess thermal comfort in outdoor spaces during the design and renovation stages. The findings provide insights into thermal evaluation scales for outdoors and are beneficial for improving thermal comfort assessments in outdoor settings.

Keywords: Outdoor thermal comfort; Thermal physiology-based model; Thermal sensation; Thermal alliesthesia; Skin temperature; Sweat rate

Publications arising from this thesis

Journal publications

[1] Jiang Y, Xie Y, Niu J. Short-term dynamic thermal perception and physiological response to step changes between real-life indoor and outdoor environments. Building and Environment 2024; 251.

[2] Jiang Y, Xie Y, Liang H, Zhang H, Goto T, Niu J. Developing a physiological-parameter-based thermal sensation model for warm-biased outdoor settings: The steady-state part. Sustainable Cities and Society. 2025;118.

[3] Jiang Y, Xie Y, Zhang H, Lai D, Niu J. Developing a physiological-parameter-based thermal sensation model for warm-biased outdoor settings: step-up phase of dynamic part. (under review)

[4] Jiang Y, Xie Y, Niu J. Developing a physiological-parameter-based thermal sensation model for warm-biased outdoor settings: step-down phase of dynamic part. (in preparation)

Conference publication

[1] Jiang Y, Xie Y, Niu J. Dynamic thermal perception in short-term transient outdoor environments – introduction of thermal variability. The 11th International Conference on Urban Climate, Sydney, Australia, 2023.

[2] Jiang Y, Xie Y, Niu J. Observation of thermal physiological and thermal sensation responses in an outdoor experimental study. Indoor Air 2024, Hawaii, USA.

[3] Jiang Y, Xie Y, Niu J. Developing a physiological-parameter-based outdoor thermal sensation model from a semi-controlled experiment: The dynamic part. COBEE 2025, Eindhoven, The Netherlands.

Acknowledgements

I would like to first acknowledge the Research Grants Council, Hong Kong, with the Theme-based Research Scheme and General Research Fund, for the financial support for this research.

My sincere appreciation goes to my supervisor, Prof. Jianlei Niu, for his rigorous research attitude, continuous support, insightful ideas, and invaluable comments. Again and again, he revised the hard copies of my drafts, building not just my thesis, but also the researcher I am today. His dedication to work and research has deeply inspired me and will continue to guide my career path. His passion for science will stay with me for life.

Big thanks to my co-supervisor, Dr. Yongxin Xie, who has supported me not only as a mentor but also senior sister throughout this journey. Her rigorous attitude to research, warm support, and meticulous feedback have always accompanied and encouraged me along the way. Her detailed and thoughtful guidance played a key role in my whole experiments in this study. We are growing together and will continue it in the future!

Warm thanks to my host supervisor, Dr. Hui Zhang, during my visiting period at UC Berkeley. Her warm support in both research and daily life, her rigorous attitude, passion for work, and positive feedback all the time have had a profound impact on my research journey and my personal growth. Her kindness and selfless support for others will always inspire me.

Thanks to our technician, Kenny Hung, for his technical support with my experiments. Many thanks to my colleagues and friends, Dr. Jianong Li, Dr. Ziwen Zhong, Dr. Yichen Yu, Dr. Haobin Liang, Ms. Siqi Zhou, Mr. Jiawei Wang, Mr. Xianzhun Zhong, Ms. Yunge Hou, Dr. Jue Wang, Dr. Dharmasastha Kumar, Mr. Junwei Lin, Ms. Peiyang Du, Mr. Cheng Zhao, Dr. Han Liu, Ms. Xinzi Xu, and Mr. Dawei Xu, also the previous colleagues in our group, Ms. Yichun Li, Ms, Junran Yang, and Mr. Yan Liang, for their kind and continuous help during my

journey. Love you all – in both work and life! Heartfelt thanks to my former roommate, Ms. Guancong Ren. I miss the time we chatted face to face every night! Thanks to all the friends and colleagues at CBE, UC Berkeley. I will cherish those shining memories.

Most importantly, many, many, many thanks to my cute parents, Mr. Xiaoxiang Jiang and Ms. Shuxiang Hao. They always support all of my choices without conditions. Their positive attitude, valuable advice, acceptance of my confession all the time, along with the happiness we share together, always encourage me to keep moving forward. It is impossible to finish this journey without their support. Love you forever!

Miss my grandparents, Mr. Zhong Jiang and Ms. Guolin Li. Thanks to them for giving me bravery, love, and happiness to overcome challenges. I will always miss them and the childhood we spent together.

Ying Jiang

Berkeley, June 2025

Table of contents

List of Figures

List of Tables

Nomenclature

ε_p	Emissivity of a clothed human body for long-wave radiation (Standard value 0.97)
σ	Stefan-Boltzmann constant ($5.67 \cdot 10^{-8}\ W/(m^2K^4)$)
ρ	Tissue density, kg/m^3
ρ_{bl}	Density of blood, kg/m^3
ω	Geometry factor, (ω=1 for polar co-ordinates, ω=2 for spheres)
a_k	Absorption coefficients of the clothed human body for short-wave radiation (Standard value 0.70)
AD	Body surface area
ADTK	Anomaly Detection Toolkit
ASV	Actual Sensation Vote
BMI	Body mass index
c	Heat capacitance, $J/kg \cdot K$
c_b	Specific heat, $W \cdot s/(K \cdot kg)$
c_{bl}	Heat capacitance of blood, $J/kg \cdot K$
$C_{sk,i}$	Critical value of each body part for classifying highly-dynamic and weakly dynamic modes
clo	Clothing insulation value
C	Convective heat transfer, W/m^2
CBE model	A multi-node human body thermal regulation model developed by the University of California-Berkeley
CFD	Computational Fluid Dynamics
COMFA	COMFort formulA model
dT	Changes in thermal sensation
dP	Changes in thermal pleasure
$dPET$	Changes in PET between two adjacent survey points, °C
$dPET/dt$	Derivative of Physiological Equivalent Temperature, °C/s
$dTSV$	Change of thermal sensation vote
$dTCV$	Change of thermal comfort vote
$dTSV/dt$	Change rate of thermal sensation vote
$dTCV/dt$	Change rate of thermal comfort vote
$dT_{sk,i}/dt$	Derivative of local skin temperature, °C/s
$dT_{sk,\mathrm{m}}/dt$	Derivative of mean skin temperature, °C/s
dT_{core}/dt	Derivative of core temperature, °C/s
$\lvert dT_{sk,\mathrm{i}}/dt \rvert$	Absolute value of the derivative of local skin temperature, °C/s
$\lvert dT_{sk,m}/dt \rvert$	Absolute value of the derivative of mean skin temperature, °C/s
DMV	Dynamic Mean thermal sensation Vote

DTS	Dynamic Thermal Sensation
E_D	Latent heat transfer to evaporate water into vapor diffusing through the skin, W/m^2
E_{Re}	Evaporative heat loss from respiration, W/m^2
E_{req}	required evaporative heat loss, W/m^2
E_{Sw}	Evaporative heat loss from sweating, W/m^2
ET^*	Effective temperature
F_{CS}	Heat transfer from body core to skin surface, W/m2
F_{SC}	Heat transfer from skin surface to clothing, W/m2
F_i	Angular factors between a person and the surrounding surfaces
HKPolyU	Hong Kong Polytechnic University
h_e	Evaporative heat transfer coefficient, W/(m^2·kPa)
h_r	Radiative heat transfer coefficient, 4.71W/M^{2}K
h_c	Convective heat transfer coefficient, W/(m^2·kPa)
i_m	Total vapor permeation efficiency: ratio of actual evaporative heat flow capability between skin and environment o sensible heat flow capability as compared to Lewis ratio
I_{cl}	Heat resistance of the clothing, $K{\cdot}m^2/kg$
k	Heat conductivity, $W/m \cdot K$
K_i	Short-wave radiation fluxes (W/m^2)
L_i	Long-wave radiation fluxes (W/m^2)
LR	Lewis ratio, equals approximately 16.5 K/kPa
M	Metabolic rate, W/m^2
m_i	Sweat rate of the i body part
MARC	Membrane-Assisted Radiant Cooling
MOCI	Mediterranean Outdoor Comfort Index
MEMI	Munich Energy-balance Model for Individuals
met	Unit of metabolic rate
MTSV	Mean thermal sensation vote
p	Possibility that the data within this period exceed the critical value
$p_{ET*,s}$	Saturated vapor pressure at ET*, kpa
p_a	Vapor pressure at a point of air temperature , kpa
PET	Physiological Equivalent Temperature
PMV	Predicted mean vote
PPD	Predicted Percentage of Dissatisfied
$Predicted\ range$	Constructs by the 10th percentile and the 90th percentile of predicted thermal sensation
q_m	Metabolism, W/m^3
Q_l	Long-wave irradiance, W/m^2
Q_s	Short-wave irradiance, W/m^2
r	Radius, m
r_s	The Spearman correlation coefficient
R	Net radiation of the body, W/m^2

RH	Relative humidity, %
R_DTE	Reverse Dynamic Thermal Environment
S	Heat storage, W/m^2
SVF	Sky View Factor
SWI	Combined Sun and Wind Conditions Index
t	Time, s
T	Tissue temperature, °C
TI	Turbulence intensity, %
T_{bla}	Arterial blood temperature, °C
T_{skin}	Skin temperature, °C
$\bar{T}_{\mathrm{sk}}$	Mean skin temperature, °C
$T_{sk,neu,i}$	Neutral skin temperature of the target local body part
T_{core}	Core temperature, ℃
$T_{\mathrm{sk},i}$	Local skin temperature, ℃
$T_{\mathrm{sk,m}}$	Mean skin temperature, ℃
T_{cl}	Mean surface temperature of the clothing, ℃
T_a	Air temperature, ℃
T_b	Black globe temperature, ℃
T_{mrt}	Mean radiant temperature, ℃
t_o	Operative temperature, ℃
TSV	Overall Thermal Sensation Vote
TSV_i	thermal sensation of local body parts
$TSV_{i,actual}$	Actual thermal sensation vote of the i body part
$TSV_{i,steady,mean}$	Mean value of the local TSV prediction of steady-state part
$TSV_{i,steady,\mathrm{10th}}$	The 10$^{\mathrm{th}}$ percentile of the local TSV prediction of steady-state part
$TSV_{i,steady,\mathrm{90th}}$	The 90$^{\mathrm{th}}$ percentile of the local TSV prediction of steady-state part
$TSV_{i,dynamic}$	Dynamic part of local TSV prediction
$TSV_{i,mean}$	Mean value of the local TSV prediction
$TSV_{i,10th}$	The 10$^{\mathrm{th}}$ percentile of the local TSV prediction
$TSV_{i,90th}$	The 90$^{\mathrm{th}}$ percentile of the local TSV prediction
$TSV_{i,steady,correction}$	SWI correction term for the steady-state part prediction
$TSV_{i,steady,ori}$	Original expression of the steady-state part prediction
$TSV_{i,steady,mean,ori}$	Mean value of the original steady-state part prediction
$TSV_{i,steady,10th,ori}$	The 10$^{\mathrm{th}}$ percentile of the original steady-state part prediction
$TSV_{i,steady,90th,ori}$	The 90$^{\mathrm{th}}$ percentile of the original steady-state part prediction
TSV_{prefer}	Preferred thermal sensation
$\overline{TSV}$	Mean value of thermal sensation vote
$TSV\ (t)$	Current thermal sensation vote at the t time
$TCV\ (t)$	Current thermal comfort vote at the t time
ΔTSV	Difference between current thermal sensation vote and the last thermal sensation vote at the previous site before thermal transitions

ΔTCV	Difference between current thermal comfort vote and the last thermal comfort vote at the previous site before thermal transitions
TCV	Thermal Comfort Vote
TA	Thermal Acceptability
TP	Thermal Pleasure
UEB	Underneath an elevated building
UTCI	The Universal Thermal Climate Index
v	Wind speed, m/s
v_b	The blood flow from body core to skin, $l/(s \cdot m^2)$
w	Skin wettedness, dimensionless
w_i	Weighting coefficient for the segment i th
w_{bl}	Blood perfusion rate, $m^3/(s \cdot m^3)$;
W	Physical work output, W/m^2
WBGT	Wet bulb globe temperature
WRF	Weather Research and Forecasting
*SET**	Standard effective temperature

Chapter 1 - **Introduction**

1.1 **Background**

Extreme heat events are becoming permanent features of summer in a growing number of countries (Ebi et al., 2021). Global warming, a universal problem that raises concerns around the world (Matthews et al., 2017), continues to bring more frequent heat waves and increased air temperatures (Du et al., 2019). This climate change, coupled with rapid urbanization, has significantly elevated urban temperatures (Oleson et al., 2013). Rising urban temperatures have deteriorated outdoor thermal conditions in urban areas at pedestrian levels (Huang et al., 2017) (Ren et al., 2022), making city dwellers' lifestyles more sedentary and indoor-focused (Obradovich & Fowler, 2017). Such behavior leading to reduced outdoor activity can potentially impact the health and well-being of urban residents.

In addition, spending a 20.5-min park visit has been shown to have an immediate positive impact on human well-being (Yuen & Jenkins, 2020). A recent study has shown that spending at least 120 min a week in natural environments reports good health or higher well-being compared with those who have no nature contact (White et al., 2019). Creating more thermally comfortable outdoor spaces may encourage city dwellers to spend more time outdoors, thereby potentially improving their overall health and well-being.

This can be achieved in two ways: by optimizing the interaction between solar shading and wind effects through building block design during the planning stage, and by implementing passive or active cooling strategies during the renovation stage. Advanced cooling strategies can be implemented to improve outdoor thermal environments. Solutions such as optimized building layout design, mist-spraying systems, and radiant cooling panels can enhance pedestrians' thermal comfort in urban settings.

While indoor thermal environments have been widely regulated through standards such as ASHRAE 55 (ASHRAE) and ISO 7730 (ISO, 2005), regulations addressing outdoor thermal conditions remain relatively limited. Germany's VDI 3787 (VDI 3787-1, 2015) provides guidance on urban microclimates, suggesting incorporating Physiological Equivalent Temperature (PET) as an indicator for heat stress assessment. Urban Climatic Map and Standards for Wind Environment from Hong Kong (Ng, 2009) offers different strategies for enhancing outdoor thermal comfort, such as breezeways and Building Height/Street Width (H/W) ratio control. CASBEE (Institute for Building & Energy, 2014) guides for improving outdoor thermal environment through measures such as enhancing wind flow, increasing shaded space, incorporating green and water elements, and managing heat vents from equipment. However, most of these standards only provide qualitative guidelines for enhancing outdoor microclimates, while quantitative assessment of outdoor thermal comfort remains largely unregulated.

Clearly, quantitative assessment requires computer-aided simulation tools to evaluate performance and to seek an optimum design that maximizes the degree of thermal comfort, and a comfort performance evaluation model that provides accurate and reliable predictions of thermal comfort (Coccolo et al., 2016). Such a model will provide 1) a quantitative prediction of outdoor thermal comfort during the design process and 2) evaluate the performance of optimization measures in terms, for example, of the proportion of people for whom that optimum solution is a satisfactory one.

Thermal sensation models for evaluating outdoor thermal environments are essential for enhancing pedestrians' thermal comfort during the design and renovation of building layouts or cooling strategies (Coccolo et al., 2016). Physiological Equivalent Temperature (PET) (Peter Höppe, 1999), Predicted Mean Vote (PMV) (Fanger, 1970), Universal Thermal Climate Index (UTCI) (Fiala et al., 2011), and Standard Effective Temperature (SET*) (Gagge et al., 1986)

are the four most widely used indices in outdoor thermal comfort studies (Potchter et al., 2018). Mainstream outdoor thermal comfort models fall into three categories, energy balance model, empirical model, and thermal physiology-based model.

The first type of model is the energy balance model, including the PET, SET*, PMV, and COMFort formula (COMFA) (Kenny et al., 2009b, 2009a). The theoretical significance of these models lies in the heat transfer between the human body and the external environment. The inputs are environmental parameters (e.g., air temperature (T_{mrt}), relative humidity (RH), wind speed (v), mean radiant temperature (T_{mrt}), and clothing insulation (I_{clo}), and the output will be an equivalent temperature or a thermal sensation. Nevertheless, most of these models are developed for steady-state conditions, thereby reducing their accuracy in dynamic outdoor environments (Fang et al., 2019).

The second type is the empirical model, such as the Actual Sensation Vote (ASV) (Nikolopoulou et al., 2003) and the Thermal Sensation (TS) (Givoni et al., 2006). Empirical models are developed based on field studies from local climates, making them more suitable for assessing thermal comfort in specific climate zones.

The third type of model is the thermal physiology-based model, which combines the characteristics of the energy balance model with the empirical model, such as the CBE model (Zhang et al., 2010b, 2010a, 2010c) and UTCI. Thermal physiology-based models integrating the developed thermoregulation model (e.g., Huizenga's model (2001), JOS-3 model (Takahashi et al., 2021), UTCI-Fiala model (Fiala et al., 2011)) would be more applicable than the empirical model since thermal sensation predictions are based on thermal physiology. Categorized by the number of nodes of the thermoregulation model, multi-node models have a higher potential for the precise prediction of thermal sensation in transient and asymmetric thermal conditions.

However, most of these models were developed based on data collected in indoor chambers, their application outdoors is restricted by the difference between physiological parameters and thermal sensation indoors and outdoors (Lai et al., 2020). Moreover, as the equivalent temperature cannot directly correspond to thermal sensation, researchers need to conduct additional subject tests to establish a connection between thermal sensation and equivalent temperature (Lai et al., 2020).

This difference between indoors and outdoors mainly comes from physical, physiological, and psychological aspects (Höppe, 2002; Nikolopoulou & Steemers, 2003). Primarily, there is a natural environmental difference between indoors and outdoors, such as dynamic wind speeds and solar radiation, resulting in dynamic thermal environments outdoors.

On a physiological level, in addition to the dynamic physiological response to highly transient thermal environments, thermal exposure outdoors is much shorter than indoors (Nikolopoulou et al., 2001). People typically remain indoors for hours, whereas exposure to the same outdoor conditions may last only a few minutes, resulting in dynamic physiological responses.

For the psychological aspect, thermal experience and thermal expectation also affect thermal perceptions, which result in different responses in thermal perception between indoor and outdoor thermal conditions. Thus, the model based on indoor chamber data may not be accurate in the prediction of outdoor thermal comfort. Cheng et al. (2012) pointed out that the PMV overestimated the thermal sensation towards the warmer end of the scale and underestimated the thermal sensation towards the cooler end of the scale, and that the PET underestimated the effect of latent heat fluxes. A field survey conducted by Li et al. (2020) in Hong Kong, it was found that the UTCI underestimated the effects of v and T_{mrt} under high air temperature conditions. Thus, the model developed from indoor chamber data may not be accurate in the prediction of outdoor thermal comfort.

There have been some attempts to establish thermal comfort models specifically tailored to outdoor environments over the past decade. A new empirical index Mediterranean Outdoor Comfort Index (MOCI) was proposed by Salata et al. (2016a) for evaluating overall thermal sensation and quantifying PET in the Mediterranean area. Lai et al. (2017b) developed a dynamic model based on outdoor data to predict overall thermal sensation, which takes into account thermal load, mean skin temperature, and the change rate of mean skin temperature as predictors. Li et al. (2020) proposed a combined sun and wind condition index (SWI) to evaluate the effect of T_{mrt} and v on outdoor thermal comfort. Xu et al. (2022) collected environmental parameters, skin temperatures of 3 body parts (i.e., chest, forearm, and calf), and thermal perceptions in transient outdoor conditions, including transitions from a sunlight area to different shading areas. A transient model was developed for the prediction of overall thermal sensation by considering the lower-arm skin temperature and its rate of change as variables. Zhang et al. (2023) revised the PET and UTCI indices and proposed PET-based and UTCI-based outdoor thermal comfort models by adding an adaptive coefficient to the rational model for outdoor use. Vellei (2024) developed a dynamic mean thermal sensation (DMV) model using datasets from previous indoor chamber studies for overall thermal sensation prediction.

However, most of these models do not account for the diversity of outdoor settings. Given the highly dynamic and variable nature of outdoor environments, investigating thermal responses across a wide range of outdoor conditions is essential for developing a reliable and applicable outdoor thermal sensation model. In addition, most models only provide overall thermal sensation prediction, and do not provide thermal sensation prediction of different body parts. Given the asymmetric nature of outdoor thermal environments, the overall thermal sensation model developed based on local thermal sensation prediction can better reveal the effect of asymmetric settings in outdoor conditions.

Due to the dynamic features of outdoor thermal environments, thermal alliesthesia and short-term thermal adaptation will highly affect human thermal perceptions outdoors. Thermal alliesthesia and short-term thermal adaptation are two well-known concepts affecting dynamic thermal perceptions (Vellei et al., 2021). They are essential theories for creating a high degree of thermal pleasure and thermal comfort feelings. The concept of thermal alliesthesia has been adopted to explain the various phenomena observed in outdoor thermal comfort studies (Lai et al., 2020).

Both short-term and long-term alliesthesia exist in our daily life. Long-term alliesthesia, such as seasonal alliesthesia, which has been observed in previous studies (Lai, Guo, et al., 2014; Yao et al., 2018; Schweiker et al., 2020), results in occupants perceiving a slightly warm thermal sensation as most comfortable in winter and a slightly cool thermal sensation as most comfortable in summer. Thermal comfort and pleasure also occur with the changes in transient thermal environments. Dzyuban et al. (2022) explored the thermal alliesthesia phenomenon in transient outdoor scenarios. They found that slight changes in microclimate conditions caused thermal pleasure. Peng et al. (2022) performed a stop-and-go experiment of transient outdoor scenarios and found that the variation of thermal environment is vital to creating thermal pleasure. Liu et al. (2021) quantified the thermal sensation into four alliesthesial potential zones based on the preceding thermal sensation deviation from the preferred thermal sensation. Linear regression and quadratic regression were used to fit the relationship between changes in thermal sensation and thermal pleasure in strong and moderate alliesthesia zones, respectively.

Sensory adaptation refers to the diminished sensitivity during the presentation of an effective stimulus (Solomon & Kohn, 2014), which is directly related to the dynamic activity of primary sensory neurons (Vellei et al., 2021). From a thermal perspective, short-term thermal adaptation refers to a short-duration (i.e., minutes or hours) adaptive process characterized by a time-dependent attenuation of the body's sensory response following non-neutral thermal

exposures (Taylor, 2006; Vellei et al., 2021), which is in a much shorter timescale than the original concept of thermal adaptation (i.e., days or months). This phenomenon has been primarily validated in local thermal stimulus experiments (Haber, 1958), while other studies focused on thermal pain perception (Edwards & Fillingim, 2001; Jepma et al., 2014).

Some studies investigated dynamic thermal perceptions under transient thermal environments in climate chambers. Zhang et al. (2017) conducted a chamber experiment collecting subjects' subjective and physiological responses to explore the effects of step-change temperature on thermal comfort. They found that thermal sensation stabilized at 20 min under warm exposure and at 1 min under cool exposure. Ji et al. (2017) experimented with 20 subjects in step-change chamber conditions, they found that thermal sensation was amplified after step-change conditions, then attenuated and stabilized after 15 min of exposure.

Nevertheless, given the large effect of thermal alliesthesia and short-term thermal adaptation phenomena on thermal perception in outdoor thermal environments, few studies have investigated the combined effects on dynamic thermal perceptions and physiological responses in outdoor settings.

Thermal sensation vote (TSV) is typically used to evaluate human thermal feelings in thermal environments. Thermal comfort vote (TCV), Thermal Acceptability (TA), and Thermal Pleasure (TP) are commonly used to assess thermal comfort conditions in various thermal environments. However, occupants have varying thermal comfort needs for different scenarios, depending on the specific use of spaces (Y. Yang et al., 2024). For instance, work environments emphasize work efficiency, sleep environments prioritize sleep quality, and urban outdoor spaces are designed to provide recreational spaces that encourage city dwellers to spend time outdoors. Due to the dynamic features in outdoor environments and pedestrians' transition between different microclimate scenarios, thermal overshoot and short-term adaptation

phenomena commonly occur (Jiang et al., 2024). Compared to indoor studies using the TCV and TA scales to evaluate occupants' thermal comfort (Ji et al., 2017; Su et al., 2020; Zhu et al., 2025), outdoor studies tend to adopt the TP scale (Liu et al., 2021; Zhang et al., 2024) as it captures the pleasant feelings that are always associated with transient environments (Cabanac, 1992; Arens et al., 2006). Consequently, thermal evaluation scales originally developed for indoor environments may not be applicable to outdoor settings. An outdoor study (S. Liu et al., 2020) compared 76 climatic adjectives and developed a semantic framework to assess outdoor thermal comfort, comprising 'thermal sensation', 'humidity', 'wind', 'solar radiation', 'thermal pleasure', and 'thermal intensity'. Few studies have explored the thermal evaluation scale specifically designed for outdoor use, thus, the applicability of different scales in outdoor settings may need further investigation.

Currently, no applicable and accurate model can provide a reliable prediction of thermal perception in different outdoor environments. There are mainly four limitations: 1) Existing classical indices are mainly developed from indoor chambers, and most developing outdoor thermal comfort models did not fully consider various outdoor thermal environments (e.g., a variety range of wind speed and solar radiation levels, transient and dynamic thermal conditions). 2) The developing outdoor thermal comfort models only considered overall thermal sensation prediction and did not consider the prediction of thermal sensation for local body parts, which are important in asymmetric outdoor conditions. 3) Few studies explored the combined effect of thermal alliesthesia and adaptation phenomena on dynamic thermal perceptions in real-life environments, especially the psycho-physiological aspect of thermal alliesthesia and short-term adaptation in step-change indoor and outdoor thermal environments. 4) Since thermal evaluation scales originally designed for indoors may not be suitable for assessing outdoor thermal environments, the applicability of these scales for outdoor use needs further investigation.

1.2 Aim and objectives

This study focuses on the development of a physiological-parameter-based model for outdoor microclimate assessment in neutral to warm-biased thermal conditions. The study aims to develop an outdoor thermal sensation model by exploring the relationship between human subjective thermal responses, in terms of local thermal sensation and overall thermal sensation, and physiological responses, in terms of local skin temperature, core temperature, and local sweat rate, in a wide range of real-life outdoor thermal environments. The thermal physiology-based model can be integrated with thermoregulation models (e.g., JOS-3 model) to predict thermal sensation based on environmental parameters.

Semi-controlled experiments and field experiments were both employed in this study to efficiently create a wide range of outdoor settings, including various combinations of wind speed and solar radiation levels, transient and dynamic conditions. The study includes the steady-state model development, the step-up phase, and the step-down phase of the dynamic model development, as well as an exploratory investigation into thermal alliesthesia and short-term adaptation phenomenon. The 'steady-state' refers to a condition where the human body maintains a relatively stable thermal status. The 'step-up' phase represents the human body experiencing an increasing thermal load, characterized by positive changes in skin temperature, while the 'step-down' phase indicates a decreasing thermal load, marked by negative changes in skin temperature. The main objectives are as follows:

1. To investigate dynamic changes in human thermal perceptions and physiological responses in various outdoor thermal environments, and explore the relationship between thermal perceptions and physiological responses in various outdoor thermal environments.

2. To discuss the applicability of different physiological parameters to predict thermal sensation of local body parts in dynamic outdoor conditions.
3. To build the thermal sensation model for overall and local body parts based on physiological parameters, under real-life outdoor conditions when the human body is in a steady state.
4. To build the thermal sensation model for overall and local body parts based on physiological parameters, under real-life outdoor conditions when the human body is in the step-up phase of dynamic states.
5. To build the thermal sensation model for overall and local body parts based on physiological parameters, under real-life outdoor conditions when the human body is in the step-down phase of dynamic states.
6. To explore the relationship between dynamic thermal perceptions and physiological response in transient thermal environments based on thermal alliesthesia and short-term thermal adaptation concepts.
7. To compare the applicability of different thermal evaluation scales (e.g., TCV, TA, TP, Thermal Stay Willingness (TSW)) in transient outdoor conditions.

1.3Research framework

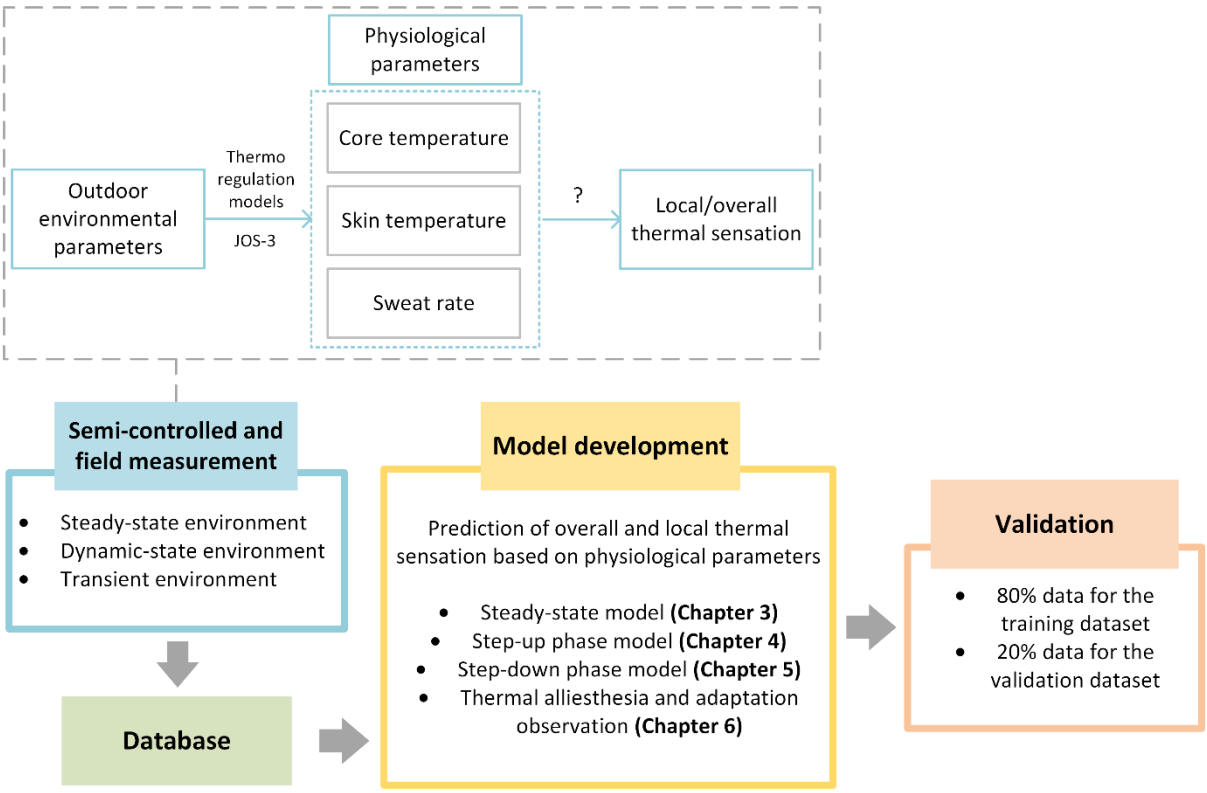

Figure 1.1 Flowchart of research framework.

1.4Thesis outline

Chapter 1 gives a brief description of the research background, points out the research gap, presents the research framework, and draws the outline of this thesis.

Chapter 2 presents a literature review of the whole study, mainly consisting of outdoor thermal comfort studies in recent years, dynamic outdoor thermal comfort research, introduction of mainstream outdoor thermal indices, developing outdoor thermal comfort models, human thermoregulatory responses, and thermal alliesthesia and short-term adaptation theory. Detailed research gaps are provided.

Chapter 3 provides the results of steady-state model development, investigates the variations of thermal sensation and physiological parameters in real outdoor conditions, as well as the

relationship between these parameters. These findings address Objectives 1, 2, and 3 of the study.

Chapter 4 provided the results of the step-up phase model development, explores the variation of thermal sensation and physiological parameters under the step-up dynamic state, and discusses the applicability of different physiological parameters to predict the dynamic thermal sensation of local body parts. The findings address Objectives 1, 2, and 4 in this study.

Chapter 5 provides the results of step-down phase model development, investigates the variation of thermal sensation and physiological parameters under the step-down dynamic state, and discusses the applicability of different thermal evaluation scales for outdoor use, especially in transient conditions. These findings address Objectives 1, 5, and 7 in this study.

Chapter 6 provides the results of dynamic thermal perceptions and physiological parameters and their correlations in transient outdoor conditions, discusses and quantifies the thermal alliesthesia and short-term thermal adaptation phenomenon. These findings address Objectives 1 and 6 in this study.

Chapter 7 summarizes the conclusion of this study and recommendations for future studies.

Chapter 2 - **Literature review**

2.1 Outdoor thermal comfort studies in recent years

2.1.1 Introduction to the research field

To give general information about this research field, the author searched the keyword 'outdoor thermal comfort' in the Web of Science. The results show an increasing concern in this field, from a record of 64 publications in 2010 to 724 publications in 2024. Figure 2.1 illustrates general information about the keyword co-occurrence network of outdoor thermal comfort studies.

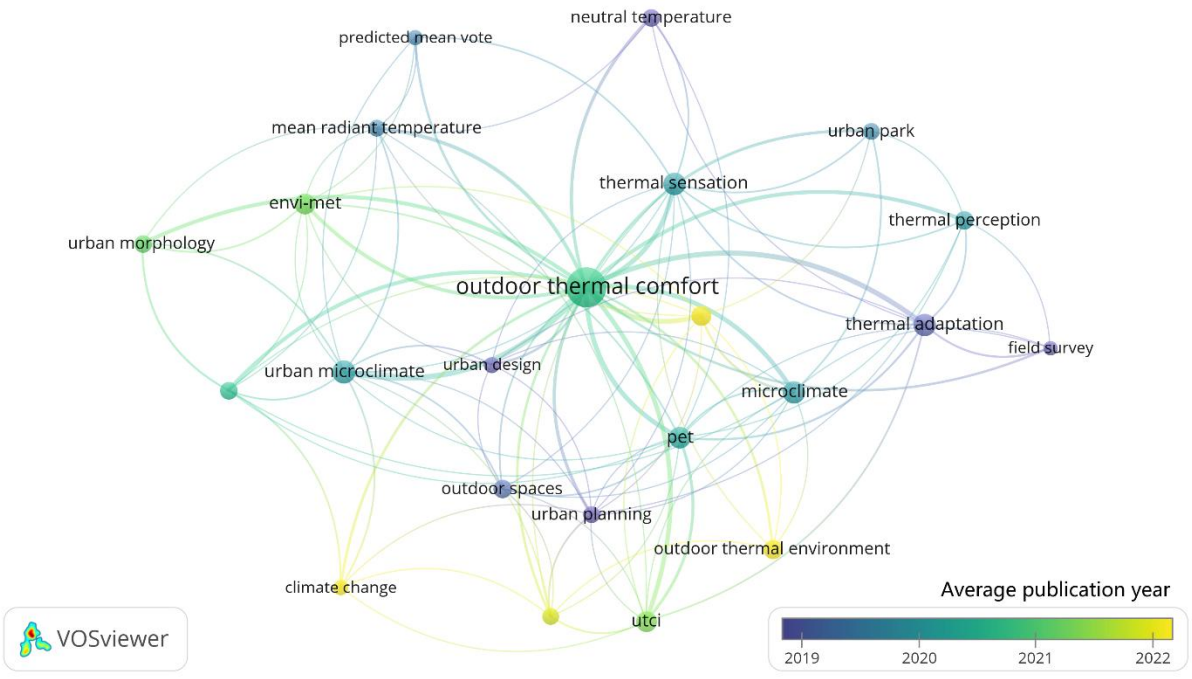

Figure 2.1 Keyword co-occurrence network of outdoor thermal comfort publications

Table 2.1 summarizes the 15 most highly cited publications in the field of outdoor thermal comfort. Among them, five studies focused on field measurement in outdoor thermal

environments (Nikolopoulou & Steemers, 2003), (Spagnolo & de Dear, 2003) (Lin, 2009) (Nikolopoulou et al., 2001) (Nikolopoulou & Lykoudis, 2006), four studies focused on developing outdoor thermal comfort models (P. Höppe, 1999) (Thorsson et al., 2007; Fiala et al., 2012; Jendritzky et al., 2012), three publications investigated strategies for enhancing outdoor thermal comfort, including green infrastructure (Norton et al., 2015) (Ng et al., 2012), and street canyon design using Computational Fluid Dynamics (CFD) simulation (Ali-Toudert & Mayer, 2006), one focused on human vulnerability under heat stress (Harlan et al., 2006), and two review papers about human thermal comfort in different thermal environments (Rupp et al., 2015), and mitigating strategies for improving thermal environments (Lai et al., 2019). Considering investigation methods, most of these studies used onsite measurement (Nikolopoulou & Steemers, 2003), (Spagnolo & de Dear, 2003) (Lin, 2009) (Nikolopoulou et al., 2001), while other studies employed simulation methods, such as ENVI-met (Ng et al., 2012) and CFD (Ali-Toudert & Mayer, 2006).

Overall, in the context of climate change and the urban heat island effect, some of these studies aimed to develop outdoor thermal comfort models to evaluate thermal conditions, while others focused on investigating cooling strategies to improve outdoor thermal environments and enhance pedestrians' thermal comfort.

Table 2.1 The most cited publications in the field of outdoor thermal comfort

Author, Year	Title	Citations	Research area
(P. Höppe, 1999)	The physiological equivalent temperature -: a universal index for the biometeorological assessment of the thermal environment	1629	Outdoor thermal comfort model

(Jendritzky et al., 2012)	UTCI-Why another thermal index?	763	Outdoor thermal comfort model
(Norton et al., 2015)	Planning for cooler cities: A framework to prioritise green infrastructure to mitigate high temperatures in urban landscapes	752	Green infrastructure
(Harlan et al., 2006)	Neighborhood microclimates and vulnerability to heat stress	728	Heat stress
(Ali-Toudert & Mayer, 2006)	Numerical study on the effects of aspect ratio and orientation of an urban street canyon on outdoor thermal comfort in hot and dry climate	703	Street canyon
(Ng et al., 2012)	A study on the cooling effects of greening in a high-density city: An experience from Hong Kong	673	Green infrastructure
(Fiala et al., 2012)	UTCI-Fiala multi-node model of human heat transfer and temperature regulation	638	Outdoor thermal comfort model
(Rupp et al., 2015)	A review of human thermal comfort in the built environment	607	Review
(Nikolopoulou & Steemers, 2003)	Thermal comfort and psychological adaptation as a guide for designing urban spaces	587	Field measurement
(Spagnolo & de Dear, 2003)	A field study of thermal comfort in outdoor and semi-outdoor environments in subtropical Sydney Australia	545	Field measurement

(Lai et al., 2019)	A review of mitigating strategies to improve the thermal environment and thermal comfort in urban outdoor spaces	526	Review
(Lin, 2009)	Thermal perception, adaptation and attendance in a public square in hot and humid regions	519	Field measurement
(Thorsson et al., 2007)	Different methods for estimating the mean radiant temperature in an outdoor urban setting	508	Outdoor thermal comfort model
(Nikolopoulou et al., 2001)	Thermal comfort in outdoor urban spaces: Understanding the human parameter	507	Field measurement
(Nikolopoulou & Lykoudis, 2006)	Thermal comfort in outdoor urban spaces: Analysis across different European countries	496	Field measurement

2.1.2 Methods for evaluating outdoor thermal environments

There are several common methods for evaluating outdoor thermal environments: indoor chamber experiments, onsite measurements, and numerical simulation methods. Table 2.2 summarizes methods used in some representative outdoor thermal comfort studies.

Table 2.2 Summary of methods used in outdoor thermal comfort studies

Research method	Author, Year
Indoor chamber experiments	(Höppe, 2002; Fiala et al., 2003; H. Zhao et al., 2024)

Onsite measurements	(Nikolopoulou et al., 2001; Lin et al., 2010; Cheng et al., 2012; Li et al., 2020; Zhang et al., 2024)
Numerical simulation	ENVI-met simulation: (Salata et al., 2016b; Ouyang et al., 2023) CFD simulation: (Wai et al., 2020; Chen et al., 2021; Yuan et al., 2022).

2.1.2.1 Indoor chamber experiments

Some classical thermal comfort models used for outdoors were developed based on experiments conducted in indoor climate chambers. Hoppe (2002) investigated the time required to reach thermal steady state when transitioning from a thermal comfort room to different simulated outdoor conditions in indoor climate chambers. The study found that for a person leaving a thermal comfort room into cold winter outdoor conditions (T_a = T_{mrt} = 0 °C, v = 1 m/s) reaching steady state will take many hours, while leaving into hot conditions (T_a = 30 °C, T_{mrt} = 60 °C, v = 0.5 m/s) will take less than 30 min. Fiala et al. (2003) developed a Dynamic Thermal Sensation (DTS) model for overall dynamic thermal sensation prediction in steady-state and various transient conditions, and the data were derived from previous indoor chamber tests. They utilized mean skin temperature and temporal changes in mean skin temperature as independent variables for overall thermal sensation prediction.

Recent studies have used advanced indoor chambers to simulate outdoor environments, allowing for more controlled experimental conditions. Zhao et al. (2024) simulated dynamic thermal radiation exposure in a climate chamber to explore the effects of dynamic thermal experience on pedestrians' thermal comfort. They found that the 'whole trip' thermal sensation vote is neither equivalent to instantaneous thermal sensation nor to the weighted average of

past thermal sensations. The whole-trip thermal sensation can be better characterized by instantaneous thermal sensation, mean skin temperature, and the heat received by the human body.

2.1.2.2 Onsite measurements

Due to the dynamic characteristics of outdoor thermal environments, indoor climate chambers cannot fully replicate real outdoor conditions. As a result, onsite measurements have become a mainstream method in outdoor thermal comfort research in recent years (Nikolopoulou et al., 2001; Lin et al., 2010; Lai, Guo, et al., 2014; Watanabe et al., 2014; Niu et al., 2015; Taleghani et al., 2015; Fang et al., 2018; Li et al., 2018; Xie et al., 2019).

Nikolopoulou et al. (2001) conducted a field measurement in outdoor urban spaces, and explored how different human parameters influence people's behaviour and usage of outdoor spaces. They found that the thermal environment is indeed of prime importance influencing people's use of outdoor spaces, while psychological adaptation, such as availability, environmental stimulation, thermal history, memory effect, and expectations, is also of great importance.

Lin et al. (2010) investigated shading effects in outdoor thermal environments and the influences on pedestrians' thermal perceptions in outdoor spaces. 12 field experiments were conducted to analyze outdoor thermal conditions on a university campus in central Taiwan to explore the annual thermal conditions instead of a particular day. The results showed that the shading effect, represented by the Sky View Factor (SVF), significantly affects outdoor thermal environments. A high SVF (barely shaded) causes thermal discomfort in summer while a low SVF (highly shaded) leads to thermal discomfort in winter.

Li et al. (2020) conducted simultaneous physical measurements and subjective surveys to investigate outdoor thermal comfort in a subtropical city, Hong Kong. T_{mrt}, sun and wind

desirability, and v were identified as the top three factors influencing thermal sensation. They found that the UTCI underestimated the effects of v and T_{mrt} at higher air temperatures, but overestimated the impacts of air temperature and relative humidity on TSV.

Zhang et al. (2024) conducted walking experiments in overhead layer and tree-shaded areas to investigate thermal comfort differences based on thermal environments and activity levels. The findings indicated that significant differences exist between the thermal environments of the two areas, with reduced T_{mrt} by approximately 3 °C and v by about 1 m/s. Subjects' thermal pleasure is influenced by the objective thermal environment, the human body's thermoregulatory mechanism, and subjective psychological expectations.

In addition to onsite measurements, some studies conducted semi-controlled experiments in real outdoor settings to address the challenges of uncontrolled environmental conditions. Cheng et al. (2012) performed a longitudinal subject study with changing wind and solar radiation conditions using a wind shield and sunshade. This experiment design allows explorations of the effects of changing environmental conditions on thermal sensation and provides information that is not possible to obtain through conventional transverse field studies. The study provided outdoor thermal sensation prediction formulas as functions of air temperature, wind speed, solar radiation intensity, and absolute humidity.

2.1.2.3 Numerical simulation

Simulation methods are also widely used in the field of outdoor thermal comfort, with ENVI-met (Salata et al., 2016b; Yilmaz et al., 2021; Elraouf et al., 2022; Fiorillo et al., 2023; Ouyang et al., 2023) and CFD being the most commonly applied tool (Wai et al., 2020; Chen et al., 2021; Yuan et al., 2022; J. Zhong et al., 2022; Chen et al., 2024).

Salata et al. (2016b) provided a proper procedure for numerical simulations using ENVI-met and compared the simulation outputs to experimental data. This study suggests that the

determination of input parameters for the ENVI-met simulations should be well considered. Ouyang et al. (2023) utilized the ENVI-met software to quantify the cooling effects of green infrastructure strategies in urban microclimate. Cooling intensity, cooling area, and cooling duration were proposed as three cooling indicators for urban planning. They found that the greatest cooling effect of green infrastructure strategies was at SVF = 0.7.

CFD is widely used to simulate different strategies to enhance outdoor thermal environments. Wai et al. (2020) coupled a CFD model to the Rayman model to study the effect of different urban forms on outdoor thermal environments, with κ–ω SST turbulent model adopted for the CFD simulations. They found that building lengths and porosity were keys to reduce heat stress in urban design. Yuan et al. (2022) employed CFD simulation to analyze the effects of different building external-wall surfaces with different reflective directional properties on outdoor thermal comfort. Chen et al. (2021) used CFD simulation to explore the impacts of different elevated walkway designs on outdoor thermal comfort. They found that the elevated walkway increased the ground-level PET by up to 2.7 °C and reduced by 2−17 °C of PET for the walkway level.

In summary, existing studies mainly use onsite measurements, numerical simulation, and indoor chamber experiments for outdoor thermal comfort research. Among these methods, onsite measurement is the most commonly used approach, as it captures the real dynamic thermal characteristics of outdoor environments. Numerical simulation is an effective tool for investigating the impacts of specific cooling strategies. Indoor chamber tests are often used to develop classical thermal indices for simulating varying thermal conditions; however, these setups may not accurately reflect the dynamic nature of outdoor environments.

2.1.3 Advanced strategies to enhance outdoor thermal comfort

In the context of climate change, cooling strategies have become a prominent research focus aimed at improving outdoor thermal conditions and alleviating pedestrians' thermal discomfort. There are several mainstream aspects to enhance outdoor thermal environments, such as urban planning, building layout design, and active cooling devices.

2.1.3.1 Urban geometry

Urban planning mainly affects urban air temperatures and wind distribution. Urban geometry with low SVF or high height-to-width ratio (H/W) can reduce solar radiation and enhance thermal comfort in hot conditions (Lai et al., 2019). Ali-Toudert et al. (2006) utilized the ENVI-met method to explore the impact of H/W and street orientation on outdoor thermal conditions in a hot and dry climate. The results revealed that H/W and street orientation highly affected the time and period of extreme heat stress, and PET distribution at street level. Charalampopoulos et al. (2013) conducted a series of field measurements at six areas with varied SVF values in Greece and found that low SVF values and dense green coverage could improve outdoor thermal conditions. Furthermore, a decrease in SVF can result in a decrease in T_{mrt} , thereby enhancing outdoor thermal conditions, as demonstrated by a field measurement study (Tan et al., 2013) and a simulation study (Wang et al., 2016). Abd Elraouf et al. (2022) investigated the different urban geometry impacts on outdoor thermal comfort in hot-humid conditions by ENVI-met software, and they found that H/W has the highest effectiveness on outdoor thermal comfort, followed by street orientation and building typology.

Street ventilation is also an important factor enhancing outdoor thermal environments (Lai et al., 2019). The direction of wind flow among urban canyons significantly affects the wind field at the pedestrian level. Hegazy et al. (2020) used ENVI-met software to explore the effect of street orientation on outdoor thermal comfort. Air temperature, wind speed, relative humidity, and pedestrian thermal comfort were examined across different sites. The results indicated that thermal comfort indices reached the highest levels of discomfort at all sites. Miao et al. (2023)

assessed outdoor thermal conditions and air quality in an urban street canyon through field measurements. The findings indicated that the middle level of the street faces higher heat stress than the bottom or roof level. He et al. (2020) indicated that precinct morphological characteristics had a strong modification effect on precinct ventilation, thereby improving outdoor thermal comfort. Zhong et al. (2022) employed the CFD method to investigate the influences of a pocket park and vegetation on the wind flows. Results indicated that the pocket park could amplify the mean and the gust flows in the street under perpendicular inflow wind.

2.1.3.2 Green infrastructures and water bodies

Green infrastructure is effective in lowering urban temperature and improving pedestrians' thermal comfort (de Quadros & Mizgier, 2023). Zölch et al.(Zölch et al., 2019) evaluated typical greening designs of rectangular public squares and their microclimatic impacts during a hot summer day, under both daytime and nighttime conditions, using a validated ENVI-met model. The results showed that at 3 pm, the greening design with the most trees and trees placed in the sunlit areas of the squares had a good cooling effect. They suggested that planting more trees to maximize the shaded areas would efficiently enhance outdoor thermal conditions. Schibuola et al. (2022) used ENVI-met to conduct a seasonal assessment of outdoor thermal environments, comparing different urban forms and green wall designs. The results showed that green walls reached the best cooling performance among different urban forms. The use of vertical green walls can help enhance outdoor thermal conditions. Galagoda et al. (2018) investigated the performance of vertical greenery systems in tropical conditions. Thermal performance, relative humidity, and CO_2 concentration were quantified for different types of vertical green walls. The results showed that living walls have the maximum temperature control performance.

Urban water bodies are an important component of urban greenery and can have a positive impact on the urban microclimate (Teshnehdel et al., 2022). A field measurement was

conducted by Xu et al. (2010) to investigate the effect of urban artificial waterbodies on outdoor thermal comfort during summer. The results showed that the artificial waterbodies could effectively improve outdoor thermal comfort in the littoral zone, especially during high temperature hours of a hot summer day, and the area 10–20 m from the water's edge showed the greatest improvement in outdoor thermal conditions. Theeuwes et al. (2013) employed a Weather Research and Forecasting (WRF) model to explore the cooling effect of water bodies on outdoor thermal conditions, with varied surface water cover, its size, spatial configuration, and temperature. The results indicated that the cooling influence of urban water bodies nonlinearly depends on factors such as water surface, lake size, and prevailing wind directions. In addition, large lakes were found to have a significant temperature impact on the surrounding edge areas and downwind regions. Cheng et al. (2022) applied the ENVI-met model to simulate the impact of water bodies and village morphological elements on outdoor thermal conditions. The results indicated that the cooling effect of water bodies was better in the afternoon than in the morning, and it was significantly influenced by the distance to water bodies. The building density of the village had a negative correlation with temperature, humidity, and PET in the microclimate conditions. Yang et al. (2025) conducted a field study to investigate outdoor microclimate conditions and sanitation workers' thermal comfort in spaces near and farther away from the water bodies. They found that sanitation workers' thermal sensation was highly influenced by T_a, RH, and v in the space near water bodies.

2.1.3.3 Building forms

Building forms can be possible to improve thermal comfort in microclimate conditions (Taleghani et al., 2015). A CFD simulation study was conducted by Sun et al. (2023) to compare the impacts of different building forms, such as building shape, orientation, and location, on outdoor thermal space in a high-density urban area. They suggested that solar radiation should be considered more than wind speed in high-density urban areas, as the wind

speed distributions were relatively low and uniform. Gamero-Salinas et al. (2021) investigated the influence of building forms on 5 types of semi-outdoor spaces in Singapore, including perimeter buffers, sky terraces, horizontal breezeways, breezeway atria, and vertical breezeways. Findings showed that vertical breezeways and horizontal breezeways are the most thermally comfortable semi-outdoor spaces. Pouri et al. (2025) investigated the effects of building forms and layout on outdoor thermal comfort of 28 residential blocks in Tabriz using ENVI-met software. The results indicated that a combination of the two scattered and peripheral block shapes was the most efficient building form for enhancing outdoor thermal comfort.

Different building shapes and layouts would affect outdoor microclimate conditions. Lee et al. (2022) did a CFD simulation to investigate the effects of wind angles in wind velocity distributions in two building configurations, namely 'T' and '+' shaped. The results showed that when the wind is lateral, the downwind length decreased by 11.5% of the 'T' shape, compared with a decrease of 15.0% of the '+' shape. Li et al. (2024) analyzed the impact of twisted wind on human thermal comfort around two tandem buildings using wind tunnel tests. The findings indicated that twisted wind surrounding two tandem non-identical-height buildings would decrease thermal comfort during summer while enhancing the thermal environment in winter.

Underneath an elevated building (UEB) is an effective building design for amplifying the wind speed and decreasing solar radiation perceived by pedestrians (Xia et al., 2017). Niu et al. (2015) conducted continuous monitoring of pedestrian-level wind and thermal parameters at three campus sites during summer, including instantaneous air temperature, globe temperature, wind speed, and humidity. Using a new PET-based index, they found that wind speed and air temperature had a significant impact on thermal comfort. Furthermore, the open ground floor UEB provides wind amplification and shading effects that significantly improve outdoor

thermal conditions. Following that, Liu et al. (2016) combined the measured thermal parameters and simulated wind velocity by the CFD method to evaluate outdoor thermal comfort. It is shown that the elevated building design modified the mean flow pattern around a building, potentially improving pedestrians' thermal comfort. A study conducted by Huang et al. (2017) simultaneously monitored environmental parameters and collected human subject surveys in Hong Kong. Their investigations indicated that, on the one hand, the elevated buildings benefit the pedestrian-level microclimate conditions and improve thermal comfort. On the other hand, three models, including the PET, UTCI, and CBE models, were compared for outdoor thermal comfort prediction, and they indicated that models need to be refined to accurately predict outdoor thermal comfort. Du et al. (2017) proposed an integrated method, combining wind tunnel tests and on-site monitoring data to investigate outdoor thermal environments around the lift-up building. The results showed that the lift-up design can provide comfortable microclimate conditions in summer while not resulting in strong cold discomfort in winter. Followed by that, Xie et al. (Xie et al., 2018; Xie et al., 2019; Xie et al., 2020) and Li et al. (Li et al., 2018, 2020) did lots of field measurements in open spaces and UEB to quantify the effect of varied sun and solar conditions on outdoor thermal comfort.

2.1.3.4 Shading

Building and trees can both provide shading space, thereby reducing air temperature, mean radiant temperature, and enhancing outdoor thermal comfort (Lin et al., 2010). Shading could be an effective cooling strategy since it can directly decrease the solar radiation perceived by pedestrians. A field measurement (Watanabe et al., 2014) analyzed different shading strategies (sunlight, building shade, and pergola shade) on improving outdoor thermal conditions. They found that under direct sunlight with total solar radiation of 800 W/m^2, building shade and pergola shade with plants created significantly cooler thermal environments than sunlight conditions. Abdallah et al. (2020) investigated the performance of two shading methods

(shaded with trees and artificial shading devices) on enhancing thermal environments in open spaces. They indicated that increasing greenery and tree density is beneficial to reduce heat stress and improve thermal comfort in outdoor open spaces. Mahmoud et al. (2022) compared the effect of different shading strategies (shading with different heights, vegetation, and hybrid) to enhance outdoor thermal comfort using the ENVI-met model in school courtyards. It is found that applying hybrid orthogonal and diagonal staggered tree shading in wide street canyons, significant reductions in PET values were achieved, reaching 18.5°C and 18.6°C, respectively.

2.1.3.5 Active cooling devices

Active cooling devices could be the most direct method to alleviate human discomfort outdoors, such as mist spraying, radiant panels, and evaporative fans.

Mist spraying systems can reduce air temperature, enhance evaporation, and lower skin temperature, thereby alleviating human thermal discomfort (Oh et al., 2019). Oh et al. (2020a) compared four modes of a mist spraying system with various amounts of water spraying, both in the absence and presence of an air blowing control. The results showed that air temperature in the mist-spraying environment decreased by -2.9 ± 1.2 °C when a larger amount of spraying water was used and decreased further by -3.6 ± 1.4 °C with the addition of an air-blowing fan. Su et al. (2022) investigated the effects of mist spraying with different nozzle densities (4, 6, and 8 nozzles) and height (2.3, 2.7, and 3.1 m) using environmental variables measured at 1.1 m above the ground, skin temperatures, and subjective surveys. The results indicated that when the nozzle number increased from 4 to 8, the effect of humidification increased from 2.60-7.03%, and the effect of reducing T_{mrt} enhanced from 9.77-31.53 °C. Subjects' thermal sensation decreased when the nozzle number was from 4 to 8 and increased when the nozzle height was from 2.3 to 3.1 m. Overall, a larger nozzle number and lower height will enhance the performance of mist spraying. Li et al. (2022) investigated the effectiveness of the stress

relief strategies, including shade, mist spraying, and mixed shade and mist spraying, on pedestrians' thermal comfort. It is found that mist spraying had a larger cooling effect than shade, while the mixed shade and mist spraying strategy provided a larger thermal comfort range. The mixed shade and mist spraying strategy reached the largest cooling effect in mean skin temperature. Another study (Y. Zhao et al., 2024) was conducted to compare the combined effect of sun sails with different coverage and mist spraying with different nozzle arrangements in a kindergarten using ENVI-met. They found that the combination of shade and mist is the most effective strategy, reducing PET by up to 14.43 °C.

Outdoor evaporative fans are found to be able to bring the UTCI down from very strong heat stress to between neutral to moderate heat stress range (Dhariwal et al., 2019). Sudprasert et al. (2021) investigated the effectiveness of evaporative air coolers for indoor use in Thailand's tropical climate and explored the variables influencing their performance. They found that the evaporative air coolers could achieve a −0.6 (slightly cool) thermal sensation. Altaf et al. (2020) investigated the performance of evaporative coolers in an open area at Thammasat University by measuring the air temperature and humidity with and without the use of evaporative coolers. Another study (Farnham et al., 2015) also explored the performance of combining a mist spraying with a fan to cool outdoor spaces, with 141 subjects participating on hot summer days. It is found that the cooling effect of the mist and fan combination is highly efficient, often exceeding the thermal load of pedestrians and resulting in a nearly immediate reduction in skin temperature.

Advanced technologies in Membrane-Assisted Radiant Cooling (MARC) (Zhong et al., 2021; Dharmasastha et al., 2023) gave us more possibilities to solve convection and condensation issues and apply them outdoors, thereby achieving direct and efficient cooling for the human body and enhancing pedestrians' thermal discomfort. Liang et al. (2024) investigated a prototype system consisting of two wall panels and one ceiling panel with a water chiller

system. Three different radiant panel surface temperatures were tested by measuring condensation and heat flux, as well as a thermal comfort survey. They found that when ambient UTCI is high, about 38.1 °C, the surface temperature of the radiant panel needs to be reduced to 14.3 °C to achieve a neutral thermal sensation. Subsequently, Yang et al. (2024) conducted a comprehensive thermal comfort survey to investigate actual human responses under membrane-assisted radiant panels. The results indicated that the asymmetric radiant cooling condition created by the membrane-assisted radiant panels can help alleviate pedestrians' thermal sensation to the neutral zone.

Many studies have focused on exploring the effectiveness of different strategies to alleviate outdoor thermal discomfort. Among them, active cooling devices would be the most effective strategies to enhance outdoor thermal comfort, especially under high heat stress conditions in the context of climate change. However, the investigation of these active cooling strategies is not enough, and the performance of different devices in improving human thermal comfort needs to be quantified. In addition, to better quantifying the performance of various cooling strategies on improving human thermal comfort, an outdoor thermal comfort model is needed to evaluate human thermal sensations under diverse outdoor conditions.

2.2Dynamic outdoor thermal comfort research

2.2.1 Dynamic features

There are differences in thermal environments between indoors and outdoors in terms of physical, physiological, and psychological aspects (Nikolopoulou et al., 2001; Höppe, 2002). Firstly, there is a natural physical difference between the indoor and outdoor thermal environments, specifically in terms of dynamic wind speed and solar radiation, which create transient and asymmetric thermal conditions outdoors.

Additionally, the predominant difference between indoor and outdoor is the time scales of thermal exposure (Höppe, 2002). A city dweller's exposure time to the same outdoor environment is typically within minutes, while it can be several hours in an indoor environment. This results in physiological parameters such as skin temperature and sweat rate fluctuating frequently to adapt to the changing thermal conditions outdoors, making it a different case from indoors.

As for the psychological aspect, thermal expectation and thermal experience highly affect outdoor thermal comfort due to the transient features outdoors. In heterogeneous outdoor scenarios, neutral temperatures for indoor settings may still be perceived as comfortable for pedestrians, but it is almost impossible to create stable thermal conditions in outdoor microclimates due to transient and dynamic characteristics. Moreover, the energy costs of maintaining a neutral thermal environment in urban settings can be prohibitively high. This encourages us to think from a different angle and take advantage of these dynamic thermal features outdoors to create comfortable thermal perceptions.

2.2.2 Real-life outdoor thermal environments

Due to the inherent dynamic characteristics in outdoor conditions, many researchers have focused on investigating human responses in real-life outdoor environments. Among four different environmental parameters, including air temperature, radiation, wind, and humidity, air temperature has been found to have the strongest association with outdoor thermal sensation (Lai, Guo, et al., 2014; Tsitoura et al., 2014). Lai et al. (2014) conducted a field study measuring the environmental parameters and subjective votes of residents in an urban residential community in central China. The study aimed to explore outdoor thermal comfort and space usage of residents. The results showed that thermal comfort is the most important factor influencing the quality of outdoor spaces, and other influencing factors include air quality,

acoustic environment, functionality, and convenience. Huang et al. (2016) conducted an on-site measurement to assess thermal conditions and attendance in a playground with shading shelters and vegetation, and they found that attendance is highly affected by the outdoor thermal environment during a period of time.

Although air temperature plays an important role in affecting outdoor thermal comfort, it is difficult to change the air temperature conditions in urban outdoor spaces (Lai et al., 2020). Niu et al. (2015) pointed out that wind speed and solar radiation have a significant impact on thermal conditions among varying open spaces.

Recent studies have focused on investigating the impact of varying wind and radiation conditions on thermal comfort in real-life outdoor environments. Lai et al. (2017a) investigated dynamic features of outdoor thermal environments under cold, mild, and hot climatic conditions in real outdoor environments. They pointed out that wind and radiation conditions changed rapidly in outdoor thermal environments, and that fluctuations in wind speed and solar radiation led to corresponding changes in convective and radiative thermal loads on the human body. Li et al. (2018) conducted field measurements in Hong Kong to investigate subjects' thermal sensation and desirability of sun and wind conditions. They indicated that the desirability of sun and wind conditions of subjects determines their thermal sensation in response to the UTCI index. Xie et al. (2019) did a comprehensive field measurement about outdoor thermal comfort in Hong Kong, and collected 1600 human subject responses as well as the concurrent meteorological parameters. The results indicated that wind and solar radiation had an interaction effect with air temperature in affecting thermal sensation and thermal comfort. In addition, in summer, wind could offset the negative impact of solar radiation when the air temperature was lower than 31 °C. A subsequent field measurement (Li et al., 2020) investigated the applicability of UTCI in varied sun and wind conditions. It is found that UTCI underestimated the effects of wind and mean radiant temperature at high air temperatures but

overestimated the effects of air temperature and relative humidity on thermal sensations. Thereby, a combined sun and wind condition index (SWI) was proposed to quantify the impacts of wind speed and mean radiant temperature on thermal comfort.

2.2.3 Transient outdoor thermal environments

Pedestrians often experience transient thermal conditions when moving between different scenarios. These transitions are worth exploring, as they can lead to significant and dynamic changes in thermal status. Some studies are dedicated to creating step-change conditions to simulate pedestrians' or commuters' thermal experience, while others focus on real walking routes to evaluate pedestrians' walking experience.

2.2.3.1 Step-change conditions

Step-change conditions frequently occur when people transition from different scenarios, such as moving from indoors to outdoors, and transition between shading and sunlit areas.

Investigating transient thermal environments resulting from indoor and outdoor conditions is important for accurately simulating the thermal experiences of commuters. Huang et al. (2020) assessed subjects' short-term thermal perceptions transitioned from an air-conditioned indoor space to a 'lift-up' outdoor condition. Subjects were asked to stay indoors for 10 minutes, then transition to a 10-minute exposure in a lift-up shaded area, followed by another 10-minute indoor stay and a final 10-minute exposure in a sunlit area. The results indicated that adopting the lift-up design significantly increased the likelihood of occupants feeling comfortable during the transition from an indoor air-conditioned space to outdoors.

Some studies focus on the transient thermal environment induced by the transition between shaded and sunlit areas. Xu et al. (2022) conducted a field experiment under transient outdoor conditions, where subjects were first exposed to direct sunlight for 20 min, and then moved to different shading areas for 45 min. This study developed a thermal sensation prediction model

for dynamic thermal status. Liu et al. (2021) designed a field experiment that created transient and dynamic thermal environments to explore the thermal alliesthesia effect. Subjects moved between direct sunlight exposure and shade conditions every 5 minutes, and then experienced artificial local thermal stimulation for 10 min, including a cooling or heating panel applied to their distal limbs, and followed by a convective heating or cooling fan in front of their legs or faces. The results revealed that larger thermal sensation changes would easily induce strong thermal pleasant feelings, and they developed a quantified thermal alliesthesia framework. Li et al. (2022) tested 48 subjects' thermal perceptions when they were exposed alternately to direct sunlight and shade at varying frequencies. Results showed that subjective thermal perceptions changed with alternating exposure to sunlight and shade at different frequencies. Higher alternating frequency could reduce thermal dissatisfaction in hot conditions and lower comfort requirements for shade.

2.2.3.2 Thermal walk scenarios

Since walking is a frequent activity outdoors, investigating thermal comfort under walking conditions is essential for understanding real-life thermal experiences and for improving the design of outdoor spaces. An increasing number of studies are focusing on pedestrians' thermal responses during walking activities.

Lau et al. (2019) investigated pedestrians' thermal sensation changes throughout the walking route and how the micro-meteorological conditions and urban geometry affect their thermal sensations. They found that large variations in micro-meteorological conditions throughout the walking route were highly affected by the urban geometry. Furthermore, the autocorrelation analysis showed that thermal sensation was highly associated with pedestrians' short-term thermal experience of about 2-3 min. Vasilikou et al. (2020) investigated thermal perception variations for pedestrians moving between interconnected spaces during walking. The findings

indicated that the sequence of space did not significantly affect microclimate conditions, but it highly affected dynamic thermal perceptions of pedestrians. Kim et al. (2022) conducted a field experiment in urban street canyons, measured microclimate conditions, and collected pedestrians' thermal behaviors. The results indicated that pedestrians tended to choose walking, sitting, or standing in the shaded area on the sidewalk. Xie et al. (2022) investigated pedestrians' thermal perceptions for urban walking spaces in Beijing during both summer and spring. The microclimate conditions were measured, and the subjective surveys of 62 subjects were collected. They found that the current thermal response was mostly affected by the short-term history of the past 20-35s. The sequential order of thermal exposure also affected pedestrians' thermal perceptions while walking. Specifically, experiencing a worse thermal environment before and an improved thermal environment after, the pedestrians' thermal perceptions will be improved than experiencing thermal environments in reverse. Li et al. (2024) conducted a 'stop-and-go' experiment to explore the subjective thermal responses during autumnal greenway walking. They found that walking status, environmental characteristics, and emotions affected pedestrians' thermal comfort. During autumnal walking, pedestrians preferred a slightly warmer thermal sensation and were sensitive to thermal stimuli.

2.2.4 Dynamic thermo-physiological responses

Dynamic environmental variations will cause dynamic variations in physiological parameters. Human physiological responses directly connect to their subjective thermal responses (Lai et al., 2020). Thermoreceptors in skin can detect temperature and send signals to the brain, which interprets the signals as thermal sensation (Zhang et al., 2010c). Physiological parameters, such as skin temperature, sweat rate, skin wettedness, heart rate, and core temperature, play important roles in regulating the heat balance of the human body.

Many researchers have explored the human dynamic physiological responses in outdoor thermal environments. Nakayoshi et al. (2015) used a wearable measurement system to measure human thermal physiological responses, including skin temperature and pulse rate, through a pathway. It is found that the skin temperature of the higher-sweating group was lower than that of the lower-sweating group, indicating thermoregulation differences among individuals. Li et al. (2023) investigated 70 human subjects' skin temperature, sweating, heart rate, as well as their subjective thermal perceptions in two complex urban continuums. The physiological response and human body heat exchange with the external environment were studied. The results indicated that when the air temperature was higher than 28 °C, 36% of the produced heat would be accumulated within the human body. Sweating rate was highly related to the environmental index, while mean skin temperature deviation from neutral skin temperature did not correlate well with the environmental index.

Furthermore, researchers have started to make connections between physiological responses and subjective responses, trying to give more reliable and foundational explanations of subjective thermal perceptions. Lai et al. (2017a) analyzed the correlations between mean skin temperature and thermal sensation, which is 0.72, and found that the correlation was weaker under hot conditions due to the phenomenon of alliesthesia. Lai et al. (2017b) further monitored environmental parameters, subjects' skin temperature, and their subjective thermal responses in real outdoor thermal conditions, and they developed a dynamic thermal comfort model. They utilized the thermal load to represent the overall outdoor thermal environment, while mean skin temperature and its change rate were used to represent dynamic thermal status. Xu et al. (2022) analyzed the correlations between local skin temperatures and thermal sensation, and built a dynamic thermal sensation prediction model for outdoor use. Their model used forearm temperature and its change rate as independent variables for the overall thermal sensation prediction.

Overall, the dynamic and transient nature of outdoor thermal environments highly affects human thermal perception, leading to fluctuating sensations that differ fundamentally from those experienced in indoor conditions. Dynamic microclimate conditions will lead to dynamic physiological responses (e.g., vasodilation, sweating, skin and core temperature variation). These physiological responses need further investigation, as they are closely linked to human thermal perception. Serving as a bridge between environmental stimuli and subjective thermal sensation, physiological responses play a crucial role in understanding outdoor thermal comfort.

2.3 Mainstream thermal indices

Thermal indices are useful tools for quantitatively assessing thermal environments and enhancing thermal comfort levels. These indices incorporate multiple environmental parameters or physiological parameters to provide a comprehensive and numerical evaluation of thermal stress or comfort.

2.3.1 Mainstream thermal indices applied outdoors

Potchter et al. (2018) summarized 110 peer-reviewed articles during 2001-2017 and found that the most commonly used models were the PET, PMV, UTCI, and SET*. Table 2.3 summarizes the differences between these models. Mainstream outdoor thermal comfort models can be classified into three categories, energy balance model, empirical model, and thermal physiology-based empirical model.

Energy balance models, including the Physiological Equivalent Temperature (PET) (Peter Höppe, 1999), Predicted Mean Vote (PMV) (Fanger, 1970), Standard Effective Temperature (SET*) (Gagge et al., 1986), Outdoor Standard Effective Temperature (OUT_SET*) (Pickup & de Dear, 2000), and COMFA (Kenny et al., 2009b, 2009a), which lie in the heat exchange between the human body and the external thermal environment. These thermal models have

theoretical significance and are easy to understand. Nevertheless, since they are developed under steady-state conditions, most of these models exhibit low accuracy when applied to dynamic outdoor environments (Lai et al., 2017b). Additionally, since the equivalent temperature cannot directly correspond to thermal sensation, researchers need to conduct subject tests to find the empirical relationship between thermal sensation and equivalent temperature (Lai et al., 2020).

The empirical model, such as the Actual Sensation Vote (ASV) (Nikolopoulou et al., 2003), Thermal Sensation (TS) (Givoni et al., 2006), Cheng et al. (2012), and the Mediterranean Outdoor Comfort Index (MOCI) (Salata et al., 2016a), are developed based on field measurement. The inputs are the environmental parameters, and the output will be the thermal sensation. However, the empirical model is not developed based on physical principles and is constrained to specific climate zones.

The thermal physiology-based empirical model, including the CBE model (Zhang et al., 2010b, 2010a, 2010c), UTCI (Fiala et al., 2011), and Dynamic Mean thermal sensation Vote (DMV) (Vellei, 2024), which can be incorporated with advanced thermoregulation models (e.g., the Huizenga model (Huizenga et al., 2001), UTCI-Fiala model (Fiala et al., 2011), and JOS-3 model (Takahashi et al., 2021)), providing enhanced reliability compared with empirical models. These models are capable of outputting thermal sensation results based on environmental conditions. Based on the number of nodes used in the physiological models, the above energy balance models can be further divided into different categories. In theory, multi-node models are better suited to transient and asymmetric thermal environments. Nevertheless, wind speed, solar radiation, and overall outdoor thermal environment are more dynamic and asymmetric compared with indoor settings (Nikolopoulou & Steemers, 2003). The availability of existing models, which are built on indoor chamber data, has been found questionable (Lai et al., 2020).

Table 2.3 Summary of mainstream thermal indices applied to the outdoors.

	Energy balance model				Empirical model		Thermal phyiology-based model	
Criteria	**PET**	**SET***	**PMV**	**COMFA**	**ASV**	**TS**	**CBE**	**UTCI**
Model	Two-node model	Two-node model	One-node model	One-node model	Linear regression	Linear regression	Multi-node model	Multi-node model
Heat transfer condition	Steady state	Steady state	Steady state	Steady state	-	-	Steady, asymmetric, and transient state	Dynamic and transient state
Output	T(equivalent)	T(equivalent)	Thermal load, TSV	Thermal load, TSV	TSV	TSV	Overall and local TSV and TCV	T(equivalent)
Intended for	Indoor and outdoor	Indoor and outdoor	Indoor	Outdoor	Outdoor	Outdoor	Non-uniform and transient environments	Outdoor
Limitations	1. Insensitive to the change in humidity and clothing 2. Based on indoor data	1. Limited accuracy of convective and radiant exchange 2. Based on indoor data	1. Not suitable for transient conditions 2. Based on indoor data	Based on indoor data	1. Limited application for other climates		Based on indoor data	1. Based on indoor data 2. Physiological responses from simulation results

2.3.2 Application of mainstream thermal indices to outdoors

Many studies have explored the applicability of these thermal indices for outdoor use. Huang et al. (2017) compared three outdoor thermal comfort models, including the PET, UTCI, and CBE models, for thermal environment assessment in UEB areas and open areas. The results indicated that the three models exhibited satisfactory results with the subjects' mean thermal sensation votes. They further divided the data into two sets: data from UEB areas and from

open areas. For the three indices, deviations were observed in both regression lines representing data from UEB and open areas, as shown in Figure 2.2. Open areas illustrated higher slope values compared with those in UEB areas. In addition, shifts in neutral indices (6.2 K, 5.8 K, and 1.1 for PET, UTCI, and the CBE model, respectively) were observed between UEB areas and open areas, indicating that the impacts of wind and solar on thermal comfort have not been accurately quantified in these indices. Model refinement would be needed to provide more accurate thermal sensation perceptions for outdoor use.

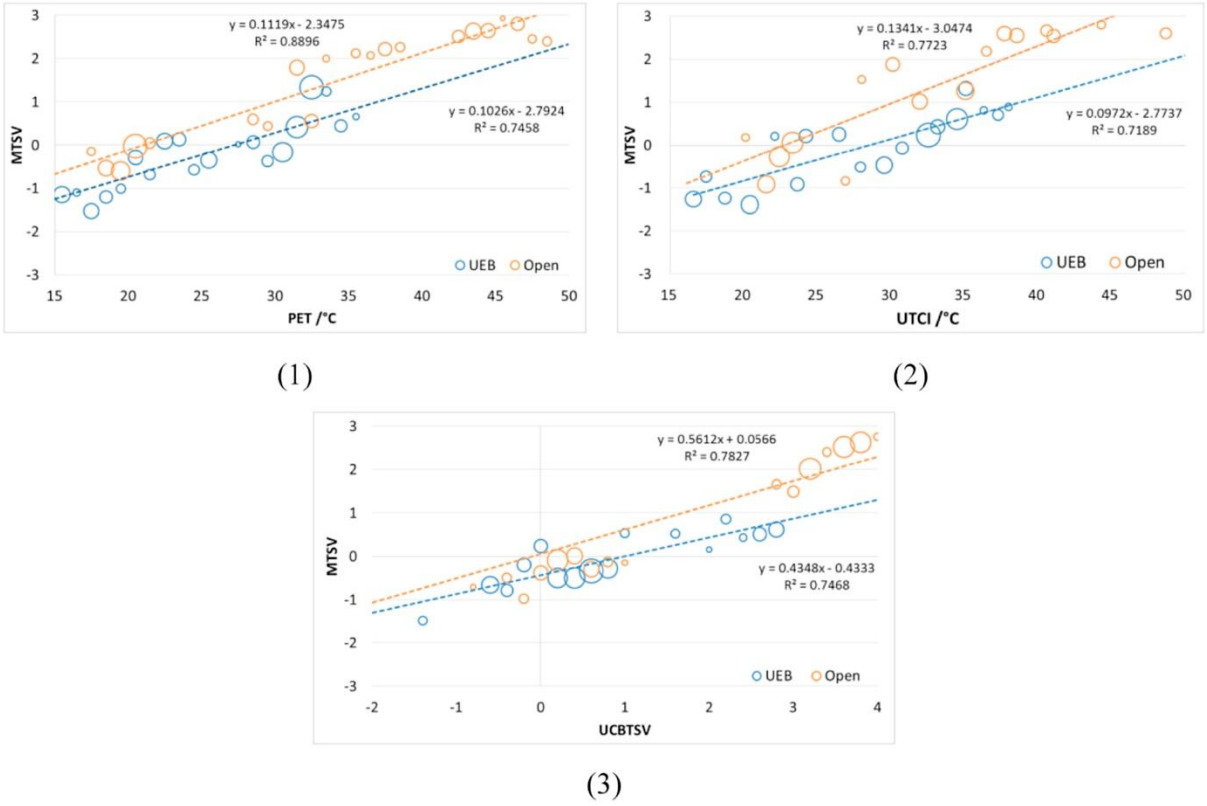

Figure 2.2 Relationship between different thermal indices and mean thermal sensation vote (MTSV) in UEB and open areas. (a). PET; (b). UTCI; (c). CBE model. Reproduced from Huang et al. (Huang et al., 2017).

Li et al. (2020) further conducted a series of field measurements in Hong Kong, collected meteorological parameters and questionnaire surveys, to explore the applicability of UTCI for outdoor thermal comfort assessment at varying sun and wind conditions. They employed multiple linear regression to analyze the correlations between UTCI, survey TSV with different environmental parameters at different temperature groups, including air temperature lower than 20 °C, between 20 °C and 30°C, and higher than 30 °C. Through the analysis of R^2 values, they indicated that at higher air temperature, the effects of T_{mrt} and v on TSV were more significant than those predicted by UTCI. In other words, UTCI may underestimate the effects of T_{mrt} and v on thermal sensation under high air temperature conditions.

Xi et al. (2012) conducted a field study to investigate the impacts of different design elements (e.g., pilotis, squares, and teaching building blocks) on outdoor thermal environments. They utilized SET* to evaluate outdoor thermal environment conditions of urban areas during summer. They found neutral SET* of young students in subtropical urban areas was about 24 ° C in summer. SET* and TSV did not show high correlations, but T_{mrt} exhibited high correlations with TSV, suggesting T_{mrt} plays an important role in subjective responses.

Fang et al. (2019) conducted a series of field measurements to comprehensively compare the differences among several outdoor thermal comfort indices, including PMV, Wet Bulb Globe Temperature (WBGT), PET, SET*, and UTCI, in subtropical climates. The relationship between different thermal indices and operative temperature is shown in Figure 2.3. WBGT, SET*, PET, T_{mrt}, T_{op}, and UTCI were calculated for the comparison with the surveyed TSV. All the thermal indices showed high linear relationships with operative temperature, with high R^2 values. T_{mrt} exhibited the highest slope compared with other indices. In outdoor conditions, although T_a is low, T_{mrt} is high due to the solar radiation.

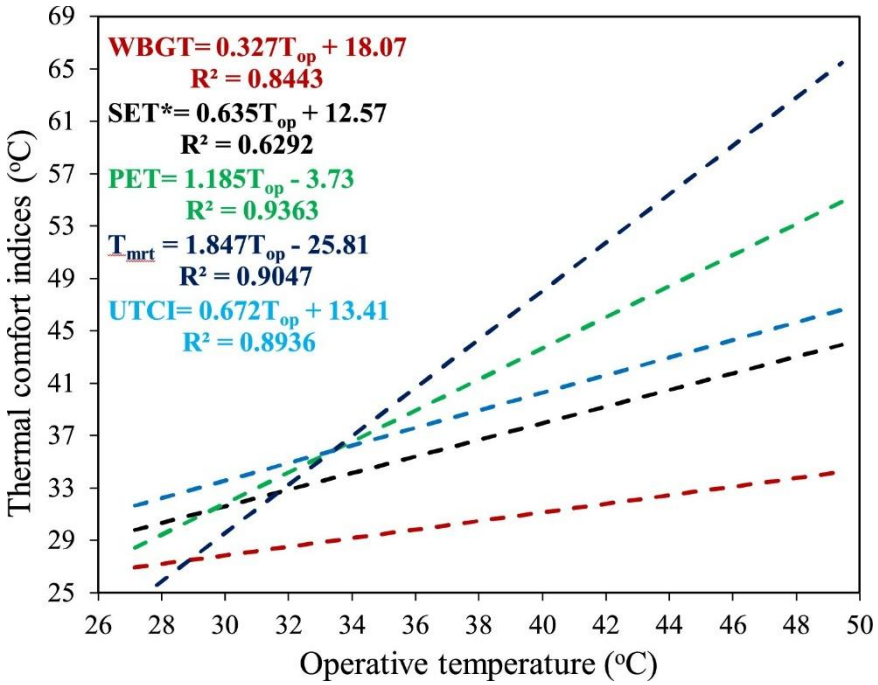

Figure 2.3 The relationship between different thermal indices and operative temperature. Reproduced from (Fang et al., 2019).

Figure 2.4 illustrates the relationship between different thermal indices and the surveyed mean thermal sensation vote (MTSV). The results indicated that when the thermal indices were lower than 38 °C, the thermal indices exhibited clear trends with MTSV. However, when the thermal indices were higher than 38 °C, MTSV showed a relatively constant value in the range of 3 and 3.5.

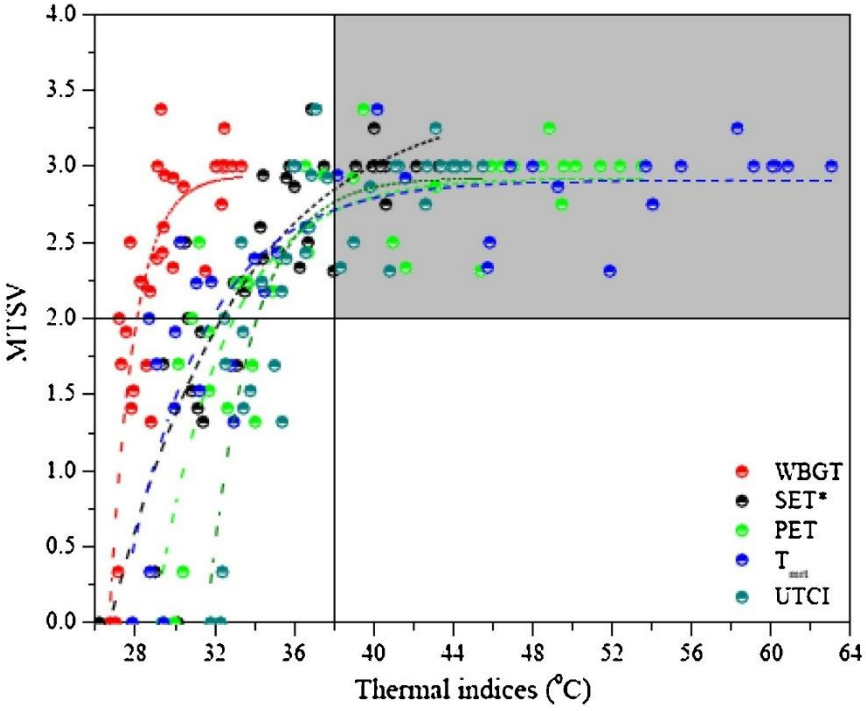

Figure 2.4 The relationship between different thermal indices and MTSV. Reproduced from (Fang et al., 2019).

The relationships of PMV, MTSV with the T_{op} are shown in Figure 2.5. A strong linear relationship was found between PMV and T_{op}. It is worth noting that when the T_{op} was higher than 34 °C, MTSV did not increase with the increased T_{op} or PMV, indicating that PMV overestimated the thermal sensation. The findings indicated that PMV may need to be modified when PMV is used to evaluate outdoor thermal conditions exceeding 34 °C.

The findings from this study suggested that the relationship between these thermal indices and the actual thermal sensation vote from subjects is unclear, especially when the operative temperature was above 34 °C. The reasons for the constant value of MTSV when in high thermal stress conditions may be due to the limited TSV scale. Thus, in this study, Fang et al. (2019) indicated that extended 7-point scales of TSV or other heat stress classification methods may need to be refined in future studies.

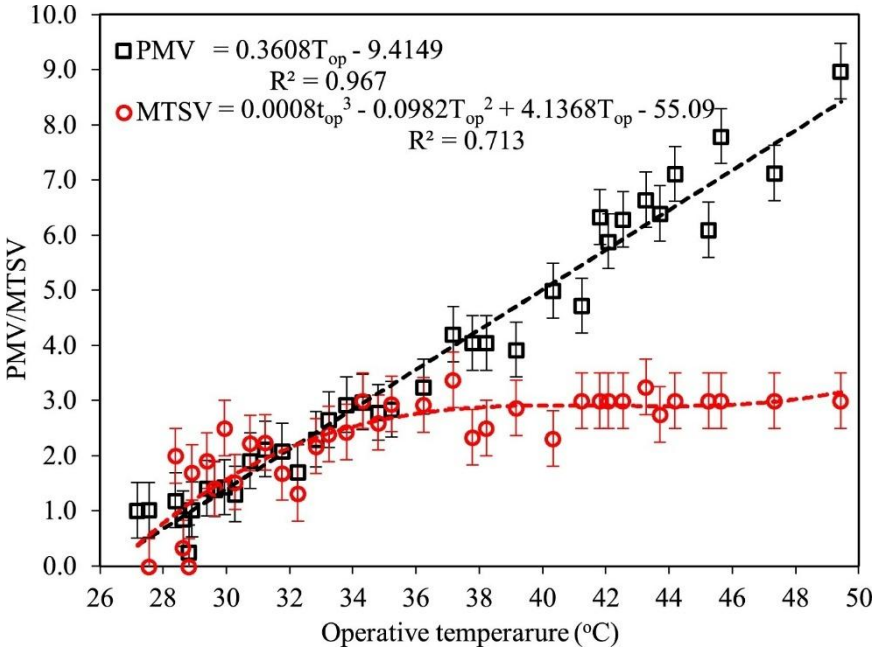

Figure 2.5 The relationship between PMV, MTSV versus operative temperature. Reproduced from (Fang et al., 2019).

Some studies have been dedicated to building the relationship between different thermal indices and TSV. Based on this relationship, thermal sensation can be directly predicted using thermal indices. Lin et al. (2011) obtained the relationship between SET* and MTSV in the hot and cool seasons, respectively, based on the field measurements collecting both subjective surveys and meteorological parameters in central Taiwan. A total of 1644 surveys were collected. Linear relationships were found between SET* and MTSV in both hot and cool seasons. Mahmoud et al. (2011) conducted field measurements in an urban park in Cairo, Egypt. They established relationships between PET and MTSV in different zones of the urban park, including the peak, entrance, spine, fountain, and lake areas. Linear regression was employed, and the regression functions varied across zones. This variation may suggest that PET may not adequately capture the influence of diverse environmental parameters on outdoor thermal comfort, as the relationship between PET and MTSV diverged under different outdoor

conditions. Lai et al. (2014) conducted a comprehensive field measurement in northern China, a cold climate zone. Microclimate conditions and subjective surveys were collected. Different thermal indices for outdoor thermal comfort assessment were compared, including PMV, PET, and UTCI. The results showed that PMV overestimated the outdoor thermal sensation, while UTCI exhibited a satisfactory prediction result.

Overall, the mainstream thermal indices have been widely used in outdoor thermal comfort assessment. However, since these indices were originally developed based on indoor conditions, discrepancies often arise between predicted and actual thermal sensations, thereby limiting their applicability in outdoor environments (Lai et al., 2020).

2.4Principles behind outdoor thermal indices

2.4.1 Physiological Equivalent Temperature (PET)

The Physiological Equivalent Temperature (PET) was developed based on the Munich Energy-balance Model for Individuals (MEMI) (Höppe, 1994), which is a thermo-physiological heat-balance model. PET (Peter Höppe, 1999) is defined as the air temperature in a typical indoor setting (without wind and solar radiation), where the heat budget of the human body has the same core temperature and skin temperature as under outdoor conditions.

The basis of MEMI was a heat-balance equation for the human body, as expressed in Eq. 2.1:

$$M + W + R + C + E_D + E_{Re} + E_{Sw} + S = 0 \quad (2.1)$$

where,

M is the metabolic rate, W/m^2;

W is the physical work output, W/m^2;

R is the net radiation of the body, W/m^2;

C is the convective heat transfer, W/m^2;

E_D is the latent heat transfer to evaporate water into vapor diffusing through the skin, W/m^2;

E_{Re} is the evaporative heat loss from respiration, W/m^2;

E_{Sw} is the evaporative heat loss from sweating, W/m^2;

S is the heat storage, W/m^2.

In order to solve the Eq. 2.1, the mean surface temperature of the clothing (T_{cl}), the mean skin temperature ($T_{sk,m}$) and the core temperature (T_c) need to be solved. Eq. 2.2 and Eq. 2.3 describes the heat transfer from body core to the skin surface (F_{CS}), and from the skin surface through clothing layer to the clothing surface (F_{SC}), respectively.

$$F_{CS} = v_b \times \rho_b \times c_b \times \left(T_c - T_{sk,m}\right) \tag{2.2}$$

$$F_{SC} = \left(\frac{1}{I_{cl}}\right) \times (T_{sk} - T_{cl}) \tag{2.3}$$

where v_b is the blood flow from the body core to the skin surface, $l/(s \cdot m^2)$, ρ_b is the blood density, kg/l, and c_b for the specific heat, $W \cdot s/(K \cdot kg)$, I_{cl} is the heat resistance of the clothing, $K \cdot m^2/kg$.

From Eqs. 2.1-2.3, the individual heat balancing for any given climatic parameters, activity, and clothing, could be characterized by heat flows and physiological parameters (e.g., body temperatures and sweat rate). A heat balance sample of the MEMI model under warm and sunny condition is shown in Figure 2.6.

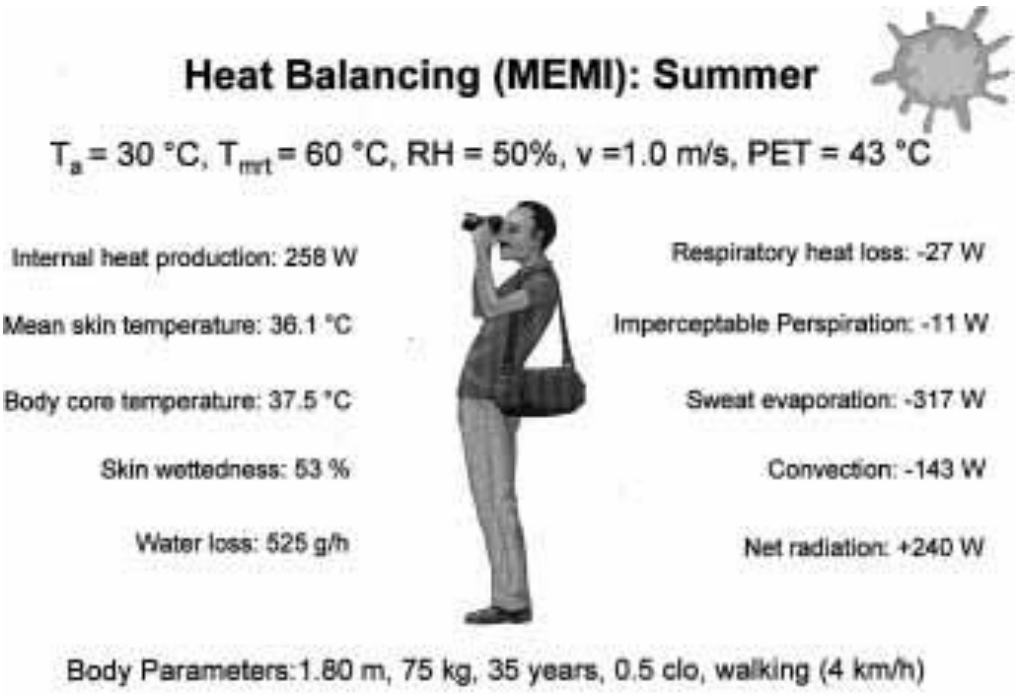

Figure 2.6 Heat-balance calculation sample of MEMI model for warm and sunny condition, reproduced from (Peter Höppe, 1999).

PET is defined as the equivalent air temperature to a typical indoor setting, in which the human body has the same core temperature and skin temperature as under other complex thermal conditions. The assumptions of the indoor setting are as below:

Mean radiant temperature equals air temperature; Air velocity is 0.1 m/s; Water vapor pressure is 12 hPa (approximately equivalent to a relative humidity of 50% at T_a=20°C) (Peter Höppe, 1999).

The PET calculating procedures include two steps: first, calculating the thermal condition with MEMI for a given meteorological condition. Then, inserting the mean skin temperatures and core temperature into the MEMI model and solving the air temperature value from Eqs. 2.1-2.3, the result is PET value.

The limitation of this model is that PET was based on the two-node model, involving core and skin, assuming that the skin temperature is distributed evenly over the whole-body surface. The

model assumes reaching a steady condition with any given meteorological conditions, which makes it more suitable for assessing stable and steady thermal conditions. Also, previous research indicated that PET is not sensitive to clothing and humidity (Fang et al., 2018).

2.4.2 Standard Effective Temperature (SET*)

SET was developed based on the Effective Temperature (ET*) (Gagge et al., 1972), combining temperature and humidity into a single index. The ET* is the temperature at 50% with the same heat loss from the skin as for the actual thermal environment (ASHRAE, 2021), as present in Eq. 2.4:

$$ET^* = t_o + wi_m LR\left(p_a - 0.5p_{ET*,s}\right) \tag{2.4}$$

where t_o is the operative temperature, °C;

p_a is the vapor pressure at a point of air temperature, kPa;

$p_{ET*,s}$ is saturated vapor pressure, kPa;

w is skin wettedness, dimensionless;

i_m is total vapor permeation efficiency: the ratio of actual evaporative heat flow capability between skin and environment to sensible heat flow capability as compared to Lewis ratio.

LR is the Lewis ratio and, at typical indoor conditions, equals approximately 16.5 K/kPa.

h_e , h_c : the evaporative heat transfer coefficient and convective heat transfer coefficient, W/(m^2·kPa).

ET* is not a universal index since it depends on clothing and activity. Standard Effective Temperature (SET*) (Gagge et al., 1986) was defined as the equivalent air temperature in an isothermal indoor environment at 50% relative humidity, where the subject wears standard clothing for the concerned activity, and has the same heat stress and physiological parameters

(i.e., skin temperature and skin wettedness) as in the actual thermal environment (ASHRAE, 2021).

The thermoregulation model of SET* is a two-node model, treating the core and skin of the human body into two concentric shells (Gagge et al., 1972). The skin is represented by a thin shell with mass, while the interior of the body is represented by a central core with mass (Gagge et al., 1972), as shown in Figure 2.7. The limitation of this model is that SET* was based on the two-node model, which is not suitable for non-uniform thermal environments. On the other hand, this model was also developed based on indoor data, which may not be suitable for outdoor use.

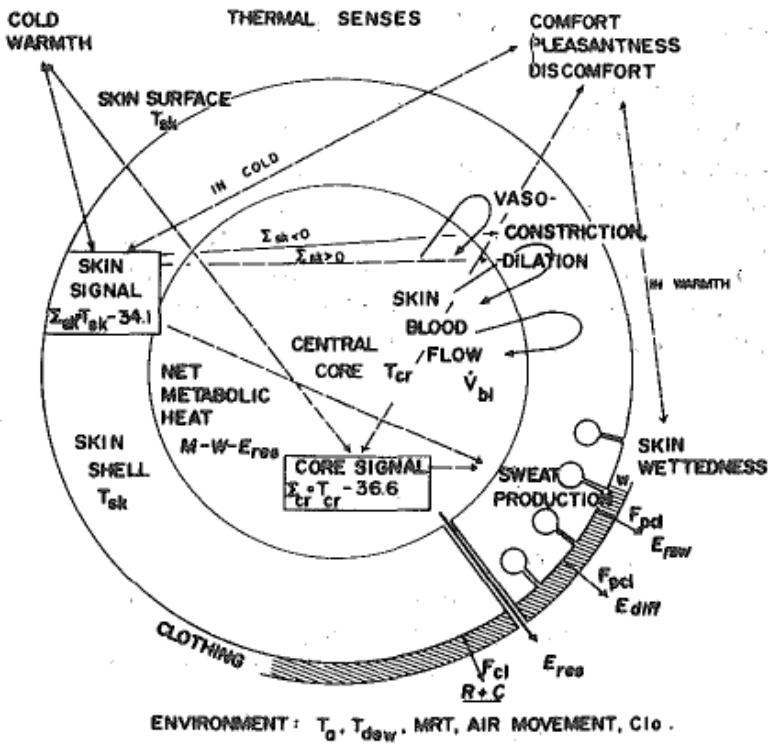

Figure 2.7 A concentric shell model of man of SET*, reproduced from (Gagge et al., 1972).

2.4.3 Universal Thermal Climate Index (UTCI)

With the development of the thermoregulation model, multi-node models were built up for the thermal physiology prediction for an extent environmental conditions, such as the Stolwijk 25-node model (Stolwijk, 1971), the Tanabe 65-node model (Tanabe et al., 2002) and JOS-3 model (Takahashi et al., 2021), and the Huizenga model (Huizenga et al., 2001). The multi-node model divides the human body into multiple segments, each consisting of four layers, including core, muscle, fat, and skin. The basis of the UTCI index (Fiala et al., 2003) is the UTCI-Fiala multi-node thermoregulation model (Fiala et al., 2011). The UTCI-Fiala model consists of 12 body segments, including head, face, neck, shoulders, thorax, abdomen, upper and lower arms, hands, upper and lower legs, and feet, as shown in Figure 2.8. Each segment consists of five layers, outer skin, inner skin, fat, muscle, and core. There are a total of 63 spatial sectors in the UTCI-Fiala model. The outer and inner skin can simulate the diffusion of heat transfer via the skin barriers. Since the heat transfer is calculated by separate body segments, the clothing insulation could be accurately considered.

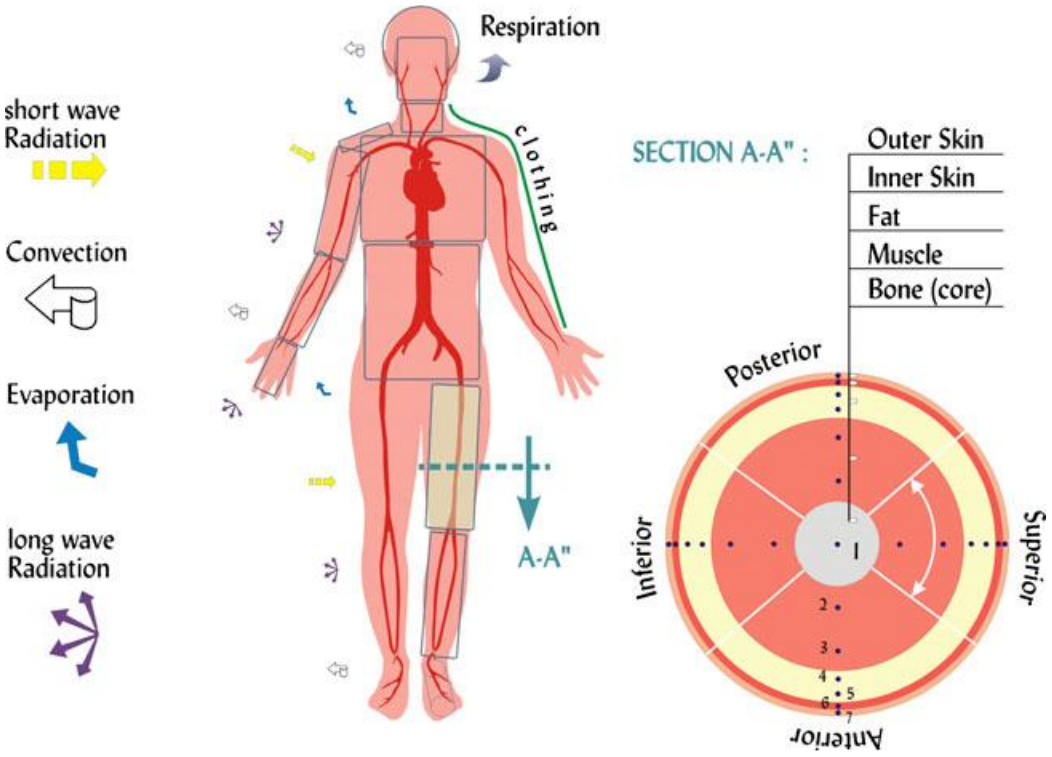

Figure 2.8 The concept of UTCI-Fiala model.

The Bio-Heat Transfer Equation of Pennes (Pennes, 1948) for polar and spherical coordinates was used for dynamic heat and mass transfer calculation, as present in Eq. 2.5:

$$\rho c \frac{\partial T}{\partial t} = k\left(\frac{\partial^2 T}{\partial r^2} + \frac{\omega}{r}\frac{\partial T}{\partial r}\right) + \rho_{bl} w_{bl} c_{bl}(T_{bla} - T) + q_m \quad (2.5)$$

where ρ: the tissue density, kg/m^3;

c: heat capacitance, $J/kg \cdot K$;

T: tissue temperature, °C;

t: time, s;

k, heat conductivity, $W/m \cdot K$;

r: radius, m;

ω: geometry factor, (ω=1 for polar co-ordinates, ω=2 for spheres);

T_{bla}: arterial blood temperature, °C;

ρ_{bl}: density of blood, kg/m^3;

w_{bl}: blood perfusion rate, $m^3/(s \cdot m^3)$;

c_{bl}: heat capacitance of blood, $J/kg \cdot K$;

q_m: metabolism, W/m^3.

The UTCI-Fiala model could predict four essential thermoregulatory responses including vasoconstriction and dilatation of the blood flow, shivering, and sweating (Fiala et al., 2001). The diagram of the thermoregulatory system model is shown in Figure 2.9. The model also

provides thermal sensation responses from physiological states, called Dynamic Thermal Sensation (DTS) (Fiala et al., 2003), as shown in Eqs. 2.6 and 2.7. The predictor variables were the mean skin temperature and its change rate, and the head core temperature.

$$DTS = 3 \times \tanh\left(\alpha \Delta T_{\mathrm{sk},m} + g + \frac{0.11\frac{dT^{-}_{\mathrm{sk},m}}{dt} + 1.91e^{-0.681t} \times \frac{dT^{+}_{\mathrm{sk},m}}{dt_{\max}}}{1+g}\right) \quad (2.6)$$

$$g = 7.94 \times \exp\left(\frac{-0.902}{\Delta T_{hy} + 0.4} + \frac{7.612}{\Delta T_{\mathrm{sk},m} - 4}\right) \quad (2.7)$$

where α is 0.30/K and 1.08/K for $\Delta T_{\mathrm{sk},m} < 0$ and $\Delta T_{\mathrm{sk},m} > 0$, respectively;

$\frac{dT^{-}_{\mathrm{sk},m}}{dt} = 0$ for $\frac{dT_{sk,m}}{dt} > 0$;

$\frac{dT^{+}_{\mathrm{sk},m}}{dt_{\max}}$ is the maximum positive change rate of mean skin temperature with the t time since the occurrence of $\frac{dT^{+}_{\mathrm{sk},m}}{dt}$;

ΔT_{hy} and $\Delta T_{sk,m}$ is the change of head core temperature and mean skin temperature, °C.

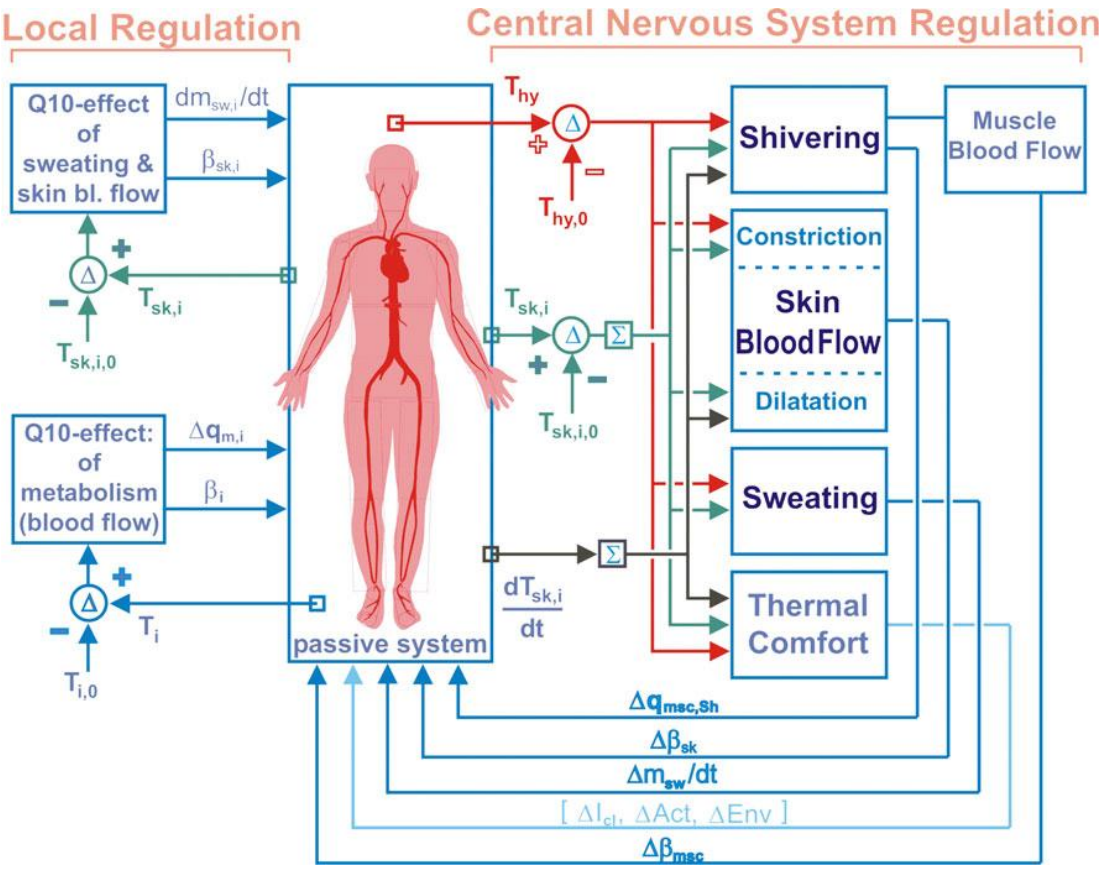

Figure 2.9 The diagram of the thermoregulatory system model of UTCI-Fiala, reproduced from (Fiala et al., 2001; Fiala et al., 2010).

The data covered 2000 subjects, a wide range of steady-state and transient thermal conditions, and activity levels for developing the DTS model. However, the data were derived from worldwide subject experiments in indoor chambers, and application in outdoor environments may be an issue to be explored.

2.4.4 The CBE model

The CBE model developed by UC Berkeley was based on the multi-node thermoregulation model, the Tanabe 65-node model (Tanabe et al., 2002), as well as the Stolwijk model (Stolwijk, 1971). Huizenga et al., (Huizenga et al., 2001) added a clothing layer into four body layers to accurately model both the heat and moisture capacitance and predicted human physiological

responses to complex thermal environments. Afterward, Zhang (Zhang, 2003) developed the thermal sensation and comfort model for predicting thermal sensation and thermal comfort based on human physiological parameters in transient and non-uniform thermal environments. Compared to the worldwide database of the UTCI model, the CBE model was developed based on their indoor experimental data. The clear logic and specific coefficients in this model development process will provide convenience and possibility for further development of outdoor models.

Up to now, multi-node thermoregulation models are well-developed for the prediction of physiological parameters based on the given environmental conditions, such as the JOS-3 model (Takahashi et al., 2021), which is an updated version of the Tanabe 65-node model. However, the relationship between physiological parameters and thermal perceptions still needs to be explored. The CBE model (Zhang, 2003) conducted human subject experiments in indoor chambers, involving steady, transient, and non-uniform thermal environments, collecting physiological parameters and subjective responses. The model was validated by passengers in automobiles in a wind tunnel. The experiment setting for non-uniform environments used ventilated air sleeves that covered specific body segments to decrease or increase the skin temperature of that body segment. As for the transient experiment setting, the subjects were asked to transfer from one climate chamber to another chamber, creating a step-change temperature. The CBE model provides the prediction of local TSV and TCV, and the overall TSV and TCV.

The transient local sensation model includes the static part and dynamic part (Zhang et al., 2010c), as shown in Eq. 2.8. The predictor variables (Eq. 2.9) are the local skin temperature ($T_{\mathrm{sk},i}$) and its change rate ($\frac{dT_{\mathrm{sk},i}}{dt}$), mean skin temperature ($\bar{T}_{\mathrm{sk}}$), and the change rate of core

temperature ($\frac{dT_{\text{core}}}{dt}$). The static part can be calculated by Eq. 2.10, while the dynamic part can be calculated by Eq. 2.11.

$$\text{Local Sensation} = \text{Sensation}_{\text{static}} + \text{Sensation}_{\text{dynamic}} \tag{2.8}$$

$$\text{Local Sensation} = f\left(T_{\text{sk},i}, \frac{dT_{\text{sk},i}}{dt}, \bar{T}_{\text{sk}}, \frac{dT_{\text{core}}}{dt}\right) \tag{2.9}$$

$$\text{Local Sensation}_{\text{static}} = 4\left(\frac{2}{1+e^{-C1(T_{\text{sk},i}-T_{\text{sk},i,set})-K1[(T_{\text{sk},i}-T_{\text{sk},i,\text{set}})-(\bar{T}_{\text{sk}}-\bar{T}_{\text{sk,set}})]}}-1\right) \tag{2.10}$$

$$\text{Local sensation}_{\text{dynamic}} = \frac{C2dT_{\text{sk},i}}{dt} + \frac{C3dT_{\text{core}}}{dt} \tag{2.11}$$

where $\bar{T}_{\text{sk,set}}$ and $T_{\text{sk},i,set}$ are the set-point temperature (neutral temperature) for overall and local body parts, respectively.

The logic of determining the overall TSV is shown in Figure 2.10 (Zhang et al., 2010b). The body parts were divided into dominant parts (i.e., chest, back, and pelvis) and the others. The sensations were divided into two groups, the negative local sensation group and the positive local sensation group. Based on the sensation classification, there will be the 'No-opposite-sensation' and the 'Opposite sensation' models. The 'TSV=0' will be classified into the bigger group. The classification of the two models is shown in Figure 2.10. If 'No-opposite-sensation' was considered, the overall sensation will be weighting averaged by local thermal sensations. If 'Opposite sensation' was considered, the overall sensation would be led by the bigger group's overall sensation and the opposite parts' modified sensation.

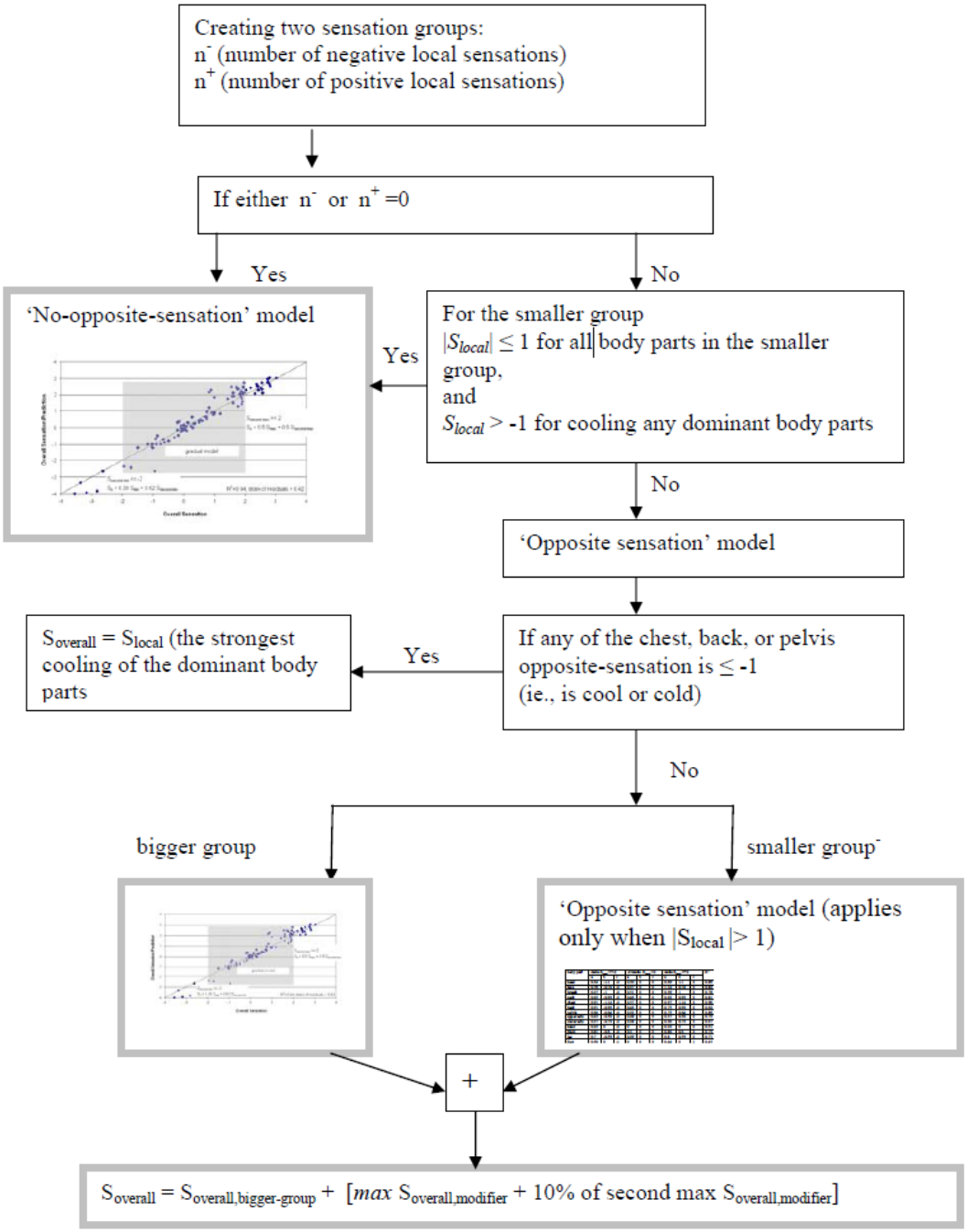

Figure 2.10 The logic of the overall thermal sensation model, reproduced from (Zhang et al., 2010b).

2.5Thermal comfort models for outdoor use

2.5.1 Developing outdoor thermal comfort models

Outdoor thermal comfort models can be utilized to assess outdoor thermal environments and improve human thermal comfort levels during the urban space design and renovation stages (Fang et al., 2018). There have been some attempts to establish thermal comfort models targeted for outdoors.

Table 2.4 summarizes and compares the limitations of the relevant studies. A new empirical index - the Mediterranean Outdoor Comfort Index (MOCI) was developed by Salata et al. (2016a) to evaluate Mediterranean people's outdoor thermal comfort. They conducted a transversal field study in Rome for an entire year and collected over 1000 surveys with meteorological parameters. MOCI was proposed by the multiple regression method, using wind speed, relative humidity, mean radiant temperature, air temperature, and clothing insulations as independent variables. However, since this model is an empirical model between environmental parameters and thermal perception, it is specifically applicable for Mediterranean people and may not be applicable for other climate zones. Melnikov et al. (2018) developed a dynamic human thermal regulation model based on Gagge's two-node model for outdoor use. They modified the skin blood flow model to improve skin temperature prediction nearly fourfold. However, the model was only validated under indoor temperature step-change conditions rather than in real outdoor conditions. Moreover, it is based on a two-node model, which limits its applicability to asymmetric thermal conditions.

Li et al. (2020) found the impacts of sun and wind were different on outdoor thermal comfort by conducting simultaneous physical measurements and questionnaire surveys in a subtropical city, Hong Kong. The results indicated that UTCI underestimated the effects of v and T_{mrt} on TSV under higher air temperature conditions, while overestimating the impacts of T_a and RH on TSV in Hong Kong. They proposed a combined sun and wind condition index (SWI) to standardize and quantify the combined effect of solar radiation and wind speed based on the UTCI index. Lai et al. (2016) developed a multi-segment thermoregulation model for transient

and non-uniform surrounding conditions based on the UTCI. They considered two-dimensional heat transfer in each segment of a human body. The heat transfer includes convection, radiation, and evaporation on bare skin and skin covered by clothing. The heat transfer between two body segments was estimated by the blood circulation. Later, they conducted a field measurement (Lai et al., 2017b) in both the USA and China, to cover a wide range of outdoor thermal environments. Skin temperatures, subjective vote, and environmental parameters were recorded during the measurements. An outdoor thermal sensation model was developed using the thermal load, mean skin temperature, and the change rate of mean skin temperature as independent variables to predict overall thermal sensation, where thermal load was calculated by the multi-segment thermoregulation model they proposed.

Xu et al. (2022) conducted a field experiment in a hot summer with 25 subjects. Subjects were asked to experience a 20-min sunlight area, and then transition to different shading areas (i.e., tree shade, building shade, and umbrella shade) for 45 min, in order to create transient thermal states. Meteorological parameters, physiological parameters (i.e., local skin temperature, tympanic temperature), and subjective vote were collected. They found that forearm temperature is more sensitive to outdoor thermal environment changes and exhibited the highest correlations with TSV. Eventually, they utilized forearm temperature and its change rate as independent variables for overall thermal sensation prediction.

Some newly developed outdoor thermal comfort models that are empirical models limit their applicability to other climate zones. Other models did not cover a wide range of outdoor thermal conditions, such as transient and non-uniform conditions, which are commonly found in outdoor thermal environments. Furthermore, most of these developing outdoor models only provided overall thermal sensation prediction, while they did not provide thermal sensation prediction for local body parts. Due to the asymmetric thermal conditions outdoors, thermal sensation for local body parts might be important to analyze human thermal conditions as well

as their whole body thermal conditions. Overall, none of them can provide reliable and accurate outdoor thermal comfort assessments based on environmental parameters or physiological responses.

Table 2.4 Summary of developing outdoor thermal comfort models.

	Salata, 2016	Melnikov, 2018	Li, 2020	Lai, 2016	Lai, 2017	Xu, 2022
Base index	-	Gagge's model	UTCI	Fiala's model	-	-
Model type	Empirical model	Thermoregulation model	Equivalent temperature	Thermoregulation model	Physiology-based model	Physiology-based model
Methods	Empirical regression: Outdoor subject tests (941 samples)	Theoretical derivation and validation	Empirical regression: Outdoor subject tests (1638 samples)	Theoretical derivation and validation	Empirical regression: Outdoor subject tests (94 samples)	Empirical regression: Outdoor subject tests (25 subjects)
Input	Ta, RH, Tmrt, v, Icl	Ta, RH, Tmrt, v, Icl	Ta, RH, Tmrt, v, Icl	Ta, RH, Tmrt, v, Icl	Thermal load, mean skin temperature, and its change rate	Forearm temperature and its change rate
Output	Overall TSV	Equivalent temperature	Equivalent temperature	Skin temperature	Overall TSV	Overall TSV
Improvements	Predict the mean thermal sensation of	Extend the dynamical properties of	Quantify the combined effect of sun	Improve the clothing, conduction, and arterial blood for	Model development based on	Consider transient outdoor conditions.

	Mediterranean people.	Gagge's classical model.	and wind conditions.	transient and non-uniform conditions.	outdoor data.	
Limitations	1. Limited applicable climate. 2. Only provide overall TSV prediction	1. Did not validate in real outdoor thermal conditions. 2. Applicability in asymmetric thermal conditions needs to be verified.	1. Applicability to other data ranges needs to be verified.	1. Validation used data from indoor climate chambers.	1. Only provide overall TSV prediction. 2. Did not cover various outdoor conditions.	1. Only provide overall TSV prediction.

2.5.2 Predictors for representing dynamic thermal status

Thermal sensation is generated by thermoreceptors in skin, which detect temperature and send signals via peripheral nerves to the brain (Darian-Smith & Johnson, 1977). Ring and de Dear (Ring & Dear, 1991) pointed out that thermoreceptor response has a static and dynamic part, expressed as the thermoreceptor response and the rate of change, as shown in Eq. 2.12. Under dynamic thermal conditions, thermoreceptors send both a static signal based on skin and core temperature, and a dynamic signal based on the rate of change of skin and core temperature (the temporal derivative) (Zhang, 2003).

$$R(x,t) = K_s\, T(x,t) + K_d \frac{dT(x,t)}{dt} \tag{2.12}$$

where K_s and K_d are the proportionality constants for the static and dynamic parts respectively, T is skin temperature, x is the depth of the thermoreceptor, and t is time.

There have been some attempts to develop thermal comfort models under dynamic thermal conditions, using both indoor chamber experiments and onsite measurements. This section summarizes different predictors used to represent the dynamic thermal status of the human body.

Supported by thermoreceptor theory, different variables have been used to reflect dynamic thermal status changes. Temporal derivatives of mean skin temperature (from now on word 'temporal' will be dropped for brevity), local skin temperature, and core temperature are three commonly used predictors. The selection of predictors may vary based on the data obtained from different experimental conditions.

Table 2.5 summarizes the use of predictors in different models for dynamic thermal status prediction. DTS model (Fiala et al., 2003) was developed using a database from chamber tests, where the derivative of mean skin temperature was chosen as predictors for the overall TSV prediction, since they found the change of the derivative of core temperature insignificant within their dataset. Similarly, DMV model (Vellei, 2024) and Takada et al. (2013), developed based on the indoor database or indoor chamber tests, also utilized the derivative of mean skin temperature as predictors for the dynamic overall TSV prediction.

Zhang et al. (Zhang et al., 2010b, 2010a, 2010c) conducted human subject experiments in an indoor chamber employing air-sleeves to heat or cool different body parts, thereby creating non-uniform thermal conditions. Significant change of derivative core temperature was observed (around 0.1 to 0.2 °C) since the cooling and heating effect of the supply air was large enough (e.g., the lowest supply air temperature of air-sleeves was 14 °C, and the highest was around 38 °C). Thus, the CBE model used the derivative of local skin temperature, representing local thermal status changes, and the derivative of core temperature, representing overall thermal status changes, for the dynamic local TSV prediction.

Other studies collected human thermal response data in real outdoor settings. Lai et al. (2017b) developed a dynamic thermal sensation model under real-life outdoor conditions. The model incorporates the independent variables of thermal load, mean skin temperature, and change rate of mean skin temperature, with the dynamic term represented by the change rate of mean skin temperature as the independent variable. Xu et al. (2022) found that high correlations exist between forearm temperature and thermal sensation, and used forearm temperature and its change rate as independent variables.

The above models are developed based on different thermal conditions, including steady, asymmetric, and transient thermal conditions. The datasets used to develop the model, which were derived from specific environmental conditions, may constrain the range of application scenarios. A wider range of environmental conditions and greater diversity in settings will enhance the model's applicability to real outdoor environments.

Table 2.5 Summary of the use of predictors for dynamic term in different outdoor thermal sensation models.

	Dependent variable	Predictors for dynamic term	Experimental conditions
DTS model (Fiala et al., 2003)	Overall TSV	$dT_{sk,m}/dt$	Indoor chamber
CBE model (Zhang et al., 2010c)	Local and overall TSV	$dT_{sk,i}/dt$, dT_{core}/dt	Indoor chamber
Takada et al. (2013)	Overall TSV	$dT_{sk,m}/dt$	Indoor chamber
Lai et al. (2017b)	Overall TSV	$dT_{sk,m}/dt$	Outdoor
Xu et al. (2022)	Overall TSV	$dT_{forearm}/dt$	Outdoor

DMV model (Vellei, 2024)	Overall TSV	$dT_{sk,m}/dt$	Indoor chamber

2.5.3 Shortcomings of current outdoor thermal comfort models

Existing thermal sensation models developed based on indoor chamber data may not be fully applicable for outdoor use. These restrictions arise mainly from the differences between indoors and outdoors in physical, physiological, and psychological aspects (Nikolopoulou & Steemers, 2003), which makes it difficult to apply existing thermal comfort models developed in indoor chambers to the real outdoors conditions.

First of all, indoor thermal environments tend to be stable and asymmetric because of the building structure and set-point control strategies of traditional HVAC systems, whereas outdoor thermal environments are primarily dynamic and asymmetric (Ahmed-Ouameur & Potvin, 2007; J. Li, J. Niu, & C. M. Mak, 2022). It has been proven that transient and intermittent wind, as well as asymmetric solar radiation, are the primary causes of thermal perception differences between indoors and outdoors (Xie et al., 2018; Yu et al., 2020).

Secondly, psychological adaptations can also affect thermal comfort perceptions outdoors, which include naturalness, expectations, experience (short-term or long-term) (Xie et al., 2022), time of exposure, perceived control, and environmental stimulation (Nikolopoulou & Steemers, 2003).

Thirdly, wide spatial and temporal variations of the thermal conditions outdoors allow for transient change of thermal sensation, and thus, high potential for thermal alliesthesia, which is a psychophysiological phenomenon of perceived pleasure or displeasure of stimuli (Liu et al., 2021). Due to these factors, evaluating outdoor thermal comfort is more challenging than evaluating indoor thermal comfort.

Nevertheless, most of the above models apply only to a limited thermal status, so they cannot account for the wide range of dynamic effects on outdoor thermal comfort (Lai et al., 2020). A few models designed for outdoor use, such as the UTCI and COMFA, and others that may be applicable to the outdoors, such as the CBE model, are not based on experimental data obtained from real-life outdoor conditions, which limits their applicability due to the differences between indoor and outdoor comfort.

The thermal comfort models developed based on real outdoor conditions are still under exploration. Most of the existing models focus solely on predicting overall thermal sensation, without addressing thermal sensation at the local body level. However, due to the asymmetric nature of outdoor thermal conditions, local thermal sensations play a crucial role in understanding both regional and whole-body thermal responses. In addition, most of them did not cover a wide range of outdoor settings, such as varying wind speed and solar radiation levels, transient and non-uniform thermal conditions, thereby limiting their applicability and accuracy in predicting complex outdoor thermal environments.

2.6Human thermoregulation under heat stress

Human thermoregulation is a vital physiological process that enables the body to maintain a relatively stable core temperature under variations in environmental conditions. This mechanism is essential for ensuring thermal comfort, protecting internal organs, and sustaining body health.

In high heat stress outdoor environments, with high solar radiation, elevated air temperatures, and varying wind conditions, human thermoregulatory mechanisms such as increasing blood flow, sweating, skin or core temperature variation, are crucial for preventing heat stroke and maintaining thermal comfort.

Many studies have focused on understanding human thermoregulatory responses under high heat stress conditions. Cramer and Jay (2016) reviewed the biophysical aspects of human core temperature regulation by explaining the human body's heat exchange, and they also elaborated on the influence of body morphology during exercise and heat stress thermal conditions. They indicated that if the whole-body sweat production remains the same, a smaller body surface area (AD) will increase sweat rates in localized regions. Regional sweat rates are frequently used to quantify regional differences in sweating. They suggested that to properly account for the influences of both required evaporative heat loss (E_{req}) and AD, local sweat rates should be evaluated at the same E_{req} per unit area (i.e., W/m²).

Prolonged exercise under heat stress could result in a rise in body core temperature and water loss (Periard et al., 2021). Periard et al. (2021) reviewed human thermoregulation during exercising under heat stress, specifically in water loss, sweating, and fluid balance. Body core temperature, such as brain, heart, and other central organs, is typically maintained around 36.6 °C (Obermeyer et al., 2017), and it can deviate significantly when the body is exposed to extreme environmental conditions. Core temperature is dependent on measurement sites since it is a result of localized heat balance (Taylor et al., 2014).

Skin temperature varies across different body parts and in response to external environments (Periard et al., 2021). They suggested that the human body temperature is generally divided into two groups, the core and the shell. Figure 2.11 showed that the highest temperature is rectal, and the foot is always the lowest temperature when the ambient temperature is lower than 32 ° C, but increases significantly with ambient temperature. When the ambient temperature is higher than 32 °C, torso temperature becomes the lowest temperature among these body parts.

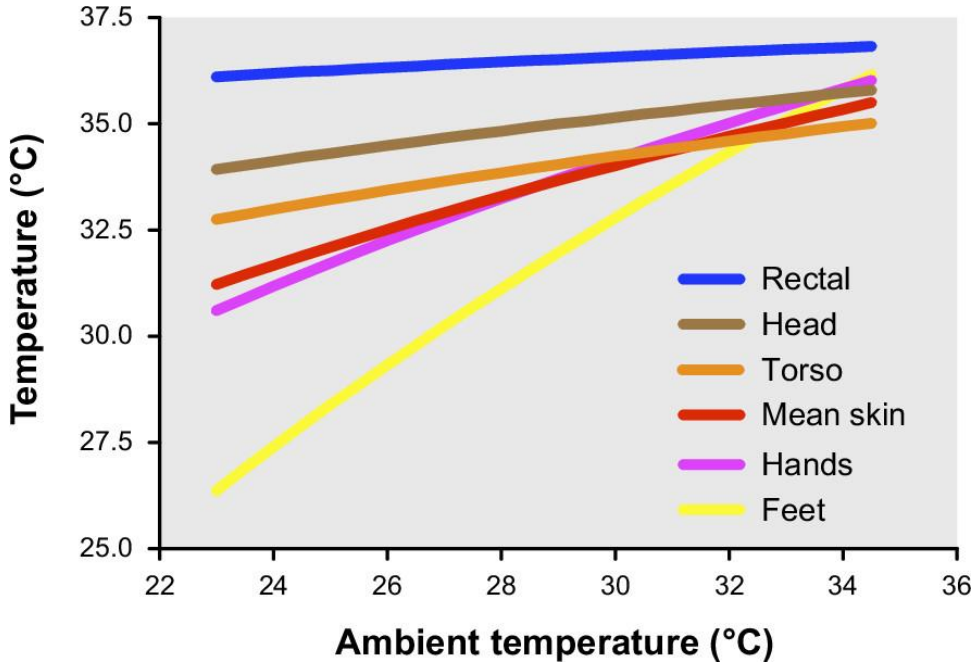

Figure 2.11 Relationship between ambient temperature and temperatures of different body parts at rest. Reproduced from (Periard et al., 2021), Original data from (Olesen, 1982)

Thermoregulatory behavior includes the control of vasomotor (i.e., cutaneous vasodilation) and sudomotor (i.e., sweating) function in the heat, along with metabolic heat production (i.e., shivering) and vasomotor function (i.e., cutaneous vasoconstriction) in cold environments (Periard et al., 2021). Human thermoregulation is governed by a proportional-control system that relies on inputs from both central and peripheral thermoreceptors. These signals are integrated in the hypothalamus, where they are compared with a set point to give appropriate thermoregulatory responses, such as vasodilation, vasoconstriction, sweating, or shivering. The magnitude of these responses is proportional to the thermoreceptor signals from the set point, enabling finely tuned thermoregulation under a wide range of environmental conditions.

Campbell et al. (2022) conducted an experiment of 13 participants experienced 5 days of 60 min heat exposure to different heat stress conditions, including hot water immersion (40°C), sauna (55°C, 54% relative humidity) and exercise in the heat (40°C, 52% relative humidity),

and a thermoneutral water immersion control (36.5°C). Physiological (thermal, cardiovascular, haemodynamic) and psychophysical strain responses were measured. The results showed that sauna reached the highest skin temperature, and exercise in the heat illustrated the highest increase in core temperature, heart rate, sweat rate, and systolic blood pressure. This study highlighted that passive heat stress in hot humid conditions has lower tolerance and more cardiovascular strain than hot water immersion.

However, few studies have explored human thermos-physiological responses in high heat stress outdoor microclimates. Otani et al. (2017) investigated the time-of-day effects of changes in solar radiation on thermoregulatory responses when subjects underwent moderate intensity exercise outdoors in summer. 8 high school baseball players were selected as subjects to experience a 3h baseball training course. Heart rate, tympanic temperature, and skin temperature were simultaneously measured during the experiment. The results indicated that skin temperature was basically higher in the morning than in the afternoon, and body heat gain was also higher in the morning than in the afternoon during exercise. In addition, evaporative heat loss was great in the afternoon compared with that in the morning. This study indicated that a greater thermoregulatory strain in the morning than in the afternoon, resulting in higher skin temperature and higher heart rate.

Li et al. (2023) studies the variable thermal exposures on walking thermal comfort of 70 human subjects from a physio-psychological aspect, with meteorological parameters, physiological responses (i.e., skin temperatures, sweating, heart rates), and thermal perceptions, collected. A Reverse Dynamic Thermal Environment (R_DTE) was proposed to quantify the variations in wind and solar radiation. The results showed that the sweating rate was highly correlated with R_DTE. Furthermore, the evaporative heat loss from sweating was dominant, taking up 35%–43% of the generated heat.

In summary, in the context of climate change, investigating human thermoregulatory responses in outdoor microclimates is crucial for mitigating heat-related health risks, particularly heat stroke, under high heat stress conditions. Understanding how the human body responds to dynamic outdoor thermal environments can guide the design and renovation of urban spaces and public cooling strategies, enhancing resilience and adaptive capacity for populations.

2.7Thermal alliesthesia and short-term adaptation

Increasing global warming continues to bring heat waves and increase air temperature, leading to thermal discomfort in urban outdoor areas at pedestrian levels (Huang et al., 2017), making city dwellers' lifestyle more sedentary and indoor-focused (Obradovich & Fowler, 2017). The enhancement of outdoor thermal environments can motivate urban residents to spend more time outdoors, resulting in improved health outcomes. Therefore, improving the microclimate of urban walking spaces requires an understanding of how outdoor thermal environments affect pedestrians' thermal perceptions.

Originating from indoor thermal comfort studies, significant efforts have been devoted to exploring a thermal neutral condition as the target of the optimum thermal environment design in outdoor thermal comfort research (Xi et al., 2012; W. Liu et al., 2016; Lin et al., 2018; Binarti et al., 2020). With the usage of different thermal indices, such as the four most widely used indices in outdoor thermal comfort studies (Potchter et al., 2018): PET, PMV, UTCI, and SET*, a large number of existing studies focus on locating a neutral temperature for a specific region.

Liu et al. (2016) found that outdoor neutral PET in Changsha, China (Cfa, Köppen climate) was 23.3 °C in summer and 14.9 °C in winter. Xi et al. (2012) found that the outdoor neutral SET* in Guangzhou, China (Cwa, Köppen climate) was 24 °C for young students in summer.

These studies contribute significantly to the understanding of long-term climate adaptation, but their relevance to practical urban design is less certain.

In heterogeneous outdoor scenarios, neutral temperatures for indoor settings may still be perceived as comfortable for pedestrians, but it is almost impossible to create stable thermal conditions in outdoor microclimates due to transient and dynamic characteristics. Thermal alliesthesia and short-term adaptation highly affect thermal perceptions (Vellei et al., 2021). In addition, the energy costs of maintaining a neutral thermal environment in urban settings can be prohibitively high. This encourages us to think from a different angle and take advantage of these dynamic thermal features outdoors to create comfortable thermal perceptions.

Research has demonstrated that the most pleasant thermal feelings occur when thermal stimulus relieves whole body thermal stress, which are typically observed in transient conditions and are of short duration (Cabanac, 1992; Arens et al., 2006). It can be explained by alliesthesia, a psycho-physiological concept describing pleasure or unpleasure aroused by a stimulus according to the person's internal state (Cabanac, 1979). A warm stimulus can arouse thermal pleasure when one is cooler-than-neutral, and a cool stimulus can arouse thermal pleasure when one is warmer-than-neutral.

Parkinson and de Dear (Parkinson & de Dear, 2014, 2015, 2016) proposed a theoretical framework of thermal alliesthesia to describe the hedonic response to thermal stimulus in transient and asymmetric thermal environments, as shown in Figure 2.12. They divided the thermal physiology into three zones, the thermoneutral zone, the moderate potential for alliesthesia zone, and the strong potential for alliesthesia zone, based on the preceding thermal perception compared with the preferred thermal perception (Parkinson & de Dear, 2015). The preferred thermal perception is the center of the thermoneutral zone (e.g., thermal sensation located in thermal neutrality and vasomotor is in fine-tuned adjustments of heat loss), while

moderate alliesthesia zone is near the thermoneutral zone by two sides (e.g., minor fluctuations in skin temperature, constriction or dilation of vessels) and strong alliesthesia zone is far from the thermoneutral zone by two ends of thermal sensation scale (e.g., shivering or sweating) (Parkinson & de Dear, 2014).

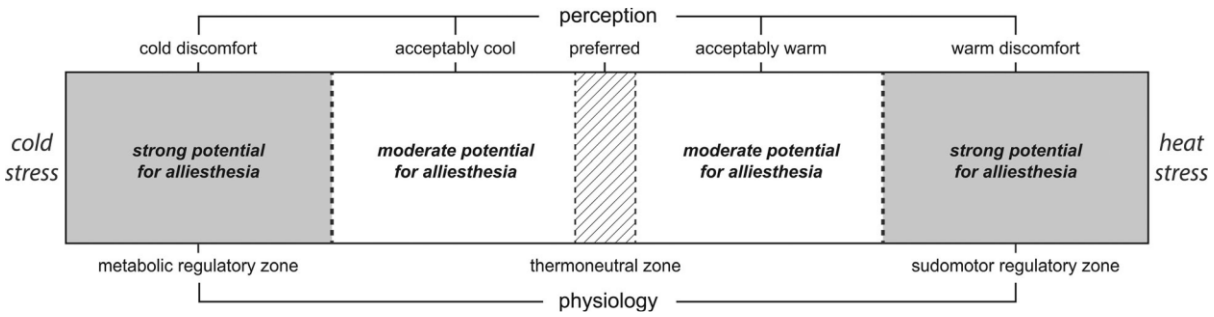

Figure 2.12 Thermal alliesthesia framework, reproduced from (Parkinson & de Dear, 2015).

The concept of thermal alliesthesia has been adopted to explain the various phenomena observed in outdoor thermal comfort studies (Lai et al., 2020). Both short-term and long-term alliesthesia exist in our daily life. Long-term alliesthesia, such as seasonal alliesthesia, which has been observed in previous studies (Lai, Guo, et al., 2014; Yao et al., 2018; Schweiker et al., 2020), results in occupants perceiving a slightly warm thermal sensation as most comfortable in winter and a slightly cool thermal sensation as most comfortable in summer.

Lai et al. (2014) investigated outdoor thermal comfort under different climate conditions, environmental conditions varied greatly with air temperature from -5.0 to 34.5 °C, 83.3% of respondents voted it as ‘acceptable’. They found that thermal preference varies seasonally, with ‘slightly warm’ conditions being most preferred during cold seasons, ‘neutral’ sensations in transitional shoulder seasons, and ‘slightly cool’ environments becoming most desirable during

hot seasons. Schweiker et al. (2020) conducted an experimental study with two groups of participants experiencing the same three thermal conditions, such as cool, neutral, and warm conditions, each lasting for 50 min. The results indicated that optimal thermal conditions varied greatly between seasons, sexes, and the dimension of thermal perceptions. They proposed a new type of alliesthesia, seasonal alliesthesia, to explain this phenomenon.

Thermal comfort and pleasure also occur with the changes in transient thermal environments. This transient alliesthesia highlights the importance of thermal variations in environmental design. Strategically incorporating thermal transitions in urban spaces, such as alternating shaded and sunny areas, ventilation corridors, or cooling features, can enhance overall thermal satisfaction beyond what steady conditions might provide.

Dayuban et al. (2022) conducted an experiment to make subjects equipped with GPS devices participate in a 1-hour walk on a hot day to explore the thermal alliesthesia phenomenon during the thermal walk in transient outdoor scenarios. Microclimate measurement and human subjective vote were simultaneously collected. The results indicated that slight changes in microclimate conditions could cause thermal pleasure. In addition, subjects' pleasant feelings were highly correlated with the mean PET they had just experienced, and estimated percent shade significantly correlated with SVF, PET, mPET, and thermal pleasure feelings. Peng et al. (2022) performed a stop-and-go experiment of transient outdoor scenarios to capture thermal perception variations during urban walks in late summer. A total of 40 subjects walked for 70 min around two different waterfront districts. The results showed that UTCI contrast could effectively predict thermal alliesthesia. They indicated that the variation of thermal environment is vital to creating thermal pleasure.

Another field measurement was conducted by Lai et al. (2017b) in West Lafayette, Indiana, USA, and Tianjin, China. They measured environmental conditions, subjects' skin

temperatures, and their subjective votes. They found that mean skin temperature decreased from 33 °C to 28.5 °C (with the thermal sensation decreasing from -0.5 to -3.0) after the 30 min exposure in cold outdoor conditions. Following that, a slight increase in mean skin temperature (0.5 °C) could cause a significant increase in thermal sensation (from -3.0 to 1.0).

Liu et al. (2021) conducted a 30-day experiment covering both summer and winter with 35 subjects and quantified the thermal sensation into four alliesthesia potential zones. Subjects experienced sunlight and shade transient conditions for three cycles, and then underwent artificial thermal stimulation for distal limbs using a contact heating (winter) or cooling (summer) panel. Following that, a convective fan was set in front of their legs or faces. This experimental setting was created to induce dynamic outdoor conditions that lead to thermal alliesthesia. Based on the results, they divided the thermal sensation into four alliesthesia potential areas, including two with moderate and two with strong alliesthesia potential, according to the preceding thermal sensation divergence from the preferred thermal sensation.

As presented in Figure 2.13, linear regression and quadratic regression were used to fit the relationship between changes in thermal sensation (dT) and thermal pleasure (dP) in strong and moderate alliesthesia zones, respectively. Good performance was shown in all regression lines. They pointed out that mild positive changes in dP occurred in a very limited range of dT in the moderate alliesthesia zone, while in the strong alliesthesia zone, dP increased when dT decreased if subjects previously felt cold. This suggests that letting people out of the thermoneutral zone (moderate alliesthesia zone in this study) could improve the potential of thermal pleasure in the next period.

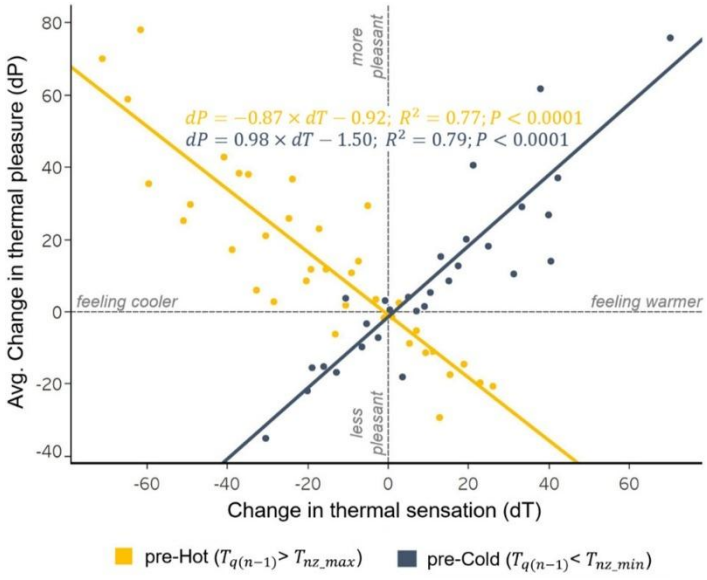

(a)

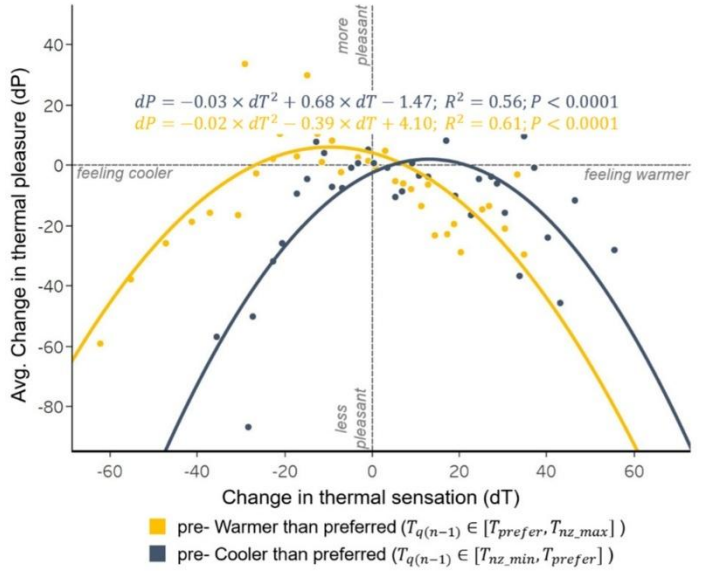

(b)

Figure 2.13 Relationships between change in thermal pleasure (dP) and change in thermal sensation (dT) with the preceding thermal sensation (a) belonged to 'Hot' or 'Cold' groups; and (b) fell in the thermoneutral zone. Reproduced from (Liu et al., 2021)

Sensory adaptation refers to the diminished sensitivity during the presentation of an effective stimulus (Solomon & Kohn, 2014), which is directly related to the dynamic activity of primary sensory neurons (Vellei et al., 2021). This phenomenon reflects a fundamental property of sensory systems that allows organisms to filter out redundant or unchanging stimuli, thereby enhancing responsiveness to novel or changing environmental inputs. Such adaptation mechanisms play a critical role in preventing sensory overload and facilitating the detection of relevant changes in the environment.

From a thermal perspective, short-term thermal adaptation is a short-duration (i.e., minutes or hours) adaptive process representing a time-dependent attenuation of the body's sensory response after non-neutral thermal exposures (Taylor, 2006; Vellei et al., 2021), which is in a much shorter timescale than the original concept of thermal adaptation (i.e., days or months). For example, thermal sensation and skin temperature were observed to overshoot first and then stabilize after cool or warm exposure (Zhang et al., 2017). This phenomenon was mostly validated in local thermal stimulus experiments (Haber, 1958), while other insights were concentrated on thermal pain perception (Edwards & Fillingim, 2001; Jepma et al., 2014).

Several studies have investigated dynamic thermal perception in response to transient thermal environments characterized by sudden temperature changes, often referred to as step-change conditions, using controlled climate chamber experiments.

Zhang et al. (2017) recruited 30 subjects exposed to different steps between a 26 °C temperature condition (neutral) and non-neutral temperature conditions ranging from 20 to 32 °C in a chamber experiment. They collected subjects' subjective and physiological responses to explore the effects of step-change temperature on thermal comfort. The results indicated that the subjective responses were anticipatory, preceding changes in skin temperature. Moreover, thermal comfort and acceptability responses were even more anticipatory, as they preceded

changes in thermal sensation. The results showed that thermal sensation stabilized at 20 min under warm exposure and at 1 min under cool exposure. Ji et al. (2017) conducted an experiment with 20 subjects experiencing five conditions in step-change chamber conditions. Subjects experienced a hot or cold temperature (i.e., 20, 23, 26, 29, 32 °C) for a period of time (differed with different conditions), and then entered into a thermal neutral condition (26 °C) for a period of time. The results indicated that thermal sensation was amplified after step-change conditions, then attenuated and stabilized after 15 mins of exposure.

Thermal alliesthesia and short-term adaptation are essential theories for creating a high degree of thermal pleasure and thermal comfort feelings. Few studies explored the combined effect of thermal alliesthesia and adaptation phenomena on dynamic thermal perceptions in real-life environments, especially the psycho-physiological aspect of thermal alliesthesia and short-term adaptation in transient outdoor thermal environments.

2.8Thermal evaluation scales for outdoor spaces

Thermal Sensation Vote (TSV) is typically used to evaluate human thermal feelings in thermal environments. Thermal Comfort Vote (TCV), Thermal Acceptability (TA), and Thermal Pleasure (TP) are commonly used to assess thermal comfort conditions in various thermal environments. TCV reflects the overall comfort level experienced by individuals, TA indicates whether the thermal environment is considered acceptable or not, and TP captures the emotional or hedonic response to thermal conditions.

However, occupants have varying thermal comfort needs for different scenarios, depending on the specific use of spaces (Y. Yang et al., 2024). For instance, work environments emphasize work efficiency, sleep environments prioritize sleep quality, and urban outdoor spaces are designed to provide recreational spaces that encourage city dwellers to spend time outdoors.

These diverse scenarios influence how individuals perceive and respond to thermal environments, highlighting the importance of context-specific thermal comfort evaluation.

Due to the dynamic features in outdoor environments and pedestrians' transition between different microclimate scenarios, thermal overshoot and short-term adaptation phenomena commonly occur (Jiang et al., 2024). Compared with indoor studies using the TCV and TA scales to evaluate occupants' thermal comfort (Ji et al., 2017; Su et al., 2020; Zhu et al., 2025), outdoor studies tend to adopt the TP scale (Liu et al., 2021; Zhang et al., 2024) as it captures the pleasant feelings that are always associated with transient environments (Cabanac, 1992; Arens et al., 2006).

Consequently, thermal evaluation scales originally developed for indoor environments may not be applicable to outdoor settings. An outdoor study (S. Liu et al., 2020) compared 76 climatic adjectives and developed a semantic framework to assess outdoor thermal comfort. In the first phase, they did an online questionnaire inviting 135 native English speakers to place 76 climatic adjectives into the semantic framework, then conducted a field study with another 22 subjects recording their thermal perceptions in the same semantic framework using the 76 adjectives. In the second phase, the results showed good correlations between the thermal adjectives for the two research phases. Finally, this study developed a six-dimensional semantic space for outdoor thermal comfort assessment, comprising 'thermal sensation', 'humidity', 'wind', 'solar radiation', 'thermal pleasure', and 'thermal intensity'.

Xi et al. (2024) conducted a semantic evaluation using Chinese words related to outdoor thermal comfort. They evaluated 63 words through online and on-site questionnaire surveys, and further used an outdoor experiment to validate the effectiveness. They found significant correlations between the 2-phase results, indicating the effectiveness of the semantic thesaurus.

They also suggested that TCV cannot systematically represent human thermal perception in outdoor thermal environments.

2.9Summary and research gap

Thermal sensation models for evaluating outdoor thermal environments are essential for enhancing pedestrians' thermal comfort during the design and renovation of building layouts or cooling strategies. There are three species of mainstream thermal sensation models, including the energy balance model, empirical model, and thermal physiology-based empirical model. Since energy balance models output equivalent temperature, additional subject experiments are required to establish the relationship between equivalent temperature and thermal sensation. Empirical models have limited application to specific climate zones. Thermal physiology-based empirical models are considered more reliable than empirical models, as they can incorporate advanced thermoregulation models to bridge environmental parameters and thermal sensation. However, most of the mainstream models are developed based on indoor chamber data. Due to the dynamic characteristics of outdoor environments, such as dynamic wind, asymmetric solar radiation, and transient pedestrian scenarios, their applicability in outdoor settings may be limited.

The developing thermal comfort models based on real outdoor conditions are still under exploration. Many of these models do not cover a wide range of outdoor settings, such as varying wind speed and solar radiation levels, transient and non-uniform thermal conditions, thereby limiting their applicability and accuracy in predicting complex outdoor thermal environments. Furthermore, most existing models focus solely on predicting overall thermal sensation, without addressing local thermal sensations. Given the asymmetric nature of outdoor thermal conditions, local thermal sensation may be critical for accurately assessing both local body parts and whole-body thermal states. Currently, none of these models offer reliable and

accurate outdoor thermal comfort assessments based on either environmental parameters or physiological responses.

Few studies explored the combined effect of thermal alliesthesia and adaptation phenomena on dynamic thermal perceptions in real-life environments, especially the psycho-physiological aspect in transient outdoor thermal environments. Given the dynamic characteristics of outdoor thermal environments, thermal alliesthesia and short-term thermal adaptation phenomenon still need investigation to create a high degree of thermal pleasure and thermal comfort feelings.

Occupants have varying thermal comfort needs depending on the specific use and context of the space (Y. Yang et al., 2024). Compared to indoor studies that commonly use the TCV and TA scales to evaluate occupants' thermal comfort, outdoor studies tend to adopt the TP, as it better captures the pleasant sensations often associated with transient outdoor environments. Consequently, thermal evaluation scales originally developed for indoor environments may not be fully applicable to outdoor settings. Thus, the applicability of various thermal evaluation scales for outdoor use needs to be further investigated.

In summary, there are several main limitations of the existing studies:

(1) Human thermoregulation is a vital process for maintaining body health under high heat stress conditions. Few studies explored the human thermoregulatory responses (e.g., skin and core temperature, sweat rate) under high heat stress outdoor thermal environments.
(2) Existing thermal physiology-based models have not been developed to cover a wide variety of real-life outdoor conditions (e.g., a wide range of wind speeds and solar radiation settings, transient and dynamic conditions), which may limit the applicability and accuracy for outdoor use.

(3) Given the asymmetric nature of outdoor thermal conditions, local thermal sensation is critical for accurately assessing both local body parts and whole-body thermal states. In most models, the overall thermal sensation was not evaluated by assessing the thermal sensation predictions of local body parts first, which limits their application for asymmetric outdoor conditions.

(4) Occupants have varying thermal comfort needs for different scenarios. Thermal evaluation scales originally developed for indoor environments may not be fully applicable to outdoor settings. The applicability of various thermal evaluation scales for outdoor use has not been extensively investigated.

(5) Thermal alliesthesia and short-term thermal adaptation highly affect dynamic thermal perceptions in outdoor thermal environments. Few studies explored the combined effect of thermal alliesthesia and adaptation phenomena on dynamic thermal perceptions in real-life environments, especially the psycho-physiological aspect of thermal alliesthesia and short-term adaptation in step-change indoor and outdoor thermal environments.

Chapter 3 - **Developing a physiological-parameter-based thermal sensation model for warm-biased outdoor settings: The steady-state part**

3.1 Summary

Outdoor thermal comfort model is essential to evaluate thermal environment conditions for residents. Currently, no applicable and accurate thermal physiology-based model can provide a reliable prediction of thermal perceptions for different outdoor environments. There are mainly two limitations: 1) Existing thermal physiology-based models have not been developed to cover a wide variety of real-life outdoor conditions (e.g., a wide range of wind speeds and solar radiation settings). 2) In most models, the overall thermal sensation was not evaluated by assessing the thermal sensation predictions of local body parts, which limits their application for asymmetric outdoor conditions. Thus, this research will develop an outdoor thermal sensation model by exploring the relationship between human subjective thermal responses, in terms of local thermal sensations and overall thermal sensation, and physiological responses, in terms of local skin temperatures and local sweat rates, in a wide range of real-life outdoor thermal environments. The model can be integrated with thermoregulation models (e.g., JOS-3 model) to predict thermal sensation based on environmental parameters. The complete outdoor thermal sensation model will include a steady-state part and a dynamic-state part, and the content of this chapter will focus on the steady-state part. This steady-state part model will contain two parts, the local TSV prediction model for 11 body parts and the overall TSV prediction model. The overall TSV model will be developed based on the local TSV of different body parts. The main objectives of this study are as follows:

1. To explore the correlations between physiological parameters (i.e., skin temperature and sweat rate) and thermal sensation under different real-life outdoor conditions.
2. To build the thermal sensation model for local body parts based on physiological parameters.
3. To develop the overall thermal sensation model based on local thermal sensation.

This chapter aims to build a thermal sensation model that correlates the subjective thermal sensation votes (TSV) with the human-body thermo-physiological responses in steady-state warm-biased outdoor conditions. The model includes a local TSV model for 11 body parts and an overall TSV model. A total of 86 human subject tests were conducted under varying wind speeds and solar radiation levels using a changeable windshield and shading device in real outdoor settings.

Results show a strong correlation between local sweat rate and skin temperature, leading to the selection of local skin temperature as the sole variable for the local TSV model. Individual differences and thermal overshoot outdoors were observed, and a new parameter accounting for the neutral skin temperature variation was introduced into the local TSV model to provide three prediction values, i.e., the mean, the 10th, and 90th percentiles. The overall TSV model, which calculates overall TSV as a weighted average of local TSVs, demonstrated a high fit with actual overall TSV ($R^2 = 0.96$). This model is designed to be used with a multi-nodal human thermoregulation model to numerically assess thermal comfort in outdoor spaces.

3.2 Methods

3.2.1 On-site experiment settings

Environmental condition monitoring. The experiments were conducted in Hong Kong which has a monsoon-influenced humid subtropical climate (Cwa, Köppen climate classification)

(Peel et al., 2007), with cool, dry winters and hot, humid summers. The experiments were conducted in hot summer, from June to August on the campus of Hong Kong Polytechnic University (HKPolyU). The semi-controlled experiment (Kircher et al., 2017) in this study is designed to cover a variety of outdoor thermal conditions. The location of the HKPolyU campus makes it possible to have high wind speeds as it is close to the harbour. There are buildings on both the north and south sides of the experimental site, forming an east-west crosswind. A windshield with different void sizes (75% void, 50% void, and 30% void) was designed to adjust the wind speed levels that people experienced. The windshield was utilized during high-wind weather conditions to generate varying levels of wind speed, while it was not employed under low-wind conditions. The sketch draft of the windshield is presented in Appendix A. To ensure a desired wind field, a CFD simulation was conducted before the processing of the windshield, as shown in Figure A2, A3. During the experiment, the middle-board was set perpendicular to the main wind direction, the angle between the side-board and the middle-board of the windshield was set at around 135°-150°, and the subjects were arranged to sit around 1.0 to 1.5 m behind the windshield. By combining it with different shading conditions, including building shade, sunshade (made of white Oxford fabric), and sunlit used to create low, medium, and high radiation levels, respectively, (Figure 3.1-a), we can create a wide range of outdoor exposure conditions. Additionally, the experiment was conducted between 10 am and 4 pm to ensure that the changes in the sunshade shadow were small.

A mobile microclimate station was placed within 1.0 m of the subjects throughout the experiments. It consists of three pairs of radiometers that measure radiant fluxes coming from six directions, an anemometer, and an air temperature and humidity sensor. A height of 1.5m is usually used to represent the pedestrian-level thermal environments in previous outdoor-focused studies (Niu et al., 2015). Considering the sitting posture of subjects in this study, the microclimate station was set at 1.3 m in height and the radiometers were set at 1.6 m to avoid

blocking solar radiation. The technical information of the instruments is listed in Table 3.1. Radiation fluxes measured by radiometers including pyranometers and pyrgeometers were used to calculate T_{mrt} according to the ISO 7726 standard (ISO, 1998). The detailed calculation method can be found in Chapter 3.

Physiological measurements. Local skin temperatures of 18 human body parts, which are similar to the body segmentation of the JOS-3 model (Takahashi et al., 2021), were collected using thermocouples. The mean skin temperature ($T_{sk,m}$) was calculated by weighting the skin temperatures at seven body parts, including forehead, abdomen, forearm, hand, thigh, calf, and foot, the weights are 0.07, 0.35, 0.14, 0.05, 0.19, 0.13, and 0.07, respectively (Hardy et al., 1938). Since sweat rate plays an important role in thermoregulation (B. Zhong et al., 2022) and is highly related to human thermal status in outdoor conditions (Li et al., 2023), sweat rate was measured in this study. The sweat rates of three body parts - forehead, left forearm, and abdomen, were measured using a commercial Vapometer (Delfin Technologies, Finland). The sweat rates of the forearm and forehead are effective in predicting the whole body's sweat condition (Baker et al., 2019), and the abdomen sweat rate was added as a reference for the unexposed body part. The measurement sites of local skin temperature and sweat rate are illustrated in Figure B. The eCelsius pills (BodyCap, France) were used for core temperature monitoring.

Table 3.1 Technical information of instruments for the on-site measurement.

Measurement type	Monitored parameter	Sensor/Equipment	Accuracy	Range of measurement	Sampling rate
Microclimate parameters	Air temperature (T_a)	R.M. YOUNG 41382	±0.3 °C	-50 ~ +50 °C	1 s
	Relative humidity (RH)		±1%	0 ~ 100%	

	Wind speed (v)	R.M. YOUNG 81000	±0.05 m/s	0 ~ 40 m/s	1 s
	Long-wave radiation (L_i)	Kipp & Zonen CNR-4	< 10%	-250 ~ +250 W	10 s
	Short-wave radiation (K_i)		< 5%	0 ~ 2000 W	10 s
Physiological parameters	Skin temperature	KPS-ZT-TT-T-30-1500-CZ	±1.0 °C	-200~ +200 °C	1 s
	Sweat rate	Delfin VapoMeter SWL5	±4%	0~200 g/m^{2}h	As needed
	Core temperature	BodyCap eCelsius	±0.2 °C	25~ 45 °C	15 s

Thermal comfort surveys. There are a total of 514 subjective surveys used for developing the steady-state model, where 80% of the data (411 subjective responses) was used as a dataset for model development, while 20% of the data (103 subjective responses) was used as a validation dataset. The questionnaire design includes two parts, the basic information survey, and the thermal comfort survey. The basic information survey includes individual characteristics and health conditions, such as gender, age, height, weight, clothing, health, and thermal experience. The thermal comfort survey was designed to collect subjective thermal responses of the human subjects, in terms of thermal sensation vote (TSV) and thermal comfort vote (TCV). Since outdoor thermal environments are more dynamic and extreme, the TSV and TCV questionnaire employed an extended nine-point scale (Zhang et al., 2010c; Xie et al., 2019) by adding 'very cold' (-4) to 'very hot' (+4) to the two ends of the ASHRAE 7-point scale (ASHRAE), and from 'very uncomfortable' (-4) to 'very comfortable' (+4) for TCV. The TSV and TCV scales are shown in Fig. C. The questionnaires were written in the subject's native language, Chinese, to facilitate understanding. Subjects' non-uniform thermal perceptions in outdoor conditions were also collected by asking for local TSVs and local TCVs for different body parts. The local TSV survey started by asking about the overall thermal sensation, then followed by a question of choosing at least three body parts that are inconsistent with their overall thermal sensation,

and the subjects were required to fill out the related TSV questions for these selected body parts. By focusing on several body parts rather than each individual part (Zhang, 2003), this survey design will save respondents time and reduce response bias when they are asked similar questions repeatedly. There are 10 body parts involved in the local TSV survey, including the forehead, neck, chest, back, upper arm, forearm, thigh, calf, hand, and foot. Chest sensation was used to represent the abdomen sensation since the abdomen thermal sensation was not asked. Due to limitations in scope, the TCV result was not included in this study.

Subjects. A total of 34 human subjects participated in the experiment, including 15 males and 19 females, most of them are college students. The sample size of subjects was estimated by G*power (Faul et al., 2009), the power level is 0.8, the significant level is set to be 0.05, and the effect size is determined to be 0.5 (Lan & Lian, 2010). The required sample size is 13. Table 3.2 summarizes the characteristics of the subjects. The weight and body fat were measured by a body composition monitor (TANITA, RD545), and the height was measured by a height ruler. For male subjects, the mean age is 23.4, the mean body mass index (BMI) is 23.5 kg/m^2, and the mean body fat is 17.7%. For female subjects, the mean age is 23.2, the BMI is 21.3 kg/m^2, and the mean body fat is 27.1%. Clothing insulation of all subjects is around 0.3 clo.

Table 3.2 Characteristics of participants

	Count	Age (years)	Height (cm)	Weight (kg)	BMI (kg/m^2)	Body fat (%)	Clothing insulation (clo)
Male	15	23.4 ± 2.7	174.8 ± 6.9	71.5 ± 13.5	23.5 ± 4.9	17.7 ± 6.4	0.3 ± 0.1
Female	19	23.2 ± 3.6	166.5 ± 4.7	59.0 ± 9.8	21.3 ± 3.8	27.1 ± 6.9	0.3 ± 0.1
Total	34	23.3 ± 3.2	170.3 ± 7.1	64.7 ± 13.1	22.3 ± 4.4	22.8 ± 8.1	0.3 ± 0.1

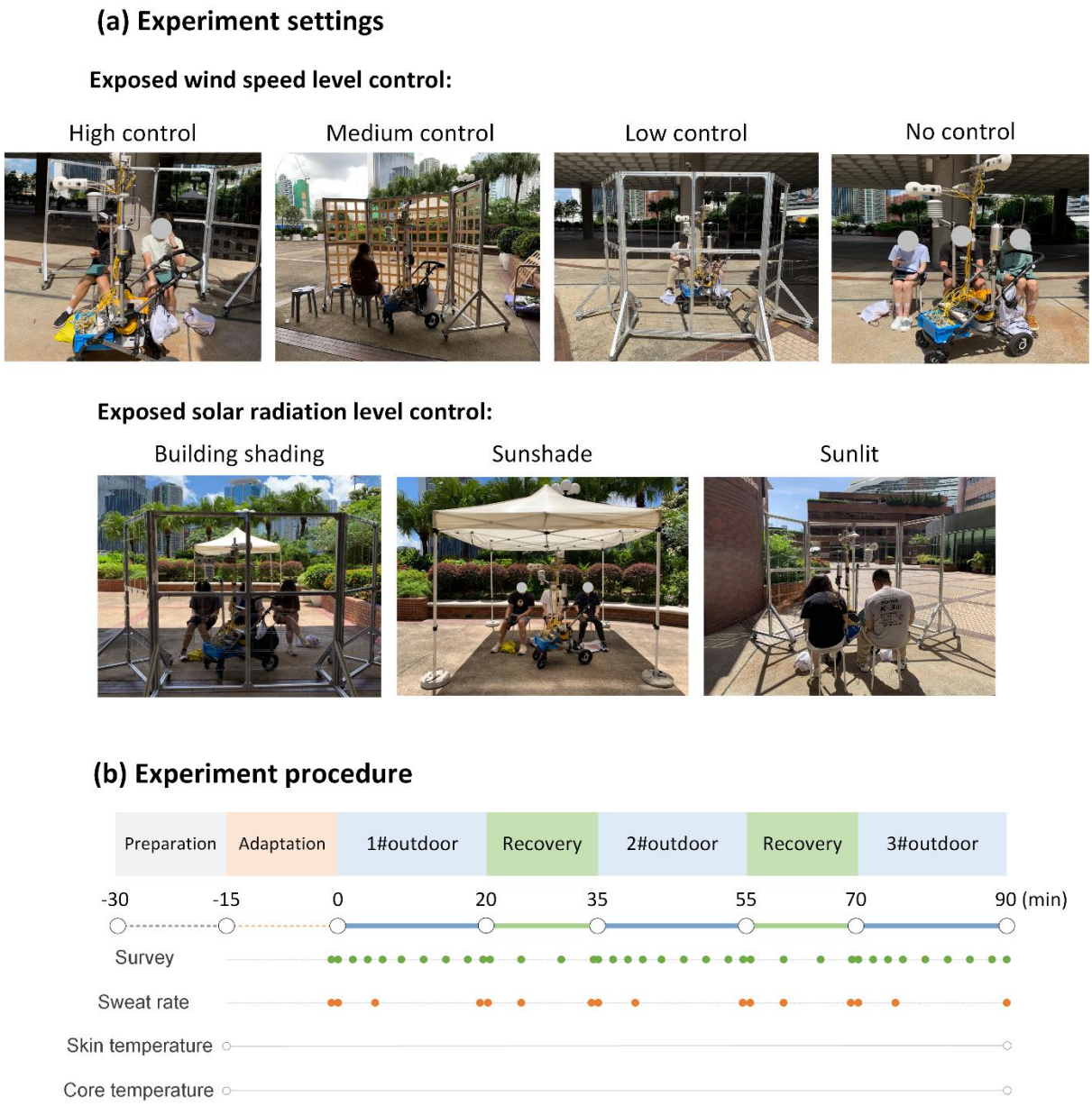

Figure 3.1 On-site experiment measurement. (a) Experiment settings, (b) Experiment procedure.

3.2.2 Experiment procedure

Figure 3.1-b shows the experimental procedure in this study. Human subjects spent a 15-min preparation period in an indoor air-conditioned sitting area (averaged environmental parameters during the measurement: T_a: 22.6 °C, v: 0.32 m/s, RH: 57.5%, T_{mrt}: 26.6 °C), during which a basic information survey was filled out and local skin temperature sensors were

attached. Then, a 15-min adaptation was conducted in the same area, to ensure a stable metabolic rate for each subject and eliminate the potential impact of previous thermal experiences on the following experiment. A subjective survey was collected at the end of this period. Following the adaptation period, three 20-min outdoor exposures were conducted under different controlled levels of wind speed and solar radiation. The indoor adaptation site and outdoor experiment site were next to each other, and the subjects moved slowly when changing sites. During each outdoor condition, subjects were asked to remain seated and fill out the subjective survey every 2 min for the first 6 min and every 3 min thereafter. An indoor air-conditioned recovery period of 15 min was set between each outdoor condition to restore the subject's thermal status to the same level as before (Zhai et al., 2019). The subjective survey was filled out every 5 min during the recovery period. Skin temperature and core temperature were monitored throughout the experiment. Since core temperature is more suitable for reflecting changes in the human body's thermal status, core temperature data will be used for future dynamic-part model development. Sweat rate was tested at the end of the adaptation period, the 0 min, the 5 min, and the end of the outdoor and recovery periods. Each subject participated 1 to 3 times in the experiment. The experiment conditions were set differently each time. A total of 86 human subject tests were performed. The human subject tests have been approved by the HKPolyU Institutional Review Board (Reference Number: HSEARS20221023001).

3.2.3 Basic mathematical model

3.2.3.1 $Local\ TSV$ model

The model development will be started with the selection of predictor variables. In order to select the most significant physiological parameters impacting local thermal sensation, the Spearman correlations and regression methods were used. The model should employ a minimal set of independent variables that can adequately predict the impact of the thermal environment

on sensation (Lai et al., 2017b). After the determination of the predictor variable, the next step was to determine the mathematical model used for the local TSV prediction. The logistic function was selected to represent the relationship between physiological parameters and thermal sensation according to previous studies (Zhang, 2003; Lai et al., 2017b; Xu et al., 2022). The general form is expressed as Eq. (3.1):

$$y = A \times \left(1 - \frac{2}{1 + e^{B \cdot x}}\right) \tag{3.1}$$

where: A is the limit coefficient, and B is the slope coefficient.

This study selected local skin temperature ($T_{sk,i}$) as the independent variable of the thermal sensation of local body parts (TSV_i) as the dependent variable. Difference between $T_{sk,i}$ and neutral skin temperature of the target local body part ($T_{sk,neu,i}$) indicates the degree to which thermal sensation deviates from thermal neutrality. The thermal sensation limits in this study were 'very cold' (-4) and 'very hot' (+4), thus the coefficient A was set as 4. The mathematical form could be organized and expressed as Eq. (3.2):

$$TSV_i = 4 \times \left(1 - \frac{2}{1 + e^{B \times (T_{sk,i} - T_{sk,neu,i})}}\right) \tag{3.2}$$

where $T_{sk,i}$ and $T_{sk,neu,i}$ are the skin temperature and neutral skin temperature for the i th body part, respectively, and B is the coefficient that controls the slope of the line.

3.2.3.2 Prediction of 'a range' instead of 'a value'

Neutral skin temperature ($T_{sk,neu,i}$) for each body part in Eq. (3.2) can provide a neutral reference of thermal sensation for local body parts, which is derived from the thermal physiological theory defining the 'load-error' output as the deviation between the skin temperature and 'set-point' temperature (Parkinson & de Dear, 2014). This means when the skin temperature deviates from the 'set-point', the skin is unable to maintain a neutral thermal sensation. The concept of 'set-point' is borrowed from the engineering field, where it denotes

a predetermined physical reference signal within a unified control system. However, given the complexity of the human body, a singular 'set-point' proves inadequate for regulating the thermoregulation system. Besides, the term 'neutral temperature' is more precise than 'set-point' when referring to a state that does not elicit any thermal sensation. Previous research has demonstrated that neutral temperature is not a constant value; rather, it can fluctuate within a range of temperatures without inducing any sensation change (Zhang, 2003; Xie et al., 2020). Zhang (2003) proposed the skin temperature adapting threshold, defining the shift range of neutral skin temperature due to skin adaptation, which was derived from the limited indoor dataset and regression results. Later, based on the observations from outdoor measurements, Xie et al. (2020) defined the concept of the 'null zone' as the fluctuations in skin temperature in a thermal neutral zone caused by transient outdoor thermal features and to address the physiological adaptation to transient thermal environments. They filtered the measured skin temperature data of the null zone by limiting the TSV data with a range of [-1,1], and the null zone was limited by the 25th and 75th percentiles of the filtered data. Other factors, such as individual differences and thermal overshoot effect, can also contribute to a shift in neutral skin temperatures. Due to the individual difference (Wang et al., 2018), different people have different neutral skin temperatures, that is, sensitivity differences to warm or cool environments. Also, since thermal overshoot effect would highly affect thermal perceptions in outdoor conditions (Lai et al., 2017b), the same sensation would correspond to different skin temperature deviations. Therefore, under given physiological parameters, the actual output of the thermal sensation model should be a range instead of a value. Originating from the concepts of the PMV and Predicted Percentage of Dissatisfied (PPD) model (Fanger, 1970) that creates a thermal environment satisfying a certain percentage of the population, this model provides three sets of TSV values for each body part in warm-biased thermal conditions, i.e. the mean value, the 90th percentile, and the 10th percentile. The 10th percentile and the 90th percentile

can construct a predicted range ($Predicted\ range$) of TSV that covers 80% of the people. Further description of the predicted range will be presented in Section 3.3.5.2.

The model added a new parameter (C) to account for the neutral skin temperature variation caused by the effect of individual differences and thermal overshoot. Combining the terms B and C together enables us to count for the three values of the predicted local TSV at a given local skin temperature, namely the mean value, the 10th percentile, and the 90th percentile. The mathematical function is expressed as Eq. (3.3):

$$TSV_i = 4 \times \left(1 - \frac{2}{1 + e^{B \times (T_{sk,i} - T_{sk,neu,i} + C)}}\right) \tag{3.3}$$

where C is the parameter that takes into account the neutral skin temperature variation. For example, people with larger C values have lower neutral skin temperatures. Under a given $T_{sk,i}$, the higher TSV_i value means that they are more sensitive to hot environments.

3.2.3.3 $Overall\ TSV$ model

Overall thermal sensation (TSV) prediction used thermal sensation for local body parts (TSV_i) as the independent variable. TSV is a weighted average of all local thermal sensations, which has been adopted in the earlier stage of CBE model development (Zhang, 2003), as shown in Eq. (3.4). The weighting coefficient is defined as the ratio of the difference between actual overall TSV and mean TSV ($\overline{TSV}$) and the difference between local TSV and mean TSV, as presented in Eq. (3.5). Mean TSV is the average value of all local thermal sensations, calculated by Eqs. (3.6), (3.5), and (3.6) are only used for calculating the weighting coefficient for each body part during the model development stage.

$$TSV = \frac{\sum(w_i \times TSV_i)}{\sum w_i} \tag{3.4}$$

$$w_i = \frac{TSV - \overline{TSV}}{TSV_i - \overline{TSV}} \tag{3.5}$$

$$\overline{TSV} = \frac{\sum_1^n TSV_i}{n} \tag{3.6}$$

where TSV_i represents the local thermal sensation for the segment i th, w_i is the weighting coefficient for the segment i th, n is the total number of body parts.

3.2.4 Data analysis

The Anomaly Detection Toolkit (ADTK) (Chakraborty et al., 2020) Python package was used for outlier detection of the wind speed data. The Savitzky-Golay Python package (Virtanen et al., 2020), a widely used wavelet smoothing method for signal processing, was used to reduce the noise of skin temperature data. We calculated a thermal index Physiological Equivalent Temperature (PET) using the Python package pythermalcomfort (2.9.0 version) (Tartarini & Schiavon, 2020) to evaluate objective outdoor thermal conditions, where a metabolic rate of 1.0 met and clothing insulation of 0.3 clo were set as the standard conditions. PET is defined as the air temperature in a typical indoor environment at which a human's energy budget governed by skin and core temperatures is the same as in complex conditions (Peter Höppe, 1999). Linear and exponential functions were employed for data regression and model development.

3.3 Results and discussion

3.3.1 Outdoor microclimate conditions

Figure 3.2 presents the distribution of air temperature, relative humidity, wind speed, mean radiant temperature, PET, mean skin temperature, and overall TSV during the outdoor measurements. The data has been averaged for each outdoor session. The mean air temperature (T_a) was between 27.3 °C to 33.1 °C, and the relative humidity (RH) ranged from 50% to 79% (Figure 3.2, b). The mean wind speed (v) was distributed in a wide range, from a lower level (about 0.5 m/s) to a medium level (about 1.5 m/s) to a higher level (about 2.8 m/s) (Figure 3.2-

c). Mean radiant temperature (T_{mrt}) was distributed uniformly between around 28 °C to 63 °C (Figure 3.2-d).

In addition to these parameters, PET was calculated to provide a reference evaluation of outdoor thermal conditions, as shown in Figure 3.2-e. PET could provide the combined effect of environmental parameters, such as T_a, RH, v, and T_{mrt}, on human thermal physiology responses. It is worth noting that, during the outdoor measurements, the range of PET was normally uniformly distributed between around 26 °C to 40 °C, ranging from slight heat stress to strong heat stress (Matzarakis et al., 1999), while there are some extreme conditions ranging from 40 °C to 45 °C. This PET range corresponds to typical neutral to warm-biased thermal conditions, as reported by Kotharkar et al. (2024) in an earlier field study.

Besides environmental parameters, mean skin temperature and overall TSV distribution are illustrated in Figure 3.2-f, e. The mean skin temperature is distributed from 32.6 °C to 37.2 °C. Overall TSV is ranged from -2 to +4, while most TSV is in the range of around 0 to +3.5.

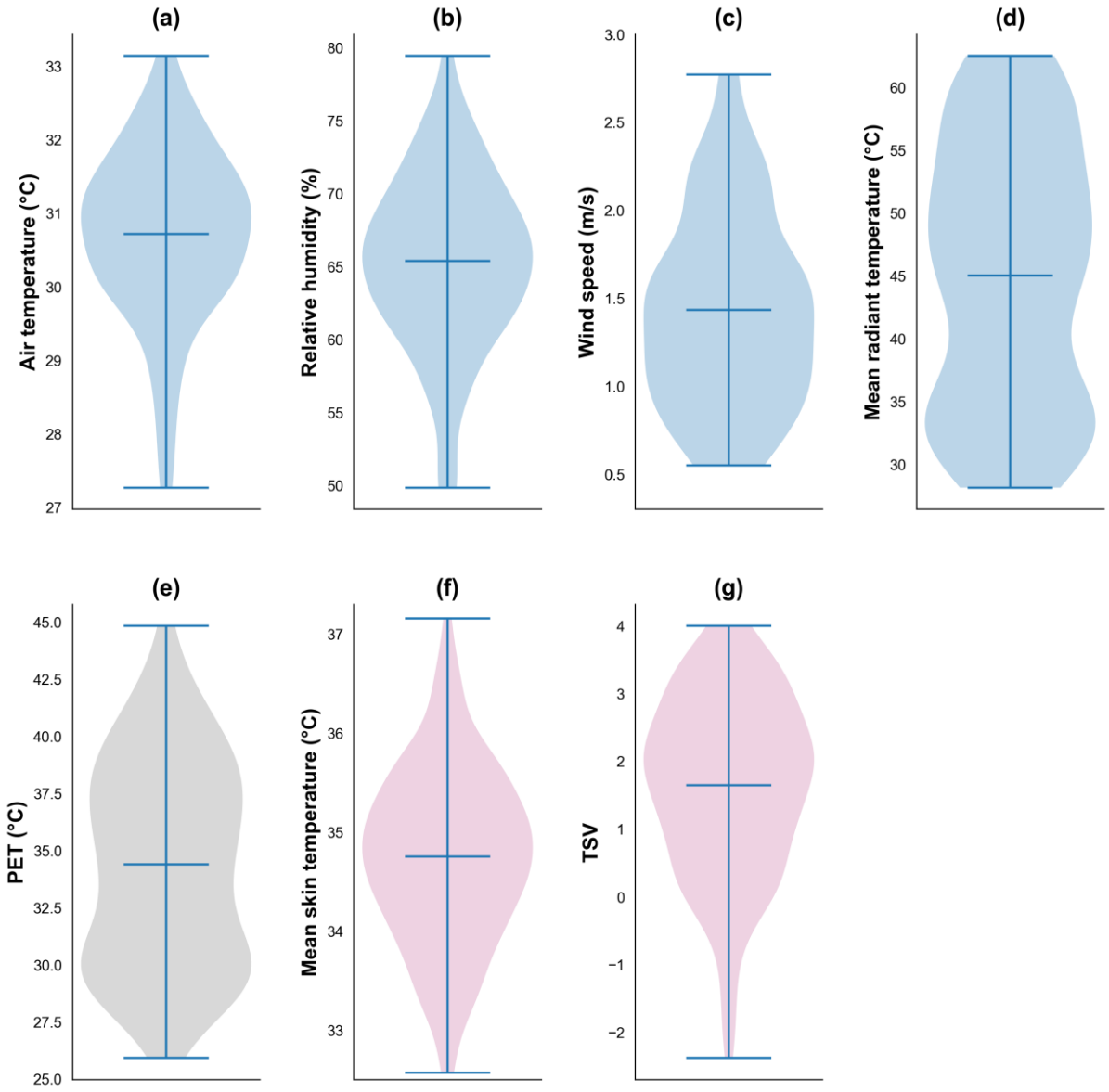

Figure 3.2 Meteorological, physiological parameters, and subjective responses during the outdoor measurements, including (a). Air temperature; (b) Relative humidity; (c) Wind speed; (d) Mean radiant temperature; (e) PET; (f) Mean skin temperature; (g) Overall TSV.

3.3.2 The effects of environmental conditions on thermal sensation

The semi-controlled experiment method enabled a relatively uniform distribution of wind speed and solar radiation levels, allowing us to analyse their effects on overall thermal sensation (Figure 3.3-a, b). The data in Figure 3.3-a were categorized into bins with wind speed

increments of 0.4 m/s and the data in Figure 3.3-b were classified into bins with T_{mrt} increments of 8 °C. The data with air temperature less than or equal to 29 °C in Figure 3.3-b were excluded to make air temperature uniformly distributed in each bin.

Linear regression was used to quantify the effect of v and T_{mrt} on TSV. Apart from the investigated independent variable, the influence of other variables on TSV is controlled to a relatively low level. The slopes of the two lines reveal that, under this study's microclimate conditions, a 1.0 m/s increase in v caused a 0.54 scale decrease in overall TSV, and a 10.0 °C increase in T_{mrt} leaded to a 0.83 scale increase in overall TSV.

Table 3.3 summarises the cooling effect of v and the heating effect and of T_{mrt} on local and overall TSVs, respectively. The effect is represented by the slope of the regression line between v or T_{mrt}, and local or overall TSV. All R^2 values for the regression lines exceed 0.65. For the cooling effect of v, exposed body segments (e.g., forehead: -0.562, upper arm: -0.520, forearm: -0.536, hand: -0.505, calf: -0.556, Neck: -0.594) have a larger slope than unexposed segments (e.g., chest and abdomen: -0.484, back: -0.507, thigh: -0.494), suggesting that exposed body segments are more likely to be affected by wind speed during outdoor conditions. There is no significant variation between body parts for T_{mrt} heating effect, but some exposed segments (upper arm: 0.083, forearm: 0.083, hand: 0.082, calf: 0.082) show slightly higher slopes. It is worth noting that the feet are insensitive to wind or radiation change. The reason might be that 78% of subjects wore sports shoes or leather shoes during the experiment, and the shoes made feet uneasily affected by the external environments.

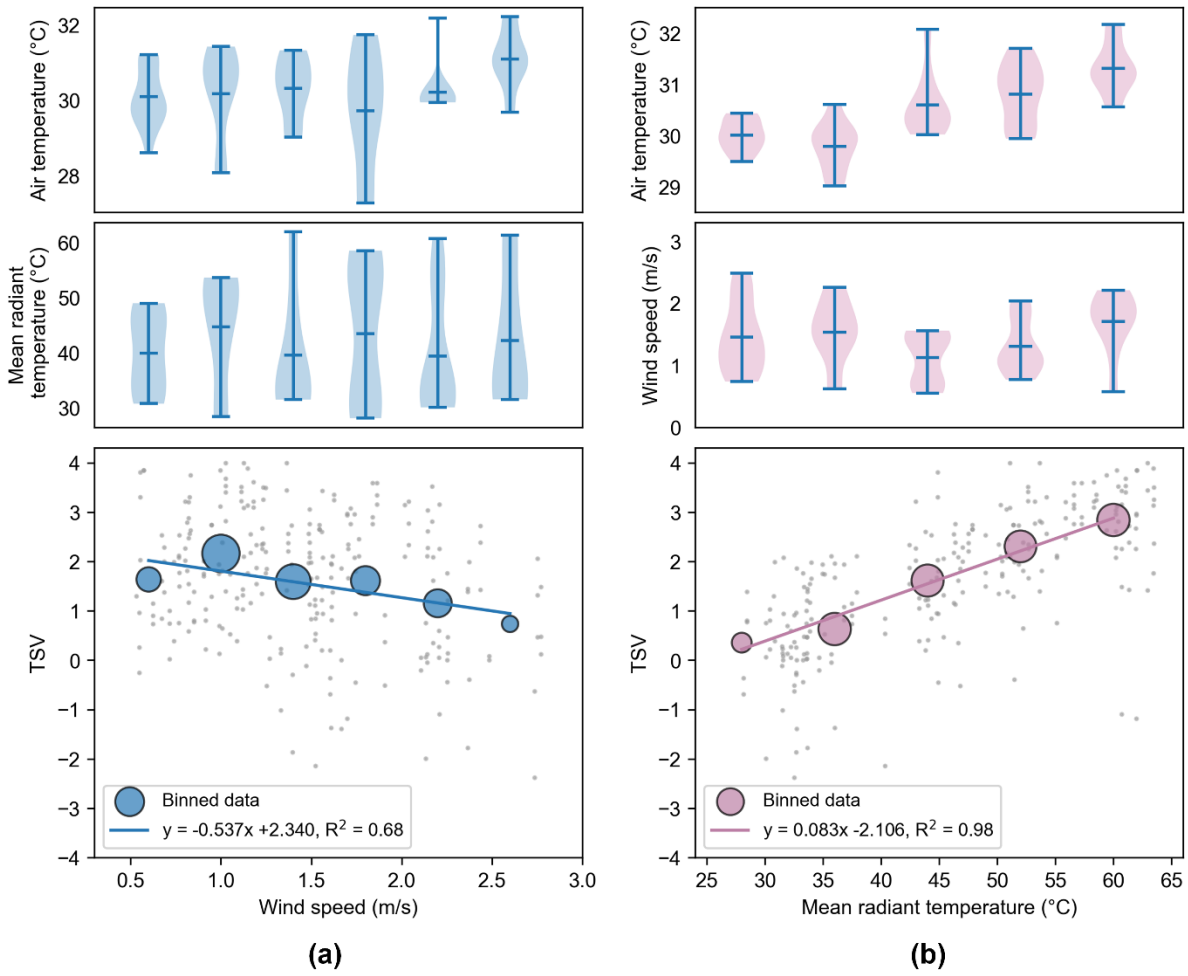

Figure 3.3 The effects of wind and radiation on overall TSV. (a). Wind speed effect; (b) Mean radiant temperature effect.

Table 3.3 Summary of the effects of wind and radiation on local and overall TSVs

	Forehead	Chest	Abdomen	Back	Upper arm	Forearm	Hand	Thigh	Calf	Foot	Neck	Overall
v	-0.562	-0.484	-0.484	-0.507	-0.520	-0.536	-0.505	-0.494	-0.556	-0.395	-0.594	-0.537
T_{mrt}	0.078	0.077	0.077	0.076	0.083	0.083	0.082	0.078	0.082	0.068	0.079	0.083

Note: the values show the slope of the regression line between v or T_{mrt}, and local or overall TSV. The negative values represent the cooling effect of a 1.0 scale increase in v on TSV, and the positive values represent the heating effect of a 1.0 scale increase in T_{mrt} on TSV.

3.3.3 Thermal physiological and subjective responses

Figure 3.4 shows an example of the variations of physiological parameters (i.e., mean skin temperature and forearm sweat rate) and overall TSV during one whole experiment session. The outdoor #1 in Figure 3.4 represents one of the most extreme situations, with PET reaching about 45 °C. Generally, $T_{m,skin}$ and arm sweat rate exhibit similar changing trends with thermal sensation.

Figure 3.4-a presents the changes in mean skin temperature and TSV during the experiment. $T_{m,skin}$ increases dramatically upon transferring from indoors to outdoors, and then gradually rises to a relatively steady state, variate within 0.5 °C within the last 5 min. TSV also significantly increases at first when transferring from indoors to outdoors, and then stabilizes at around the last three questionnaires (about 5 min before the end of each outdoor exposure). $T_{m,skin}$ and TSV show slight fluctuations in outdoor conditions, which may be mainly due to the dynamic wind environment outdoors.

Since forearm sweat rate is highly correlated with the whole body's sweat condition (Baker et al., 2019), and it seems easily affected by the external environment, the change in forearm sweat rate and TSV is selected to be illustrated in Figure 3.4-b. Since the measurement interval of sweat rate was between 5-10 min, changes in TSV cannot be accurately captured by the collected sweat rate data, but it shows a similar trend with TSV. When the subject transfers from indoors to outdoors, the forearm sweat rate slightly decreases at first due to the increased wind speed outdoors compared with indoors, and then gradually increases from the 1 min, the 5 min to the 15 min. Accordingly, different outdoor settings create different intensities of sweat

rates. For instance, sweat rates are highest under sunlit conditions, lowest under building shading conditions, and at middle level under sunshade conditions. Since the measurement frequency is limited by technical restrictions of the measurement device, the sweat rate data in this study show less accuracy than skin temperature in quantifying the dynamic changes of TSV in outdoor conditions.

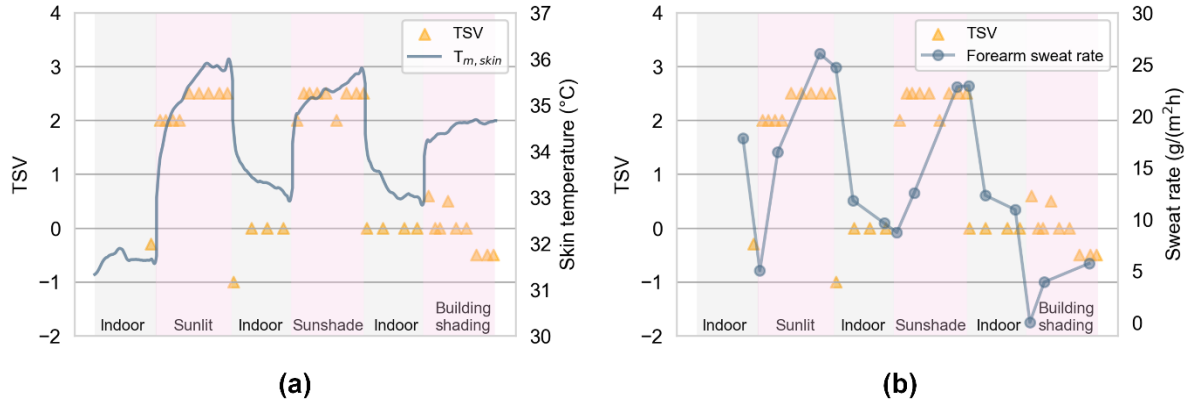

Figure 3.4 Variations in physiological responses and overall TSV during the whole experiment session. (a). Mean skin temperature and TSV; (b). Forearm sweat rate and TSV.

3.3.4 Relationships between physiological parameters and TSV under steady state

3.3.4.1 Data filtering for steady-state part

The sample data from section 3.3.3 indicates that each outdoor exposure in this experiment involved a dynamic-state condition, during which subjects transferred from indoors to outdoors and gradually adapted to the outdoor thermal environment, then reached a steady-state condition. This study focuses on the thermal responses of subjects under steady-state thermal conditions. The data in section 3.3.3 shows that the skin temperature and thermal sensation tend to stabilize at around the last 5 min, ignoring small fluctuations in environmental parameters that are inevitable for any outdoor environment. In order to develop the steady-state

part of the model, we selected data with exposure time exceeding 900 s in each outdoor condition. Air temperature and solar radiation were relatively stable among the environmental parameters during each outdoor session. However, the wind environment kept fluctuating. Previous research has shown that sudden changes in wind speed highly affect outdoor thermal comfort (Xie et al., 2020). Therefore, this study compared the differences in wind speed data from the first 15 min (dynamic-state) and the remaining data of each outdoor condition (steady-state) in order to filter out the outdoor sessions with sudden changes in the wind environment. The calculation of differences in turbulence intensity (TI) and mean v between dynamic-state and steady-state conditions were used for data filtering. TI is the ratio of the standard deviation of wind speed to the mean wind speed (ASHRAE). The TI difference and v difference were calculated as Eqs. (3.7) and (3.8):

$$TI\ difference = TI_{steady} - TI_{dynamic} \tag{3.7}$$

$$v\ difference = \frac{v_{steady} - v_{dynamic}}{v_{dynamic}} \tag{3.8}$$

where $TI_{dynamic}$ and $v_{dynamic}$ (m/s) are the TI value and v value of the first 15 min (dynamic-state) during each outdoor condition, TI_{steady} and v_{steady} (m/s) are the TI value and v value of the remaining data except for the first 15 min (steady-state) during each outdoor condition. The boxplots of TI difference and v difference are presented in Figure D1. The experimental data within the range of the lower and the upper error bars were selected for steady-state part model development. There are 203 out of 258 sets of outdoor sessions retained after filtering. Two wind speed data samples after filtering are shown in Figure D2.

3.3.4.2 Correlations between physiological parameters and TSV

Spearman analysis can provide a reference for the weight of independent variable parameters affecting dependent variables. The correlations from Spearman analysis (r_s) between local skin temperature and overall thermal sensation under steady-state conditions are summarized in

Table 3.4. The results show that there are certain associations between local and mean skin temperatures and overall TSV. Most of the r_s between local skin temperature and TSV are between 0.3 and 0.5. $T_{m,skin}$ has the strongest correlation (r_s = 0.57) with overall TSV. Among the local body parts, thigh and forearm temperatures highly correlate with overall TSV (thigh: 0.56, forearm: 0.51). A previous study focusing on dynamic outdoor thermal sensation prediction also reported similar results, with r_s between overall TSV and forearm temperature, $T_{m,skin}$ being 0.517 and 0.443, respectively (Xu et al., 2022). It should be noted that the correlations between local skin temperature and overall TSV were relatively low for the forehead, foot, and neck (forehead: 0.26, foot: 0.19, neck: 0.26). The possible reasons will be further discussed in 3.3.5.2.

Table 3.5 shows the Spearman correlations (r_s) between the local sweat rate on the forehead, abdomen, forearm ($m_{forehead}$, m_{abdo}, $m_{forearm}$), overall TSV, and $T_{m,skin}$ respectively under steady conditions. The technical limitation of instantaneous sweat rate measurement prevents the simultaneous collection of sweat rate data and survey data. Therefore, each sweat rate data was filled backward by 60 s when calculating the correlations between local sweat rate and overall TSV. In general, the correlations between local sweat rate and $T_{sk,m}$ are higher than that with overall TSV. Specifically, the abdomen sweat rate shows the highest correlation with overall TSV of 0.39, while the forehead sweat rate has the lowest correlation of 0.26. However, local sweat rate shows strong correlations with $T_{sk,m}$, with values of 0.54, 0.62, and 0.67 for the forehead, abdomen, and forearm, respectively. Among the three body parts, the forearm sweat rate correlates the best with $T_{sk,m}$. Based on the above observation, we conclude that the changes in skin temperatures may have directly reflected changes in sweat rate in outdoor conditions.

Table 3.4 Spearman correlations (r_s) between local skin temperature and overall TSV under steady state.

	$T_{forehead}$	T_{chest}	T_{abdo}	T_{back}	$T_{upper\ arm}$	$T_{forearm}$	T_{hand}	T_{thigh}	T_{calf}	T_{foot}	T_{neck}	$T_{sk,m}$
TSV	0.26	0.40	0.39	0.32	0.41	0.51	0.37	0.56	0.39	0.19	0.26	0.57

Table 3.5 Spearman correlations (r_s) between local sweat rate, overall TSV, and $T_{m,skin}$ under steady state.

	$m_{forehead}$	m_{abdo}	$m_{forearm}$
TSV	0.26	0.39	0.33
$T_{m,skin}$	0.54	0.62	0.67

3.3.4.3 Relationships between local skin temperature and local sweat rate

This section further explores the relationship between local skin temperature and local sweat rate. An exponential function was employed to explore the relationship between sweat rate and skin temperature of the forehead, forearm, and abdomen under the steady-state condition, as shown in Figure 3.5. The data were categorized into bins with an increment of 0.2 °C in skin temperature. Bins containing less than or equal to three data points were excluded from the regression to ensure robustness. The results show a close exponential relationship between the skin temperature of the three body parts and their sweat rate. A high coefficient of determination (R^2) of 0.90 illustrates the significant exponential relationship between forearm skin temperature and its sweat rate, corroborating findings from previous studies. Libert et al. (1979) reported a linear relation between mean skin temperature and arm sweat rate for resting men under heating-cooling cycles, where air and wall temperatures varied from 28 °C to 45 °C and the airspeed was 0.3 m/s. Nadel et al. (1971) found an exponential relationship between thigh skin temperature and its sweat rate for resting men in a controlled environment with air

temperatures between 25 °C and 35 °C and minimal air movement, noting a linear regression between mean skin temperature and thigh sweat rate. Thus, local skin temperature was selected as the independent variable for TSV prediction under steady-state conditions.

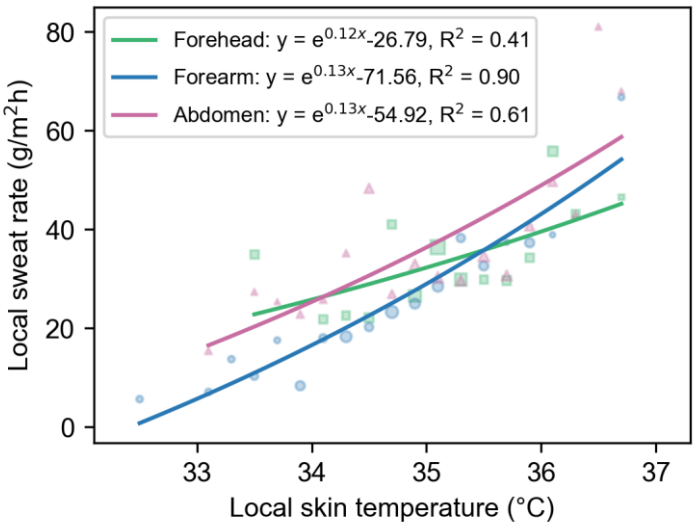

Figure 3.5 The relationship between local skin temperature and local sweat rate, including forehead, forearm, and abdomen.

3.3.5 Thermal sensation prediction for local body parts

3.3.5.1 Neutral temperature for local body parts ($T_{sk,neu,i}$)

The concept of the 'null zone' for the neutral skin temperature range is defined by Xie et al. (2020). The lower and upper limits of the null zone are defined as the values located at the 25th and 75th percentiles of the filtered data, which filters the corresponding local or overall TSV in the range [-1, 1]. The results are reproduced as shown in Figure 3.6-b (Xie et al., 2020). Adopting the same method, this study further adjusted the TSV range to [-0.5, 0.5], in order to gain a more accurate range of neutral temperature, the results are shown in Figure 3.6-a. The neutral temperature is defined as the mean value of the filtered data (shown as the mean bar in Figure 3.6-a). The neutral zone and warm-side adapting threshold from the CBE model are also

reproduced for comparison (Figure 3.6-c) (Zhang, 2003). Generally, the neutral temperatures for different body parts show a similar trend among these three studies. The neutral zone of most local body parts measured in this study (Figure 3.6-a) is narrower than those reported in Xie et al. (Figure 3.6-b, referred to as 'null zone') and Zhang's study (Figure 3.6, referred to as 'adapting threshold'), and the neutral temperature in this study are more similar to that from the 'adapting threshold' while higher than that from the 'null zone' results. The difference may be due to the different experimental conditions. The subjects in this study were exposed to more extreme conditions than those in Xie's study, which would strengthen their thermal tolerance to hot environments due to the short-term heat acclimatization effect (Cândido et al., 2012). The mean skin temperature could exceed 36 °C under sunlit conditions in this study (Figure 3.2-f), whereas the maximum mean skin temperature in Xie's study was around 35.2 °C. The subjects in Zhang's study were also exposed to high ambient temperatures, and the maximum skin temperatures could reach 36 °C. All in all, this study reinforces the idea that the neutral temperatures do change with ambient exposure. The calculated neutral temperature for local body parts ($T_{sk,neu,i}$) will be further used as the neutral sensation reference in the local thermal sensation model development part. Table 3.6 summarizes the $T_{sk,neu,i}$ value. Additionally, as the model was primarily developed for neutral to warm-biased thermal environments, a small proportion of data with $T_{m,skin}$ lower than the lower limit of the neutral zone for $T_{m,skin}$ (about 33.91 °C) will be excluded in the next step of model development.

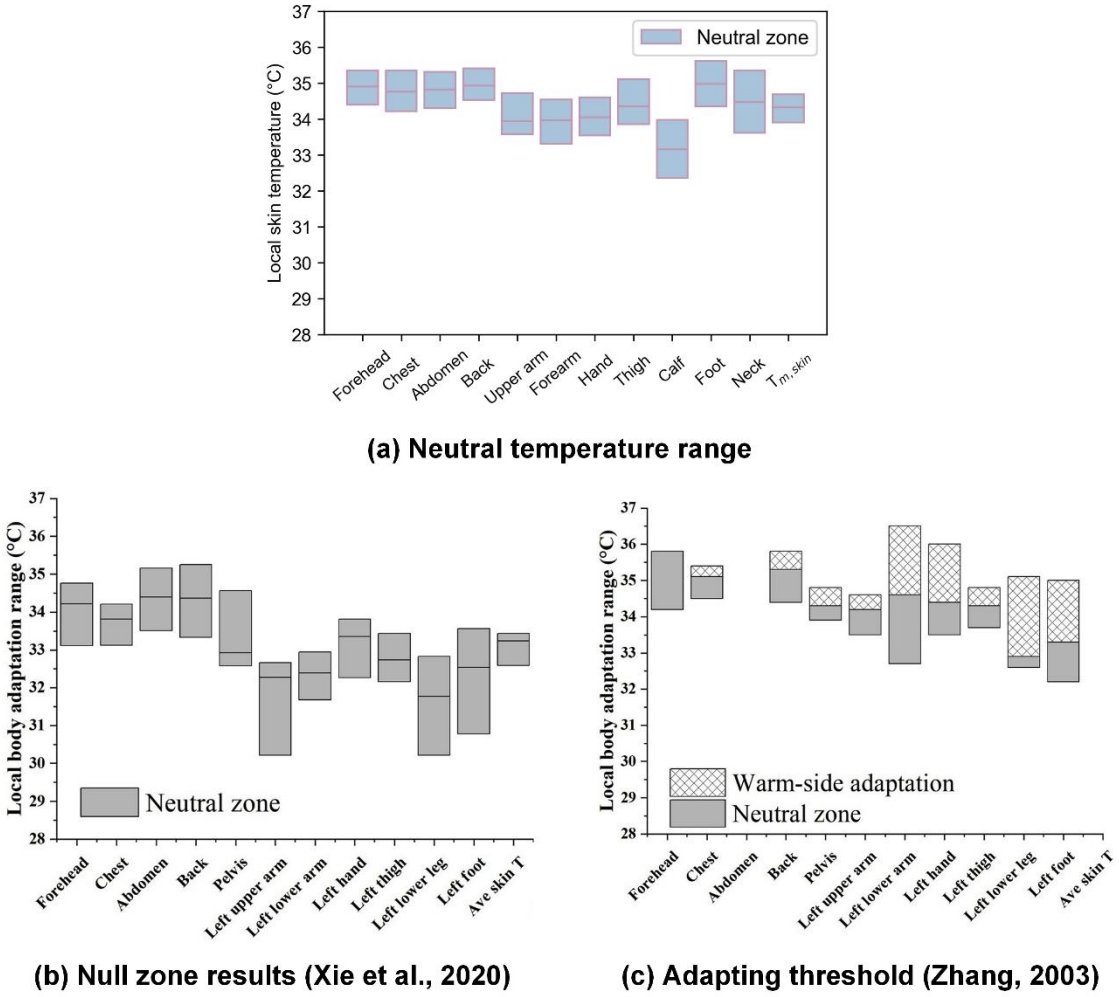

Figure 3.6 Neutral temperature range of local body parts. (a) Neutral temperature range while local or overall TSV is [-0.5,0.5] in this study; (b) Null zone results derived from Xie's study, reproduced from (Xie et al., 2020); (c). Adapting threshold derived from Zhang's study (Zhang, 2003), reproduced from (Xie et al., 2020).

Table 3.6 Summary of $T_{sk,neu,i}$ value for model development.

	Forehead	Chest	Abdomen	Back	Upper arm	Forearm	Hand	Thigh	Calf	Foot	Neck	$T_{sk,m}$
$T_{sk,neu,i}$ (°C)	34.90	34.75	34.81	34.93	33.94	33.96	34.04	34.35	33.15	34.97	34.47	34.33

3.3.5.2 $Local\ TSV$ prediction model

Figure 3.7 presents the thermal sensation regression results for different body parts, following the logistic format described in Eq. (3.3). The original data were binned by 0.2 scales of skin temperature, and bins containing less than or equal to three data points were excluded from the regression. The exponential function was employed for local thermal sensation (local TSV) regression. It is worth noting that the thermal sensation prediction range in this study considers the different neutral temperatures for different people, covering about 80% of people. In each 0.2-scale skin temperature bin, the values at the 10^{th} percentile were used to construct the lower prediction limit of the local TSV model, while the values at the 90^{th} percentile were used to construct the upper prediction limit. In the same manner, mean local TSV predictions were made using the mean values. In each regression plot from Figure 3.7, the dashed lines are the 10^{th} percentile prediction and the 90^{th} percentile prediction, respectively, while the middle solid line is the mean value prediction. Three different regression lines have different C values, which means that different people have different neutral skin temperatures. For instance, the C value of the 90^{th} percentile line is larger than that of the 10^{th} percentile line, which means that the people at the 10^{th} percentile line have a higher neutral skin temperature than the people at the 90^{th} percentile line, indicating that the people at the 10^{th} percentile line may be less sensitive to warm environments. The terms B and C are combined to control the three predicted lines of local TSV. The higher the B value, the sharper the prediction line, which means a more sensitive response to the thermal environment. Most of the body parts show a higher B value of the 90^{th} percentile line than the lines of mean and 10^{th} percentile, suggesting that the people at the 90^{th} percentile line have a higher thermal sensitivity than those at the mean and 10^{th} percentile lines.

Most of the R^2 is in the range of 0.4-0.8, which means a good regression result. Generally, the predicted TSV range around the neutral-skin-temperature condition (approximately 33.0-

34.0 °C) is wider than that around the high-skin-temperature condition (approximately above 36.0 °C). The regression results of most body parts, such as the chest, upper arm, forearm, hand, thigh, and calf, show a high coefficient of determination, while other body parts (i.e., forehead, foot, and neck) do not show satisfactory regression results. One possible reason is that the thermal sensations of the foot and neck, always remain at high values and are not affected by local skin temperatures. People are insensitive to the skin temperature changes from these body parts in warm-biased conditions, thus the coefficients between local TSV and skin temperature are relatively weak. On the other hand, in our experiment, the measured forehead and foot temperatures are limited to relatively small ranges compared to other body parts, and the relationship between skin temperature and sensation may not be significant within these ranges. For example, the foot results (Figure 3.7-j) and neck results (Figure 3.7-k) show a constant line (mean value of local TSV is about 2.06 and 2.22, respectively), which will be temporarily regarded as a constant value in the local TSV prediction model for warm-biased outdoor conditions. Other low R^2 appear especially at the lower limit line, such as forehead, abdomen, back, and upper arm results. It can be seen that when the local TSVs fall within the neutral range (from -1 to 1), the trend between local skin temperature and local thermal sensation is unclear. The reason might be that the subjects are always ambiguous about the voting semantics for thermal sensation within the neutral range. Table 3.7 summarizes the coefficients and R^2 for local thermal sensation prediction, including the prediction of mean value, upper limit (the 90^{th} percentile), and lower limit (the 10^{th} percentile).

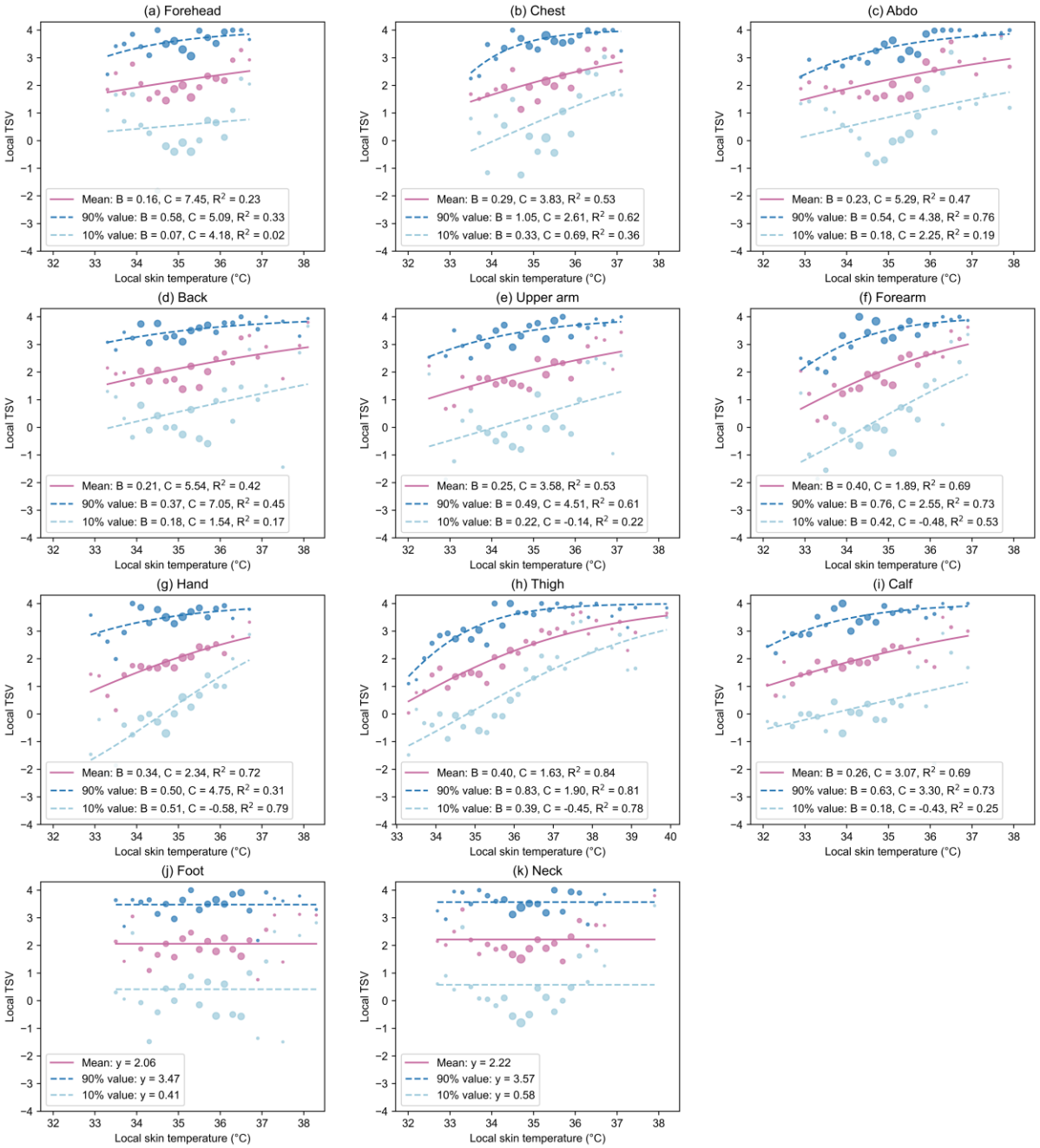

Figure 3.7 The regression analysis of the local TSV for different body parts.

Table 3.7 The coefficients and R^2 for local TSV prediction model.

	Mean			Upper limit (the 90th percentile)			Lower limit (the 10th percentile)		
	B	C	R^2	B	C	R^2	B	C	R^2
Forehead	0.16	7.45	0.23	0.58	5.09	0.33	0.07	4.18	0.02

Chest	0.29	3.83	0.53	1.05	2.61	0.62	0.33	0.69	0.36
Abdomen	0.23	5.29	0.47	0.54	4.38	0.76	0.18	2.25	0.19
Back	0.21	5.54	0.42	0.37	7.05	0.45	0.18	1.54	0.17
Upper arm	0.25	3.58	0.53	0.49	4.51	0.61	0.22	-0.14	0.22
Forearm	0.40	1.89	0.69	0.76	2.55	0.73	0.42	-0.48	0.53
Hand	0.34	2.34	0.72	0.50	4.75	0.31	0.51	-0.58	0.79
Thigh	0.40	1.63	0.84	0.83	1.90	0.81	0.39	-0.45	0.78
Calf	0.26	3.07	0.69	0.63	3.30	0.73	0.18	-0.43	0.25
Foot	y = 2.06			y = 3.47			y = 0.41		
Neck	y = 2.22			y = 3.57			y = 0.58		

3.3.5.3 Validation for $local\ TSV$ prediction model

The local TSV prediction model could provide three values at a given local skin temperature, including mean value, lower limit (the 10th percentile), and upper limit (the 90th percentile). The 10th percentile and the 90th percentile provide a $predicted\ range$. *Accuracy* is defined by the percentage of actual local TSV ($TSV_{i,actual}$) located in the $predicted\ range$, as shown in Eq. (3.9). The *Accuracy* of local TSV prediction for different body parts is summarized in Table 3.8. All of the *Accuracy* are between 0.6 and 0.8, indicating good prediction results since the model was initially developed to cover 80% of people.

$$Accuracy = \frac{Count\left(TSV_{i,actual} \in Predicted\ range\right)}{Count\left(TSV_{i,actual}\right)} \tag{3.9}$$

Table 3.8 The *Accuracy* of body parts for local TSV prediction model.

Segment	Forehead	Chest	Abdomen	Back	Upper arm	Forearm	Hand	Thigh	Calf	Foot	Neck
$Accuracy$	0.74	0.73	0.61	0.70	0.73	0.75	0.76	0.64	0.69	0.73	0.67

3.3.6 Overall thermal sensation prediction

3.3.6.1 General description of local and overall TSV

Table 3.9 presents the local and overall TSV from four subjects as examples. Both local and overall TSV values for each subject are calculated as the average of three consecutive votes obtained during one outdoor exposure under steady-state conditions. The results reveal that there is no significant variation in local TSV among different body parts. Some exposed body segments (e.g. forehead, forearm) may have a cooler sensation than other body parts, as reported by one subject (code 009), and another subject (code 028) reported significantly higher thermal sensation in unexposed body segments than other parts. In general, overall TSV tends to closely align with the average of all body parts, following the 'gradual model' when compared to other sub-models stated in the CBE model that derived overall TSV from local TSVs (Zhang et al., 2010b).

Table 3.9 Local and overall TSVs from subject samples.

	Actual local and overall TSV											
Subject code	Forehead	Chest	Abdomen	Back	Upper arm	Forearm	Hand	Thigh	Calf	Foot	Neck	**Overall**
009 (3 votes)	0.9	1.3	1.3	1.2	1.1	0.9	1.1	1.2	1.2	1.1	1.1	**1.1**
011 (3 votes)	3.1	2.7	2.7	2.7	2.7	2.9	2.8	2.7	2.8	3	2.7	**2.7**
021 (3 votes)	0.9	0.8	0.8	0.9	0.9	1.0	0.9	1.0	0.9	1.0	0.2	**0.9**

028 (3 votes)	0.3	0.8	0.8	1.5	0.3	0.3	0.3	0.3	0.3	0.3	0.8	**0.3**

3.3.6.2 $Overall\ TSV$ prediction model

Overall thermal sensation prediction for the steady-state model adopted the weighted average of the local sensations, as proposed by (Zhang, 2003) in the earlier stage of CBE model development. The weighting coefficients (w_i) for each local body part are summarized in Figure 3.8, which are obtained using Eq. (3.5) via regression analysis. The horizontal axis is the difference between the local TSV and mean TSV, and the vertical axis is the overall TSV minus mean TSV. The data were binned by 0.03 scales of the horizontal axis, and the bins with data count less than or equal to five were not used in the regression. The linear regression was employed for the weighting coefficient calculation, where the slope of the line represents the weighting coefficient (w_i). Figure 3.8 shows that the R^2 for linear regression for most body parts is larger than 0.5 except for the chest and abdomen. From the w_i results, distal body parts show higher values than those of core body parts, suggesting that the thermal sensation of distal parts highly affects overall thermal sensation in outdoor conditions. This finding is consistent with previous research (Xie et al., 2020; Xu et al., 2022), proving that the body segments exposed to the external environment (e.g., leg and arm) provide high accuracy in predicting overall thermal sensation outdoors. However, Zhang's experiment (Zhang, 2003) observed that the back and chest have a larger impact on overall sensation than the distal body parts (e.g., arm, hand, or foot) when local body parts experience cooling in a warm-biased environment. Physical differences between indoor and outdoor thermal environments may be the main reason for such a difference. As Zhang used an indoor chamber to conduct experiments, when human subjects are actively cooled for local body parts, core body parts like the chest and back have a larger impacted surface area than other parts, making them more dominant in terms of overall

sensation. For this study, in section 3.3.1, the statistics of environmental parameters and mean skin temperatures are given, illustrating that the current study is undertaken for combined effects of warm-biased, breezy, solar radiation, and humid outdoor conditions, with $T_{m,skin}$ ranging from around 32.6-37.2 °C. Likewise, the statistics of skin temperatures of each body part are given in section 3.3.5.2, showing the temperature ranges for each body part are different in this study, which are basically higher than in Zhang's experiment. In this kind of microclimate, dynamic wind speed and asymmetric solar radiation will be the dominant environmental factors influencing overall thermal sensation. In fact, in the further developed overall sensation model by Zhang (Zhang et al., 2010b), the 'gradual model' also showed that the warmer or cooler of the local body parts (like the exposed body parts in the current study), the bigger the impact on the overall thermal sensation. The distal body segments are always exposed to the external environment in summer, which are easily affected by the wind and solar radiation, therefore, these segments would have high weights on overall sensation. The weighting coefficients of different body parts for the overall TSV prediction model are summarized in Table 3.10.

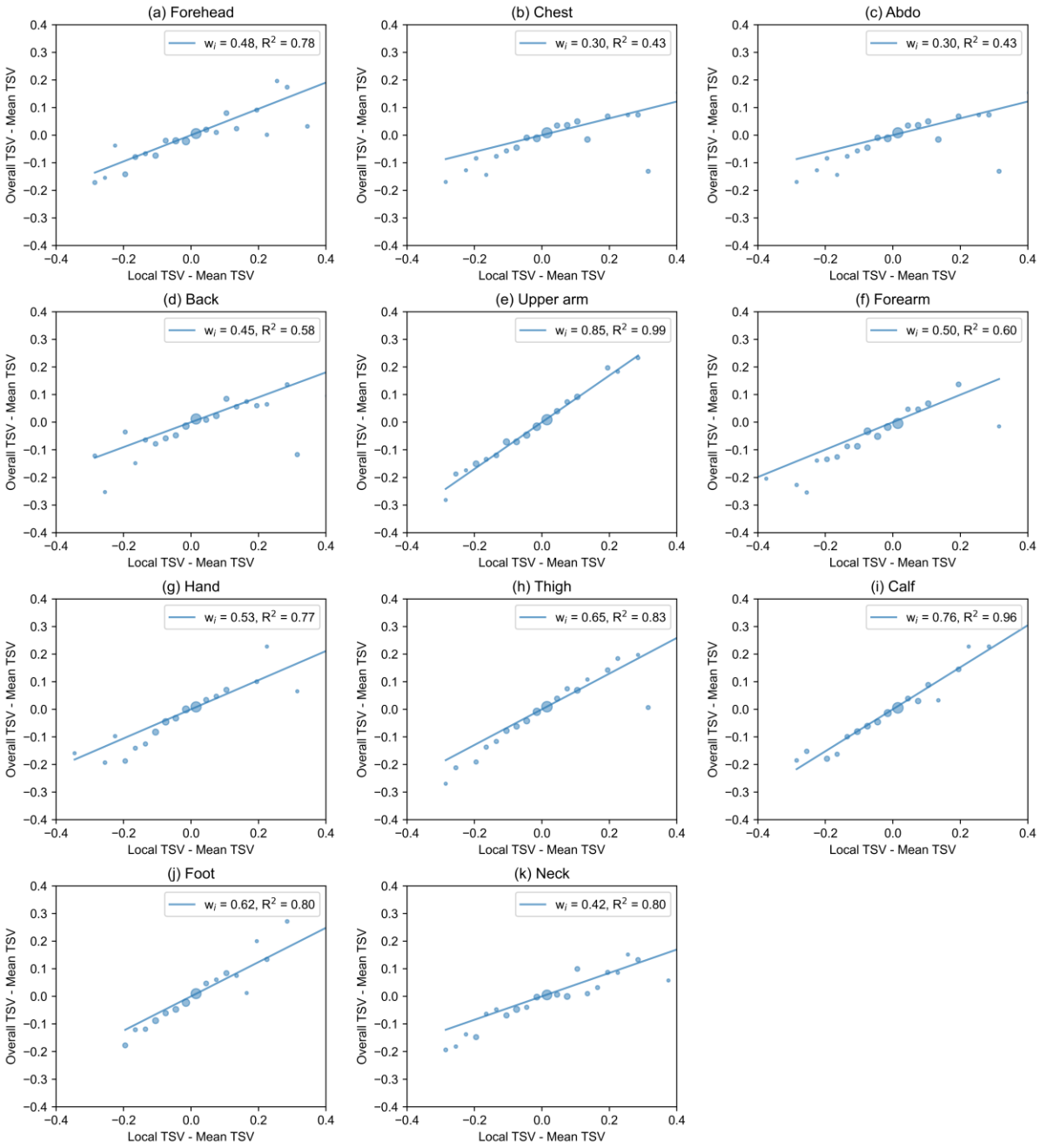

Figure 3.8 The regression results of weighting coefficients for local body parts.

Table 3.10 Summary of weighting coefficients of local body parts for the overall TSV prediction model.

Forehead	Chest	Abdomen	Back	Upper arm	Forearm	Hand	Thigh	Calf	Foot	Neck

w_i	0.48	0.30	0.30	0.45	0.85	0.50	0.53	0.65	0.76	0.62	0.42
R^2	0.78	0.43	0.43	0.58	0.99	0.60	0.77	0.83	0.96	0.80	0.80

3.3.6.3 Validation for *overall TSV* prediction model

The comparison between actual and predicted overall TSV is shown in Figure 3.9. The result shows a high R^2 between the actual and predicted overall TSV of 0.96, representing that the validated data fits well with the deviation line (y = x). Thus, the model can predict overall thermal sensation accurately based on local thermal sensations.

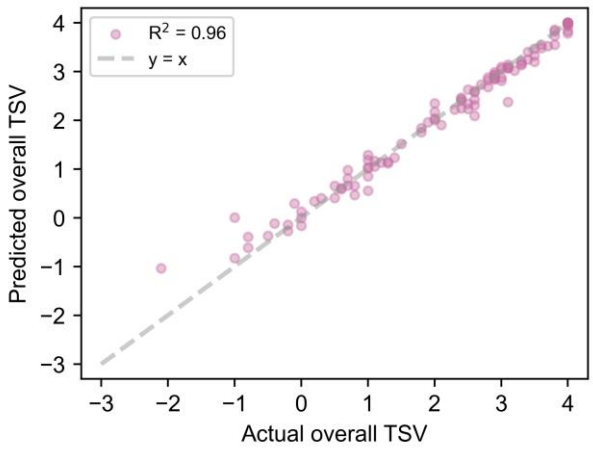

Figure 3.9 Deviation of validation dataset for overall TSV prediction model.

3.4 Implication of outdoor thermal sensation model

Small variations of any thermal environmental parameters can be easily detected by the skin (de Dear et al., 1993), and the prediction of physiological parameters in a given environmental condition can be accurately obtained by the thermoregulation models (e.g., JOS-3 model (Takahashi et al., 2021)). Current outdoor thermal sensation models are mostly developed based on indoor data and do not fully consider different outdoor conditions, this model takes

account of various outdoor settings (i.e., wind speed and solar radiation levels) from an experimental study. It contains two parts, one is the local TSV prediction model based on thermal physiological response, and another part is the overall TSV prediction model based on local TSV. The framework of the outdoor thermal sensation model in this study is presented in Figure 3.10. This model can be further integrated with the thermoregulation model (e.g., JOS-3 model) to provide thermal sensation prediction at given environmental conditions under complicated outdoor environments.

The local TSV model could output three sets of values (i.e., mean, the 10^{th} percentile, and the 90^{th} percentile) of TSV for 11 body parts, with local skin temperature as the only independent variable. The overall TSV model would output three values (i.e., mean, the 10^{th} percentile, and the 90^{th} percentile) of overall TSV, established by a weighted average of local TSV. The 10^{th} percentile and 90^{th} percentile construct a predicted range of TSV. The validation dataset was used to test the whole model's accuracy. Local skin temperatures of 11 body parts serve as the input variables, and the output consists of three values of overall TSV, as visualized in the 3D plot in Figure 3.10. In this plot, the x-axis variable is the overall TSV predicted by the model, the y-axis variable represents the mean skin temperature from the validation dataset to illustrate the trend of local skin temperature, and the actual overall TSV from the validation dataset is the z-axis variable. In the y-z projection plane, the scatters show that, from the raw data, the actual overall TSV is distributed in a range instead of a value at the same mean skin temperature. As the mean skin temperature increases, the TSV distribution range gradually becomes smaller. The x-y plane illustrates the three TSV prediction values of the model. The x-y plane illustrates the three TSV prediction values of the model. The validation result is shown in the x-z plane, indicating that 69.9% of the actual overall TSVs in the validation dataset are within the predicted 10^{th} percentile and 90^{th} percentile range.

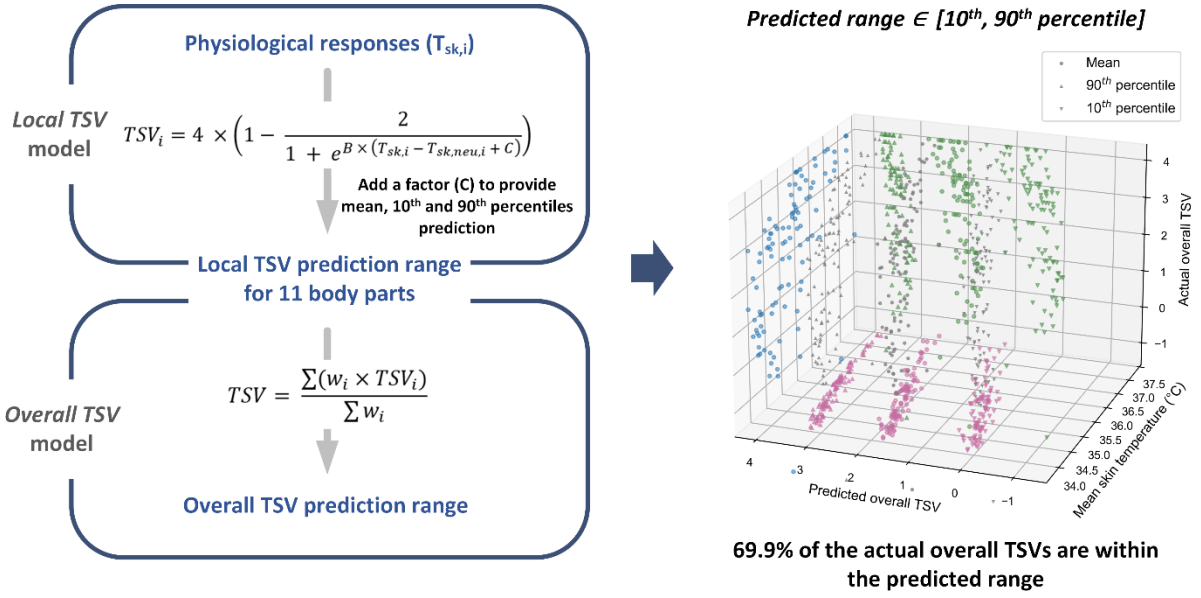

Figure 3.10 Implication and validation of the outdoor thermal sensation model in this study.

3.5 Future work

This Chapter only illustrates the development of the steady-state part of the model, other chapters will take into account the dynamic-state part (e.g., subjects transform between indoors and outdoors).

In this study, a semi-controlled experiment was used to develop a new model for outdoor thermal sensation that provides thermal sensation prediction ranges covering 80% of people. A new parameter C was first added to the local TSV prediction model by considering individual differences and thermal overshoot effect outdoors, which could provide thermal sensation prediction of a mean, 10th percentile (lower limit), and 90th percentile (upper limit) of people. In future studies, this range can be adjusted to cover fewer or more people. Experimental samples with large wind speed fluctuations have been excluded from developing the steady-state model, but the solar radiation parameter has not been screened before model development. This is because there are currently no clear indicators to quantify the intensity and frequency of solar radiation fluctuations that will cause thermal perception fluctuation, and

the solar radiation condition during a short-term outdoor session is relatively stable. The quantified impact of solar radiation fluctuation on thermal sensation needs to be further explored. The sweat rate measured in this study is not continuous, to better explore the relationship between sweat rate, skin temperature, and thermal responses, especially under high sweat rates, continuous sweat rate measurement technology is needed in future studies. Due to the unclear relationships between local skin temperatures of several body parts (i.e., forehead, foot, and neck) and local TSV, the local TSV prediction of these body parts will be further explored in a future study. Since outdoor activities (e.g., walking and standing) and individual characteristics (e.g., age, body fat, and thermal history) affect thermal perception, the model can be further developed for different activities and populations using the above approach. In addition, due to the climate characteristics of the region, the model focuses on hot summer conditions, and models for cool conditions can also be developed in future studies.

For the outdoor thermal sensation model developed in this study, there are three main differences from other mainstream models. Firstly, this study proposed a semi-controlled experiment to obtain real-life outdoor data for model development, creating various outdoor settings (i.e., 9 combination settings of different levels of solar radiation and wind speed) by a changeable windshield and shading devices. The semi-controlled experiment could improve the efficiency of data collection, realize a wide range of data under various outdoor conditions, and not cause physiological or psychological differences due to differences in indoor and outdoor environments. Thus, this model will have a higher potential for outdoor use. Secondly, the model provides thermal sensation prediction for 11 body parts. Outdoor thermal environments are more asymmetric due to the solar radiation and wind speed, the local TSV prediction model will facilitate the thermal assessment for local body segments. The local TSV prediction could also provide a performance assessment for outdoor cooling devices (e.g., radiant cooling panels (Dharmasastha et al., 2024) and mist-spraying cooling (Oh et al.,

2020b)). Lastly, considering individual differences, the model provides a prediction range of thermal sensation covering around 80% of people, which provides a new prospect for outdoor thermal comfort model development and guidance for the design of comfortable outdoor thermal environments.

3.6 Chapter conclusions

Through a series of experiments in semi-controlled outdoor environments, a model was developed that correlates the subjective thermal sensation with the thermal physiology of the human body in a relatively steady state for neutral to warm ambient conditions.

The experiment collected environmental parameters, physiological parameters (e.g., skin temperature of 18 body parts and sweat rate of 3 body parts) of the subjects, and their subjective vote (e.g., overall and local TSV). Since skin temperature and sweat rate are crucial physiological parameters affecting human thermal sensation, this study elaborated on the applicability of these parameters to predict thermal sensation and develop a model for local and overall thermal sensation prediction under relatively steady states. The findings are as follows:

1. The experiment is undertaken for warm-biased, breezy, humid outdoor conditions, under a wide range of wind speed levels (around 0.5-2.8 m/s) and solar radiation levels (T_{mrt} around 28-63 °C), with $T_{m,skin}$ ranging from around 32.5-36.5 °C. The results show that a 1.0 m/s increase in v will cause a 0.54 scale decrease in overall TSV, and a 10.0 °C increase in T_{mrt} will lead to a 0.83 scale increase in overall TSV.
2. The applicability of physiological parameters (i.e., skin temperature and sweat rate) in predicting outdoor thermal sensation has been assessed. Skin temperatures are highly associated with TSV, showing correlations of around 0.3-0.5. There is an exponential association between the local skin temperature and local sweat rate with high R^2, and

the correlations between skin temperatures and sweat rate of three measured body parts, namely the forehead, forearm, and abdomen, are around 0.6. Since the strong correlation between sweat rate and skin temperature and the fact that skin temperature is more easily predictable, local skin temperature was used to be the only predictor variable for the local TSV prediction under steady state.

3. Local TSV prediction model for 11 body parts was developed. The neutral temperature of each body part was provided to give a neutral sensation reference in the local TSV prediction model. A new parameter C was first added to the local TSV prediction model by considering individual differences and thermal overshoot effect outdoors, which could provide a prediction range covering around 80% of people, including mean, 10^{th} percentile, and 90^{th} percentile prediction.
4. Overall TSV prediction model was established by the weighted average of local TSVs. Distal body parts have a higher weighting coefficient than core parts. The predicted overall TSV fits well with the actual overall TSV, with an R^2 of 0.96, suggesting a satisfactory prediction result.
5. The whole outdoor thermal sensation model in this study could provide three values of overall TSV (i.e., the mean, the 10^{th} percentile, and the 90^{th} percentile) based on the local skin temperatures. The model can be integrated with thermoregulation models to predict thermal sensation based on environmental parameters. The 10^{th} and 90^{th} percentiles construct a predicted range of overall TSV. 69.9% of the actual overall TSVs in the validation dataset are within the predicted 10^{th} percentile and 90^{th} percentile range.

This study lays the foundation for developing a more advanced outdoor thermal sensation model. By advancing the ability to predict a range of thermal sensations rather than a single value, this study opens up new possibilities for more realistic and accurate thermal comfort

assessments. Our future work will involve other human thermal states to enhance the model's accuracy and applicability.

Chapter 4 - **Developing a physiological-parameter-based thermal sensation model for warm-biased outdoor settings: Step-up phase of the dynamic part**

4.1 Summary

There are two main limitations in the existing models above: 1) Most dynamic models were developed in indoor chambers and were not built in real-life outdoor environments. 2) Most outdoor thermal comfort models only provided overall thermal sensation prediction and did not provide the prediction of thermal sensation for local body parts, which might be important in assessing asymmetric outdoor conditions (Jiang et al., 2025). Chapter 3 filtered the steady-state data obtained from the experiments, providing the local and overall TSV prediction based on local skin temperatures when the human body is under a relatively steady state. Building upon this work, the present study uses the dynamic-state dataset obtained from the same experiments when subjects transition from indoors to outdoors. Specifically, the 'step-up' phase represents the human body experiencing an increasing thermal load, characterized by positive changes in skin temperature. This study will develop the step-up phase of dynamic local TSV predictions, which is an extension of Chapter 3. This study collected both human subjective thermal responses, in terms of local thermal sensations, and physiological responses, in terms of local skin temperatures and core temperatures, in a wide range of real-life outdoor thermal environments. There are three main objectives:

1. To explore the correlations between physiological parameters (i.e., local and mean skin temperature, and core temperature) and thermal sensation of local body parts under dynamic thermal status.
2. To discuss the applicability of different physiological parameters to predict thermal sensation of local body parts in dynamic outdoor conditions.

3. To provide the dynamic thermal sensation prediction of local body parts based on physiological responses in real-life outdoor environments.

In this study, a thermal sensation model is developed that correlates subjective thermal sensation votes (TSV) with human thermo-physiological responses in step-up dynamic thermal states under warm-biased outdoor conditions. Human subject tests (n = 86) were conducted across a realistic range of wind speeds (0.5–2.8 m/s) and solar radiation levels (T_{mrt}: 28–63 °C), using an adjustable windshield and shading device. Environmental parameters, physiological responses (e.g., local skin and core temperatures), and local and overall TSVs were collected. To address naturally occurring thermal fluctuations outdoors, two fluctuation modes are defined, namely, the highly-dynamic mode and the weakly-dynamic mode. A classification method was developed based on empirical critical values of the derivative of local skin temperature ($dT_{sk,i}/dt$), categorizing data according to the percentage of values exceeding the critical threshold within a 30 s window. The step-up phase of the dynamic model was developed via linear regression, utilizing the derivative of mean skin temperature ($dT_{sk,m}/dt$) as the independent variable for the weakly-dynamic mode, while both $dT_{sk,i}/dt$ and $dT_{sk,m}/dt$ were used for the highly-dynamic mode. The dynamic part model, integrated with the previously published steady-state part model, will improve local TSV predictions, enhancing thermal comfort assessments in outdoor environments.

4.2 Methods

4.2.1 On-site experiment settings

Environmental condition monitoring. Detailed descriptions of the experimental setups can be found in Chapter 3. The experiment site is in Hong Kong, a monsoon-influenced humid subtropical climate (Cwa, Köppen climate classification) (Peel et al., 2007), with cool dry winters and hot humid summers. The experiment was conducted on the campus of Hong Kong

Polytechnic University from June to August. Semi-controlled experimental design was adopted to create various outdoor settings efficiently. A windshield with different void sizes (75% void, 50% void, and 30% void) was used to adjust the wind speed levels people experienced. Different shading conditions, including building shade, sunshade, and sunlit, were created to adjust the solar radiation levels, as shown in Figure 4.1-a. Combining the different wind speed and solar radiation levels, the experiment settings were able to cover a wide range of outdoor thermal conditions. A mobile weather station was placed within 1.0 m of the subjects during the experiments. It consists of an air temperature and relative humidity sensor, an anemometer, and three radiometers to measure the radiant fluxes in six directions. The weather station was set at 1.3 m in height, and the radiometers were set at 1.6 m to avoid the blocking of solar radiation by other instruments. The technical information of the instruments is listed in Table 4.1.

Physiological measurements. Local skin temperatures of 18 body parts were measured by thermocouples, including the forehead, chest, back, abdomen, upper arm (left and right), forearm (left and right), hand (left and right), thigh (left and right), calf (left and right), foot (left and right), neck, and pelvis. Mean skin temperature ($T_{sk,m}$) was calculated by the seven-point weighting method (Hardy et al., 1938), including forehead, abdomen, forearm, hand, thigh, calf, and foot, and the weights were 0.07, 0.35, 0.14, 0.05, 0.19, 0.13, and 0.07, respectively. Core temperature was monitored by the eCelsius pills.

Thermal comfort surveys. A total of 1442 subjective surveys were collected from the dynamic state experiment. Among them, around 900 votes were used for developing the step-up phase model, with 80% of the data (around 720 surveys) used for model development, and 20% of the data (around 180 surveys) used for model validation. The surveys utilized in this study encompass basic information survey, such as gender, age, clothing, and health condition, as well as subjective survey of thermal environment, in terms of thermal sensation vote (TSV),

and thermal comfort vote (TCV). The TSV and TCV questionnaires employed an extended 9-point scale (Zhang et al., 2010c; Xie et al., 2019). The questionnaire asked both local and overall TSVs and TCVs. Subjects were prompted to select at least three body parts that were most different from their prior overall thermal sensation, and were then asked to provide TSV ratings for these specific body parts. In total, 10 body parts were involved in the local TSV survey, including the forehead, neck, chest, back, upper arm, forearm, thigh, calf, hand, and foot. Chest sensation was used to represent the abdomen sensation since the abdomen thermal sensation was not asked. Due to the length constraints, TCV results will not be analysed in this study.

Subjects. A total of 34 human subjects participated in the experiments, including 15 males and 19 females. Subjects were asked to wear typical summer clothes, such as T-shirt, shorts or thin trousers. From the statistics of basic information questionnaire, 78% of subjects wore sneakers or leather shoes during the experiments. The mean age is 23.4 years, the mean body mass index (BMI) is 23.5 kg/m^2, and the mean body fat is 17.7%. Detailed subject information can be found in Chapter 3.

Table 4.1Technical information of instruments for the on-site measurement, reproduced from Chapter 3.

Measurement type	Monitored parameter	Sensor/Equipment	Accuracy	Range of measurement	Sampling rate
Microclimate parameters	Air temperature (T_a)	R.M. YOUNG 41382	±0.3 °C	-50 ~ +50 °C	1 s
	Relative humidity (RH)		±1%	0 ~ 100%	
	Wind speed (v)	R.M. YOUNG 81000	±0.05 m/s	0 ~ 40 m/s	1 s
	Long-wave radiation (L_i)	Kipp & Zonen CNR-4	< 10%	-250 ~ +250 W	10 s

	Short-wave radiation (K_i)		< 5%	0 ~ 2000 W	10 s
Physiological parameters	Skin temperature	KPS-ZT-TT-T-30-1500-CZ	±1.0 °C	-200 ~ +200 °C	1 s
	Sweat rate	Delfin VapoMeter SWL5	±4%	0 ~ 200 g/m^{2}h	As needed
	Core temperature	BodyCap eCelsius	±0.2 °C	25 ~ 45 °C	15 s

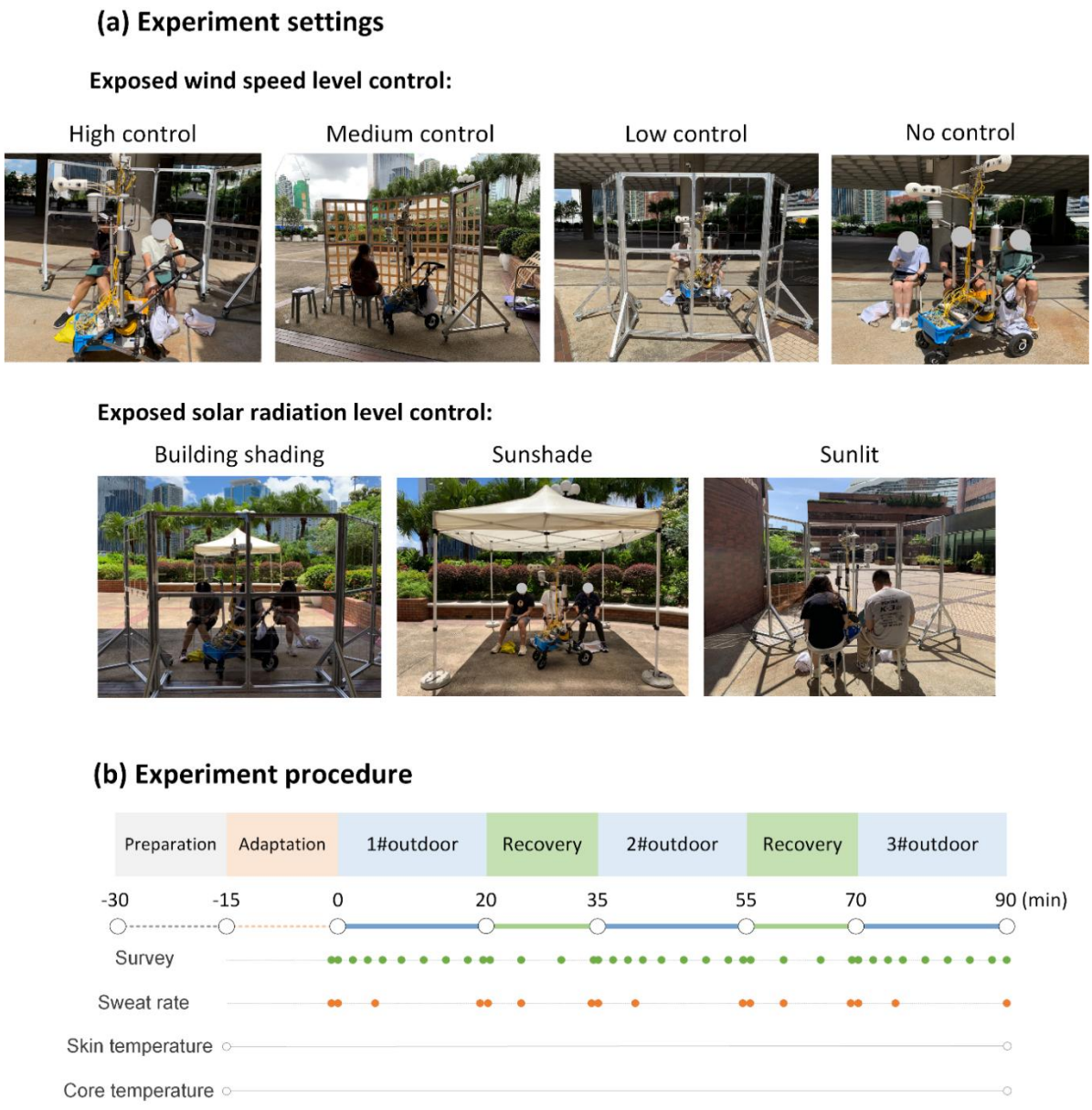

Figure 4.1 On-site measurement settings. (a). Experiment settings; (b). Experiment procedure, reproduced from Chapter 3.

4.2.2 Experiment procedure

Figure 4.1-b illustrates the experiment procedure. Subjects experienced a 15-min preparation, during which sensors were attached while they filled out a basic information survey, followed by a 15-min adaptation period to stabilize their metabolic rate in an air-conditioned indoor space (averaged environmental parameters during the adaptation period: T_a: 22.6 °C, v: 0.32 m/s, RH: 57.5%, T_{mrt}: 26.6 °C) during which they also filled out a subjective survey. Then, they experienced three different 20-min outdoor conditions, separated by two 15-min recovery periods in an air-conditioned indoor space to restore the subjects' thermal status to the initial level (Zhai et al., 2019). The subjects filled out the subjective survey every 2 min in the first 6 min and every 3 min thereafter during each outdoor session, and every 5 min during each recovery period.

Skin temperature and core temperature were monitored during the whole experiment. Each subject took part in the experiment 1-3 times, with varying experimental conditions for each session, resulting in a total of 86 human subject tests conducted. A smaller number of the subjects participated in core temperature measurement by ingesting core temperature pills 4 hours before the experiment, while 19 core temperature samples were collected, a total of 16 valid core temperature samples were usable due to the inappropriate ingestion time of some subjects. Data with an exposure duration from 0 to 15 min in each outdoor exposure were utilized for the dynamic model development in this study. The human subject tests have been approved by the HKPolyU Institutional Review Board (Reference Number: HSEARS20221023001).

4.2.3 Basic mathematical local thermal sensation model

Previous studies used the change rate of physiological parameters to represent the dynamic change in thermal sensation. CBE model (Zhang et al., 2010c) used the derivative of local skin

temperature to depict changes in local thermal status and the derivative of core temperature to represent changes in overall thermal status. Some studies (Fiala et al., 2003; Lai et al., 2017b; Vellei, 2024) adopted the derivative of mean skin temperature as the predictor to reflect changes in overall thermal status. Xu et al. (2022) employed the derivative of forearm temperature, and the derivative of tympanic temperature representing core temperature changes, to reflect changes in overall thermal status. Generally, the derivative of local skin temperature is commonly utilized to indicate changes in local thermal status, while the derivatives of mean skin temperature and (or) core temperature are used to reflect changes in the overall thermal status in previous research.

To determine the most appropriate predictor variables for quantifying dynamic thermal sensation in outdoor conditions, this study examined the changing trend of the above potential predictor variables and local thermal sensation, as well as the correlations between these variables and local thermal sensation. Due to strong correlations between the derivative of local skin temperature and dynamic local TSV, the derivative of local skin temperature was chosen as the predictor to represent changes in the corresponding local thermal status. Since the derivative of mean skin temperature showed higher correlations with dynamic local TSV than the derivative of core temperature, it was selected to represent changes in overall thermal status (detailed analysis is presented in Section 4.3.5). Previous studies indicated a highly linear association between the derivative of skin temperatures and dynamic thermal sensation (Zhang et al., 2010c; Lai et al., 2017b), thus, the basic mathematical function in this model is expressed as Eq. (4.1).

$$TSV_{i,dynamic} = K_1 dT_{sk,i}/dt + K_2 dT_{sk,m}/dt + K_3 \quad (4.1)$$

where $TSV_{i,dynamic}$ is the dynamic term of local thermal sensation, calculated by the actual local thermal sensation ($TSV_{i,actual}$) minus the mean value of steady-state local thermal sensation ($TSV_{i,steady,mean}$) which can be calculated by Chapter 3, as shown in Eq. (4.2), (4.3).

$dT_{sk,i}/dt$ is the derivative of local skin temperature, °C/s. $dT_{sk,m}/dt$ is the derivative of mean skin temperature, °C/s. K_1 and K_2 are the empirical coefficients to control the slope of lines. K_3 is an empirical constant term that arises from minor shifts of neutral skin temperature and sensation due to different exposure periods of dynamic and steady parts, and is primarily attributed to changes in thermal tolerance over time.

$$TSV_{i,dynamic} = TSV_{i,actual} - TSV_{i,steady,mean} \tag{4.2}$$

The mathematical equation of local thermal sensation under steady-state conditions, $TSV_{i,steady}$ of the model (Chapter 3), can be generally expressed as:

$$TSV_{i,steady} = 4 \times \left(1 - \frac{2}{1 + e^{B \times (T_{sk,i} - T_{sk,neu,i} + C)}}\right) \tag{4.3}$$

where $T_{sk,i}$ and $T_{sk,neu,i}$ are the skin temperature and neutral skin temperature for the ith body part, respectively, and B is an empirical coefficient. C is the new parameter that takes into account the neutral skin temperature variation for different people. The steady-state model has three sets of B and C values for each body part, which could provide a local TSV prediction range covering around 80% of people, including the mean ($TSV_{i,steady,mean}$), 10th percentile ($TSV_{i,steady,10th}$), and 90th percentile ($TSV_{i,steady,90th}$) predictions.

It is emphasized that, when the local TSV model is applied, the calculated local thermal sensation (TSV_i) would have three output values for each body part, including the mean value ($TSV_{i,mean}$), the 10th percentile ($TSV_{i,10th}$), and the 90th percentile ($TSV_{i,90th}$), which will be determined by adding the dynamic term ($TSV_{i,dynamic}$) to the three values of the steady-state terms ($TSV_{i,steady,mean}, TSV_{i,steady,10th}, TSV_{i,steady,90th}$) (Chapter 3), as presented in Eqs. (4.4-4.6).

$$TSV_{i,mean} = TSV_{i,dynamic} + TSV_{i,steady,mean} \tag{4.4}$$

$$TSV_{i,10th} = TSV_{i,dynamic} + TSV_{i,steady,10th} \tag{4.5}$$

$$TSV_{i,90th} = TSV_{i,dynamic} + TSV_{i,steady,90th} \tag{4.6}$$

The equation of TSV_i can be generally expressed as:

$$TSV_i = 4 \times \left(1 - \frac{2}{1 + e^{B \times (T_{sk,i} - T_{sk,neu,i} + C)}}\right) + K_1 dT_{sk,i}/dt + K_2 dT_{sk,m}/dt + K_3 \quad (4.7)$$

where TSV_i is the local thermal sensation calculated by this model.

4.2.4 Data analysis

The Savitzky-Golay Python package (Virtanen et al., 2020), a wavelet smoothing method for signal processing, was employed to reduce the noise of raw skin temperature data. The derivative of skin temperature is calculated using the difference between two successive skin temperature data points taken every second, denoted in units of °C/s. The exponential weighted moving average method was further employed for smoothing the calculated derivatives. The core temperature and its derivative smoothing were carried out using the same method. Figure E in the Appendix shows a sample of the smoothed results for skin temperature and its derivative. Physiological Equivalent Temperature (PET) was used to characterize the overall thermal conditions of the outdoor environments, calculated by the Python package pythermalcomfort (2.9.0 version) (Tartarini & Schiavon, 2020) with a metabolic rate of 1.0 met and clothing insulation of 0.3 clo. Linear functions were utilized for data regression.

4.3 Results

4.3.1 Outdoor thermal environment

Table 4.2 summarizes the environmental parameters during the outdoor measurements, including mean, standard deviation, maximum, and minimum values of air temperature (T_a), relative humidity (RH), wind speed (v), mean radiant temperature (T_{mrt}), and PET. T_a ranges from 27.3 to 33.1 °C, v from 0.55 to 2.77 m/s, and T_{mrt} from 28.1 to 62.5 °C. PET value ranges from 25.9 to 44.8 °C, indicating slight heat stress to extreme heat stress (Matzarakis et al.,

1999), and this range corresponds to the typical neutral to hot thermal conditions based on the observation of a previous field study (2024). The mean skin temperature and thermal sensation ranges are also illustrated in Table 4.2, with $T_{sk,m}$ ranges from 32.6 to 37.2 °C, and overall TSV ranges from -2.4 to 4.0, representing cool to extremely hot conditions. According to these environmental and physiological results, the thermal conditions during the measurements were neutral to warm-biased, covering the typical climate conditions of the Cwa climate zone.

Table 4.2 General information of environmental parameters, $T_{sk,m}$ and overall TSV during the outdoor measurement

	T_a (°C)	RH (%)	v (m/s)	T_{mrt} (°C)	PET (°C)	$T_{sk,m}$ (°C)	TSV
Average	30.7	65.4	1.43	44.9	34.4	34.8	1.64
Standard deviation	1.2	5.9	0.55	10.4	4.4	0.89	1.3
Maximum	33.1	79.4	2.77	62.5	44.8	37.2	4.0
Minimum	27.3	49.8	0.55	28.1	25.9	32.6	-2.4

4.3.2 Dynamic variation of TSV

When individuals experience a thermal stimulus in an indoor chamber, four main types of thermal response behaviour may be observed: quick overshooting, longer overshooting, flat pattern, and gradual pattern (Zhang, 2003), according to monitored changing trends of skin temperature and thermal sensation. The quick overshooting pattern shows a rapid and sudden jump following thermal stimuli, whereas the longer overshooting pattern shows a prolonged jump lasting approximately 5-8 minutes after thermal stimuli (Zhang, 2003). The flat pattern is characterized by a relatively constant thermal sensation value when exposed to thermal stimuli, whereas the gradual pattern means that thermal sensation changes gradually along with the variations in skin temperature (Zhang, 2003).

The trends of overall thermal sensation and mean skin temperature for four samples throughout the experiment are shown in Figure 4.2. Some TSVs follow the variations in $T_{sk,m}$, displaying a gradual pattern (e.g., Figure 4.2-b-outdoor#1, Figure 4.2-d-outdoor#1&#3). Some demonstrate sensitivity to dynamic changes in thermal condition, exhibiting a quick overshooting pattern (e.g., Figure 4.2-b-outdoor#2&#3, Figure 4.2-d-outdoor#2) or longer overshooting pattern (e.g., Figure 4.2-a-outdoor#3, Figure 4.2-c-outdoor#2&#3), while some show a flat pattern under outdoor conditions (e.g., Figure 4.2-a-outdoor#1&#2). However, due to the dynamic outdoor features, irregular pattern can be observed from some votes have, but the changing trends highly accord with the change rates of $T_{sk,m}$ (e.g., Figure 4.2-c-outdoor#1). These abrupt jumps resulting from variations in physiological parameters will be quantified in the dynamic local TSV model, by exploring the relationship between the change rate of physiological parameters and the dynamic term of local TSV.

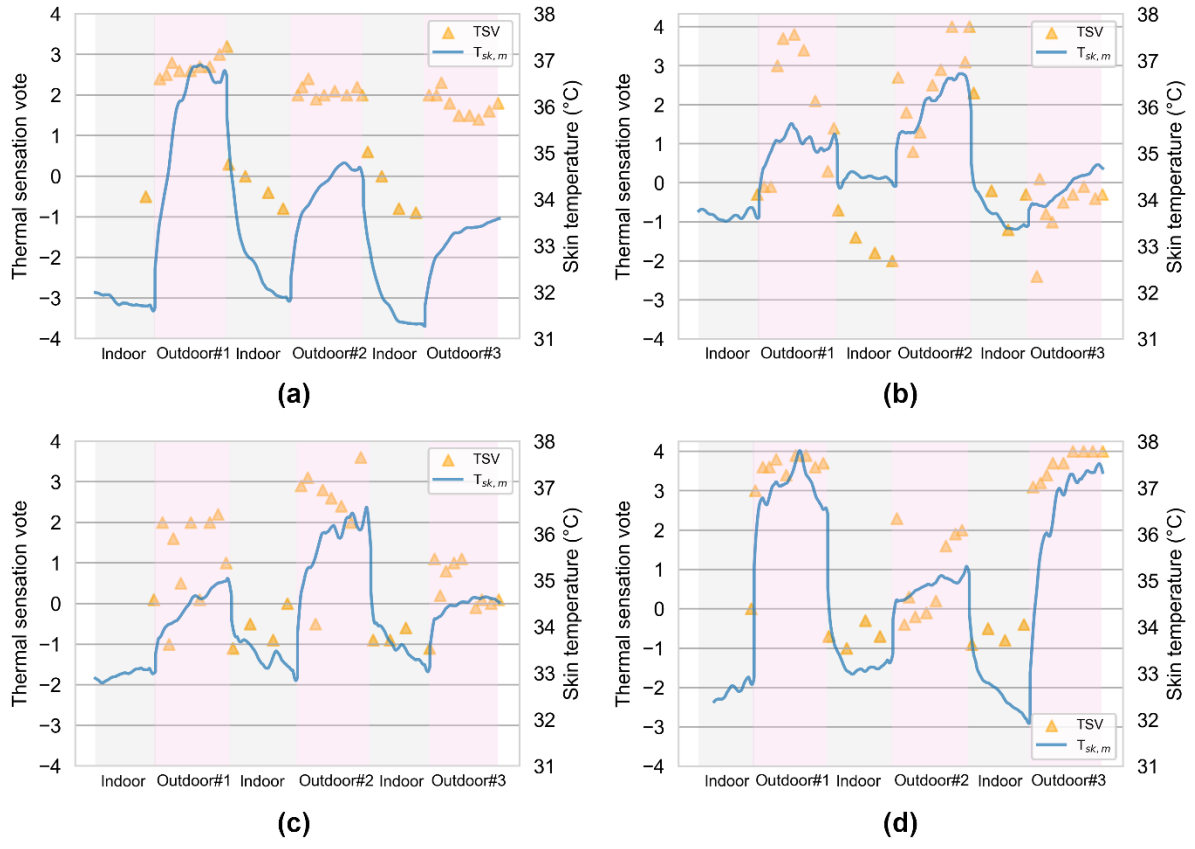

Figure 4.2 Temporal variation of overall thermal sensation and mean skin temperature during the experiment (four samples). (a). 23072023_018 (DD/MM/YYYY_subject code); (b). 08072023_021; (c). 07082023_034; (d). 14072023_025.

4.3.3 Dynamic variations of physiological parameters and local TSV

Local skin temperature can be used as an indicator of local thermal status, while mean skin temperature and core temperature could serve as indicators of overall thermal status. Since the large arteries of the pelvis region always represent core of human body (Hymczak et al., 2021), pelvis temperature is included as a comparison with measured core temperature due to its proximity to the body's core and the ease of measurement. Since a strong correlation has been observed between the forearm temperature and thermal sensation (Jiang et al., 2024), the forearm is chosen as the local body part to observe the variation trends between physiological parameters and local TSV.

Figure 4.3-a, b shows the variations of physiological parameters (i.e., forearm temperature, mean skin temperature, pelvis temperature, and core temperature) and forearm TSV during one experiment. Since local TSVs were not acquired during indoor recovery periods, overall TSV is illustrated in the indoor conditions in Figure 4.3 (blue triangle). Subjects swallowed the pills about four hours before the experiment. In general, pelvis temperature does not reflect the changes in forearm TSV well. While $T_{sk,m}$ and forearm temperature show co-variation with forearm TSV, core temperature exhibits an opposite variation with forearm TSV, showing similar results with Zhang's study (Zhang, 2003). The observed decrease in core temperature during the transition from a cool indoor environment to a hot outdoor environment can be attributed to the physiological response of skin vasodilation. While in the cool indoor condition, peripheral blood temperature remains relatively low. Upon exposure to the hot outdoor environment, vasodilation increases peripheral blood flow, allowing a greater volume of cooler

blood to exchange heat with body core, resulting in a temporary reduction in core temperature. This mechanism is consistent with predictions made by well-known thermoregulation models, such as the Stolwijk model (Stolwijk, 1971) and the JOS-3 model (Takahashi et al., 2021).

It should be noted that during our measurements, most core temperature samples exhibited an opposite variation with local TSV, while a small number of samples showed irregular trends. A sample in Figure 4.3-c shows irregular trends between core temperature and forearm TSV. This is mainly because the real-life outdoor conditions may not induce notable changes in core temperature. Further explanation will be provided in Section 4.4.1. Therefore, given the trendless results shown in the collected core temperature from our existing samples, it may not be a reliable indicator for thermal perception modelling in this study.

Among these parameters, local skin temperatures exhibit the strongest correlation with local TSV compared to $T_{sk,m}$ and core temperature. Accordingly, forearm skin temperature may serve as a reliable parameter for representing the influence of local thermal status variations influencing forearm TSV under non-uniform thermal conditions, while $T_{sk,m}$ and core temperature could be utilized as parameters to represent the impact of overall thermal status on local TSV.

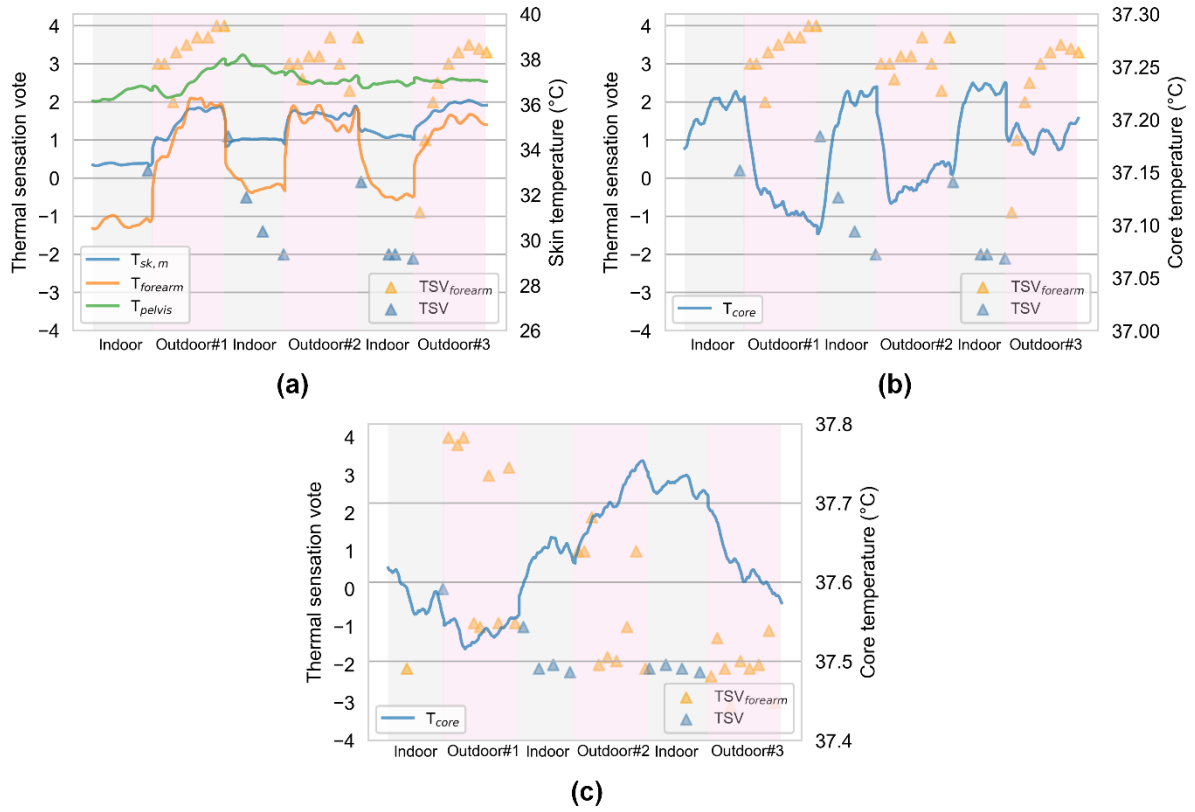

Figure 4.3 Temporal variations of physiological parameters and local TSV. (a). Forearm temperature, mean skin temperature, pelvis temperature, and forearm TSV; (b). Core temperature and forearm TSV; (c). Core temperature and forearm TSV from another sample.

4.3.4 Distribution of TSV and skin temperature during outdoor exposure

This study focuses only on the periods when the derivative local or mean skin temperature is positive, called step-up phase. The variations in thermal sensation, including overall, forearm, and chest TSV of all subjects during the 20-min outdoor exposures (time "0" represents the first vote outdoors), are presented in Figure 4.4. The forearm and chest are selected to represent the exposed and unexposed body segments, respectively. The boxplot represents the statistical distribution of the data with the exposure time, and the mean dots show the mean value of each box. Figure 4.4 illustrates that the average TSV of all subjects shows a quick increase between the first and second votes (whin 2 min after transitioned to outdoor). After that, the overall

thermal sensations remain generally stable. There are no significant differences among overall, forearm, and chest TSVs, although chest TSVs are slightly higher compared with overall and forearm TSVs during the final phase (9-20 min).

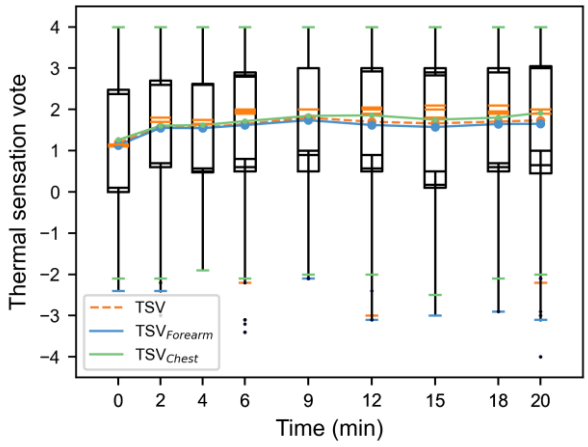

Figure 4.4 Variations and distribution of thermal sensation during outdoor exposure.

Figure 4.5 illustrates the dynamic variations of skin temperatures (i.e., $T_{sk,m}$, forearm, and chest temperature) and their derivatives of all subjects during 20-min outdoor exposures. Mean skin temperature (Figure 4.5-a) initially started at the lowest point with a mean value of $T_{sk,m}$ around 34.1 °C, then increased to approximately 34.7 °C within the first 6 min, and eventually stabilized with minor fluctuations around 35.0 °C after the 9th min. Among the measured $T_{sk,m}$, forearm, and chest temperature, the chest temperature is the highest, with the forearm temperature being the lowest (Figure 4.5-a). This phenomenon can be attributed to the forearm's distal location and its constant exposure to the external environment during summer. Accordingly, the temperature change in the forearm is bigger than the changes of skin temperatures of chest and mean.

The derivatives of mean skin temperature (Figure 4.5-b) initially peaked at a rate of approximately 0.006 °C/s (mean value of $dT_{sk,m}/dt$), then dramatically declined to about

0.001 °C/s within the first 6 minutes. After the 9th min, all the derivatives gradually stabilize, maintaining a low value (close to zero). The derivative of forearm temperature is higher than that of the chest and $T_{sk,m}$ (as shown in Figure 4.5-b).

According to the above observations, notable differences exist in the derivatives of local skin temperatures ($dT_{sk,i}/dt$) between the first 6 minutes and the period after the 9th min during the 15-minute outdoor exposures. Consequently, the data will be divided into two phases: the highly-dynamic period in the initial period 0-450 s, characterized by significant variations, and the weakly-dynamic period in the later period 450-900 s, marked by minor fluctuations. During the highly-dynamic period, results from transitions between indoor and outdoor environments caused large $dT_{sk,i}/dt$. Conversely, the weakly-dynamic period arises from minor natural environmental variations with small $dT_{sk,i}/dt$. It is worth noting that the slight variations with small derivatives of skin temperature commonly exist in outdoor settings due to its dynamic thermal features, such as variations caused by breeze, which may not be observed in steady indoor conditions.

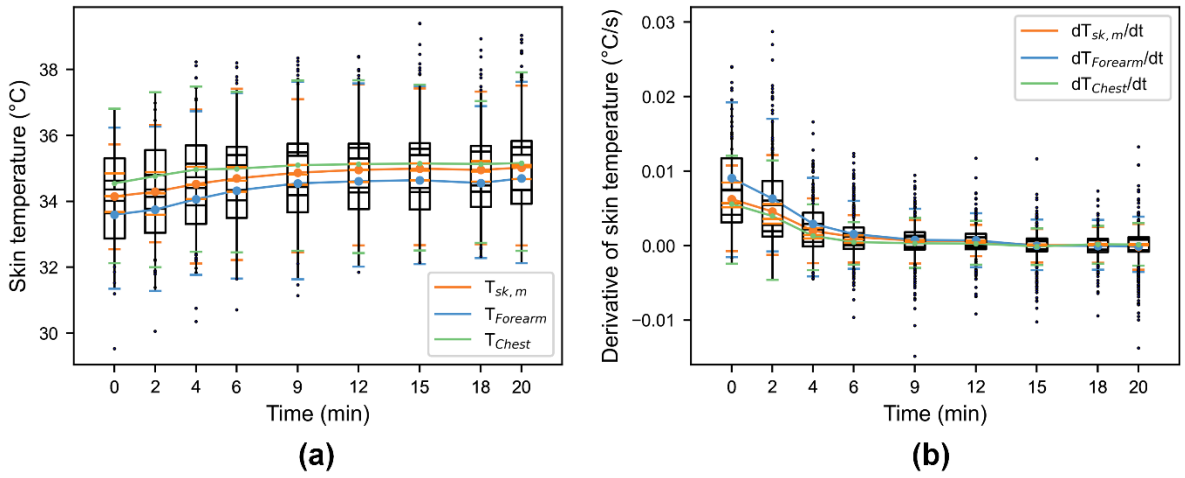

Figure 4.5 Variations and distribution of skin temperatures and their derivatives during outdoor exposures. (a). Skin temperatures; (b). Derivative of skin temperatures.

4.3.5 Selection of predictor variables

Table 4.3 shows the Spearman correlations (r_s) and p-values between local skin temperature, $T_{sk,m}$ and local TSV of the highly-dynamic and weakly-dynamic periods. In general, the correlations of most body parts (e.g., chest, abdomen, arm, and thigh) in the weakly-dynamic period are slightly larger than those in the highly-dynamic period. All the p-values are zero indicating statistically significant correlations. Among different body parts, the correlations of the back, forearm, and thigh are higher than others in the highly-dynamic period, while in the weakly-dynamic period, the correlations of the chest, forearm, and thigh are higher.

The change rate of skin temperatures affect thermal sensations (Lai et al., 2017b). Table 4.4 shows the r_s and p-values between the derivative of local skin temperature and the dynamic term of local TSV ($TSV_{i,dynamic}$) of highly-dynamic and weakly-dynamic periods. To find the correlations in the step-up phase, data with $dT_{sk,i}/dt$ larger than zero were selected for further correlation analysis between $dT_{sk,i}/dt$ and $TSV_{i,dynamic}$. In general, the correlations are much lower between $dT_{sk,i}/dt$ and $TSV_{i,dynamic}$ than those between $T_{sk,i}$ and local TSV. The p-values are below 0.05, except for the thigh during the highly-dynamic period, and the hand, thigh, and neck during the weakly-dynamic period. The results exhibit insignificant differences in the correlations between the highly-dynamic and weakly-dynamic periods.

Table 4.5 illustrates the r_s and p-values between the $dT_{sk,m}/dt$, the derivative of core temperature (dT_{core}/dt), and $TSV_{i,dynamic}$ of highly-dynamic and weakly-dynamic periods. Data with $dT_{sk,m}/dt$ larger than zero were selected for further correlation analysis between $dT_{sk,m}/dt$ and $TSV_{i,dynamic}$. Given the reverse variation between core temperature and thermal sensation (Zhang, 2003), data with dT_{core}/dt smaller than zero were selected for correlation analysis between dT_{core}/dt and $TSV_{i,dynamic}$. Generally, $dT_{sk,m}/dt$ exhibits notably higher correlations (p-values < 0.05, except for the thigh) with $TSV_{i,dynamic}$ compared

with dT_{core}/dt (p-values > 0.05), thereby $dT_{sk,m}/dt$ would be a more suitable predictor for outdoor applications compared with dT_{core}/dt. The reason might be the fact that core temperature tends to be insensitive to external environment changes in real-life outdoor conditions, thereby limiting its effectiveness in capturing thermal status changes in outdoor environments. In addition, as mentioned in Section 4.3.3, core temperature samples did not exhibit consistent trends. Consequently, some values of dT_{core}/dt showed negative correlations with $TSV_{i,dynamic}$, while others exhibited positive correlations, thereby limiting the applicability for modelling.

Therefore, given the strong associations between $dT_{sk,i}/dt$, $dT_{sk,m}/dt$, and $TSV_{i,dynamic}$ in the highly-dynamic period, $dT_{sk,i}/dt$ and $dT_{sk,m}/dt$ will be used as the independent variables in the highly-dynamic period. $dT_{sk,i}/dt$ would better capture local body sensation changes when the whole body experiences significant dynamic and asymmetric conditions. $dT_{sk,m}/dt$ could reflect the impact of overall thermal sensation changes on local TSV, and incorporating $dT_{sk,m}/dt$ for some body parts may enhance the stability of the predicted results. Due to the high correlations between $dT_{sk,m}/dt$ and $TSV_{i,dynamic}$ in the weakly-dynamic period, $dT_{sk,m}/dt$ is selected as the independent variable for the TSV prediction in this period. The weakly-dynamic period is induced by minor environmental changes, such as slight fluctuation in wind speed, which do not lead to significant dynamic and asymmetric thermal conditions. Consequently, $dT_{sk,i}/dt$ is not employed as the independent variable for the weakly-dynamic period.

Table 4.3 Spearman correlation analysis between local skin temperature and local TSV (TSV_i) of highly-dynamic and weakly-dynamic periods.

			$T_{forehead}$	T_{chest}	$T_{abdomen}$	T_{back}	$T_{upper\ arm}$	$T_{forearm}$	T_{hand}	T_{thigh}	T_{calf}	T_{foot}	T_{neck}	$T_{sk,m}$ with overall TSV
Local TSV	Highly-dynamic period	r_s	0.38	0.33	0.27	0.44	0.38	0.48	0.39	0.46	0.38	0.17	0.37	0.44
		p-value	0	0	0	0	0	0	0	0	0	0	0	0
	Weakly-dynamic period	r_s	0.36	0.45	0.40	0.35	0.42	0.52	0.39	0.53	0.39	0.16	0.30	0.55
		p-value	0	0	0	0	0	0	0	0	0	0	0	0

Table 4.4 Spearman correlations analysis between the positive derivative of local skin temperature and dynamic term of local TSV ($TSV_{i,dynamic}$) of highly-dynamic and weakly-dynamic periods.

			$dT_{forehead}/dt$	dT_{chest}/dt	$dT_{abdomen}/dt$	dT_{back}/dt	$dT_{upper\ arm}/dt$	$dT_{forearm}/dt$	dT_{hand}/dt	dT_{thigh}/dt	dT_{calf}/dt	dT_{foot}/dt	dT_{neck}/dt
$TSV_{i,dynamic}$	Highly-dynamic period	r_s	0.09	0.16	0.23	0.16	0.15	0.14	0.09	0.05	0.15	0.11	0.11
		p-value	0.04	0	0	0	0	0	0.01	0.21	0	0	0.01
		r_s	0.12	0.24	0.13	0.21	0.22	0.12	0.03	0.02	0.25	0.34	0.04

Weakly-dynamic period	p-value	0.04	0	0.01	0	0	0.02	0.54	0.71	0	0	0.49

Table 4.5 Spearman correlations analysis between the positive derivative of mean skin temperature and negative derivative of core temperature, and dynamic term of local TSV ($TSV_{i,dynamic}$) of highly-dynamic and weakly-dynamic periods.

			$TSV_{i,dynamic}$										
			Forehead	*Chest*	*Abdomen*	*Back*	*Upper arm*	*Forearm*	*Hand*	*Thigh*	*Calf*	*Foot*	*Neck*
$dT_{sk,m}/dt$	Highly-dynamic period	r_s	0.13	0.18	0.18	0.14	0.19	0.15	0.17	-0.01	0.16	0.12	0.18
		p-value	0	0	0	0	0	0	0	0.70	0	0	0
	Weakly-dynamic period	r_s	0.26	0.22	0.24	0.26	0.30	0.21	0.21	0.08	0.23	0.28	0.25
		p-value	0	0	0	0	0	0	0	0.12	0	0	0
dT_{core}/dt	Highly-dynamic period	r_s	-0.02	-0.11	-0.08	-0.05	-0.10	0.02	0.02	-0.11	-0.01	0.05	-0.04
		p-value	0.87	0.29	0.43	0.59	0.34	0.91	0.84	0.26	0.94	0.64	0.70
	Weakly-dynamic period	r_s	-0.01	-0.10	-0.12	-0.16	0.13	0.14	0.20	-0.15	0.18	0.19	0.12
		p-value	0.93	0.53	0.49	0.35	0.42	0.41	0.23	0.36	0.28	0.24	0.45

4.3.6 Classification of highly-dynamic and weakly-dynamic modes

In the previous section, we divided the data into highly-dynamic and weakly-dynamic periods based on the data received during exposure outdoors. Figure 4.6 shows the boxplot of the absolute value of the derivative of mean skin temperature ($|dT_{sk,m}/dt|$) in the highly-dynamic and weakly-dynamic periods. There is a notable difference in the $|dT_{sk,m}/dt|$ between the two periods, the 25th percentile of the highly-dynamic period is obviously higher than the 75th percentile of the weakly-dynamic period. The 25th and 75th percentiles of the $|dT_{sk,m}/dt|$ in the highly-dynamic period are 0.00171 and 0.00393, respectively, while in the weakly-dynamic period, the values are 0.00061 and 0.00160, respectively.

The 25th percentile of the highly-dynamic period or the 75th percentile of the weakly-dynamic period might be the critical value to classify the two data groups, because they are similar in both periods, indicating a transition between the two periods. The weakly-dynamic data group consists of minor variations caused by natural environmental fluctuations outdoors that remain within a certain threshold, while the highly-dynamic data group exhibits relatively larger variations due to abrupt transient or dynamic environmental changes caused by space changes and activation of active cooling. Given that the 75th percentile of the weakly-dynamic data group statistically represents the upper bound of natural environmental fluctuation outdoors, it serves as a more appropriate threshold for distinguishing the two variation modes, namely, the highly-dynamic mode, characterised by large variations in skin temperature, and the weakly-dynamic mode, marked by minor variations in skin temperature. Hodges et al. (Hodges et al., 2009) found that skin vasodilation was significantly attenuated at a skin temperature heating rate of 0.0017 °C/s compared with that at a heating rate of 0.033 °C/s. This indicates that the skin temperature change rate of around 0.00160 °C/s corresponds to a relatively low level of skin vasodilation. It further proves that a derivative of mean skin temperature at 0.00160 (°C/s)

can serve as the critical value to classify the data into highly-dynamic and weakly-dynamic modes.

With this classification method, data will no longer be categorized based on the exposure period. Consequently, some data points collected within the 0–450 s period may be classified as belonging to the weakly-dynamic mode, and vice versa. For example, in Figure 4.6, there are some high values of $|dT_{sk,m}/dt|$ within the weakly-dynamic period that are identified as outliers, potentially resulting from significant changes in environmental conditions (e.g., wind gusts or sudden changes in solar radiation). Under this classification approach, these data points will be reassigned to the highly-dynamic mode due to their high $|dT_{sk,m}/dt|$ values. Likewise, some data in the initial indoor-outdoor transition period will be categorized within the weakly-dynamic mode. In essence, the classification approach is based on empirically derived critical values of skin temperature changes from the experiments.

Outdoor thermal environment is usually non-uniform, meaning that the variation rate of skin temperatures of different body parts would differ from that of the mean skin temperature. Therefore, in real non-uniform situations, the absolute value of the derivative of local skin temperatures ($|dT_{sk,i}/dt|$) is more indicative of the highly-dynamic and weakly-dynamic modes for each body part compared with $|dT_{sk,m}/dt|$, and the 75th percentile of the weakly-dynamic period is selected as the critical value ($C_{sk,i}$) for each body part, as summarized in Table 4.6.

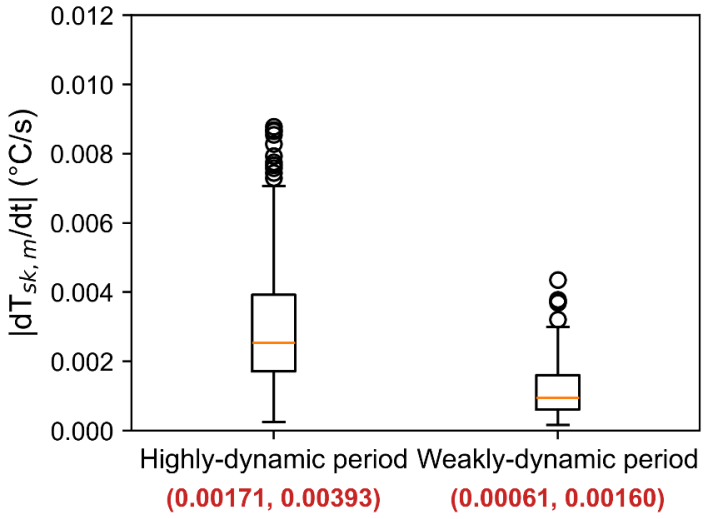

Figure 4.6 The distribution of $|dT_{sk,m}/dt|$ in the highly-dynamic and weakly-dynamic periods.

Table 4.6 Critical values ($C_{sk,i}$) of different body parts.

Part	Forehead	Chest	Abdomen	Back	Upper arm	Forearm	Hand	Thigh	Calf	Foot	Neck
$C_{sk,i}$ (°C/s)	0.00176	0.00152	0.00141	0.00201	0.00179	0.00209	0.00244	0.00356	0.00179	0.00137	0.00188

However, due to the instability of time series data, using a simple $C_{sk,i}$ for classification is unrealistic, as it may lead to frequent data jumps between the highly-dynamic and weakly-dynamic modes. A previous study indicated that the outdoor thermal sensation of pedestrians is indeed influenced by the past 20-35s thermal history (Xie et al., 2022). An applicable classification method for highly-dynamic and weakly-dynamic modes is proposed, using a 30 s window to calculate the possibility (p) that the data within this period exceed the critical value, as described in Eq. 4.8. If the p is larger than 0.5, the 30 s data will be classified into the highly-dynamic mode, otherwise, it will be classified into the weakly-dynamic mode. Figure 4.7 illustrates a sample of the classification results of the forearm. In the first 180 s period, subjects transferred from indoors to outdoors, reaching a high value of $|dT_{forearm}/dt|$, and

the p is 1.0. Subsequently, due to fluctuations in solar radiation and wind conditions, forearm temperature changed rapidly, exhibiting transitions between highly-dynamic and weakly-dynamic modes.

$$p = \frac{count\left(\left|\frac{dT_{sk,i}}{dt}\right| > C_{sk,i}\right)}{30} \tag{4.8}$$
$$if\ p > 0.5, data \in highly-dynamic\ mode$$
$$else, data \in weakly-dynamic\ mode$$

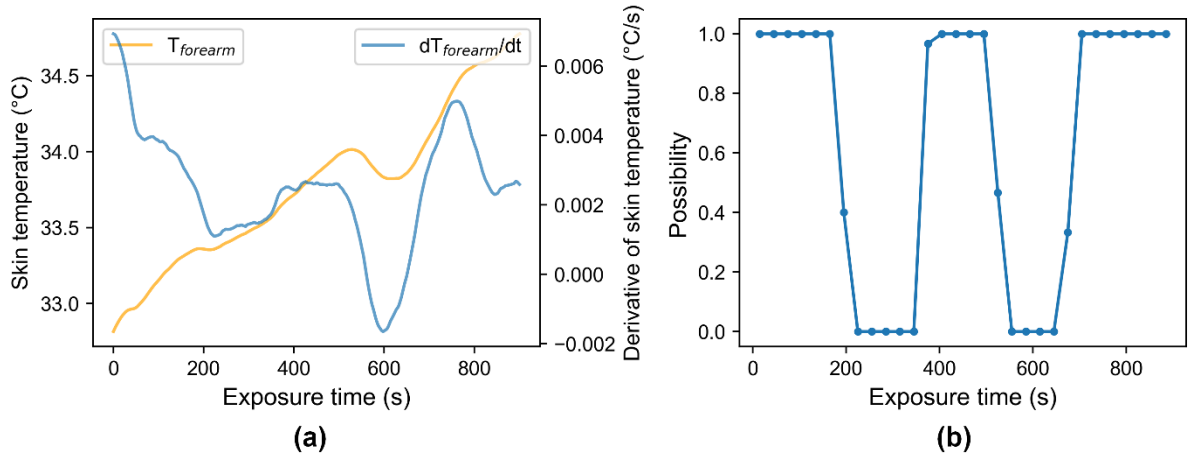

Figure 4.7 A sample of the grouping results of the forearm of highly-dynamic and weakly-dynamic modes. (a). Forearm temperature and its derivative; (b). Grouping results with p calculation.

4.3.7 Dynamic model for step-up conditions

Since the outdoor thermal sensation of pedestrians is influenced by the past 20-35 s thermal history (Xie et al., 2022), the derivative of local skin temperature value at each vote was averaged backward 30 s for the model development. Similarly, the derivative of local skin temperature will be averaged backward 30 s during model application. To ensure the model under warm-biased conditions, data from each outdoor session were chosen for dynamic model

development if the mean value of $T_{sk,m}$ at the steady state (after 15 minutes at each session) exceeded the lower limit of the neutral zone for $T_{sk,m}$ (33.91 °C (Chapter 3)).

4.3.7.1 Highly-dynamic mode prediction

Positive derivatives of skin temperature mean that the body part is experiencing a heating condition, and negative derivatives indicate the body part is undergoing a cooling condition. Given that the human body's thermal response to cooling is typically more significant than its response to heating, due to stronger signals sent from cold thermoreceptors than warm thermoreceptors when exposed to the same level of external stimuli (Zhang, 2003), and considering that majority of data collected in this study corresponds to heating conditions, the dynamic model is divided into a step-up phase and a step-down phase. The regression for the step-up phase of the dynamic model in the highly-dynamic mode, where $dT_{sk,i}/dt$ larger than zero, is conducted and presented in Figure 4.8. For the calf, both $dT_{sk,i}/dt$ and $dT_{sk,m}/dt$ are utilized as the independent variables; for other body parts only $dT_{sk,i}/dt$ is used as the independent variable. A further explanation for the inclusion of both derivatives in the calf model will be provided in a subsequent section. To obtain a more robust model, the original calf data were binned in increments of 0.0015°C/s for $dT_{sk,i}/dt$ due to small variations $dT_{sk,m}/dt$, while the original data of other parts were binned in increments of 0.0025°C/s for $dT_{sk,i}/dt$. Bins containing less than or equal to three data points were excluded from the regression.

Most of the body parts exhibit a high R^2 value, typically ranging from 0.5 to 0.8, indicating a strong correlation result. Among different body parts, parameter K_1 of the abdomen, upper arm, and hand are higher than those of other body parts. This suggests a greater impact of the change rate of abdomen, upper arm, and hand temperature on local TSV compared with the other body parts. However, low R^2 were found for the forehead and foot, which may be attributed to

excessive sweating on the forehead, which leads to irregular skin temperature derivatives. In contrast, foot temperature variations were smaller than other body parts during the experiments (Chapter 3), which may lead to an unclear relationship between the derivative of foot temperature and its dynamic TSV. For the calf, the parameters K_1 and K_2 control the effect of the changes in local and overall thermal status on local TSV, respectively (Figure 4.8-i). K_1 and K_2 exhibit both positive values, indicating positive impacts of the change rate of local and mean skin temperature on local TSV. It is worth noting that K_2 is much larger than K_1, indicating $dT_{sk,m}/dt$ has a larger impact on dynamic calf TSV than that of dT_{calf}/dt. This may be attributed to that people are less sensitive to leg thermal status changes in real outdoor thermal environments, compared with some core body parts (e.g., chest, abdomen) or exposed body parts (e.g., arm, hand). Hence, calf sensation is more influenced by and closely tracks changes in whole-body thermal status rather than the local thermal status. Similar phenomenon is observed in the thigh data, and weak correlations are found between dT_{thigh}/dt, $dT_{sk,m}/dt$ and dynamic thigh TSV (Table 4.4 and Table 4.5), the dynamic thigh TSV approaches zero (Figure 4.8-h). Table 4.7 summarizes the coefficients for the highly-dynamic mode.

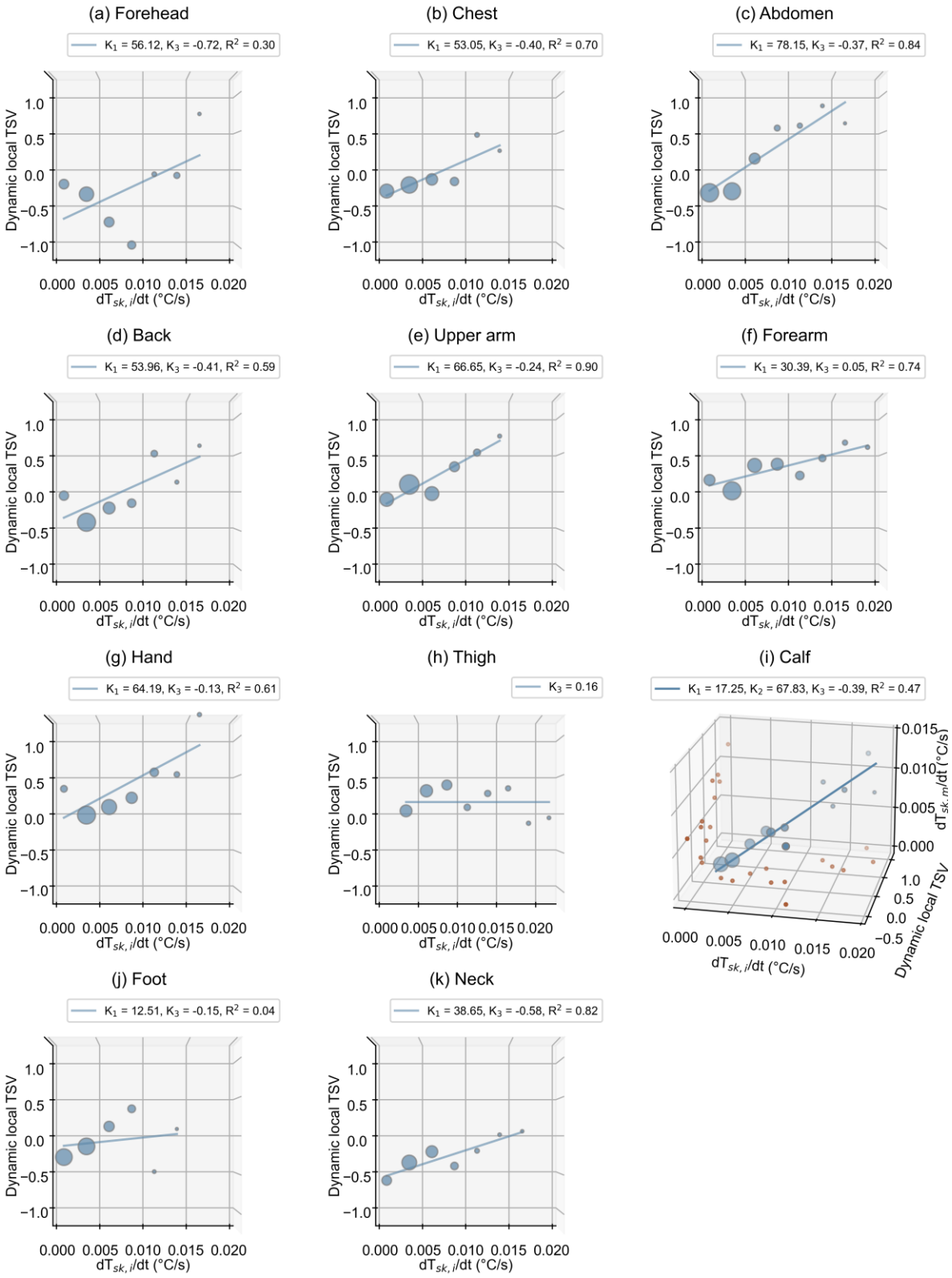

Figure 4.8 Regression results of highly-dynamic mode of the dynamic model.

Table 4.7 The coefficients for the highly-dynamic mode of the dynamic model.

Segment	K_1	K_2	K_3	R^2
Forehead	56.12	-	-0.72	0.30
Chest	53.05	-	-0.40	0.70
Abdomen	78.15	-	-0.37	0.84
Back	53.96	-	-0.41	0.59
Upper arm	66.65	-	-0.24	0.90
Forearm	30.39	-	0.05	0.74
Hand	64.19	-	-0.13	0.61
Thigh	-	-	0.16	-
Calf	17.25	67.83	-0.39	0.47
Foot	12.51	-	-0.15	0.04
Neck	38.65	-	-0.58	0.82

4.3.7.2 Weakly-dynamic mode prediction

Figure 4.9 summarizes the regression results. $dT_{sk,m}/dt$ is employed as the independent variable. Original data of $dT_{sk,m}/dt$ have been binned by 0.0005°C/s increment, and bins containing less than or equal to six data points were excluded from the regression. The regression for the step-up phase of the dynamic model in the weakly-dynamic mode, where $dT_{sk,m}/dt$ larger than zero, is conducted and presented in Figure 4.9. Most body parts illustrate a high R^2, ranging from 0.5-0.8. Foot exhibits a low R^2 mainly due to the limited foot temperature change during the experiments, as it is covered by sneakers or leather shoes. It is worth noting that the thigh illustrates a trendless result, indicating that the thigh may not be significantly affected by the minor changes in thermal status. Among the body parts, the K_2 of some exposed body segments (i.e., upper arm, forearm, hand, and calf) are notably higher than other body parts. This may be attributed to the fact that the TSVs of exposed body

segments are easily affected by external environments outdoors, while the TSV changes of trunk body segments are less obvious. Table 4.8 summarizes the model coefficients for the weakly-dynamic mode.

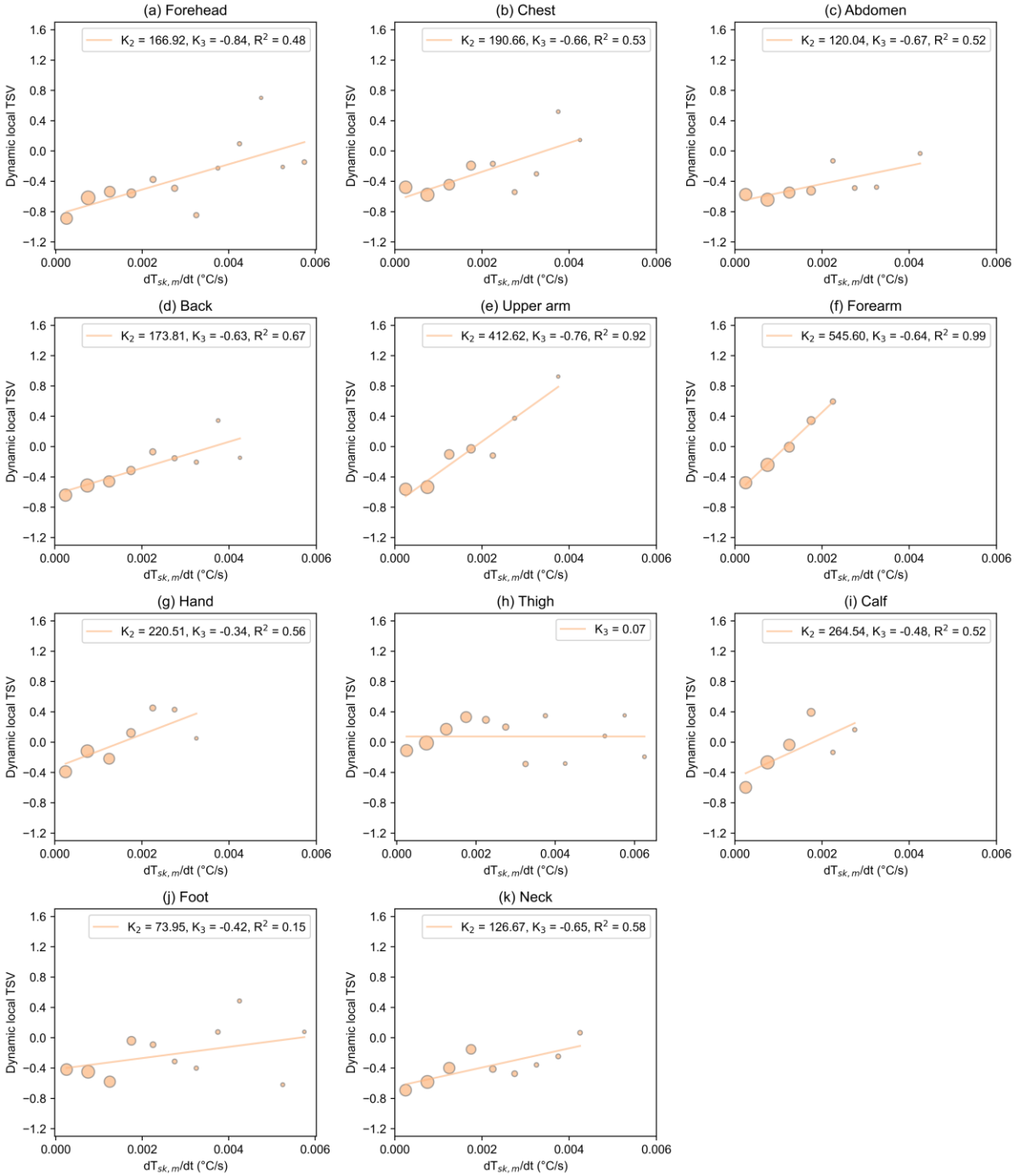

Figure 4.9 Regression results of weakly-dynamic mode of the dynamic model.

Table 4.8 The coefficients for the weakly-dynamic mode of the dynamic model.

Segment	K_2	K_3	R^2
Forehead	166.92	-0.84	0.48
Chest	190.66	-0.66	0.53
Abdomen	120.04	-0.67	0.52
Back	173.81	-0.63	0.67
Upper arm	412.62	-0.76	0.92
Forearm	545.60	-0.64	0.99
Hand	220.51	-0.34	0.56
Thigh	-	0.07	-
Calf	264.54	-0.48	0.52
Foot	73.95	-0.42	0.15
Neck	126.67	-0.65	0.58

4.3.8 Validation of the dynamic model for step-up conditions

The actual local TSV ($TSV_{i,actual}$) is predicted as the sum of the prediction values from the steady-state part and the dynamic part, as presented in Eq. (4.2). The steady part could provide three values, including the mean value, the 10th percentile, and the 90th percentile. The 10th percentile and the 90th percentile can construct a predicted range ($Predicted\ range$) of local TSV that covers 80% of the people. *Accuracy* is calculated by the percentage of actual local TSV ($TSV_{i,actual}$) located in the $predicted\ range$. Table 4.9 and Table 4.10 show the *Accuracy* of body parts for the highly-dynamic and weakly-dynamic modes, respectively. Most of the *Accuracy* are ranged from around 0.65-0.85, indicating good satisfactory results as the model is developed to cover 80% of the population. The average *Accuracy* of the highly-dynamic mode is 74.2%, while the average *Accuracy* of the weakly-dynamic mode is 73.8%.

Table 4.9 The *Accuracy* of body parts for the highly-dynamic mode.

Segment	Forehead	Chest	Abdomen	Back	Upper arm	Forearm	Hand	Thigh	Calf	Foot	Neck
Accuracy	0.72	0.70	0.74	0.73	0.85	0.81	0.83	0.63	0.80	0.71	0.67

Table 4.10 The *Accuracy* of body parts for the weakly-dynamic mode.

Segment	Forehead	Chest	Abdomen	Back	Upper arm	Forearm	Hand	Thigh	Calf	Foot	Neck
Accuracy	0.74	0.78	0.62	0.65	0.76	0.80	0.86	0.67	0.79	0.76	0.69

4.3.9 Demonstration of the dynamic model

We developed steady-state model that provides three sets of local TSVs for 11 body parts and three values of overall TSVs based on local skin temperatures, including mean, the 90th percentile (upper limit), and the 10th percentile (lower limit) value. The dynamic model predicts the dynamic part of local TSVs based on the change rates of local and mean skin temperatures. The final local TSV prediction value is obtained by summing the steady-state and dynamic parts.

Figure 4.10 shows a sample output of the completed local TSV model for different body parts. By integrating the steady-state part model, the three local TSV values (mean, 90th percentile, and 10th percentile) for each body part are shown on the y-axis. Generally, satisfactory prediction performance is shown, as most actual local TSV values are close to the predicted mean value, and all local TSV values fall within the predicted range. The grey shaded area in each sample indicates periods of negative skin temperature derivatives, called step-down phase, for which predictions were not generated. Due to the inclusion of both highly-dynamic and weakly-dynamic modes in the dynamic component, sudden jumps may occur at transition points. To mitigate these abrupt changes during the model application, smoothing functions

will be incorporated in future studies when the step-down phase of the dynamic model is completed.

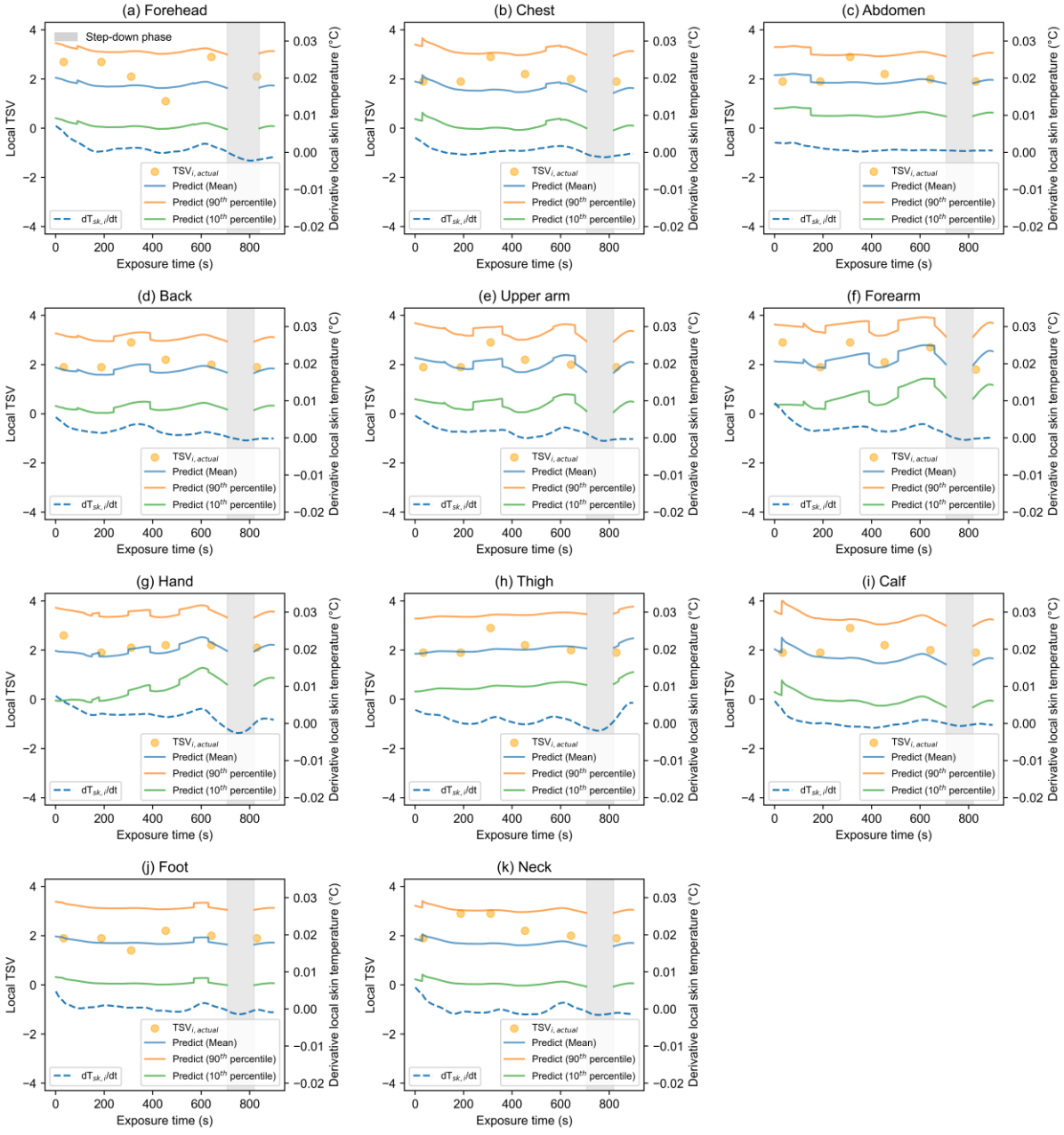

Figure 4.10 Implication samples of step-up phase of the dynamic model for different body parts.

4.4 Discussion

4.4.1 Selection of dynamic predictors for outdoor thermal sensation model

In this study, the derivative of core temperature exhibits lower correlations with dynamic local TSV compared with the derivative of mean skin temperature. The main reason may be attributed to the insignificant changes in core temperature caused by the indoor-outdoor transition in this experiment. In the CBE model (Zhang, 2003; Zhang et al., 2010c), the large cooling effect of air-sleeves resulted in the core temperature change reaching 0.2 °C. However, in our measurement, the maximum observed changes in core temperature during the indoor-outdoor transition was about 0.12 °C (Figure 4.3-b), while its fluctuations in natural outdoor environments resulted in smaller changes (within 0.05 °C). Changes in skin temperature were sufficient to maintain thermal balance in the human body, resulting in insignificant changes in core temperature.

Another challenge is the variability in core temperature measurements across different studies, which can lead to consistency issues. One source of variation is the selection of measurement sites. For example, some studies have used the invasive measurement (e.g., core temperature pills (Song et al., 2020; Brown et al., 2024), rectal temperature measured by thermocouple (Jay et al., 2011; Schulze et al., 2015)), while other studies have utilized the non-invasive measurement to represent core temperature (e.g., tympanic temperature (Xu et al., 2022; Watanabe et al., 2024)). Additionally, the timing of ingesting core temperature pills can affect measurement outcomes. Previous studies have instructed participants to ingest the pills at different time intervals before the experiment (e.g., 2-4 hours (Deng et al., 2020; Song et al., 2020; Xu et al., 2023), 8 hours (Brown et al., 2024), or even immediately before the experiment (Zhang, 2003)).

Moreover, inconsistent core temperature trends were observed across subjects in our measurements. The unclear trend between core temperature and thermal responses led to weak correlations between the derivative of core temperature and dynamic local TSV, thereby limiting the applicability for modelling. Therefore, the selection of the derivative of core temperature as a dynamic term predictor should be determined by the model application scenarios. In outdoor scenarios measured in our study, the derivative of core temperature might not be an ideal predictor for dynamic TSV prediction. Conversely, derivative of mean skin temperature could serve as a more effective indicator of overall thermal status changes. However, for higher metabolic rate conditions, core temperature may show a clear increasing trend, and the applicability of the derivative of core temperature could be further investigated in different conditions.

For the local thermal status changes, derivative of local skin temperature always serves as a dynamic term to predict local TSV in indoor settings (Zhang et al., 2010c). In outdoor settings, where the changes in skin temperatures of different body parts may vary due to localized environmental fluctuations, derivative of local skin temperature would also be a suitable parameter for indicating changes in local thermal status.

4.4.2 Differences in dynamic model development: indoors vs outdoors

The main difference between indoor and outdoor thermal environments is the physical difference (Nikolopoulou & Steemers, 2003). Indoor thermal environment is more stable, whereas outdoor thermal environment is more dynamic and non-uniform due to the dynamic wind speed and asymmetric solar radiation. The dynamic thermal status indoors may arise during transitions between different indoor environments or when utilizing personal comfort systems. Thermal sensation models developed for indoor conditions always use one dynamic term to calculate changes in thermal status, e.g., DTS model (Fiala et al., 2003) and CBE model (Zhang et al., 2010c).

In outdoor conditions, apart from transitioning between different scenarios, the natural thermal environment inherently exhibits dynamic characteristics, resulting in fluctuations in human thermal status. However, the intensity of these two changes in thermal status is significantly different. During the highly-dynamic period, the derivative of mean skin temperature can reach approximately 0.006 °C/s (Figure 4.5-b), whereas in the weakly-dynamic period, it remains around 0.001 °C/s.

Although the previous outdoor model only adopted one form of the dynamic part (Lai et al., 2017b; Xu et al., 2022), this study found different correlations between physiological parameters and thermal sensation in the two forms of thermal status change. The dynamic part is divided into the highly-dynamic mode, e.g., caused by transient scenarios with large $dT_{sk,i}/dt$, and the weakly-dynamic mode, e.g., caused by natural environmental fluctuations with small $dT_{sk,i}/dt$, by empirical critical values of $dT_{sk,i}/dt$. Additionally, some large changes in natural environmental fluctuations (e.g., wind gusts, sudden change in solar radiation) would reach a strong variation in derivative skin temperatures, these data will also be classified into the highly-dynamic mode according to the classification method by critical values.

4.4.3 Detailed application of the outdoor thermal sensation model

The relationship between environmental parameters and physiological responses can be predicted by thermoregulation models (e.g., JOS-3 model (Takahashi et al., 2021)). The thermal sensation model in this study can be integrated with thermoregulation models to provide thermal sensation prediction based on environmental conditions for outdoor conditions. The dynamic model in this study is the second part of the whole outdoor thermal sensation model, serving as dynamic part of the local TSV prediction. It will be integrated with the steady-state part (Chapter 3) to provide local and overall TSV predictions. The completed local TSV prediction is the sum of the steady-state part and dynamic part calculation results, as

presented in Eq. (4.2), while the overall TSV prediction is output by the weighted average of local TSVs, which has been developed in the steady-state part. The whole model could give the completed local and overall TSVs prediction (i.e., three sets of local TSVs for 11 body parts and three values of overall TSVs).

4.4.4 Limitations

Given the experiment settings of indoor-outdoor transition in this study, the dynamic part developed only predicts dynamic thermal sensation when the derivative local or mean skin temperature is positive, called it step-up phase of the dynamic part. In Chapter 5, the step-down phase of the dynamic part will be quantified by collecting additional data when subjects experience cooling changes in thermal status.

To identify naturally occurring thermal fluctuations outdoors, the 75^{th} percentile of the weakly-dynamic period is selected as the empirical critical value to group outdoor skin temperature data into two groups. Alternative approaches based on theoretical considerations are worth exploring in future studies.

The current model is applicable when the core temperature changes are small, corresponding to small values of the derivative of core temperature. During various outdoor activities, core temperature may respond differently, and a clear trend might be possible for the core temperature change (e.g., higher metabolic level corresponds to higher core temperatures (Lee et al., 2010; Brown et al., 2024)), and the applicability of the current model in higher activity levels needs further investigation.

Different outdoor activities and populations are not considered in this study. Since the model output is based on physiological parameters, there may be differences in the results between different outdoor activities (e.g., walking and running) and populations. The applicability of this model for these different cases should be further validated.

4.5 Chapter conclusions

By conducting a series of semi-controlled outdoor experiments, the step-up phase of the dynamic part of an outdoor thermal sensation model was developed for neutral to warm-biased thermal conditions. This provides the dynamic part of local thermal sensation prediction using temporal derivatives of physiological parameters.

Using an adjustable windshield and shading device in actual outdoor settings, a wide range of outdoor conditions were created, with wind speeds ranging from 0.5-2.8 m/s, and T_{mrt} varying 28-63 °C. Subjects transitioned from indoors to outdoors creating dynamic thermal status, a total of 86 sets of human subject tests were completed, with environmental parameters, physiological parameters (e.g., skin temperatures of 18 body parts and core temperature), and subjective votes (e.g., local and overall TSVs) collected. The following findings emerge:

1. Significant differences in $dT_{sk,m}/dt$ were observed between different exposure periods during outdoor conditions. In the initial 0–450 s (highly-dynamic period), $dT_{sk,m}/dt$ peaked at approximately 0.006 °C/s caused by transient scenarios, while in the 450–900 s (weakly-dynamic period), it declined to about 0.001 °C/s mainly induced by natural environmental fluctuations.
2. Addressing naturally occurring thermal environmental fluctuations in outdoor settings, skin temperature data were classified into highly-dynamic and weakly-dynamic modes for model development and application. The classification is performed using an empirical critical value of $dT_{sk,i}/dt$, defined as the 75th percentile in the weakly-dynamic period. A 30 s moving window approach determines whether data belong to the highly-dynamic or weakly-dynamic mode based on the percentage of values exceeding the critical value.

3. The correlations between $dT_{sk,i}/dt$, $dT_{sk,m}/dt$, dT_{core}/dt, and $TSV_{i,dynamic}$ were analyzed. $dT_{sk,i}/dt$ and $dT_{sk,m}/dt$ exhibited stronger correlations with dynamic local TSV than dT_{core}/dt. Furthermore, weakly-dynamic period showed higher correlations between $dT_{sk,m}/dt$ and $TSV_{i,dynamic}$ than the highly-dynamic period. Since natural environmental fluctuations do not cause significant asymmetric thermal conditions, the weakly-dynamic mode utilizes $dT_{sk,m}/dt$ as the independent variable, whereas the highly-dynamic mode primarily use $dT_{sk,i}/dt$ as independent variables, and $dT_{sk,m}/dt$ is added for calf.
4. The step-up phase of the dynamic model of each local body part during highly-dynamic and weakly-dynamic modes was developed using linear regression, with corresponding regression coefficients provided for model application. Model validation shows a satisfactory performance, with an average Accuracy of 74.2% for the highly-dynamic mode, and 73.8% for the weakly-dynamic mode.

The dynamic part will be integrated with the steady-state part to provide local TSV prediction, the completed local TSV output is the sum of the steady-state and dynamic parts calculation results, including three sets of local TSVs for 11 body parts. The whole model can be applied in conjunction with a multi-nodal human thermoregulation model to assess the thermal comfort condition of outdoor spaces during the design and renovation stage.

Chapter 5 - **Developing a physiological-parameter-based thermal sensation model for warm-biased outdoor settings: Step-down phase of the dynamic part**

5.1 Summary

There are two main limitations of existing studies: 1) Few studies developed the outdoor thermal comfort model under transient and dynamic conditions in real-life outdoors, and most did not consider thermal sensation prediction for local body parts. 2) The applicability of various thermal evaluation scales for outdoor use has not been extensively investigated. Previous Chapters (steady-state part (Chapter 3), step-up of dynamic part (Chapter 4)) provided steady-state thermal sensation prediction as well as the dynamic part when the human body experiences positive changes in skin temperatures. This study focuses on the step-down side of the dynamic part of the whole outdoor thermal sensation model, where the human body experiences negative changes in skin temperatures. This study collected thermal perceptions, in terms of TSV, TCV, TA, and TP, and physiological responses, in terms of local skin temperatures, in transient outdoor environments. In addition, to explore the applicability of different thermal evaluation scales outdoors, this study introduced a new scale, thermal stay willingness (TSW), for evaluating pedestrians' willingness in outdoor space. There are three main objectives:

1. To explore the correlations between physiological parameters (i.e., local and mean skin temperatures) and thermal sensation of local body parts under dynamic thermal status.
2. To quantify dynamic thermal sensation of local body parts based on physiological responses in real-life outdoor conditions.

3. To initially investigate the applicability of different thermal evaluation scales in transient outdoor conditions (TCV, TA, TP, TSW).

In this Chapter, a thermal sensation model is developed that correlates subjective thermal sensation votes (TSV) with human-body thermo-physiological responses in step-down dynamic thermal status under warm-biased outdoor conditions. 142 human subjects tests were completed, transferring from step-change thermal environments, with environmental parameters, skin temperature of 12 body parts, and subjective votes (i.e., TSV, TCV, TA, TP, TSW) collected.

According to the results from Chapter 4, skin temperature data were classified into two fluctuation modes, the highly-dynamic and weakly-dynamic modes. Lower correlations were found between the $dT_{sk,i}/dt$ and dynamic local TSV, and between the derivative of PET and $dT_{sk,i}/dt$, in the weakly-dynamic mode than those in the highly-dynamic mode. Comparing the two phases, the step-up phase showed higher associations between dPETs and dTSVs than those of the step-down phase. The step-down phase model was developed using linear regression, utilizing $dT_{sk,i}/dt$ as the independent variable for both the highly-dynamic and weakly-dynamic modes. Comparing thermal evaluation scales, TSW is suitable for outdoor thermal evaluation during transition stages and occupancy periods. The findings provide insights into thermal evaluation scales for outdoors, and the model can be integrated with thermoregulation models to numerically assess outdoor thermal environments.

5.2 Methods

5.2.1 On-site experiment settings

Experiment sites. The experiment site is in Hong Kong, a monsoon-influenced humid subtropical climate (Cwa, Köppen climate classification) (Peel et al., 2007), with cool, dry winters and hot, humid summers. The experiments were conducted at Hong Kong Polytechnic

University from July to October. Three sites were selected to cover classical scenarios of pedestrians, including indoor (site 1), underneath-elevated building (referred to as UEB, site 2), and sunlit (site 3), as shown in Figure 5.1. Site 1 is a typical indoor environment with air-conditioning. Site 2 is a semi-outdoor UEB area with high wind speed and low solar radiation due to the wind amplification and shading effects created by the building structure (Huang et al., 2020), while site 3 is a sunlit area with high wind speed and direct solar radiation.

Figure 5.1 Measurement sites in the field study.

Instruments. A mobile weather station comprising an air temperature and relative humidity sensor, an anemometer, and three sets of radiometers providing for short- and long-wave radiation monitoring for six directions was placed within 1.0 m of the subjects. Mean radiant temperature (T_{mrt}) was calculated following ISO 7726 (ISO, 1998). The detailed calculation method is described in our previous study (Jiang et al., 2024). On several measurement days when radiation data were available only in two directions (ground and sky), a correction method was applied to improve the calculation accuracy, as

detailed in Appendix F. The weather station was installed at a height of 1.3 m, while the radiometers were placed at 1.6 m to avoid blocking radiation. Skin temperature was measured using quick-response resistance temperature detectors (RTDs) with a time constant of 0.1 s. The RTDs employed in this study consist of a thin 0.01-inch Platinum resistance wire encased in flexible Polyimide material, allowing for seamless adaptation to the skin surface. Skin temperatures of 12 body parts were measured, including the forehead, chest, back, abdomen, upper arm (right), forearm (right), hand (right), thigh (right), calf (right), foot (right), neck, and pelvis. Mean skin temperature ($T_{sk,m}$) was determined using the seven-point weighting method (Hardy et al., 1938), which considers the forehead, abdomen, forearm, hand, thigh, calf, and foot. The corresponding weights assigned to these body parts are 0.07, 0.35, 0.14, 0.05, 0.19, 0.13, and 0.07, respectively. Table 5.1 summarizes the technical information of the equipment.

Table 5.1 Technical information of equipment used for the field measurement.

Measurement type	Monitored parameter	Sensor/Equipment	Accuracy	Range of measurement	Sampling rate
Microclimate parameters	Air temperature (T_a)	R.M. YOUNG 41382	±0.3 °C	-50 ~ +50 °C	1 s
	Relative humidity (RH)		±1%	0 ~ 100%	
	Wind speed (v)	R.M. YOUNG 81000	±0.05 m/s	0 ~ 40 m/s	1 s
	Long-wave radiation (L_i)	Kipp & Zonen CNR-4	< 10%	-250 ~ +250 W	10 s
	Short-wave radiation (K_i)		< 5%	0 ~ 2000 W	10 s
Physiological parameters	Skin temperature	Minco S17422PDZ40A	EN60751, Class B, ±(0.3+0.005|t|) °C	-73 ~ +200 °C	1 s

Thermal comfort surveys. There are 3359 outdoor subjective surveys collected in this study. Around 700 subjective surveys are used for the step-down phase of dynamic part model development in this study, with 80% of the data (about 560 surveys) used for model development and 20% of the data (about 140 surveys) used for model validation. The surveys include the basic information survey, such as gender, age, height, weight, and clothing, as well as the subjective survey of thermal environments, in terms of TSV, TCV, TA, TP, and TSW. The TSV and TCV questionnaires employed an extended 9-point scale (Zhang et al., 2010c; Xie et al., 2019), from 'very cold' to 'very hot', and 'very uncomfortable' to 'very comfortable'. Local and overall TSVs and TCVs were both asked in the questionnaire. The TSV survey first asked the overall TSV. Following that, subjects were prompted to select at least three body parts that were inconsistent with their prior overall thermal sensation, and were then asked to provide TSV ratings for these specific body parts (Jiang et al., 2025). 11 body parts were involved in the local TSV survey, including the forehead, neck, chest, abdomen, back, upper arm, forearm, thigh, calf, hand, and foot. The survey of TA and TP employed a 7-point scale. The new evaluation scale, TSW, asked subjects, 'Do you expect to stay in this thermal environment (willingness)? The scale is from 'very unwilling' to 'very willing', adopting a 7-point scale as the same as TA and TP. The survey scales used in this study are shown in Figure G.

Subjects. 142 subjects participated in this study, including 59 males and 83 females. Table 5.2 summarizes the characteristics of the subjects. The weight and body fat were measured by a body composition monitor (TANITA, RD545). Subjects were asked to wear typical summer clothes, such as T-shirt, shorts or thin trousers. 84.5% of subjects wore sneakers or leather shoes during the experiment. For male subjects, the mean age is 24.5 years, the mean body mass index (BMI) is 23.8 kg/m^2, and the mean body fat is 17.5%. For female subjects, the mean

age is 22.8 years, the mean body mass index (BMI) is 21.1 kg/m^2, and the mean body fat is 26.1%.

Table 5.2 Characteristics of subjects.

	Count	Age (years)	Height (cm)	Weight (kg)	BMI (kg/m^2)	Body fat (%)	Clothing insulation (clo)
Male	59	24.5 ± 7.1	176.3 ± 6.4	74.6 ± 22.8	23.8 ± 6.0	17.5 ± 7.0	0.25 ± 0.06
Female	83	22.8 ± 4.0	163.0 ± 5.6	56.2 ± 9.2	21.1 ± 3.2	26.1 ± 7.3	0.28 ± 0.07
Total	142	23.5 ± 5.5	168.6 ± 8.8	63.9 ± 18.5	22.2 ± 4.7	22.5 ± 8.2	0.27 ± 0.07

5.2.2 Experiment procedure

The experiment procedure is shown in Figure 5.2. Subjects experienced a 15-min preparation period in an indoor air-conditioned area to attach sensors and complete a basic information survey. This was followed by a 10-min adaptation period in the same area to stabilize their metabolic rate, after which they filled out a subjective survey before proceeding outdoors. Then, subjects transitioned from the UEB area (UEB#1 period in Figure 5.2) to a sunlit area, and returned to the UEB area (UEB#2 period in Figure 5.2), spending 15 min in each condition.

It is worth noting that the arrangement of the transitional area sequences is designed to induce varying levels of thermal stress changes, thereby resulting in different step changes in skin temperatures. The step change from the indoor to the UEB#1 area aims to evoke a slight step-up or step-down in skin temperature depending on the wind conditions on the experimental day. Conversely, significant step-up changes occurred when transitioning from the UEB#1 area to the sunlit area, while large step-down changes were induced during the transition from the sunlit area to the UEB#2 area. During the outdoor measurement, the subjects were asked to fill out the subjective survey every 2 min. Skin temperatures of 12 body parts were continuously

monitored throughout the experiment. The human subject tests have been approved by the HKPolyU Institutional Review Board (Reference Number: HSEARS20221023001).

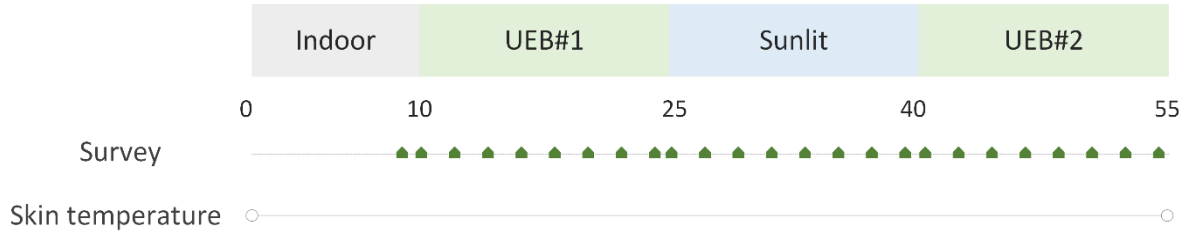

Figure 5.2 Experiment procedure.

5.2.3 Data smoothing and outlier detection

Physiological Equivalent Temperature (PET) was employed to assess thermal conditions of the outdoor environments, calculated by the Python package pythermalcomfort (2.9.0) (Tartarini & Schiavon, 2020) with a metabolic rate of 1.2 met and clothing insulation of 0.27 clo. The skin temperature data was processed using the Savitzky-Golay Python (Virtanen et al., 2020), a wavelet smoothing technique commonly used in signal processing to minimize noise. The temporal derivative of skin temperature ($dT_{sk,i}/dt$) (from now on word 'temporal' will be dropped for brevity) was computed by the difference between two adjacent skin temperature data, with measurements recorded every second and expressed in °C/s. The exponential weighted moving average method was utilized to further smooth the derivative of skin temperature data. Similarly, the PET data was smoothed using the Savitzky-Golay Python and its derivative ($dPET/dt$) using the exponential weighted moving average method. Linear functions were utilized for data regression.

The Anomaly Detection Toolkit (ADTK) Python package (Chakraborty et al., 2020) was employed to detect outliers in wind speed data by using a sliding window to compare each time series data with the mean value of the preceding window. To address the issue of poor contact between skin temperature sensors and the skin surface, especially under high-sweat conditions

in summer, an additional outlier detection method was applied to improve the reliability of skin temperature data. However, due to large variations in skin temperature under outdoor conditions, the previously mentioned mathematical outlier detection method was not suitable for identifying anomalies in outdoor experiments. An empirical method was used for outlier detection in skin temperature data, with the detailed procedure described in Appendix H.

5.2.4 Basic mathematical model

5.2.4.1 SWI correction term

Wind and solar radiation influence thermal comfort with varying intensities, which may not be fully captured by current outdoor thermal indices (Li et al., 2020). Li et al. (2020) pointed out that UTCI underestimated the effects of v and T_{mrt} at high temperature conditions. They proposed a Combined Sun and Wind Conditions Index (SWI) to quantify the combined effects of solar radiation and wind speed on thermal sensation. SWI is obtained by the 0–1 scaling standardization method, defined as the difference between the standardized mean radiant temperature and wind speed, as expressed in Eq. (5.1).

$$SWI = T'_{mrt} - v' = \frac{T_{mrt} - 12}{64 - 12} - \frac{v - 0}{4.0 - 0} = \frac{T_{mrt} - 12}{52} - \frac{v}{4.0} \quad (5.1)$$

where T_{mrt} is mean radiant temperature, °C, v is wind speed, m/, T'_{mrt} and v' are the standardized T_{mrt} and v, The index was applied in the range: 12.0 ⩽ T_{mrt} ⩽ 64.0 °C and 0 < v ⩽ 4 .0 m/s.

Section 5.3.4.2 elaborates on how varying SWI values affect thermal sensation. Even with similar $T_{sk,m}$, TSV differs between the UEB and sunlit areas under steady-state conditions. Consequently, a SWI correction term is proposed to enhance the accuracy of thermal sensation prediction for the previous steady-state part (Chapter 3) under varying sun and wind conditions.

The SWI correction term for the steady-state part ($TSV_{i,steady,correction}$) can be expressed as Eq. (5.2).

$$TSV_{i,steady,correction} = k \times SWI + b \tag{5.2}$$

where k is the slope of the line, b is the intercept.

The steady-state part of local TSV prediction ($TSV_{i,steady}$) is the sum of the original expression of steady-state part ($TSV_{i,steady,ori}$) (Chapter 3) and the correction term ($TSV_{i,steady,correction}$), as shown in Eqs. (5.3), (5.4):

$$TSV_{i,steady,ori} = 4 \times \left(1 - \frac{2}{1 + e^{B \times (T_{sk,i} - T_{sk,neu,i} + C)}}\right) \tag{5.3}$$

$$TSV_{i,steady} = 4 \times \left(1 - \frac{2}{1 + e^{B \times (T_{sk,i} - T_{sk,neu,i} + C)}}\right) + k \times SWI + b \tag{5.4}$$

where $T_{sk,i}$ and $T_{sk,neu,i}$ are the skin temperature and neutral skin temperature for the ith body part, respectively, and B is the coefficient that controls the slope of the line, C is the factor that takes into account the neutral skin temperature variation. The steady-state part has three sets of B and C values for each body part, which provides three predicted local TSV values: the mean ($TSV_{i,steady,mean}$), 10th percentile ($TSV_{i,steady,10th}$), and 90th percentile ($TSV_{i,steady,90th}$). The 10th percentile and the 90th percentile can construct a predicted range ($Predicted\ range$) of local TSV that covers 80% of the people. The corrected prediction of the three values should be the sum of the original value ($TSV_{i,steady,mean,ori}$, $TSV_{i,steady,10th,ori}$, $TSV_{i,steady,90th,ori}$) and the correction term ($TSV_{i,steady,correction}$).

5.2.4.2 Local TSV model

According to Chapter 4, the mathematical equation of the dynamic term of local TSV model can be expressed as Eq. (5.5).

$$TSV_{i,dynamic} = K_1 dT_{sk,i}/dt + K_2 dT_{sk,m}/dt + K_3 \tag{5.5}$$

where $TSV_{i,steady}$ and $TSV_{i,dynamic}$ is the steady-state and dynamic local thermal sensation, respectively. $dT_{sk,i}/dt$ is the derivative of local skin temperature, °C/s. $dT_{sk,m}/dt$ is the derivative of mean skin temperature, °C/s. K_1 and K_2 are the coefficients to control the slope of the line. K_3 is an empirical constant term that arises from minor shifts of neutral skin temperature and sensation due to different exposure periods of dynamic and steady parts, and is primarily attributed to changes in thermal tolerance over time. Detailed information can be found in Chapter 4.

$TSV_{i,dynamic}$ can be calculated by the actual local thermal sensation ($TSV_{i,actual}$) minus the mean value of the steady-state term of local thermal sensation ($TSV_{i,steady,mean}$) calculated from Chapter 3, as shown in Eq. (5.6).

$$TSV_{i,dynamic} = TSV_{i,actual} - TSV_{i,steady,mean} \tag{5.6}$$

When applying the model, the calculated local thermal sensation (TSV_i) would have three output values, including the mean value ($TSV_{i,mean}$), the 90th percentile ($TSV_{i,90th}$), and the 10th percentile ($TSV_{i,10th}$), which will be determined by adding the dynamic term ($TSV_{i,dynamic}$) to the three values of the steady-state term ($TSV_{i,steady,mean}$, $TSV_{i,steady,90th}$, $TSV_{i,steady,10th}$) calculated by Chapter 3, and the SWI correction term in Section 5.2.4.1, as presented in Eq. (5.7), (5.8), (5.9).

$$TSV_{i,mean} = TSV_{i,dynamic} + TSV_{i,steady,mean} \tag{5.7}$$

$$TSV_{i,90th} = TSV_{i,dynamic} + TSV_{i,steady,90th} \tag{5.8}$$

$$TSV_{i,10th} = TSV_{i,dynamic} + TSV_{i,steady,10th} \tag{5.9}$$

5.3 Results

5.3.1 Environmental parameters

Figure 5.4 illustrates the variation of environmental parameters during the measurement, including air temperature (T_a), humidity ratio (d), wind speed (v), mean radiant temperature (T_{mrt}), and the PET averaged per minute. The environmental conditions of the indoor area were as follows: T_a: 25.6 °C, d: 12.6 g/kg, v: 0.2 m/s, T_{mrt}: 26.9 °C. The mean value of T_a, d, and v were similar in UEB and sunlit, which were around 29.8 °C, 16.0 g/kg, and 1.5 m/s, respectively. The mean value of T_{mrt} in the sunlit area (around 49.4 °C) was much higher than the UEB (approximately 29.4 °C). Additionally, PET results indicate the overall thermal stress level of thermal environments. In the sunlit area, PET showed the highest value at approximately 34.7 °C, followed by the UEB area with a PET value of 28.0 °C, while the indoor area exhibited the lowest PET value at around 26.3 °C.

In summary, during outdoor conditions, most of the PET values were in the range of 25.0 to 40.0 °C, covering slight heat stress to strong heat stress, corresponding to slightly warm to very hot thermal perceptions (Matzarakis et al., 1999).

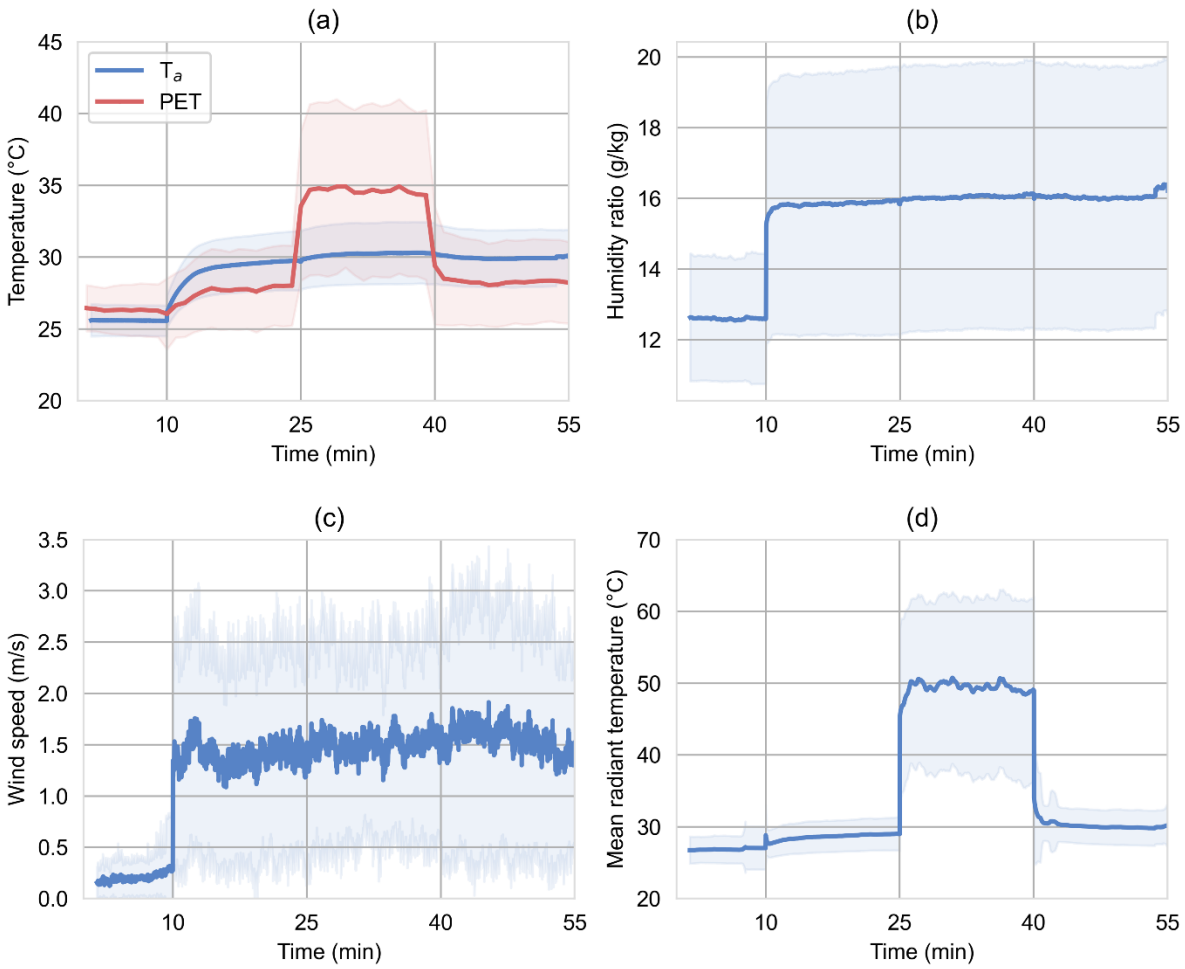

Figure 5.3 Environmental parameters during the measurement. (a). Air temperature and PET; (b). Humidity ratio; (c). Wind speed; (d). Mean radiant temperature.

5.3.2 Dynamic thermal perceptions

Figure 5.4 presents the variations of thermal perceptions during the experiment, including TSV, TCV, TA, TP, and TSW. In general, TSV is the highest in the sunlit area, while TCV, TA, TP, and TSW are the lowest in the sunlit area. When subjects transferred from indoors to the UEB#1 condition, mean TSVs initially decreased, then exhibited a slight increase before stabilizing and remaining unchanged (Figure 5.4-a). Conversely, when subjects transferred from the UEB#1 condition to the sunlit condition, mean TSVs dramatically increased and then

stabilized. Similarly, when subjects transferred from the sunlit to the UEB#2 condition, mean TSV significantly dropped and then exhibited minor fluctuations.

Mean TCVs exhibited a reverse trend with TSV. In Figure 5.4-b, mean TCVs slightly increased and then gradually dropped when subjects transferred from indoors to the UEB#1 condition. It is worth noting that when subjects transitioned from UEB#1 to the sunlit condition, there was no sudden drop in mean TCVs, compared with the transition from the sunlit to UEB#2 condition. Conversely, mean TCVs gradually decreased in the sunlit condition. This may suggest that the impact of solar radiation on TCVs differs from that of wind speed, as the solar radiation effect on TCVs is a time-accumulated result.

Mean TAs, TPs, and TSWs exhibit similar trends with TCVs, except for the transition from indoors to the UEB#1 condition. Compared with TCVs, mean TAs, TPs, and TSWs were initially highest in indoor conditions and then gradually decreased when the subjects transferred to the UEB#1 condition. This may be attributed to the semantic differences between TCV and the three thermal evaluation scales (i.e., TA, TP, TSW). TA, TP, and TSW provide clearer semantic interpretations for thermal evaluation, such as acceptability, pleasure, and willingness, compared with TCV, whose definition of comfort is somewhat ambiguous, particularly in the context of outdoor thermal assessments as reported by Xi et al (2024). It is worth noting that TSW exhibited the most significant response during the step change from the UEB#1 to the sunlit condition compared with TA and TP, suggesting that the semantics of TSW may be more sensitive to assessing transient outdoor thermal environments. Since TSW focuses on the users' willingness to stay in outdoor thermal environments, a fundamental requirement for outdoor spaces, it may serve as a more effective scale for outdoor thermal evaluation. Detailed discussions will be illustrated in Section 5.4.4.

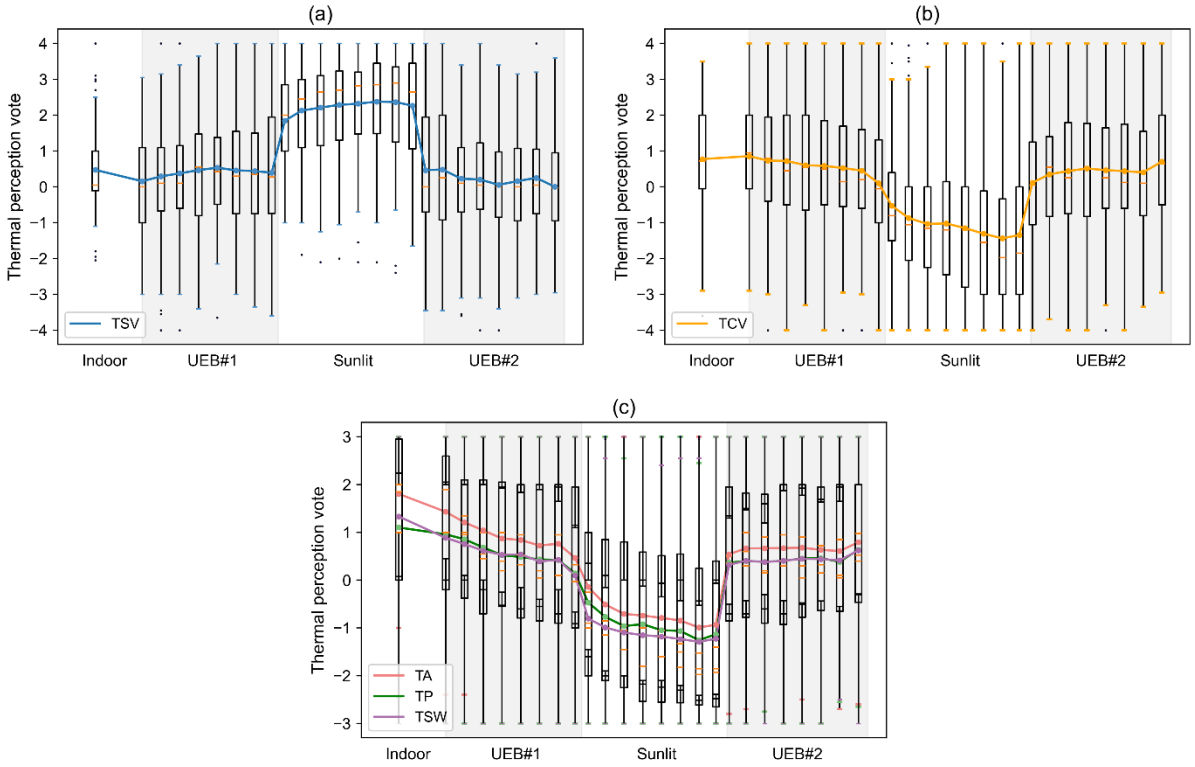

Figure 5.4 Variations in thermal perceptions. (a). TSV; (b). TCV; (c). TA, TP, and TSW.

5.3.3 Dynamic skin temperatures

The variation in skin temperatures during the experiment is shown in Figure 5.5-a, including mean skin temperature ($T_{sk,m}$), forearm temperature, and chest temperature. The forearm and chest are chosen to represent exposed and unexposed body segments, respectively. The boxplot illustrates the statistical distribution over exposure time, with dots indicating the mean value for each group. In general, forearm temperature exhibited the most significant changes during the step-change conditions compared with chest temperature and $T_{sk,m}$, mainly because the forearm is an exposed body segment and is easily affected by the external environment. Mean value of $T_{sk,m}$ kept unchanged when subjects transferred from indoors to the UEB#1 condition (around 34.3 °C), slightly increased then remained stable (approximately 34.4 °C) in the UEB#1 condition, dramatically increased and then kept unchanged (about 35.6 °C) as they

moved from the UEB#1 to the sunlit condition, and gradually dropped (around 34.7 °C) when they moved from the sunlit to the UEB#2 condition. Forearm and chest temperature exhibited similar trends to $T_{sk,m}$ throughout the experiment.

Figure 5.5-b illustrates the variation in derivatives of skin temperatures, including $dT_{sk,m}/dt$, derivative of forearm temperature and derivative of chest temperature. Generally, derivatives of skin temperature were initially the highest when the subjects experienced step-change conditions, and gradually decreased to a small value (nearly zero) when they stayed in a condition for around 6 mins. For example, mean value of $dT_{sk,m}/dt$ was the highest when the subjects initially transferred to the next condition, where the mean value of $dT_{sk,m}/dt$ were 0.001, 0.004, and -0.003 °C/s when they arrived at the UEB#1, sunlit, and UEB#2 conditions, respectively. When the subjects stayed in a condition for more than 6 mins, the $dT_{sk,m}/dt$ gradually decreased to a near-zero value.

Notable differences are observed in the derivatives of skin temperatures between the first 6 mins and the period after the 8 mins during each outdoor condition. Consequently, a time duration of 420s was selected to divide the data into two periods in this study, including the highly-dynamic period and the weakly-dynamic period. According to Chapter 4, different from indoor conditions, slight variations with small derivatives of skin temperature are common in outdoor conditions due to the dynamic features, such as breeze and slight solar radiation changes. The highly-dynamic period is characterized by significant variations, for instance, results from transitions between step-change environments with large $dT_{sk,i}/dt$. The weakly-dynamic period is marked by minor fluctuations arising from minor natural environmental variations with small $dT_{sk,i}/dt$.

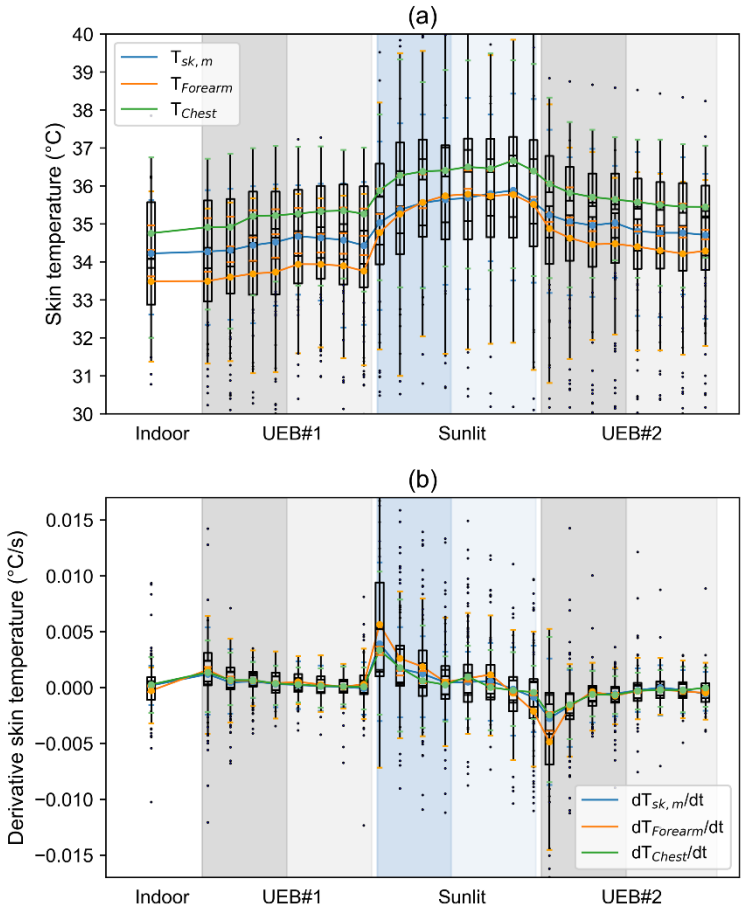

Figure 5.5 Variations in skin temperatures and the derivatives of skin temperature. (a). Mean skin temperature, forearm, and chest temperature; (b). Derivatives of mean skin temperature, forearm, and chest temperature.

5.3.4 Steady-state part description

5.3.4.1 Steady-state part development of abdomen, foot, and neck

Since abdomen TSV data were collected in this study, and a wider data range was obtained for the foot and neck, the local TSV prediction of the steady-state part ($TSV_{i,steady,ori}$) of the abdomen, foot, and neck are supplemented using the data from this study, as presented in Figure 5.6. The data with exposure time larger than 13 min were regarded as the steady-state data. Following that, to build the model for warm-biased conditions, the filtered data with $T_{sk,m}$ larger than the lower limit of neutral skin temperature (33.9 °C) (Chapter 3) were utilized for

the regression. The three body parts show satisfactory results with high R^2. Table I summarizes the updated coefficients of different body parts in the steady-state part model.

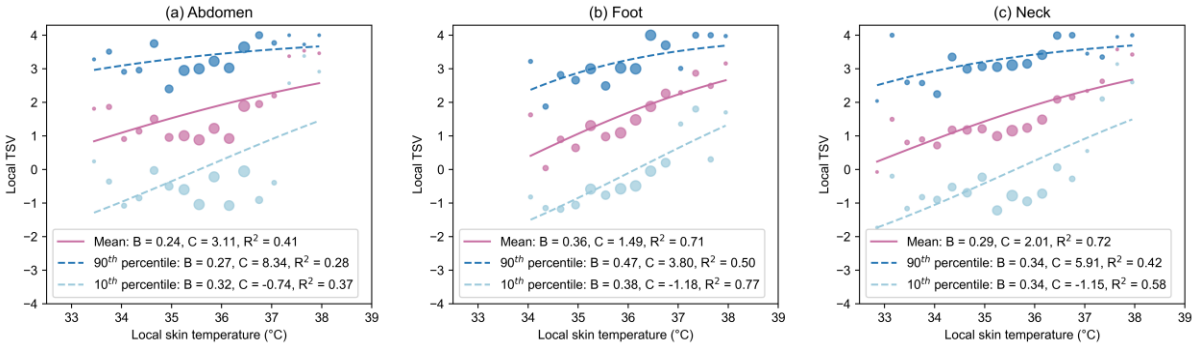

Figure 5.6 The supplemented regression results of abdomen, foot, and neck for steady-state part model. (a). Abdomen; (b). Foot; (c). Neck.

5.3.4.2 Sun and wind correction term

SWI combines the effects of solar radiation and wind speed on thermal comfort (Li et al., 2020). With similar $T_{sk,m}$, variations in SWI could lead to different TSV responses. As illustrated in Figure 5.7, similar values of $T_{sk,m}$ were observed in the steady state of the sunlit and UEB#2 conditions. However, the SWI was considerably higher in the sunlit condition. This difference contributed to the variation in TSV responses, which were approximately -0.7 in the sunlit condition and -2.5 in the UEB#2 condition. The above observation reveals that different combinations of solar radiation and wind conditions can lead to varied thermal sensation responses. Consequently, a SWI correction term is added to the steady-state part of the model for the local TSV prediction.

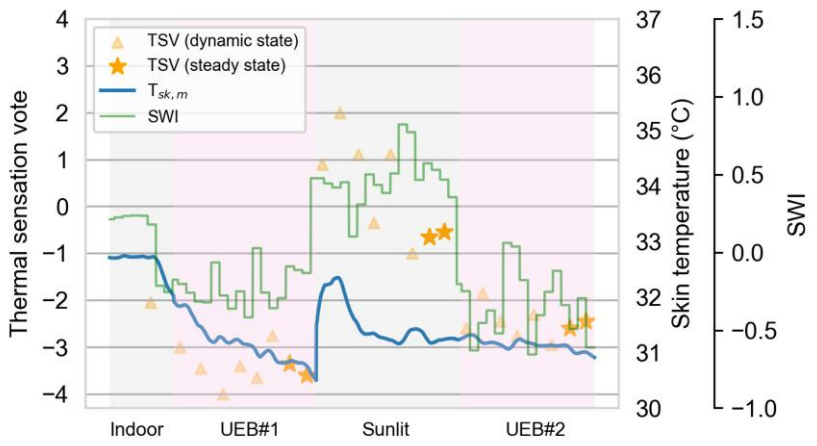

Figure 5.7 A sample of skin temperature and thermal sensation response under different SWI values.

To better improve the accuracy of the steady-state model, both the data utilized for developing the steady-state model (Chapter 3) (referred to as steady-state data here) and the data obtained in this study (referred to as this study data here) are used to build the SWI correction term. The regression results of the SWI correction term for local body parts are shown in Figure 5.8. Linear function was employed for the regression. The deviation was calculated as the difference between the actual ($TSV_{i,actual}$) and the original predicted range of local TSV ($[TSV_{i,steady,10th,ori}, TSV_{i,steady,90th,ori}]$) for the steady-state part. The results show strong associations between SWI and the deviations, with high R^2 for each body part. Generally, deviation decreased with the decrease in SWI, suggesting a lower actual value than the predicted value when the SWI is low. The results illustrate that the original steady-state model underestimates the TSV under high solar radiation conditions (e.g., SWI larger than 0.6 for forehead), whereas it overestimates the TSV under high wind speed conditions (e.g., SWI lower than 0.3 for thigh). Similar results were found in Li et al. (2020), mean value of TSV increases with the increase in SWI. Table 5.3 summarizes the coefficients of the SWI correction term for local body parts. $Accuracy$ is calculated by the percentage of actual local TSV ($TSV_{i,actual}$)

located in the *predicted range*. As shown in Table 5.4, after adding the SWI correction term, the *Accuracy* of steady-state part for body parts are improved, ranging from 0.6-0.8.

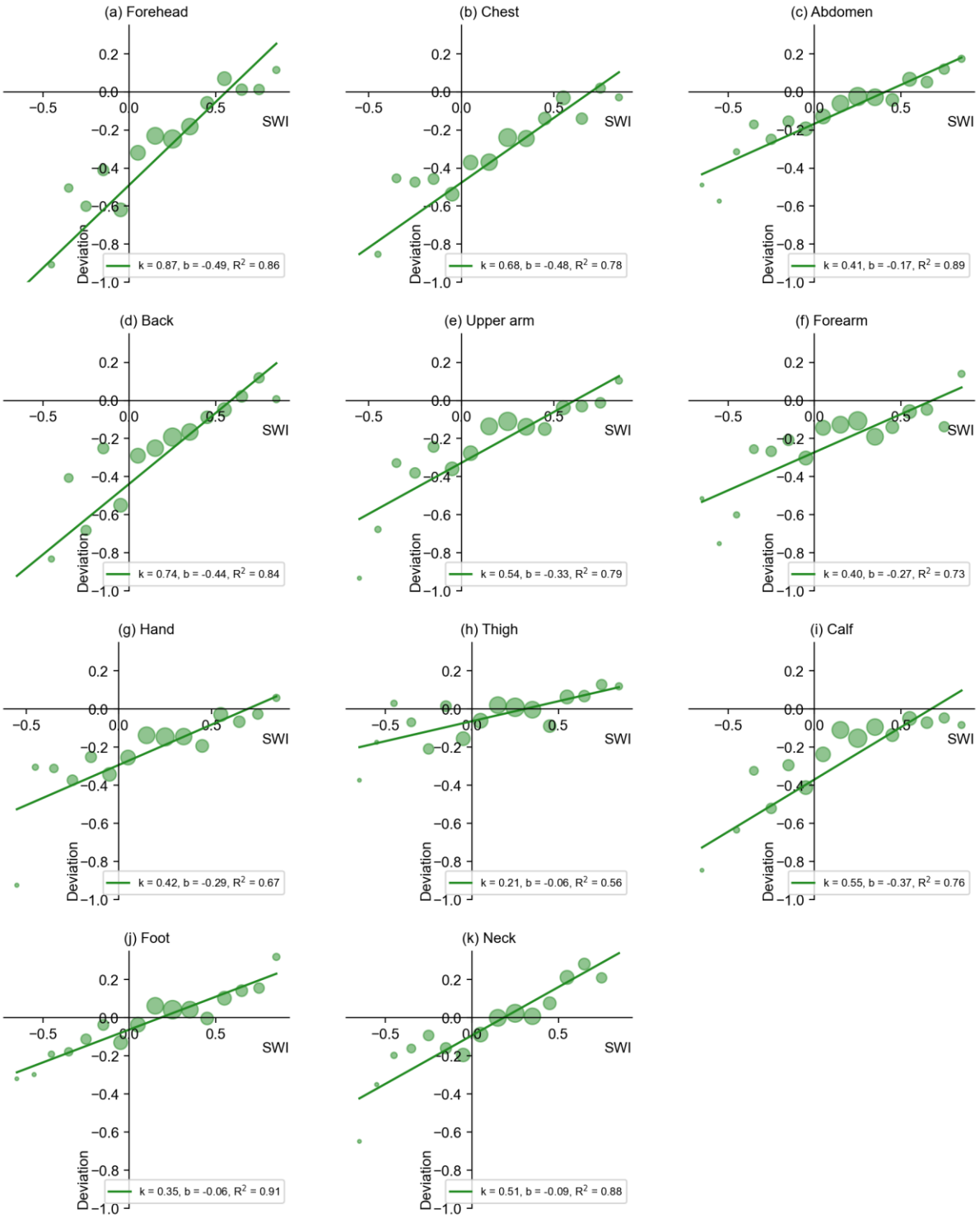

Figure 5.8 The regression results of the SWI correction term for local body parts.

Table 5.3 Coefficients of the SWI correction term for local body parts.

Segment	k	b	R^2
Forehead	0.87	-0.49	0.86
Chest	0.68	-0.48	0.78
Abdomen	0.41	-0.17	0.89
Back	0.74	-0.44	0.84
Upper arm	0.54	-0.33	0.79
Forearm	0.40	-0.27	0.73
Hand	0.42	-0.29	0.67
Thigh	0.21	-0.06	0.56
Calf	0.55	-0.37	0.76
Foot	0.35	-0.06	0.91
Neck	0.51	-0.09	0.88

Table 5.4 The *Accuracy* of the steady-state part after SWI correction.

	Forehead	Chest	Abdomen	Back	Upper arm	Forearm	Hand	Thigh	Calf	Foot	Neck
Original	0.62	0.60	0.71	0.60	0.67	0.66	0.66	0.64	0.64	0.70	0.69
After correction	0.68	0.64	0.72	0.64	0.69	0.66	0.67	0.65	0.68	0.71	0.71

5.3.5 Classification of highly-dynamic and weakly-dynamic modes

In the previous section, two periods of data were found, the highly-dynamic and weakly-dynamic periods, based on the exposure time outdoors. Due to the naturally dynamic characteristic outdoors, two fluctuation modes are defined in Chapter 4, namely, the highly-

dynamic mode, characterized by significant variations, and the weakly-dynamic mode, marked by minor fluctuations. The 75th percentile of the absolute value of the derivative of local skin temperatures ($|dT_{sk,i}/dt|$) of the weakly-dynamic period can serve as a critical value ($C_{sk,i}$) for distinguishing the highly-dynamic and weakly-dynamic modes. Steady-state data and this study data are combined to obtain the $C_{sk,i}$ of different body parts. Since the sitting or standing posture significantly affects the variations in the thigh temperature (e.g., the convective heat transfer coefficient would be different, or the subjects prefer to put their hands on the thigh when sitting), the $C_{sk,i}$ of thigh for standing posture utilizes the data in this study and uses the previous steady-state data for sitting posture. Table 5.5 summarizes the $C_{sk,i}$ for different body parts.

Table 5.5 Critical values ($C_{sk,i}$) of different body parts.

Part	Forehead	Chest	Abdomen	Back	Upper arm	Forearm	Hand	Thigh	Calf	Foot	Neck
$C_{sk,i}$ (°C/s)	0.00216	0.00123	0.00122	0.00125	0.00153	0.00186	0.00272	Sitting for 0.00356, standing for 0.00118	0.00151	0.00095	0.00281

The classification method of highly-dynamic and weakly-dynamic modes uses the same method as the step-up phase model (Chapter 4). The classification method uses a 30 s window to determine the possibility (p) that the data within this 30 s window exceed the $C_{sk,i}$, as shown in Eq. 5.10. If the p is larger than 0.5, the 30 s data will be classified into the highly-dynamic mode, otherwise, it will be classified into the weakly-dynamic mode.

$$p = \frac{count\left(\left|\frac{dT_{sk,i}}{dt}\right| > C_{sk,i}\right)}{30} \tag{5.10}$$
$$if\ p > 0.5, data \in highly-dynamic\ mode$$
$$else, data\ \in weakly-dynamic\ mode$$

5.3.6 Correlations between skin temperatures and thermal sensation

Table 5.6 shows the Spearman correlations (r_s) between local skin temperature and local TSV of the highly-dynamic and weakly-dynamic modes after classification by the 30s window method. Generally, most of the correlations are between 0.3 and 0.6, and most body parts exhibit higher correlations in the highly-dynamic mode than in the weakly-dynamic mode. Among different body parts, the forehead, forearm, and hand illustrate higher correlations than other body parts in the highly-dynamic mode, while in the weakly-dynamic mode, the forearm, hand, and calf show higher correlations than others.

The step-up phase model employed derivatives of local skin temperatures and derivatives of mean skin temperatures as predictors to predict the dynamic local TSV. Table 5.7 shows the r_s between the derivative of local skin temperature and the dynamic term of local TSV ($TSV_{i,dynamic}$) of highly-dynamic and weakly-dynamic modes. The $TSV_{i,dynamic}$ is computed by Eq. (6). To build the step-down phase model, the data with $dT_{sk,i}/dt$ smaller than zero were selected for the correlation analysis. In general, the correlations between $dT_{sk,i}/dt$ and $TSV_{i,dynamic}$ are much lower than those of $T_{sk,i}$ and local TSV. The correlations in the highly-dynamic mode are slightly higher than those in the weakly-dynamic mode. Among different body parts, in the highly-dynamic mode, the back and upper arm show higher correlations than other body parts, while the back illustrates a higher correlation than other body parts in the weakly-dynamic mode.

The r_s between the derivative of mean skin temperature and the dynamic term of local TSV ($TSV_{i,dynamic}$) in the two modes are further illustrated in Table 5.8. The data with $dT_{sk,m}/dt$ smaller than zero were selected for the correlation analysis. The correlations between $dT_{sk,m}/dt$ and $TSV_{i,dynamic}$ in the highly-dynamic mode are higher than those in the weakly-dynamic mode, similar to the correlation results between $dT_{sk,i}/dt$ and $TSV_{i,dynamic}$.

In the step-up phase model, $dT_{sk,i}/dt$ and $dT_{sk,m}/dt$ are used as the independent variables for the local TSV prediction in the highly-dynamic mode, and $dT_{sk,m}/dt$ is selected as the independent variable in the weakly-dynamic mode. For the step-down phase model in this study, $dT_{sk,i}/dt$ and $dT_{sk,m}/dt$ are still used as the independent variables for the local TSV prediction in the highly-dynamic mode. Given the slightly larger correlations between $dT_{sk,i}/dt$ and $TSV_{i,dynamic}$ compared to that of $dT_{sk,m}/dt$, $dT_{sk,i}/dt$ will be employed as the independent variable for weakly-dynamic mode. Nevertheless, lower correlations are exhibited in the step-down phase than in the step-up phase. The detailed explanation is provided in Section 5.4.1.

Table 5.6 Spearman correlations (r_s) between local skin temperature and local TSV (TSV_i) of highly-dynamic and weakly-dynamic modes.

		$T_{forehead}$	T_{chest}	$T_{abdomen}$	T_{back}	$T_{upper\ arm}$	$T_{forearm}$	T_{hand}	T_{thigh}	T_{calf}	T_{foot}	T_{neck}
TSV_i	Highly-dynamic mode	0.41	0.33	0.22	0.25	0.35	0.53	0.43	0.37	0.35	0.32	0.33
	Weakly-dynamic mode	0.35	0.26	0.16	0.23	0.3	0.37	0.4	0.36	0.42	0.32	0.26

Table 5.7 Spearman correlations (r_s) between the negative derivative of local skin temperature and dynamic term of local TSV ($TSV_{i,dynamic}$) of highly-dynamic and weakly-dynamic modes.

		$dT_{forehead}/dt$	dT_{chest}/dt	$dT_{abdomen}/dt$	dT_{back}/dt	$dT_{upper\ arm}/dt$	$dT_{forearm}/dt$	dT_{hand}/dt	dT_{thigh}/dt	dT_{calf}/dt	dT_{foot}/dt	dT_{neck}/dt
$TSV_{i,dynamic}$	Highly-dynamic mode	0.04	-0.01	-0.03	0.1	0.15	0.01	-0.1	0.04	0.05	-0.04	-0.16
	Weakly-dynamic mode	0.03	0.02	0	0.11	-0.02	-0.02	0.05	0	0.07	0.06	-0.04

Table 5.8 Spearman correlations (r_s) between the negative derivative of mean skin temperature and dynamic term of local TSV ($TSV_{i,dynamic}$) of highly-dynamic and weakly-dynamic modes.

		$TSV_{i,dynamic}$										
		Forehead	*Chest*	*Abdomen*	*Back*	*Upper arm*	*Forearm*	*Hand*	*Thigh*	*Calf*	*Foot*	*Neck*
$dT_{sk,m}/dt$	Highly-dynamic mode	-0.04	0.13	0.08	0.07	0.13	0.1	0.04	0.11	0.11	0.05	0
	Weakly-dynamic mode	0.03	-0.02	0.01	-0.06	0.03	0.05	0.01	-0.05	0.01	-0.01	0.03

5.3.7 Dynamic model for step-down conditions

The derivative of local skin temperature at each vote was averaged backward 30 s during the model development since the outdoor thermal sensation of pedestrians is influenced by the past 20-35 s thermal history (Xie et al., 2022). Data from each outdoor session were selected for dynamic model development if the mean value of $T_{sk,m}$ at the steady state (after 13 minutes at each session) exceeded the lower limit of the neutral zone for $T_{sk,m}$ (33.91 °C (Chapter 3)), to construct a warm-biased model.

5.3.7.1 Highly-dynamic mode prediction

This study will develop the step-down phase model, with negative derivatives of skin temperatures. The regression results of the highly-dynamic mode of different body parts for the step-down phase is presented in Figure 5.9. All body parts used $dT_{sk,i}/dt$ as the independent variable. The original data were binned to improve the accuracy of the regression analysis. To better preserve the characteristics of the raw data, a relatively small bin interval was used, which resulted in lower R^2 among different body parts. Parameter K_1 of the chest, abdomen, and upper arm are higher than those of other body parts, indicating a larger impact of the change rate of skin temperature of these three body parts on local TSV compared with the others. Foot exhibits a low regression result, mainly attributed to the limited variation range in this study, as most subjects wore sneakers during the experiment.

Hand and neck exhibit irregular trends in the data. The low R^2 may be attributed to excessive sweating, which causes irregular fluctuations in the derivative of skin temperature. Thus, the dynamic TSV prediction of hand and neck in the highly-dynamic mode may require further modelling in future studies. Table 5.9 summarizes the coefficients of highly-dynamic mode of step-down model for different body parts.

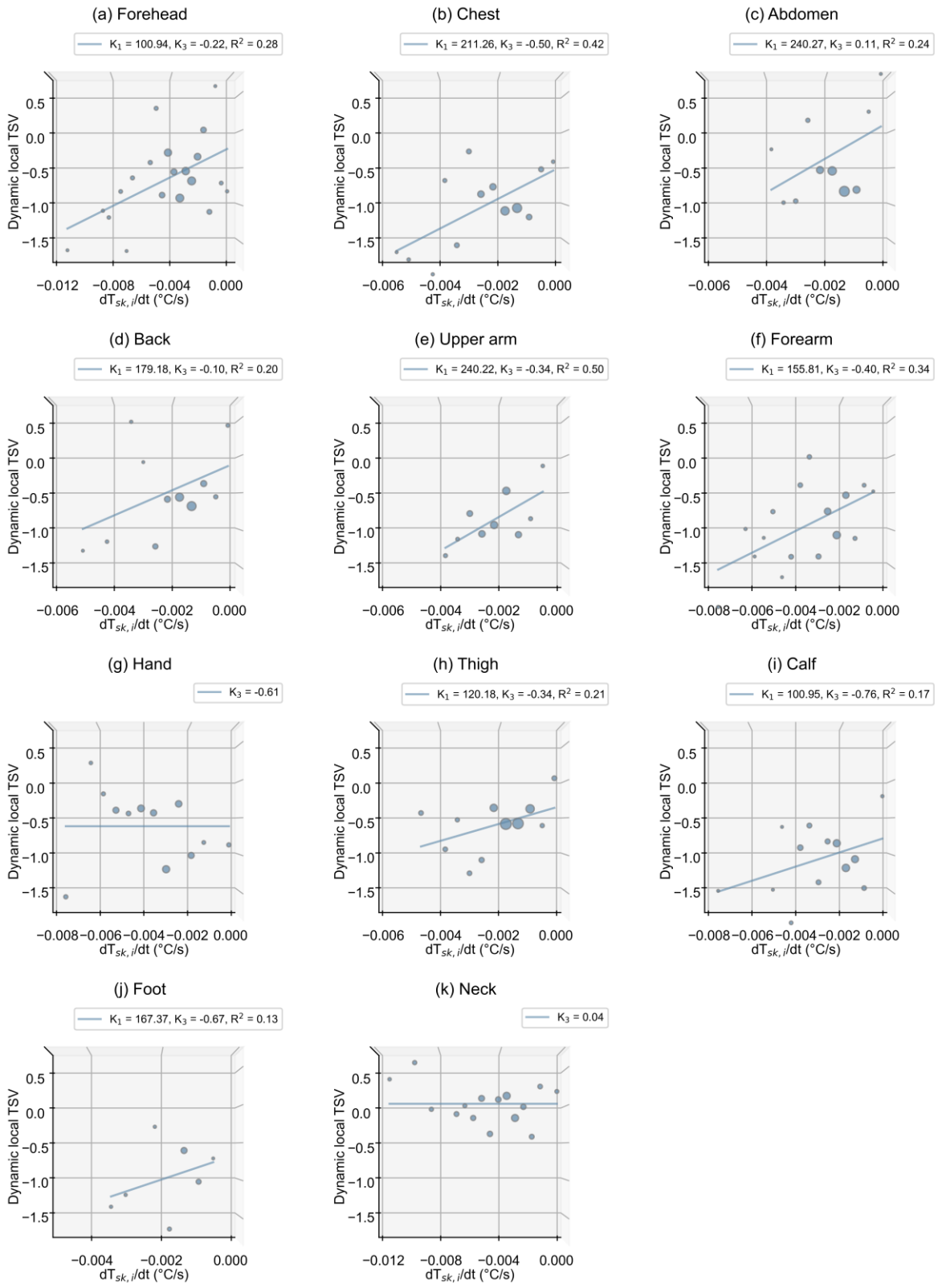

Figure 5.9 Regression results of highly-dynamic mode of the dynamic model.

Table 5.9 The coefficients for the highly-dynamic mode of the dynamic model.

Segment	K_1	K_3	R^2
Forehead	100.94	-0.22	0.28
Chest	211.26	-0.50	0.42
Abdomen	240.27	0.11	0.24
Back	179.18	-0.10	0.20
Upper arm	240.22	-0.34	0.50
Forearm	155.81	-0.40	0.34
Hand	-	-0.61	-
Thigh	120.18	-0.34	0.21
Calf	100.95	-0.76	0.17
Foot	167.37	-0.67	0.13
Neck	-	0.04	-

5.3.7.2 Weakly-dynamic mode prediction

The regression results of the weakly-dynamic mode of the step-down phase of different body parts are shown in Figure 5.10. The weakly-dynamic mode utilizes $dT_{sk,i}/dt$ as the independent variable. The original data were binned to enhance the accuracy of the regression analysis. Only the chest, back, and foot show satisfactory regression results, whereas other body parts exhibit irregular trends between the derivative of skin temperature and dynamic local TSV. The main reason might be that, as the environmental variations are minor in the weakly-dynamic mode, the minor environmental variations may not lead to significant changes in skin temperature during the step-down phase. The detailed explanation will be addressed in Section 5.4.2. Consequently, other body parts in the weakly-dynamic part use a constant line (K_3) to represent the minor shifts of neutral skin temperature and sensation due to different

exposure periods of the dynamic and steady-state periods. Table 5.10 summarizes the coefficients of weakly-dynamic model in the step-down model.

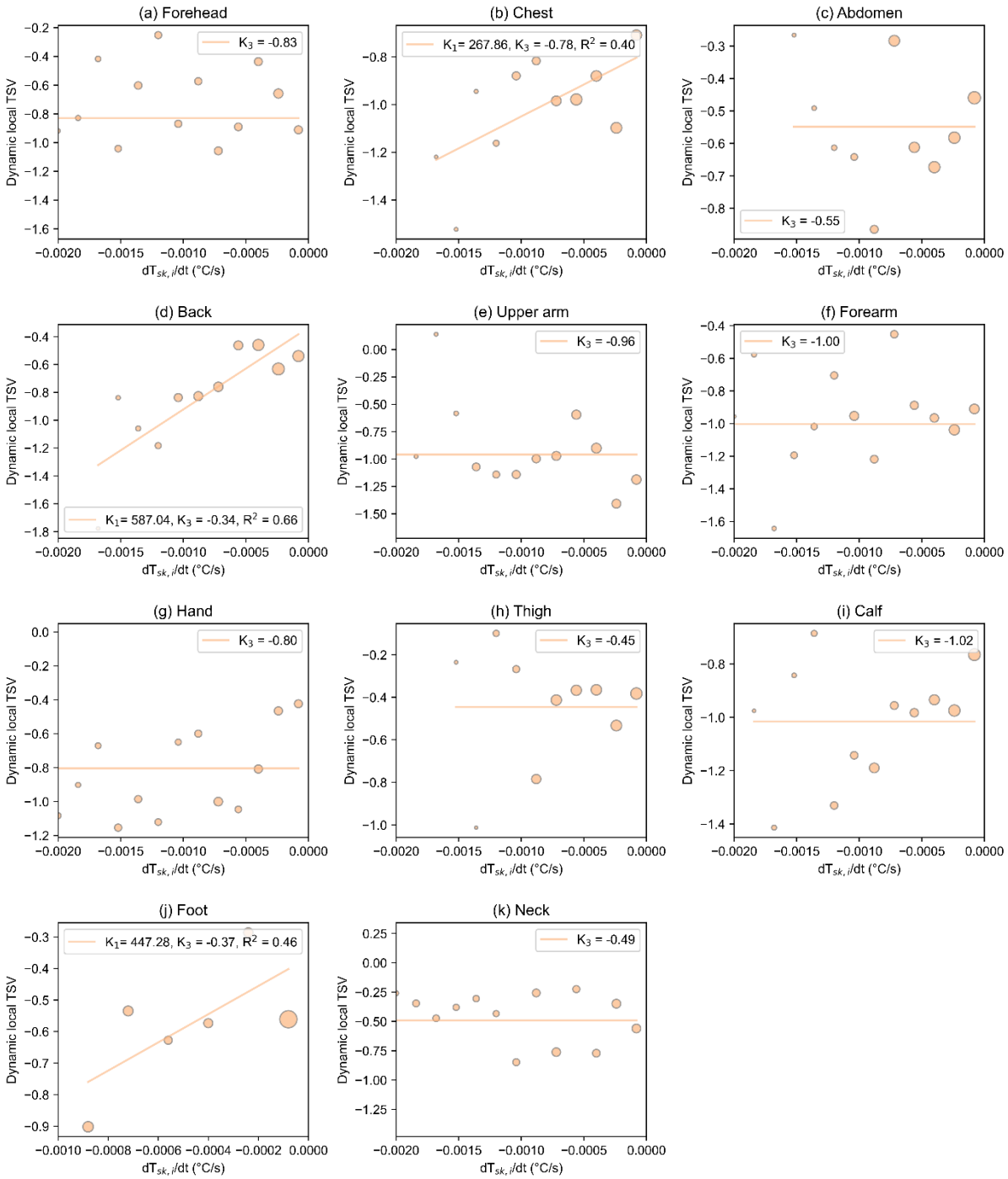

Figure 5.10 Regression results of weakly-dynamic mode of the dynamic model.

Table 5.10 The coefficients for the weakly-dynamic mode of the dynamic model.

Segment	K_1	K_3	R^2
Forehead	-	-0.83	-
Chest	267.86	-0.78	0.40
Abdomen	-	-0.55	-
Back	587.04	-0.34	0.66
Upper arm	-	-0.96	-
Forearm	-	-1.00	-
Hand	-	-0.80	-
Thigh	-	-0.45	-
Calf	-	-1.02	-
Foot	447.28	-0.37	0.46
Neck	-	-0.49	-

5.3.8 Validation of the dynamic model for step-down conditions

The predicted local TSV is the sum of the steady-state part and the dynamic part, as shown in Eq. (5.6). The predicted local TSV will also output three values, including the mean value, the 10th percentile, and the 90th percentile, as presented in Eq. (5.7), (5.8), (5.9). $Accuracy$ is calculated by the percentage of actual local TSV ($TSV_{i,actual}$) located in the $predicted\ range$. Table 5.11 and Table 5.12 summarize the $Accuracy$ of different body parts for the highly-dynamic and weakly-dynamic modes of the step-down phase. Most body parts illustrate a satisfactory result, with the $Accuracy$ ranging from 0.5-0.8, as the predicted range is originally designed to cover 80% of people. The average *Accuracy* of the highly-dynamic mode is 62.1%, while the average $Accuracy$ of the weakly-dynamic mode is 69.0%.

Table 5.11 The *Accuracy* of body parts for the highly-dynamic mode.

Segment	Forehead	Chest	Abdomen	Back	Upper arm	Forearm	Hand	Thigh	Calf	Foot	Neck
$Accuracy$	0.53	0.56	0.70	0.61	0.60	0.59	0.59	0.60	0.52	0.80	0.73

Table 5.12 The *Accuracy* of body parts for the weakly-dynamic mode.

Segment	Forehead	Chest	Abdomen	Back	Upper arm	Forearm	Hand	Thigh	Calf	Foot	Neck
$Accuracy$	0.71	0.58	0.71	0.64	0.71	0.72	0.65	0.68	0.75	0.68	0.77

5.4 Discussion

5.4.1 Difference between step-up and step-down phases of the dynamic part

Lower correlations between $dT_{sk,i}/dt$, $dT_{sk,m}/dt$, and $TSV_{i,dynamic}$ in both highly-dynamic and weakly-dynamic modes of the step-down phase compared with those of the step-up phase is found in Section 5.3.6. To further explore the reasons, the impacts of dPETs on dTSVs are analyzed when the dPET is in the step-up or step-down phases, where the step-up phase corresponds to a positive value of dPET and the step-down phase means a negative value of dPET. The dPETs and dTSVs of each survey point are used in this section, which are defined as the difference between the two adjacent values, as expressed in Eq. (5.11), (5.12).

$$dPET = PET_i - PET_{i-1} \tag{5.11}$$

$$dTSV = TSV_i - TSV_{i-1} \tag{5.12}$$

where the i is the current survey point, $i-1$ is the preceding survey point.

The relationships between dPETs and dTSVs in the step-up and step-down phases for different body parts are shown in Figure 5.11. Generally, the step-up phase shows higher associations (e.g., forehead: 0.25, upper arm: 0.30, forearm: 0.32) between dPETs and dTSVs than those of

the step-down phase (e.g., forehead: 0.00, upper arm: 0.02, forearm: 0.05) for each body part. However, the slopes of the regression lines do not show significant differences between the step-up and the step-down phases. The results suggest that the impacts of dPET on dTSV in the step-up phase are more regular than in the step-down phase in warm-biased conditions. In other words, when people are in warm-biased conditions, the impacts of environmental changes on thermal sensation changes are more irregular when the human body experiences cooling conditions compared with when the human body undergoes heating conditions.

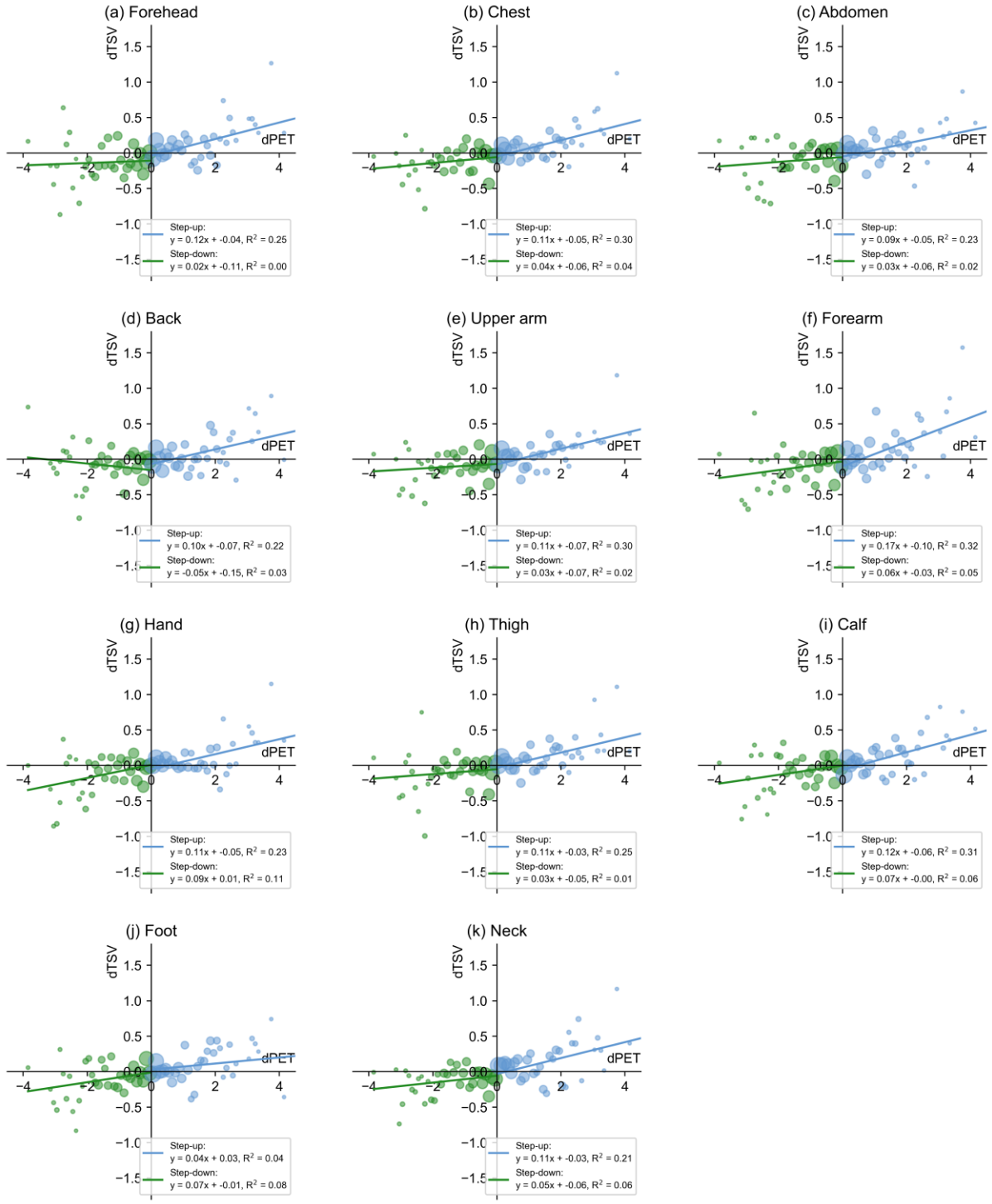

Figure 5.11 The impact of dPETs on dTSVs of step-up and step-down phases of the dynamic part.

5.4.2 Relationship between environmental conditions and physiological responses in highly-dynamic and weakly-dynamic modes

Previous Section 5.3.7.2 illustrates the low R^2 between $dT_{sk,i}/dt$ and $TSV_{i,dynamic}$ in the weakly-dynamic mode. Since the changes in physiological responses are caused by environmental changes, the correlations between environmental conditions and physiological responses in highly-dynamic and weakly-dynamic modes are further analyzed. Table 5.13 summarizes the (r_s) between the $dPET/dt$ and negative $dT_{sk,i}/dt$ of highly-dynamic and weakly-dynamic modes. The r_s between $dPET/dt$ and $dT_{sk,i}/dt$ are much higher in the highly-dynamic mode than those in the weakly-dynamic mode, where the r_s in the highly-dynamic mode are around 0.3 and most of the r_s are lower than 0.1 in the weakly-dynamic mode. The r_s for the foot is the lowest among all body parts in the highly dynamic mode, approaching zero. This is attributed to that most subjects wore sports shoes or leather shoes during the experiments, thereby their feet were uneasily affected by the external environmental changes.

The above analysis suggests that fluctuations in environmental conditions in the weakly-dynamic mode, such as a breeze blowing, did not create significant changes in skin temperature. As a result, the relationship between skin temperature changes and thermal sensation remained unclear in the weakly-dynamic mode during the step-down phase.

Table 5.13 Spearman correlations (r_s) between the negative derivative of local temperature and the derivative of PET of highly-dynamic and weakly-dynamic modes.

		$dT_{forehead}/dt$	dT_{chest}/dt	$dT_{abdomen}/dt$	dT_{back}/dt	$dT_{upper\ arm}/dt$	$dT_{forearm}/dt$	dT_{hand}/dt	dT_{thigh}/dt	dT_{calf}/dt	dT_{foot}/dt	dT_{neck}/dt
$dPET/dt$	Highly-dynamic mode	0.26	0.19	0.28	0.2	0.22	0.32	0.19	0.26	0.35	0.06	0.38
	Weakly-dynamic mode	0.1	0.05	0.07	0.03	0.02	0.14	0.14	0.11	0.08	0.01	0.12

5.4.3 Demonstration of the outdoor thermal sensation model

The series work constructs the entire outdoor thermal sensation model, steady-state part (Chapter 3), provides the steady-state local TSV prediction and overall TSV prediction model; step-up phase of the dynamic part (Chapter 4), provides the heating side of dynamic local TSV prediction model; step-down phase of the dynamic part (this study), provides the cooling side of the dynamic local TSV prediction model. The whole model could provide three sets of local TSV predictions for 11 body parts, as well as three values of overall TSV prediction based on local skin temperatures, the derivatives of local and/or mean skin temperatures. The model could be incorporated with the thermoregulation model (e.g., JOS-3 model), providing local and overall TSV prediction based on environmental conditions.

Figure 5.12 illustrates the output samples of the local TSV prediction model for several body parts. Three values of TSV will be predicted for each body part based on local skin temperatures, the derivative of local and/or mean skin temperatures, including the mean value, 10th percentile, and 90th percentile. The 10th percentile and the 90th percentile can construct a predicted range ($Predicted\ range$) of local TSV that covers 80% of the people. The predicted results show that most of the actual local TSVs are in the $Predicted\ range$, indicating a satisfactory result.

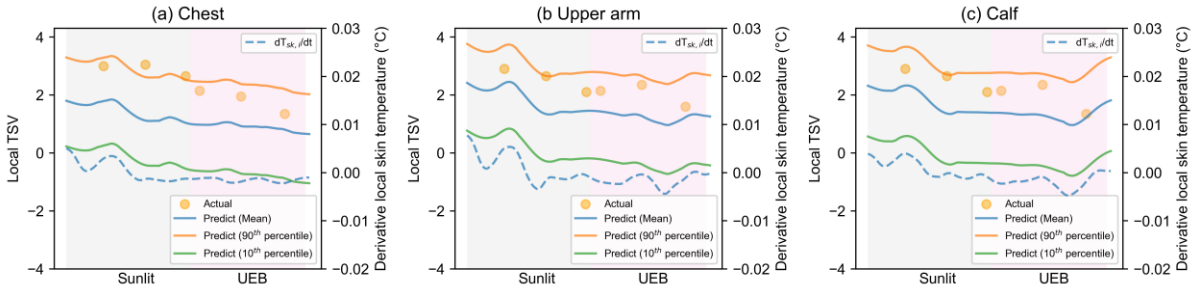

Figure 5.12 Demonstration of the outdoor thermal sensation model during step-change conditions.

5.4.4 Applicability of different voting scales in outdoor thermal environment assessment

Occupants' thermal comfort needs may vary across different scenarios based on the specific use of the space (Y. Yang et al., 2024). Outdoor spaces are commonly designed for recreation and encourage city dwellers to enjoy outdoor activities. As such, thermal evaluation in outdoor environments may require different considerations compared to indoor settings. The thermal stay willingness, TSW, was preliminarily raised in this study and provided a different aspect for the thermal comfort evaluation for the outdoor spaces.

Section 5.3.2 found that TSW exhibited the most significant response during the step changes compared with TA and TP. Thermal overshoot and adaptation are commonly abrupt when pedestrians experience step-change thermal environments (Jiang et al., 2024). Since environmental parameters respond quickly to these changes, their correlations with different thermal evaluation scales may reflect how the scales capture responses to thermal overshoot or adaptation.

Spearman correlations (r_s) between the PET and different thermal evaluation scales with different outdoor exposure durations are further analysed, as presented in Table 5.14. Generally, the r_s between the PET and TSW are the largest. When the exposure duration is smaller than 120 s, r_s difference between TSW and other scales is the largest (TSW: 0.53, others around 0.46-0.48). As exposure duration increases, this difference gradually decreases. For instance, when the exposure duration exceeds 600 s, the r_s between PET and TSW is 0.60, compared to 0.55 for TA. Among the other scales, TP shows a higher correlation with PET than TCV and TA, although its correlation is lower than that of TSW when the exposure duration is under 120 s. However, when exposure exceeds 120 s, TP's correlation with PET becomes similar to that of TSW. Therefore, for step-change outdoor environments, TSW may be suitable for thermal comfort evaluation for outdoor spaces during the transition period (exposure time ≤

120s) as well as prolonged exposure period (exposure time > 120s), and TP would be applicable for the evaluation during prolonged exposure periods (exposure time > 120s).

Table 5.14 Spearman correlations (r_s) between the PET and different voting scales under different exposure durations.

Exposure time (s)	TCV	TA	TP	TSW
≤ 120	0.46	0.44	0.48	0.53
120-300	0.52	0.51	0.55	0.56
≥300	0.56	0.54	0.58	0.59
≥600	0.58	0.55	0.59	0.60

5.4.5 Limitations

The study developed a step-down phase of the dynamic part model, which will be integrated with the steady-state part and step-up phase of the dynamic part to provide the local and overall TSV predictions. However, non-uniform thermal conditions created by localized irradiation and cooling devices (e.g., radiant cooling panel and localized fan) have not been considered in this study. Future studies could explore the thermal responses of different body parts in non-uniform thermal conditions.

The current model is developed based on sitting and standing postures. Higher metabolic rates may result in different changes in core temperature responses. Future studies are needed to explore its application across different activity levels (e.g., walking, running) and diverse populations.

Continuous sweat rate was not measured in this study. The rate of change in sweat rate may serve as a rapid physiological indicator of dynamic thermal status, especially during the step-down phase. Future research should explore the relationship between the derivative of sweat rate and dynamic local TSV, which may help improve the model accuracy in the step-down phase.

For different outdoor scenarios, the applicability of thermal evaluation scales may be different. For example, the thermal acceptability, TA, might be more applicable and sensitive than other scales when pedestrians are under high heat stress conditions. The applicability of different thermal evaluation scales under varying outdoor scenarios could be explored in future studies.

5.5 Chapter conclusions

This study conducted a series of step-change thermal environments, including indoor, UEB, and sunlit conditions. As an extension of the step-up phase model (Chapter 4), the step-down phase of the dynamic part of the outdoor thermal sensation model was developed for neutral to warm-biased thermal conditions. Subjects transferred from different step-change environments, a total of 142 human subject tests were completed, with environmental parameters, skin temperature of 12 body parts, and subjective votes (i.e., TSV, TCV, TA, TP, TSW) collected. The findings are as follows:

1. The steady-state part prediction of the abdomen, foot, and neck has been rebuilt due to the wider range of skin temperature and abdomen TSV data collected in this study. Since different effects of v and T_{mrt} on TSV under high temperature conditions, a SWI correction term was added to enhance the accuracy of the steady-state part.
2. Skin temperature data were classified into the highly-dynamic mode and the weakly-dynamic mode based on the empirical critical value. Critical values, defined as the 75th percentile of $dT_{sk,i}/dt$ value of the weakly-dynamic mode, which were updated using both our previous experiment data and the data from this study. In the weakly-dynamic mode, the correlations between the $dT_{sk,i}/dt$ and dynamic local TSV are lower than those in the highly-dynamic mode, mainly attributed to that the minor negative fluctuations in environmental conditions, did not induce effective changes in skin temperature.

3. The step-up phase showed higher associations between dPETs and dTSVs than those of the step-down phase for each body part. This suggests that when people are in warm-biased conditions, the impacts of environmental changes on thermal sensation changes are more irregular during cooling than during heating.
4. The step-down phase of the dynamic model of 11 body parts during highly-dynamic and weakly-dynamic modes was developed. For the step-down phase, both highly-dynamic and weakly-dynamic modes employ $dT_{sk,i}/dt$ as the independent variable. The average Accuracy for the highly-dynamic mode is 62.1%, and 69.0% for the weakly-dynamic mode.
5. The applicability of different thermal evaluation scales in outdoor spaces was assessed. For step-change outdoor environments, TSW may be more suitable than TCV and TA for thermal comfort evaluation during both the transition period (≤ 120 s) and prolonged exposure period (> 120 s), while TP would be applicable for prolonged exposure period (> 120s).

The steady-state part, step-up phase, and step-down phase of the dynamic model would be combined for the local and overall TSV prediction model, providing three sets of local TSVs for 11 body parts as well as three values of overall TSV. The outdoor thermal sensation model can be integrated with the advanced multi-nodal thermoregulation model for the outdoor thermal environment assessment during the design and renovation stages.

Chapter 6 – **Thermal alliesthesia and short-term adaptation response to step changes between real-life indoor and outdoor environments**

Short-term dynamic thermal perception and physiological response to transient outdoor environments

6.1 Summary

Thermal alliesthesia and short-term thermal adaptation are two well-known concepts affecting dynamic thermal perceptions (Vellei et al., 2021), and they are essential theories for creating a high degree of thermal pleasant and thermal comfort feelings. However, few studies explored the combined effect of thermal alliesthesia and adaptation phenomena on dynamic thermal perceptions in real-life environments, especially the psycho-physiological aspect of thermal alliesthesia and short-term adaptation in step-change indoor and outdoor thermal environments. Thus, this Chapter will investigate the dynamic thermal perceptions (i.e., thermal sensation and thermal comfort) and physiological responses (i.e., local and mean skin temperatures and sweat rate) in transient indoor and outdoor exposures based on thermal alliesthesia and adaptation concepts. The specific objectives are as follows:

1. To investigate the short-term dynamic change of human thermal perceptions in step-change thermal environments based on thermal alliesthesia and short-term thermal adaptation concepts.
2. To investigate the short-term dynamic change of human physiological response in step-change thermal environments.

3. To explore the relationship between short-term thermal perceptions and physiological response in transient thermal environments.

This study examined the short-term dynamic thermal perceptions and physiological responses of 50 subjects exposed to step-change indoor and different outdoor environments, including underneath an elevated building (UEB) and sunlit areas. Environmental parameters were monitored using a microclimate station, while physiological parameters were characterized by mean and local skin temperatures and sweat rate.

Results show that short-term transitions lead to thermal alliesthesia and adaptation. When thermal environment changed, overshoot in thermal sensation persisted for at least 5 mins, and its influence on thermal comfort increased and then diminished at around the 5 min, at which point thermal adaptation began to occur. The current thermal comfort was affected by the preceding thermal status: in the strong alliesthesia zone, a 1.00 scale decrease in dTSV resulted in a 0.44 scale increase in dTCV; whereas in the moderate alliesthesia zone, a slight dTSV within 1.00 scale could positively affect dTCV. Skin temperature of exposed segments correlated better with TSV than that of unexposed ones. Still, skin temperatures had lower correlations with TSV compared with experiments at static conditions conducted by other researchers. Besides thermal alliesthesia and adaptation effects, sweat accumulation and evaporation are possible reasons for the low correlations. The findings may have implications in adopting dynamic features outdoors for better design of thermal environment.

6.2 Methods

6.2.1 On-site settings

The experiment was conducted in the campus of Hong Kong Polytechnic University. Hong Kong has a monsoon-influenced humid subtropical climate (Cwa) based on the Köppen climate

classification (Peel et al., 2007), with mild, dry winters and hot, humid summers. The experiments were conducted in both mild spring conditions from February to April and hot summer conditions from August to September. Three sites were selected to cover different environmental conditions of pedestrians, as shown in Figure 6.1. Site 1 is an indoor transitional area with air-conditioning, which will be referred to as the indoors in this study. Site 2 is a semi-outdoor area located underneath an elevated building (UEB), which will be referred to as the UEB here. The UEB area at a ground level supported by pillars and shaded by building structure (Huang et al., 2020) has proven to improve local thermal comfort conditions in hot and humid summers due to the wind amplification and the shading effects (Niu et al., 2015). Site 3 is an open area that receives direct sunlight, which will be called the sunlit area in this study. The three sites are next to each other.

Figure 6.1 Measurement sites in the field study, reproduced from Chapter 5.

The pedestrian level meteorological data were collected by a microclimate station that consists of radiometers, an anemometer, and an air temperature and humidity sensor, as shown Figure 6.2-a. All of the instruments on the microclimate station were set at a height of around 1.5 m. During the experiment, the microclimate station was located within 1 m of the subjects. The technical information of these instruments is listed in Table 6.1. Specifically, the pyranometer and pyrgeometer from Kipp & Zonen CNR-4 were used to measure short-wave radiation fluxes (K_i) and long-wave radiation fluxes (L_i) for the calculation of the mean radiant temperature (T_{mrt}). The local skin temperatures of 7 body parts of human subjects were collected, as shown in Figure 6.2-b. The foot skin temperature was measured using the i-buttons for convenient movement. The other local skin temperatures were collected using thermocouples with portable data loggers. Sweat rate was measured by a commercial VapoMeter (Delfin Technologies, Finland) in this study which can provide instant sweat measurement from transepidermal water loss (also known as insensible sweat, sweat in the form of vapor) to sensible sweat (sweat in the form of liquid).

The mean skin temperature ($T_{m,skin}$) was calculated by Eq. (6.1) as follows:

$$T_{m,skin} = 0.07T_{forehead} + 0.35T_{abdomen} + 0.14T_{arm} + 0.05T_{hand} + 0.19T_{thigh} + 0.13T_{calf} + 0.07T_{foot} \quad (6.1)$$

Table 6.1 Technical information of equipment used for the field test.

Measurement type	Monitored parameter	Sensor/Equipment	Accuracy	Range of measurement	Sampling rate
Microclimate parameters	Air temperature (T_a)	R.M. YOUNG	±0.3 °C	-50 ~ +50 °C	1 s
	Relative humidity (RH)	41382	±1%	0 ~ 100%	

	Wind speed (v)	R.M. YOUNG 81000	±0.05 m/s	0 ~ 40 m/s	1 s
	Long-wave radiation (L_i)	Kipp & Zonen CNR-4	< 10%	-250 ~ +250 W	1 s
	Short-wave radiation (K_i)		< 5%	0 ~ 2000 W	1 s
Physiological parameters	Skin temperature	i-button TT-T-30-SLE	±0.5 °C ±(0.4% or 0.5 °C)	-40 ~ +85 °C -200 ~ +150 °C	1 s
	Sweat rate	Delfin VapoMeter SWL5	±0.4%	0 ~300 g/m^{2}h	As needed

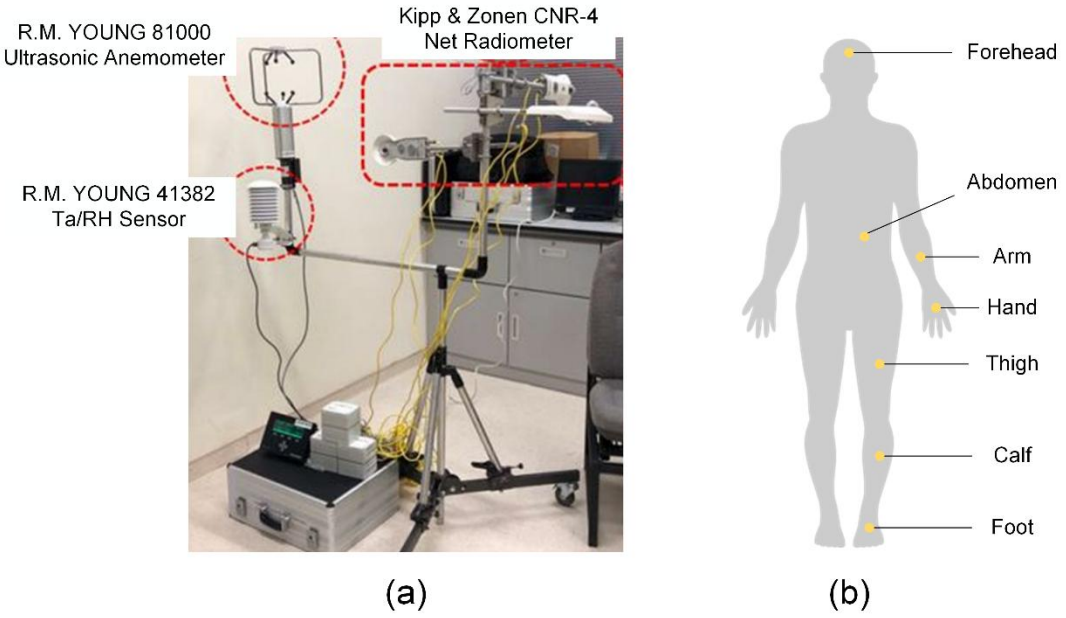

Figure 6.2 Specific devices on microclimate station and graphical explanation of local skin temperature measurement points (a) Microclimate station (Xie et al., 2018); (b) Measurement points of local skin temperatures.

6.2.2 Questionnaire

The questionnaire includes two parts: basic information and subjective evaluation. The basic information includes gender, height, weight, age, health, activity level, and clothing information. The subjective evaluation part was designed for collecting thermal responses from human subjects, which includes local thermal sensation and thermal comfort for different body parts, as well as the overall thermal sensation and comfort. An extended nine-point scale (Zhang et al., 2010c; Xie et al., 2019) was used for both thermal sensation vote (TSV) and thermal comfort vote (TCV), as shown in Figure 6.3. The extended TSV scale followed the ASHRAE 7-point scale (ASHRAE) with 'very cold' (-4) and' very hot' (+4) added at the ends. The extended TCV scale was from very uncomfortable (-4) to very comfortable (+4).

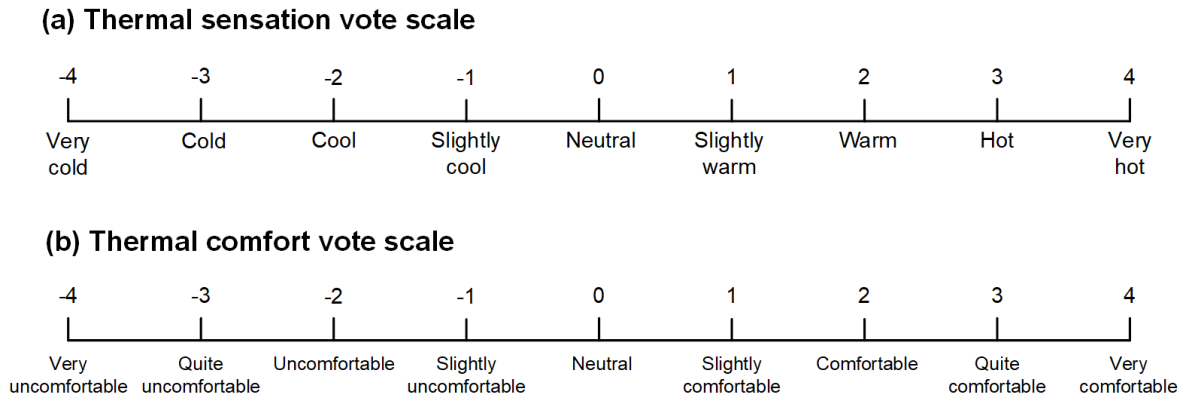

Figure 6.3 The extended TSV scale and TCV scale.

6.2.3 Experiment procedure

Figure 6.4 shows the experimental procedure of this study. Human subjects had a 15-min preparation period, during which skin temperature sensors were attached to local body parts and the experiment procedure was explained in an air-conditioned indoor sitting area. The human subjects were then provided with a 10-min adaptation period in the air-conditioned indoor environment (Site 1). In this period, the basic information questionnaire and the first

subjective evaluation questionnaire were filled out. The arrangement of this period was also for eliminating the potential influence of previous thermal experience on the following experiment and ensuring that each human subject reached a stable metabolic rate and thermal status. According to the results from Zhang et al. (2020), the metabolic rate can be stabilized within a 10-min period. Then, the human subjects were asked to walk slowly from Site 1 to Site 2 (the UEB area) to have a 10-min exposure, and to vote at the 1st min, the 5th min, and the 10th min, starting with their first arrival. Then, they were asked to return to Site 1 to have a repeated 10-min indoor exposure (indoor#2) and to vote at the 1st min and the 5th min after arriving at Site 1. The indoor#2 exposure was then followed by a 10-min sunlit exposure at Site 3, and three votes were conducted similar to Site 2. The local skin temperatures were measured during the whole experiment. The measurements of sweat rate were taken at the 5th min after entering Site 1, the 5th min, and the 10th min after entering Site 2 and Site 3. Since people rarely sweat during mild thermal conditions, sweat rate was measured only during several summer experiments (10 samples). A total of 450 subjective evaluation questionnaires were collected in this study.

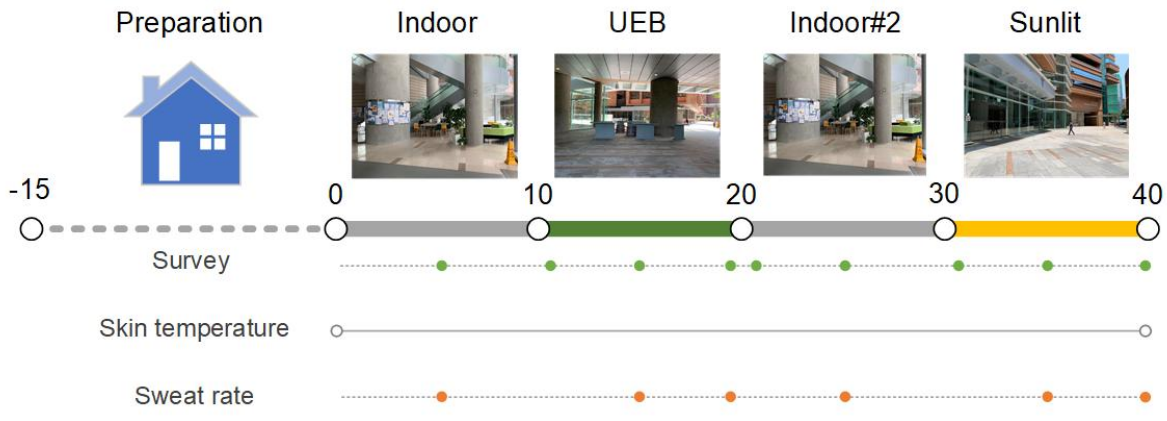

Figure 6.4 Experimental procedure of this study (The 'o' markers indicate the point of time at which questionnaires were filled in and measurements were conducted).

6.2.4 Participants

A total of fifty human subjects (30 males and 20 females) participated in the experiment. Thirty-six (22 males and 14 females) and fourteen (8 males and 6 females) human subjects participated in spring and summer experiments, respectively. Table 6.2 summarizes the detailed characteristics of the participants. The mean age of subjects was around 24.5 in the spring experiments and 22.9 in the summer experiments, and the mean body mass index (BMI) was around 21.0 kg/m^2. The clothing insulation of subjects was around 0.55 clo for spring and 0.25 clo for summer.

Table 6.2 Characteristics of participants

		Count	Age (years)	Height (cm)	Weight (kg)	BMI (kg/m^2)	Clothing insulation (clo)
Spring	**Male**	22	26.5 ± 9.6	174.5 ± 6.0	66.3 ± 10.9	21.7 ± 2.8	0.5 ± 0.3
	Female	14	22.5 ± 3.2	161.1 ± 3.9	53.0 ± 5.0	20.4 ± 1.6	0.6 ± 0.2
Summer	**Male**	8	24.1 ± 11.6	169.9 ± 8.4	61.9 ± 10.8	21.2 ± 1.9	0.2 ± 0.1
	Female	6	21.7 ± 0.8	160.5 ± 5.2	54.8 ± 7.8	21.2 ± 2.2	0.3 ± 0.0

6.2.5 Data analysis methods

6.2.5.1 Calculation of mean radiant temperature (T_{mrt})

One of the main differences between indoor and outdoor thermal environments is the solar radiation. Mean radiant temperature (T_{mrt}) is a crucial index to quantify the radiative heat transfer between a human body and the surrounding environment. The pyranometer from CNR-4 measured short-wave radiation fluxes (K_i) and the pyrgeometer measured long-wave radiation fluxes (L_i). The six individual measurements of short-wave radiation and long-wave

radiation fluxes need to be multiplied by the angular factors F_i $(i = 1 - 6)$ between a human body and the surrounding surfaces according to Eq. (6.2) (ISO, 1998):

$$T_{mrt} = \sqrt[4]{\sum_{i=1}^{6} \frac{F_i\left(a_k K_i + \varepsilon_p L_i\right)}{\varepsilon_p \sigma}} - 273.15 \tag{6.2}$$

K_i : Short-wave radiation fluxes $(i = 1 - 6)(W/m^2)$

L_i : Long-wave radiation fluxes $(i = 1 - 6)(W/m^2)$

F_i : Angular factors between a person and the surrounding surfaces $(i = 1 - 6)$ was set to 0.06 for standing or walking posture (or 0.13 for sitting posture) for two vertical directions, 0.22 for standing or walking posture (or 0.185 for sitting posture) for four horizontal directions if a person is approximated as a cylinder (Holmer et al., 2018)

α_k : Absorption coefficient of a clothed human body for short-wave radiation (Standard value 0.70)

ε_p : Emissivity of a clothed human body for long-wave radiation (Standard value 0.97)

σ : Stefan - Boltzmann constant $(5.67 \cdot 10^{-8}\ W/(m^2K^4))$

6.2.5.2 Thermal alliesthesia effect

Thermal alliesthesia effect can be quantified by the difference between current thermal perception and preceding thermal perception. Based on Liu's research (Liu et al., 2021) and the thermal alliesthesia framework developed by Parkinson and de Dear (Parkinson & de Dear, 2015; Parkinson et al., 2016), the change of thermal sensation vote ($dTSV$) and change of thermal comfort vote ($dTCV$) are defined by Eqs. (6.3) and (6.4):

$$dTSV = TSV\ (t_2) - TSV\ (t_1) \tag{6.3}$$

$$dTCV = TCV\ (t_2) - TCV\ (t_1) \tag{6.4}$$

Accordingly, the change rate of thermal sensation vote ($dTSV/dt$) and change rate of thermal comfort vote ($dTCV/dt$) are defined by Eqs. (6.5) and (6.6):

$$\frac{dTSV}{dt} = [\,TSV\ (t_2) - TSV\ (t_1)]/(t_2 - t_1) \tag{6.5}$$

$$\frac{dTCV}{dt} = [\,TSV\ (t_2) - TSV\ (t_1)]/(t_2 - t_1) \tag{6.6}$$

where $TSV\ (t_2)$ and $TCV\ (t_2)$ represent the current thermal sensation and thermal comfort votes at the t_2 time, $TSV\ (t_1)$ and $TCV\ (t_1)$ represent the preceding votes at the t_1 time, and $(t_2 - t_1)$ represents the time interval between two surveys.

6.2.5.3 Short-term thermal adaptation effect

In order to quantify the changes in thermal perceptions with different time scales after thermal transition, and further analyse the changes in short-term thermal adaptation effect, ΔTSV and ΔTCV are defined by the current thermal perception vote ($TSV\ (t_2)$ or $TCV\ (t_2)$) minus the last thermal perception vote at the previous site before thermal transitions ($TSV\ (t_0)$ or $TCV\ (t_0)$), as shown in Eqs. (6.7) and (6.8). It should be noted that the $TSV\ (t_2)$ and $TCV\ (t_2)$ can be referred to as any votes after thermal transition.

$$\Delta TSV = TSV\ (t_2) - TSV\ (t_0) \tag{6.7}$$

$$\Delta TCV = TCV\ (t_2) - TCV\ (t_0) \tag{6.8}$$

6.2.5.4 Data outlier detection and smoothing

The Anomaly Detection Toolkit (ADTK) Python package (Chakraborty et al., 2020) was used for the outlier detection in wind speed data. This study used PersistAD of ADTK, a method using a sliding window to compare each time series data with the median or mean value of its preceding time window (Chakraborty et al., 2020). Regarding skin temperature measurement, thermocouples are well-known for their fast response, but they are less stable and are more

likely to generate noise signals if sampled at a high frequency. Therefore, the wavelet smoothing method, commonly used in signal processing, was used to smooth skin temperature in this study. The Savitzky-Golay Python package (Virtanen et al., 2020), a kind of signal processing method, is used in this study to eliminate noise in skin temperature measurement data.

6.2.5.5 Statistical analysis

A universal thermal index, Physiological Equivalent Temperature (PET) was adopted in this study to represent the objective thermal environment (Peter Höppe, 1999; Walther & Goestchel, 2018). PET is defined as the air temperature in a typical indoor environment at which the body's energy budget, maintained by skin and core temperatures, is the same as under complex outdoor conditions (Peter Höppe, 1999). It is suitable for both indoor and outdoor thermal environment assessment as it has closer connection with human thermal physiology mechanisms (Matzarakis & Amelung, 2008; Morakinyo et al., 2016). The calculation results of the PET index were obtained using the Python package pythermalcomfort (Tartarini & Schiavon, 2020). The metabolic rate was set at 1.2 met, and the clothing values were set according to the clothing of subjects in this study (0.25 clo in summer and 0.55 clo in spring). Shapiro-Wilk test was used to test whether the subjective data (i.e., TSV, TCV) fit the normal distribution. If the data is normally distributed, the paired-sample t-test was used to verify the difference in the voting results. Otherwise, wilcoxons test for nonparametric paired samples was used. The critical *p-value* was set as 0.05. The Spearman analysis was used for analyzing the correlations between mean and local skin temperatures and TSV. The preferred thermal sensation, and the relationship between the changes of thermal sensation vote (dTSV) and thermal comfort vote (dTCV) were explored by regression methods, including linear and non-linear regressions.

6.3 Results

6.3.1 Thermal conditions

Figure 6.5 provides mean values and ranges of variation of the environmental parameters for 50 sets of field experiments (14 sets in summer and 36 sets in spring), including air temperature, humidity ratio, wind speed, mean radiant temperature, and the PET averaged per minute. The mean air temperature (T_a) in UEB and sunlit was around 31.0 °C in summer and 23.5 °C in spring (Figure 6.5-a, b). The spring record showed little variation between indoor and outdoor air temperatures (within 0.9 °C), while the summer records showed a difference of about 4.0 °C. The indoor air temperature was relatively stable during the experiment, while the air temperature measured in the indoor#2 condition in summer experiments showed a decreasing trend. It should be noted that the decreasing trend in air temperature was a system error. Indeed, both summer and spring indoor thermal environments were stable. This phenomenon was caused by low air speed (below 0.5 m/s) indoors and a radiation shield surrounding the sensor, which limited the air from passing through the shield and being detected effectively by the sensor. It was inevitable that air temperature measurement would be delayed when switching from the UEB to indoor#2 in summer, where obvious differences in air temperature existed (Figure 6.5-a). The mean humidity ratio (d) was about 12.6 to 15.2 g/kg indoors, 17.2 g/kg in UEB area, and 17.6 g/kg in sunlit area during summer experiments, whereas the humidity ratio in the indoors, UEB area, and sunlit area showed little variation (within 1 g/kg) at around 11.2 g/kg during spring experiments (Figure 6.5-c, d). The wind speed in UEB and sunlit areas variated in the range of 0.7 m/s to 2.5 m/s in summer and 0.6 m/s to 1.4 m/s in spring (Figure 6.5-e, f). Compared with that, wind speeds indoors were normally within the unnoticeable range of human body (below 0.5 m/s) (Lawson & AD, 1977) (Figure 6.5-e, f). The mean radiant temperature (T_{mrt}) in indoor and UEB area showed little difference in summer (around 29.0 °C)

and in spring (around 25.0 °C), and the T_{mrt} in sunlit was relatively high (around 45 °C in both summer and spring), as shown in Figure 6.5-g, h. In addition, the averaged PET values representing thermal conditions were calculated in this study (Figure 6.5-a, b). In summer experiments, the PETs were around 30.3 °C, 28.5 °C, and 33.5 °C in indoors, UEB area, and sunlit area, respectively. In spring experiments, the PETs were around 25.4 °C indoors and 21.6 °C in UEB area and 28.8 °C in sunlit area. A significant difference between PET and air temperature was observed both during summer and spring experiments in the UEB area. It was mainly due to the high wind speed drastically reducing PET.

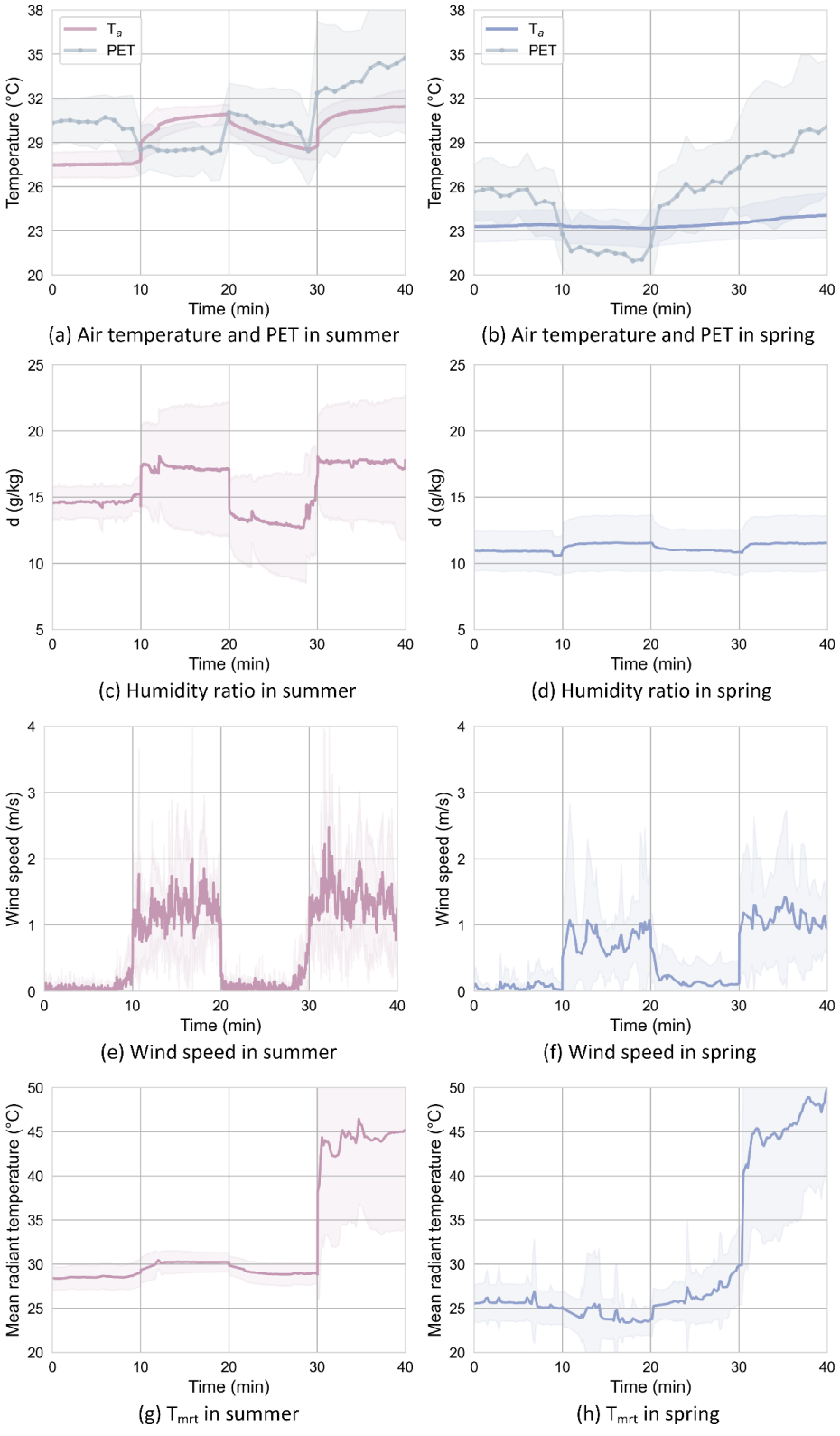

Figure 6.5 Environmental parameters during the whole experiment. (a)(b). Air temperature and PET in summer and spring; (c)(d). Humidity ratio in summer and spring; (e)(f). Wind speed in summer and spring; (g)(h). Mean radiant temperature in summer and spring.

6.3.2 Thermal alliesthesia and short-term thermal adaptation

6.3.2.1 Dynamic thermal sensation

Figure 6.6 shows the results of variations in TSV and the change rate of TSV (dTSV/dt). Table 6.3 summarizes the statistical significance results of current TSV and TCV compared with the last voting at the previous sites in detail. In general, thermal sensation in UEB area was lower than indoors, and thermal comfort in UEB area was higher than indoors. Conversely, thermal sensation in sunlit area was higher than indoors, and thermal comfort in sunlit area was lower than indoors.

The boxplots of TSV for summer and spring experiments are shown in Figure 6.6-a, b. In summer, when subjects transferred from indoors to UEB area, mean TSV decreased by up to 1.71 scales, possibly due to the cool effects of wind. All three TSV results from UEB area showed significant differences from that of the indoors (*p-value* < 0.05). Conversely, when subjects transferred from indoors to sunlit area, mean TSV increased by up to 1.50 scale with the 2nd questionnaire showed significant differences with that of the indoors (*p-value* < 0.01). In spring, when subjects transferred from the indoors to UEB area, mean TSV was decreased by up to 1.51 scales, and all three votes in the UEB area showed significant differences with that of the indoors (*p-value* < 0.01). Conversely, when subjects transferred from indoors to sunlit area, mean TSV was increased by up to 0.99 scales with significant differences (*p-value* < 0.05) between indoors and all three votes from sunlit area.

By comparing the time-sequential votes each time human subjects changed sites, thermal overshoot was observed. The maximum absolute mean TSVs for both UEB and sunlit conditions were observed during the 2nd questionnaire (the 5th min) following transfer from indoors to outdoors. It is evident from Figure 6.6-a that, in summer, when thermal conditions

changed, both cool and warm overshoots lasted for 5 mins and weakened afterward. In spring, cool and warm overshoots were the highest at the 5th min, then slightly attenuated or lasted till moving to the next location (Figure 6.6-b). Part of this finding corresponds to the findings of Zhang et al. (Zhang et al., 2017), who conducted temperature step-change experiments in a climate chamber, where the overshoot of warm sensation was observed when thermal condition changed, and reached its maximum around the 5th to 6th min in their warming step-change experiments. In their cooling step-change experiments, however, the cool sensation overshoot reached its maximum immediately right after thermal environment changed.

The change rate of thermal sensation vote (dTSV/dt) is shown in Figure 6.6-c, d. We considered TSV stable when dTSV/dt is within ±0.1 scale in this study. Considering the long duration of the first indoor stay and the slight change in thermal response during the second indoor stay, the thermal response before leaving the indoors was considered stabilized and the same as the last indoor questionnaire. The dt in the calculation of dTSV/dt was taken as 1 min in the 1st questionnaire of each transition, and 5 mins in the 2nd and 3rd questionnaires. The fast decline of dTSV/dt for each transition illustrates obvious time-dependent attenuation of both cold and heat sensory response: dTSV/dt for all conditions stabilized in the 3rd questionnaire. That is to say, TSV does not keep rising or dropping over the short time exposure period. Hence, short-term thermal adaptation takes place, which is also observed in the repeated indoor (indoor#2) exposure. Following 10 mins of cool thermal perception in the UEB area, human subjects in the indoor#2 exposure had a lower TSV record than in the first indoor exposure in both spring and summer experiments. This finding is consistent with Zhang's findings pertaining to the cyclical temperature variation experiment, in which air temperature variations were created with amplitudes of 3-4 °C and 5-7 °C (Zhang et al., 2016). They demonstrated that human subjects' TSVs decreased gradually under the second and subsequent cyclical heating exposures.

6.3.2.2 Dynamic thermal comfort and thermal alliesthesia

Figure 6.7 shows the results of variations in TCV and the change rate of TCV (dTCV/dt). In summer, when subjects transferred from indoors to the UEB area, mean TCV was increased by up to 1.50 scale with significant differences at all three sites. Conversely, when subjects transferred from indoors to the sunlit area, mean TCV was decreased by up to 1.00 scale. In spring, when subjects transferred from indoors to the UEB area, the TCV was first slightly increased by 0.27 scales in the 2nd questionnaire and then decreased to 0.92 scales in the 3rd questionnaire. Conversely, when subjects transferred from indoors to the sunlit area, the TCV was decreased by up to 1.75 scales with significant differences in the three questionnaires. By comparison to the maximum TSV, the maximum absolute TCV did not show a clear trend with the warm or cool thermal stimulus. In particular, the comparison of TCVs between UEB and the previous indoor voting during spring experiments, and the comparison between the first vote at the sunlit condition and the vote at indoor#2 during summer experiments showed no significant difference. It is evident from Figure 6.7-a, b that the 25% and 75% TCV values at the UEB in spring and sunlit areas in summer varied greatly, which may be due to individual differences in thermal preference for high wind speed and strong solar radiation. Thus, the finding that maximum overshoot in thermal sensation occurs in about 5 mins might not be applicable when it comes to comfort perception.

While variations in thermal comfort could still be observed in the time-series data, the overshoot of thermal comfort is less obvious than thermal sensation, as shown in Figure 6.7-c, d. The assumption of treating dTCV/dt within ±0.1 scale as stable is made similarly as for dTSV/dt. Thermal alliesthesia, which is an overshoot of thermal comfort, has been empirically confirmed by Parkinson and de Dear (Parkinson & de Dear, 2015) that its intensity is closely associated with the original thermal status and the change of thermal stimulus. Several findings can be revealed by combining Figure 6.6 and Figure 6.7-c, d. First, thermal comfort would only

change if thermal sensation changed. dTCV/dt remained stable when dTSV/dt remained stable. It can be observed through the UEB-2nd, UEB-3rd, indoor#2-2nd, and sunlit-3rd questionnaires from the summer experiment, as well as the UEB-2nd, UEB-3rd, sunlit-2nd, and sunlit-3rd questionnaires from the spring experiment. Furthermore, we have observed several cases that support Cabanac's (Cabanac, 1971) classification of thermal alliesthesia. Cabanac defines positive alliesthesia as the reduction of 'thermoregulatory load-error' while negative alliesthesia refers to the exacerbation of load-error. In our dataset, both the UEB-1st questionnaire from summer and the UEB-1st questionnaire from spring experiments have recorded a warm-biased signal of preceding TSV and a negative value of dTSV/dt, which belong to the case of minimizing load-error, leading to positive changes of thermal comfort. In contrast, the sunlit-2nd questionnaire in summer and the sunlit-1st questionnaire in spring experiments both led to a negative change in thermal comfort due to exacerbating load error. Lastly, there is a question of whether deviation from neutral status is welcomed when people's TSV is in the thermal neutral zone (e.g., [-0.5, +0.5]). From the point of view of the mean value, one case (the indoor#2-1st from the summer experiment) had preceding mean TSV of -0.36, and mean dTSV/dt of 0.86, which resulted in a negative value of dTCV/dt (-1.64). However, one case from the spring experiment, the indoor#2-1st questionnaire, had the preceding mean TSV of -0.31, and mean dTSV/dt of 1.00, resulting in a positive value of 0.12 scale dTCV/dt. In light of these controversial results, we will further explore the relationship between dynamic thermal sensation and comfort in the discussion section.

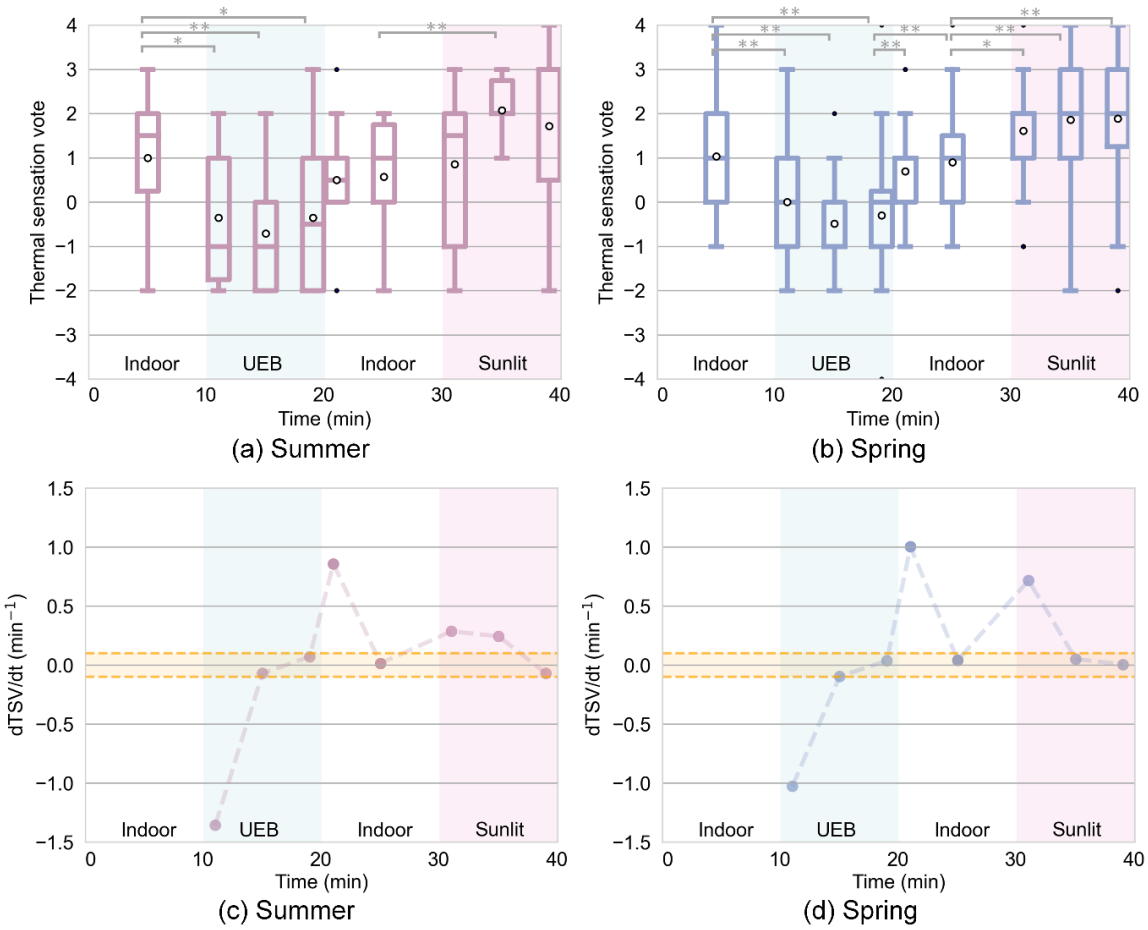

Figure 6.6 Variations in thermal sensation vote (TSV) and change rate of thermal sensation vote (dTSV/dt); significance levels: *p < 0.05, **p < 0.01. (a). TSV in summer; (b). TSV in spring; (c). dTSV/dt in summer; (d). dTSV/dt in spring.

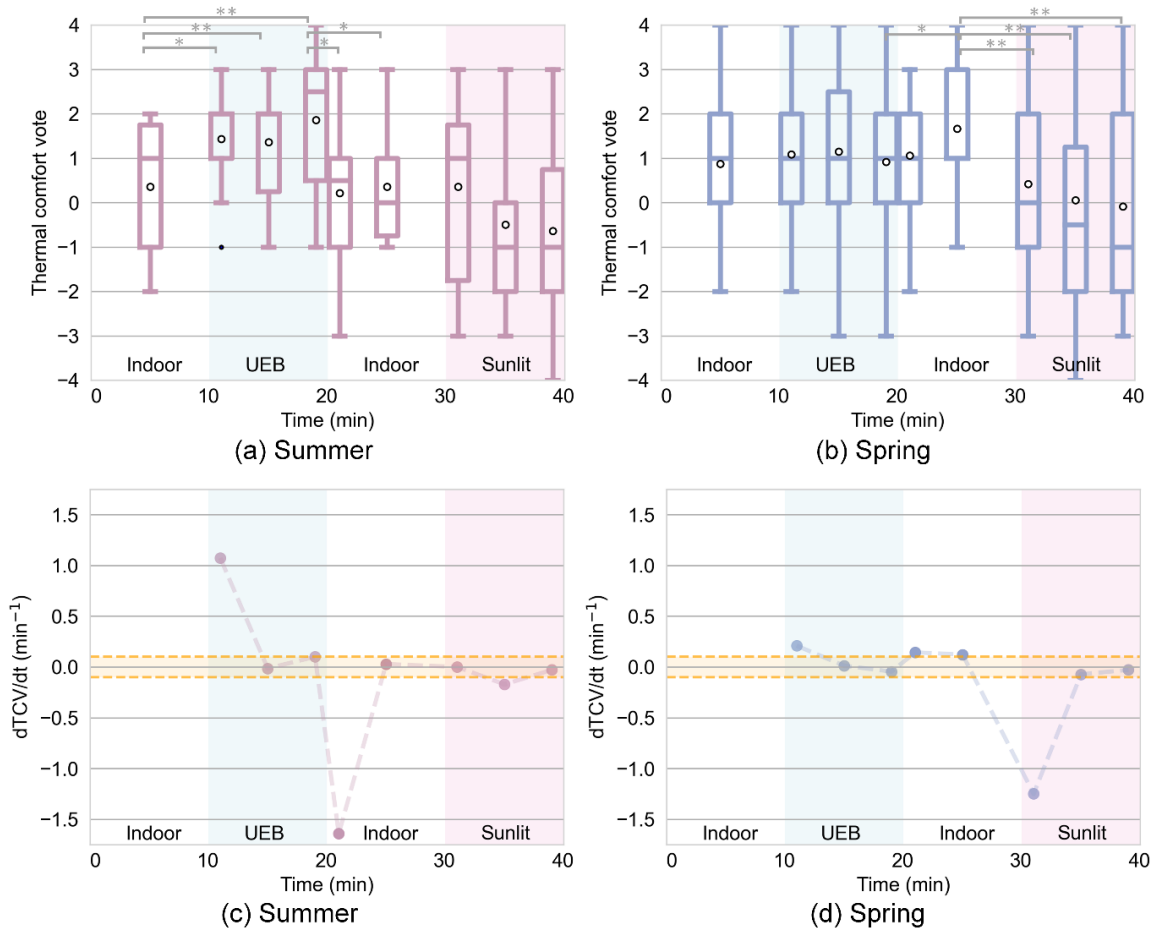

Figure 6.7 Variations in thermal comfort vote (TCV) and change rate of thermal comfort vote (dTCV/dt); significance levels: *p < 0.05, **p < 0.01. (a). TCV in summer; (b). TCV in spring; (c). dTCV/dt in summer; (d). dTCV/dt in spring.

Table 6.3 Statistical significance results of current thermal sensation and thermal comfort vote compared with last voting at previous locations (*p-value*): Significant level, *p < 0.05, **p < 0.01.

		UEB-1st	UEB-2nd	UEB-3rd	Indoor#2-1st	Indoor#2-2nd	Sunlit-1st	Sunlit-2nd	Sunlit-3rd
Summer	TSV	0.011*	0.006**	0.048*	0.079	0.078	0.653	0.005**	0.182
	TCV	0.016*	0.008**	0.003**	0.018*	0.012*	1.000	0.103	0.152
Spring	TSV	0.000**	0.000**	0.000**	0.002**	0.000**	0.015*	0.005**	0.005**
	TCV	0.283	0.515	0.910	0.831	0.018*	0.002**	0.002**	0.007**

6.3.2.3 The influence of exposure time on ΔTSV and ΔTCV

To discover the influence of exposure time on thermal perceptions after thermal transitions, Figure 6.8 presents the relation between ΔTSV and ΔTCV of the 1st, 2nd, and 3rd questionnaires obtained from both the UEB and sunlit sites. The mean ΔTCV of each 1.0 scale of ΔTSV was binned and used for regression. Quadratic regression was used to explore the relationship between ΔTSV and ΔTCV. The results show that the influence of thermal sensation on thermal comfort is more prominent in the warm side than in the cool side. From a parallel comparison of its influence from different time scales, the absolute value of the coefficient of the quadratic term increased from the 1st to the 2nd questionnaire (from 0.14 to 0.23) and then decreased from the 2nd to the 3rd questionnaire (from 0.23 to 0.11), meaning that the change magnitude of ΔTSV to ΔTCV increased from the 1st to the 2nd questionnaire, and weakened from the 2nd to the 3rd questionnaire. A gradual decrease in R^2 with exposure time also shows that ΔTCV is less predicted by merely taking ΔTSV as an independent variable. These results indicate that when the thermal environment changes, a sudden change in thermal sensation helps to create a change in thermal comfort feelings. As time passes, the influence increases and then diminishes at around the 5th min, at which point sensory adaptive process begins to occur and gradually increases to affect thermal perception.

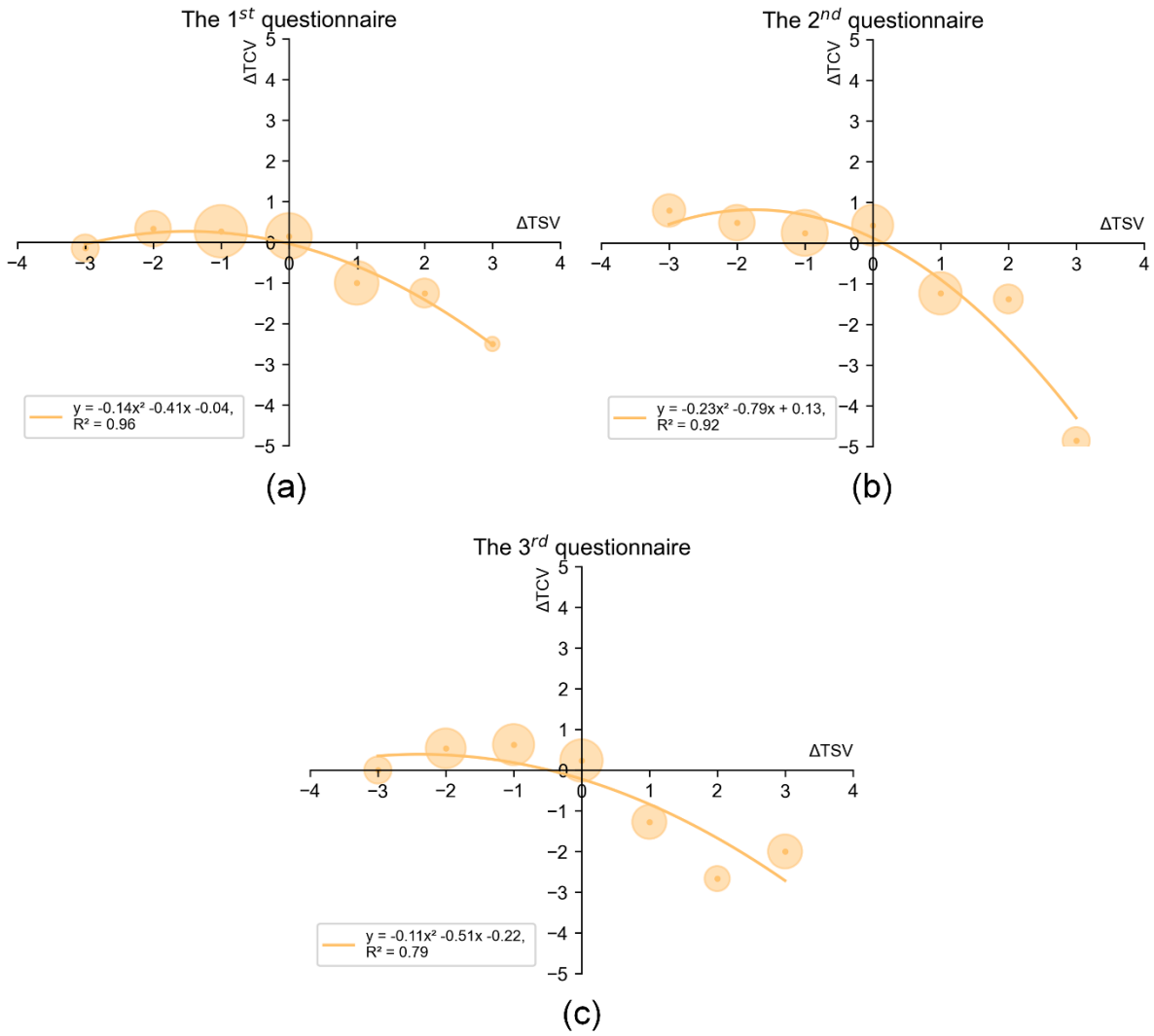

Figure 6.8 The change of thermal sensation vote and thermal comfort vote in different questionnaire stages. (a). The 1st questionnaire; (b). The 2nd questionnaire; (c). The 3rd questionnaire.

6.3.3 Dynamic variations of physiological response

6.3.3.1 Sweat rate

In the summer experiment, sweat rate was measured on the back, arm, and calf, and its variation is shown in Figure 6.9. It is noted that the sweat rate measurements ranged from transepidermal water loss (insensible sweat) to sensible sweat in this study. Human subjects' sweat rate

dropped dramatically when they moved from indoors to UEB area, indicating that the higher air movement in UEB area evaporated sweat more efficiently than in indoor environments. Sweat rate increased when they returned indoors due to a sudden decrease in air movement. In the sunlit condition, sweat rate measurements taken during the 2nd questionnaire were higher than those taken in the indoor#2 condition, and the back's sweat rate dramatically increased during the measurement of the 3rd questionnaire. Wind conditions in UEB and sunlit areas were similar (Figure 6.5-e), but solar radiation in the sunlit area was much higher (Figure 6.5-g). The enhanced evaporation process caused by higher air movement outdoors was unable to counteract the increased amount of sweat caused by higher solar radiation. As a result, sweat accumulated on skin surface and lead to an increase in sweat rate. Also, the sweat rate of back in sunlit condition during 2nd and 3rd questionnaire were higher than that of arm and calf, which suggests that the sweating process is intense at back when exposed to high solar radiation environments.

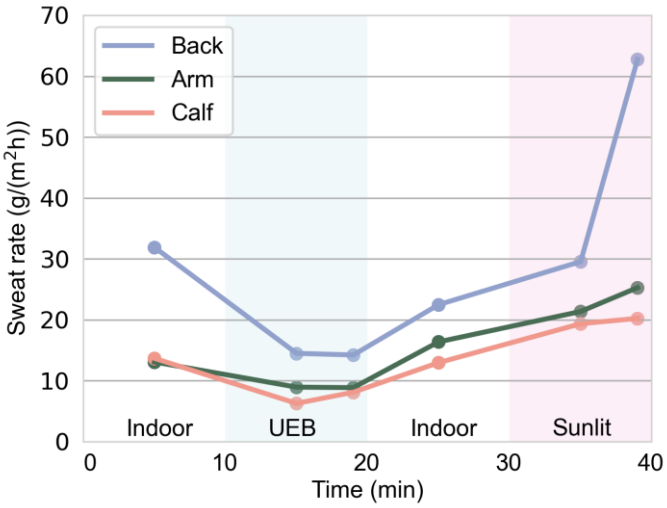

Figure 6.9 The results of sweat rate on back, arm, and calf (10 samples).

6.3.3.2 Variations of mean and local skin temperatures with thermal sensation

Figure 6.10 shows the variations in $T_{m,skin}$ during transient scenario changes. The skin temperature was averaged every minute. During summer experiments, human subjects' $T_{m,skin}$ increased gradually as they moved from indoors to UEB area (from about 32.3 °C to 32.6 °C), dropped dramatically and then increased gradually when they moved from the UEB to indoors (minimum 31.8 °C), and dramatically increased (maximum 33.5 °C) then dropped (minimum 32.7 °C) when they moved from indoors to the sunlit area (Figure 6.10-a). In spring experiments, human subjects' $T_{m,skin}$ kept decreasing when they moved from indoors to the UEB area (from about 32.6 °C to 32.0 °C), then rose when they moved back indoors (stabilized at 32.2 °C), and significantly increased when they were exposed to the sunlit condition (maximum 33.6 °C) (Figure 6.10-b).

The fluctuation of mean TSV did not always correspond to the fluctuation of $T_{m,skin}$. During spring experiments, the fluctuation of mean TSV was mainly explained by the fluctuation of $T_{m,skin}$. Summer experiments, however, revealed several cases of fluctuation of mean TSV that were in the opposite direction of $T_{m,skin}$ fluctuations. In particular, when human subjects moved from indoors to the UEB area, they voted lower TSVs in UEB than they voted indoors, and TSV overshoots were observed. In contrast, the $T_{m,skin}$ recorded in the UEB was relatively higher than that recorded indoors. Additionally, this converse fluctuation was also observed when human subjects moved back indoors, resulting in an increase in TSV, but a decrease in mean skin temperature. A similar phenomenon was observed in the step-change experiment conducted by Zhang et al. (Zhang et al., 2017). In their neutral to warm step-change experiments, where thermal overshoot was recorded, the maximum TSV appeared at 5 min, decreased afterward, and then adapted to the warm condition after 20 mins. Meanwhile, the $T_{m,skin}$ kept increasing for the whole 60 min warm-up experiment.

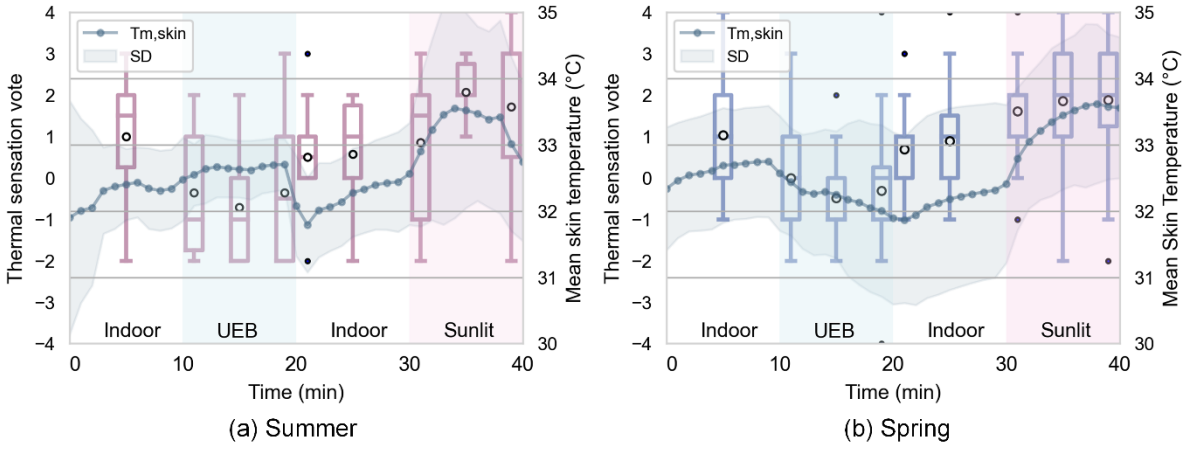

Figure 6.10 The results of mean skin temperature and TSV change. (a). Summer; (b). Spring.

The fluctuation of local skin temperature was further analysed to understand the relation between skin temperature and dynamic thermal sensation. Previous studies have proven that the body parts in contact with the external environment have high accuracy in predicting overall thermal sensation in outdoor environments (K. Liu et al., 2020; Xie et al., 2020). Therefore, this study divided local body parts into two groups based on whether they were covered by clothing: the exposed segments (e.g., forehead and arm) (Figure 6.11-a, b), and the unexposed segments (e.g., abdomen and thigh) (Figure 6.11-c, d).

Compared with unexposed body segments, the fluctuations of exposed segments correlate better with mean TSV in summer experiments (Figure 6.11-a). A noticeable decrease in arm temperature was observed when subjects moved from indoors to UEB (from about 32.3 °C to 31.9 °C). Besides, the transition from indoors to the sunlit area resulted in significant increases then drops in both forehead and arm. The fluctuations described above are in line with that of mean TSV. The fluctuation of exposed body segments cannot, however, fully explain the change in mean TSV. Sweating accumulation and evaporation might be the main reasons

(Figure 6.9). As sweat evaporation increased with enhanced wind speed in the UEB area, caused a decrease in arm skin temperature. When returning indoors, the combined effect of reduced wind speed and sweat accumulation resulted in an increase in skin temperature and mean TSV. In the sunlit conditions, such accumulation processes continued and intensified, creating a large amount of sweating for evaporation, resulting in the initial increase in skin temperatures and mean TSVs. Then, due to the gradual increase in latent heat loss from the skin surface, skin temperatures began to decline and thus led to cooler thermal sensation. The sweat accumulated on the skin amplified hot thermal sensations, and the sweat evaporation amplified cool sensations.

Unexposed segments such as abdomen and thigh displayed in Figure 6.11-c showed a limited range of fluctuations (within 1.5 °C) compared to exposed segments (within 2.5 °C) and different fluctuation trends compared with mean TSV. Specifically, during UEB conditions, the limited fluctuation of skin temperatures of unexposed segments was probably because of their less contact with wind. When moved from indoors to the sunlit area, the sweating process intensified, accumulated, and became trapped in clothing. Increasing wind speed in sunlit areas accelerated the evaporation of wet clothing, decreased the clothing temperature, and when it contacted local body segments, it resulted in the unexposed body parts experiencing dramatic reductions in skin temperature (Havenith, 2002).

Both exposed and unexposed segments showed similar fluctuation trends with mean TSV in spring experiments (Figure 6.11-b, d). Despite the lack of sweat rate data collected during spring experiments, low air temperature and low activity level suggest that sensible sweat did not occur.

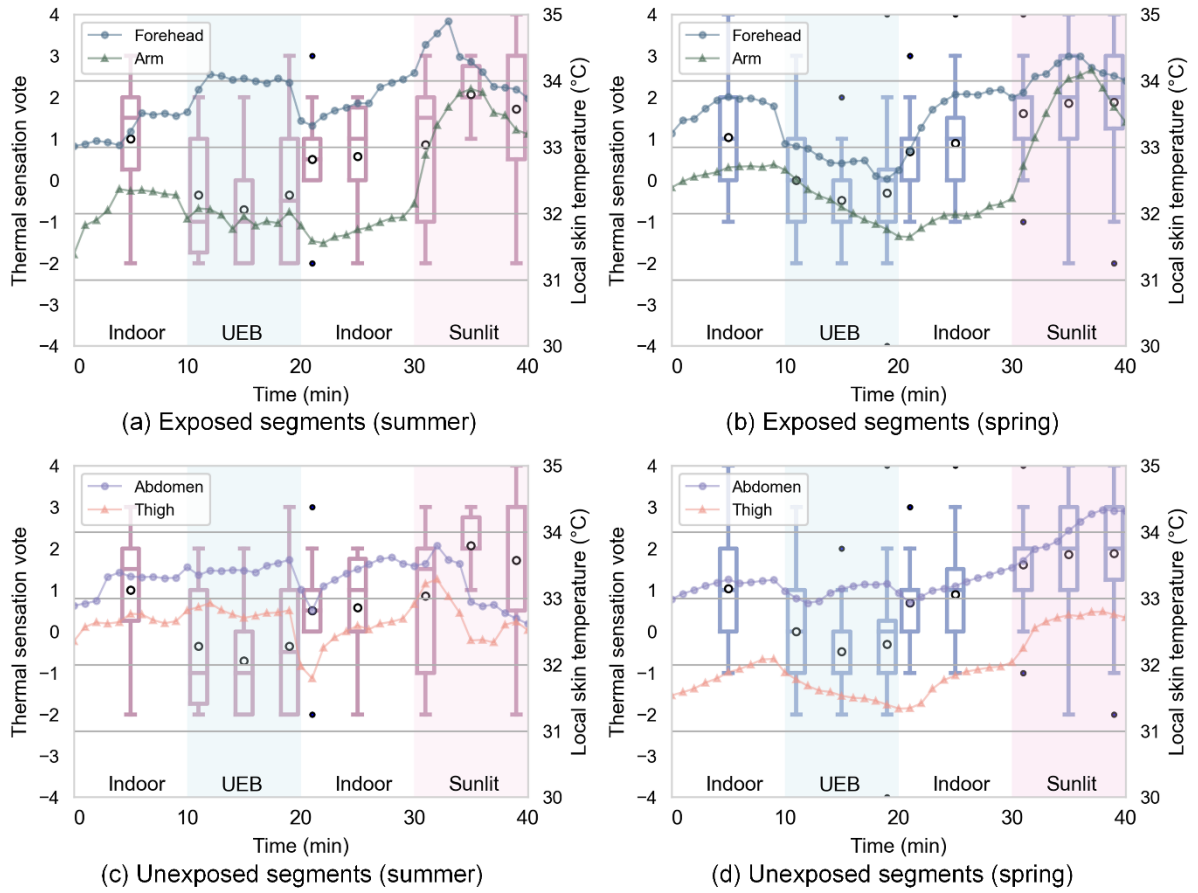

Figure 6.11 The results of local skin temperature and TSV change. (a). Exposed segments (summer); (b). Exposed segments (spring); (c). Unexposed segments (summer); (d). Unexposed segments (spring).

6.3.3.3 Correlations between local and mean skin temperatures and thermal sensation

The correlation coefficients from Spearman analysis (r_s) between local and mean T_{skin}, change rate of local and mean T_{skin} (dT_{sk}/dt), TSV, and $dTSV/dt$ for UEB and sunlit conditions are presented in Table 6.4 and Table 6.5. The dt was calculated here by the interval between two adjacent votes. Most of the r_s between local T_{skin} and TSV are between 0.3 and 0.5. The r_s between $T_{sk,m}$ and TSV are 0.47 for spring and 0.44 for summer. Still, the correlation coefficients between skin temperatures and mean TSV in this study are much lower than that in non-transient outdoor environments. Two previous studies that exposed human subjects for

60 mins to an outdoor environment have reported r_s of around 0.8 between exposed body segments and TSV, such as head, face, and hand. (Lai et al., 2017b; K. Liu et al., 2020). A transient experiment that conducted a 20-min sunlight exposure followed by a 45-min shading exposure, has found that r_s between TSV and skin temperatures of the lower leg, lower arm, chest, and mean skin temperature were 0.28, 0.52, 0.48, and 0.44 respectively (Xu et al., 2022). Comparing summer and spring results, the r_s between T_{skin} and TSV of exposed body segments in spring (forehead: 0.51, arm: 0.50, hand: 0.46) was higher than that in summer experiment (forehead: 0.16, arm: 0.41, hand: 0.15). Though dT_{sk}/dt has been proved to be more suitable in predicting dynamic TSV in transient thermal environment, the results in Table 6.5 showed low correlations between dT_{sk}/dt and $dTSV/dt$, but the coefficients in spring experiment were higher than that in summer experiment.

The low r_s between mean or local skin temperatures and TSVs in transient outdoor environments might be attributed to three reasons. Firstly, the time difference between thermal perception and physiological response. There was a noticeable difference between peak arrival time from local skin temperature (e.g., exposed segments such as arm and forehead) and TSV in the sunlit condition (Figure 6.11). Secondly, the fluctuation inconsistency between local skin temperatures of unexposed body segments and TSVs caused by insufficient sweat evaporation or absorption by clothing, and the sweating process of exposed body segments (e.g., forehead and hand) influenced by wind, might explain why a much lower r_s between dT_{sk}/dt and $dTSV/dt$ is obtained in summer experiments than in spring. In addition, thermal variations and different microclimate scenarios may cause strong psychological effects (Nikolopoulou & Steemers, 2003), which might undermine the relationship between physiological parameters and thermal sensation. In light of the above reasons, the following part discusses the challenges of designing in-situ experiments for transient outdoor thermal comfort studies.

Table 6.4 The correlation coefficients between local and mean T_{skin}, and TSV in summer and spring experiments (Results from Spearman analysis).

		$T_{sk,forehead}$	$T_{sk,abdo}$	$T_{sk,arm}$	$T_{sk,hand}$	$T_{sk,thigh}$	$T_{sk,calf}$	$T_{sk,foot}$	$T_{sk,m}$
TSV	Summer	0.16	0.31	0.41	0.15	0.45	0.57	0.48	0.44
	Spring	0.51	0.25	0.50	0.46	0.30	0.45	0.37	0.47

Table 6.5 The correlation coefficients between local and mean dT_{skin}/dt, and $dTSV/dt$ in summer and spring experiments (Results from Spearman analysis).

		$dT_{sk,forehead}/dt$	$dT_{sk,abdo}/dt$	$dT_{sk,arm}/dt$	$dT_{sk,hand}/dt$	$dT_{sk,thigh}/dt$	$dT_{sk,calf}/dt$	$dT_{sk,foot}/dt$	$dT_{sk,m}/dt$
dTSV/dt	Summer	0.21	0.16	0.22	0.16	0.17	-0.03	0.29	0.16
	Spring	0.33	0.27	0.29	0.34	0.25	0.31	0.30	0.38

6.4 Discussion

6.4.1 Relationship between environmental index and thermal sensation

The comparison results of thermal sensation and PET are shown in Figure 6.12. In general, there were similar trends between PET and mean TSV during both the summer and spring experiments. However, PET was unable to identify thermal overshoot and adaptation triggered by changing thermal conditions. Specifically, PET showed limited variations at the same site (e.g., UEB and sunlit), but mean TSV showed the highest overshoot in UEB and sunlit areas at the 2nd questionnaire and then attenuated at the 3rd questionnaire during our step-change experiment (Figure 6.12-a). The inaccuracy of PET in predicting thermal sensation is primarily due to thermal overshoot phenomenon after thermal transitions, including the results of warm and cool stimulus. Thermal overshoot might be caused in part by physiological effects, such as large changes in skin temperature, sweating accumulation and evaporation, and in part by

psychological effects (e.g., visual effects caused by strong sunlight). This phenomenon has not been fully understood by researchers and needs further exploration (Vellei et al., 2021). Thermal overshoot occurs along with short-term thermal adaptation, and its intensity varies with exposure time. Current studies on this phenomenon mainly focus on alliesthesia phenomenon (Lai et al., 2017a), adaptation duration (Xiong et al., 2016) and qualitative explanations (Ji et al., 2017; Zhang et al., 2017). Yet, a quantitative model of short-term thermal adaptation is needed in the future.

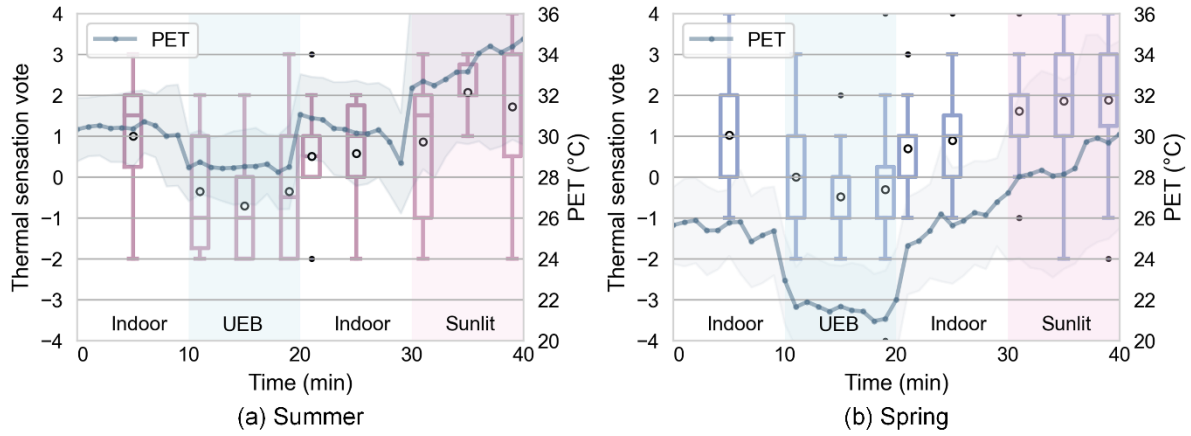

Figure 6.12 The relationship between environmental indices and TSV. (a). Summer; (b). Spring.

6.4.2 Relationship between thermal sensation and thermal comfort

6.4.2.1 Calculation of preferred thermal sensation (TSV_{prefer})

The prediction of human thermal comfort in dynamic thermal environments is more complex than that in steady thermal environments, mainly due to thermal alliesthesia effects. According to the thermal alliesthesia framework, current thermal perceptions are dependent on preceding thermal conditions and the change of thermal conditions (Parkinson & de Dear, 2014; Liu et

al., 2021). Figure 6.13 shows the relationship between TSV and TCV in quadratic regression in this study. The mean TCV of subjects in each 1.0 TSV interval group was calculated and used for regression, resulting in an R^2 of 0.96. When TCV is the highest, the corresponding thermal sensation can be regarded as the most desired, which is termed the preferred thermal sensation (TSV_{prefer}). The calculated preferred thermal sensation is -1.10, suggesting that subjects generally prefer slightly cool conditions during the experiment seasons.

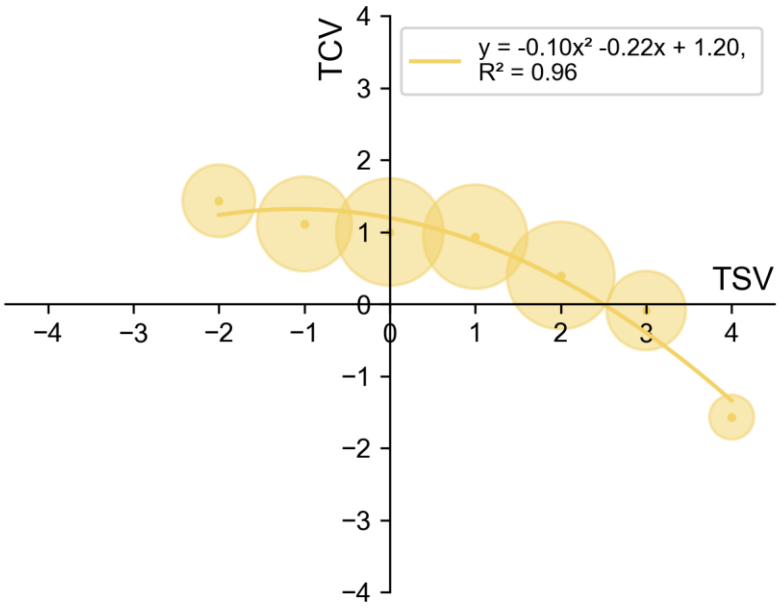

Figure 6.13 The quadratic regression between TSV and TCV.

6.4.2.2 Relationship between $dTSV$ and $dTCV$ in different alliesthesia zones

Based on Liu's research (Liu et al., 2021) and the thermal alliesthesia framework (Parkinson & de Dear, 2015; Parkinson et al., 2016), the collected data were classified into four zones (cold discomfort, acceptably cool, acceptably warm, and warm discomfort) according to the preceding thermal sensation ($TSV\ (t_1)$), as shown in Figure 6.14. The four zones are defined as follows:

Cold discomfort: $TSV\ (t_1)\ \leq\ TSV_{n,min}$

Acceptably cool: $TSV\ (t_1)\ \in (TSV_{n,min}, TSV_{prefer})$

Acceptably warm: $TSV\ (t_1)\ \in (TSV_{prefer}, TSV_{n,max})$

Warm discomfort: $TSV\ (t_1)\ \geq\ TSV_{n,max}$

The boundary of different alliesthesia zones is defined below. First, TSV_{prefer} is calculated as -1.10 in Section 6.4.2.1. Then, the boundaries between 'cold discomfort' and 'acceptably cool', 'warm discomfort' and 'acceptably warm' are defined as the thermal sensation corresponded to 'TCV = 1 (slightly comfortable)', which are calculated to be -2.87 ($TSV_{n,min}$) and 0.67 ($TSV_{n,max}$) based on the quadratic regression stated in Figure 6.13. Therefore, the preceding thermal sensation in the moderate alliesthesia zone can be classified as -2.87 < TSV < 0.67, among which, -2.87 < TSV < -1.10 belongs to the acceptably cool zone, and -1.10 < TSV < 0.67 belongs to the acceptably warm zone. The thermal sensation in cold discomfort and warm discomfort zones can be classified as TSV ≤ -2.87 and TSV ≥ 0.67, respectively.

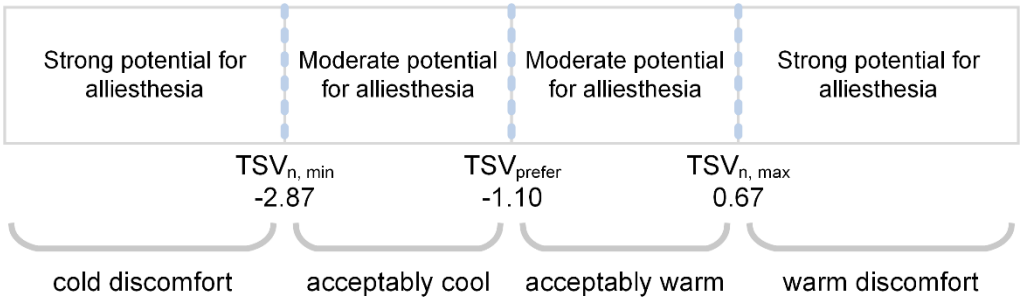

Figure 6.14 The boundary and classification of four thermal alliesthesia zones in this study.

According to the classification of alliesthesia zones, the relationship between dTCV and dTSV in strong and moderate alliesthesia zones are calculated and shown in Figure 6.15. Due to the limited data for cold discomfort and acceptably cool zones, Figure 6.15 only shows the regression results of warm discomfort and acceptably warm zones. Linear regression is employed for those preceding thermal sensations falling in the warm discomfort zone which is deemed to possess strong alliesthesia potential (Figure 6.15-a), whereas quadratic regression is employed for the acceptably warm zone, which is supposed to have moderate alliesthesia potential (Figure 6.15-b). The R^2 for strong alliesthesia potential caused by warm discomfort is 0.63, and the R^2 for moderate alliesthesia potential caused by acceptably warm is 0.98. Each 1.00 scale decrease in dTSV results in a 0.44 scale increase in dTCV when the preceding thermal sensation falls in the strong alliesthesia potential zone. The contribution of dTSV to dTCV varies in the moderate alliesthesia potential zone. It is worth noting that if the preceding thermal sensation falls within the moderate alliesthesia potential zone, moderate changes in the thermal environment can contribute to positive changes in thermal comfort while extreme changes can result in negative changes in thermal comfort. To be specific, when the preceding thermal sensation is within an acceptably warm zone, a change in the thermal environment that alters the absolute thermal sensation within a range of about 1.0 scale can have a positive effect on thermal comfort, while exceeding such a range can have a negative effect on thermal comfort. The results support Liu's findings (Liu et al., 2021) and can be explained by the psycho-physiological alliesthesia conceptual framework (Parkinson & de Dear, 2014).

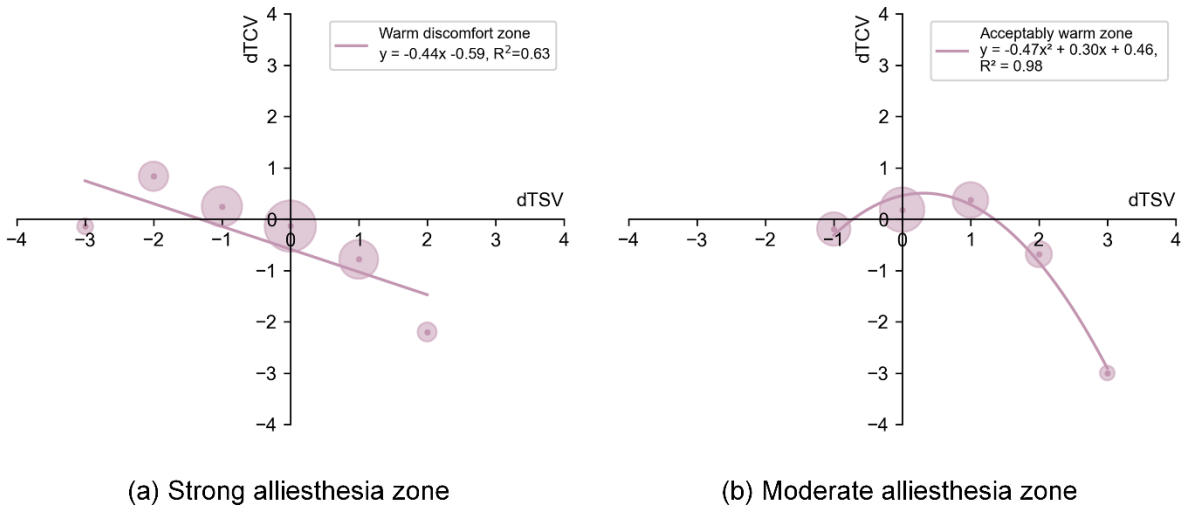

(a) Strong alliesthesia zone (b) Moderate alliesthesia zone

Figure 6.15 The relationship between dTSV and dTCV. (a). Strong alliesthesia zone; (b). Moderate alliesthesia zone.

6.4.3 Challenges for in-situ experiment design

Based on the above discussion, here are some challenges and suggestions for the in-situ experiment design in outdoor thermal comfort research. The first challenge is to make sure that the sampling rate of physiological parameters and subjective questionnaire can reflect the transient fluctuations. A quick-response sensor with a suitable sampling rate could help researchers capture the actual and accurate skin temperature fluctuation. In addition, the voting interval of subjects should be selected carefully for better comparison with the physiological responses. In Table 6.6, we summarize the sampling rates of skin temperature sensors and voting intervals for recently published studies targeted at outdoor thermal comfort. Generally, the sampling rate of skin temperature was ≥10s, and the voting interval varied from 2 to 5 mins during transient experiments. The correlation coefficients for transient experiment settings were much lower than the static settings. To capture the possible thermal alliesthesia and adaptation effects, the findings in the current study suggest that the sampling rate of skin temperature and voting interval should be carefully considered and may be set shorter than the

existing studies due to the highly changed environmental conditions and possible psychological effects in transient outdoor thermal environment research. The second challenge is continuous measurement or frequent data collection of local sweating rate for warm-biased experiments. The accumulated liquid sweat on the skin surface hinders skin temperature from changing while thermal sensation keeps increasing, making the fluctuation of skin temperature unable to reflect thermal sensation change. The evaporation rate of accumulated sweat on the skin surface changes fast with the surrounding air movement, and strong evaporation of sweat will create a sudden cool sense. With the accumulated sweat and absorbed by clothing, wet clothing will cool down the skin and induce a cool sensation. Thus, the measurement of transient sweating rate and quantifying its thermal effect might be the key to quantifying thermal alliesthesia and adaptation effects in a warm-biased transient outdoor thermal environment.

Table 6.6 A summary of sampling time of skin temperature and subjective vote interval in previous studies

Studies	Experiment settings	Sampling rate of skin temperature	Voting interval	Correlations
(Lai et al., 2017b)	Static, 60 min outdoors	1 s	5 min	Spearman coefficient around 0.8
(Xu et al., 2022)	Transient, 20 min sunlight and 45 min shade outdoors	10 s	2~5 min	Spearman coefficient < 0.52
(Peng et al., 2022)	Transient, scenarios change outdoors	1 min	5 min	$R^2 < 0.17$

6.4.4 Implications of dynamic thermal environments in thermo-spatial environment design

Current outdoor thermal comfort research emphasizes 'thermal neutrality' over 'thermal comfort', ignoring the natural differences between indoor and outdoor thermal environments, and the fact that 'thermal neutrality' originated in indoor thermal comfort studies aimed at forming steady thermal conditions. The most pleasant thermal feelings, however, are highly associated with transient conditions (Arens et al., 2006). Previous studies show that creating dynamic thermal environments is efficient in mitigating thermal discomfort outdoors, including the UEB design as a transition process from indoor to outdoor (Huang et al., 2020), frequent alternating exposure to sunlight and shade (J. Li, J. Niu, T. Huang, et al., 2022), and microclimate diversity in urban contexts (Peng et al., 2022). The findings in this study suggest that the classical transient scenarios when pedestrians move outdoors can result in temporal thermal alliesthesia, which can push people out of thermoneutral zone and create the probability of achieving a higher thermal comfort level. Besides, the influence of thermal sensation overshoot on thermal comfort increased and then diminished with the exposure time to the thermal stimulus, which means short-term thermal adaptation phenomenon. Combining the synthesis effect of thermal alliesthesia and short-term thermal adaptation, our findings suggest that dynamic thermal environments may result in a higher level of thermal comfort. Thus, thermal variations in urban microclimate design may have potentials to improve pedestrians' thermal perceptions.

6.4.5 Limitations and future work

Recent studies showed that physiological parameters could predict thermal sensation (e.g., local and mean skin temperatures, derivative mean skin temperatures, core temperatures, and thermal load) in steady and transient outdoor environments (Fiala et al., 2003; Lai et al., 2017b; K. Liu et al., 2020). The relationships between these variables and environmental parameters

have been extensively developed by thermoregulation models (e.g., Gagge's two-nodal model, Fiala's multi-nodal model, the JOS-3 model) (Gagge et al., 1986; Fiala et al., 2011; Takahashi et al., 2021). However, the findings in this study have shown low correlations between thermal sensation and skin temperature in a warm-biased short-term transient outdoor environment. Future experiments should think over the transient sweating rate of local body parts, as well as the sampling rate of physiological devices and voting intervals. The voting intervals in this study do not allow us to determine the exact peak time of the thermal overshoot and adaptation phenomena. To capture the variations in thermal perception in transient environments, future experiments should increase the voting intervals.

Thermal alliesthesia and adaptation phenomena highly affect pedestrians' thermal perceptions. Dynamic thermal environments may achieve a higher thermal comfort level. Further studies are also needed to explore the impact of more diverse thermal variations in transient outdoor environments on pedestrians' thermal perceptions.

6.5 Chapter conclusions

The purpose of this study is to explore the short-term dynamic thermal perception and physiological response in step-change indoor and outdoor environments. A total of 50 human subjects participated in experiments held in spring and summer. Human subjects were asked to transfer between three different indoor and outdoor thermal conditions and vote their instant thermal perceptions at specific time points. In the meantime, their physiological data were collected, including skin temperature and sweat rate, and a micro-weather station continuously measured the micro-thermal environment. The relationship between transient thermal environment and dynamic thermal perceptions, including the mechanism, influencing factors, and potential applications, are discussed in this study.

The following findings have emerged:

1. Overshoot in thermal sensation persisted for at least 5 mins when the thermal environment changed. In contrast, the influence of ΔTSV on ΔTCV increased and then diminished at around the 5th min, at which point short-term thermal adaptation phenomenon began to occur and such effect gradually increased.
2. The influence of dTSV on dTCV was explored in different thermal alliesthesia zones. The relation between dTSV and dTCV can be modelled by linear regression in the warm discomfort zone, and by quadratic regression in the acceptably warm zone. A 1.00 scale decrease in dTSV resulted in a 0.44 scale increase in dTCV when the preceding thermal sensation fell in the warm discomfort zone (one type of the strong alliesthesia zone). Near thermal neutrality, a proper fluctuation of thermal sensation is still encouraged. When the preceding thermal sensation fell within the acceptably warm zone (one type of moderate alliesthesia zone), a change in an environment that alters the absolute thermal sensation within about 1.00 scale could have a positive effect on thermal comfort, however, exceeding this range may negatively impact thermal comfort.
3. Skin temperatures from exposed body segments correlated better with transient TSV than those from unexposed ones. Even so, the correlation between local skin temperatures and TSV was lower than in other static outdoor studies, especially during summer experiments. Sweat accumulation on skin and absorption by clothing in heat-stressed conditions, and transient sweat evaporation affected by high wind speed levels are possible reasons. Also, thermal alliesthesia and short-term thermal adaptation highly influenced thermal perceptions in transient outdoor environments.

The findings suggest that outdoor thermal comfort research could explore non-steady-state conditions to enrich pedestrians' thermal experience during walking, providing insights in adopting dynamic features outdoors for better design of thermal environment. This study

encourages architects and urban designers to consider dynamic thermal environments in the design of building layouts and landscape planning.

Chapter 7 **Conclusions and recommendations for future study**

7.1 Conclusions

Semi-controlled experiments and field experiments were both employed in this study to efficiently create a wide range of outdoor settings, including various combinations of wind speed and solar radiation levels, as well as dynamic and transient conditions.

The study investigated the dynamic changes in human thermal perceptions and physiological responses in outdoor thermal environments, and aims to develop an outdoor thermal sensation model based on thermal physiology. The study includes the steady-state model, the step-up phase, and the step-down phase of the dynamic model, as well as an exploratory investigation into thermal alliesthesia and short-term adaptation phenomenon.

The environmental parameters, human subjective thermal responses, in terms of local thermal sensation and overall thermal sensation, and physiological responses, in terms of local skin temperature, core temperature, and local sweat rate, were collected. The following findings have emerged:

1. The steady-state part model development study found that (1) Mean skin temperature changed rapidly when the thermal environment changed. Skin temperatures are highly associated with TSV, showing correlations of around 0.3-0.6. The correlations between skin temperatures and sweat rate of three measured body parts are around 0.60. Exponential function was used for arm skin temperature and its sweat rate regression, with a high R^2 of 0.92. Thus, local skin temperature was used to be the only predictor variable for the local TSV prediction under steady state. (2) Local TSV prediction for 11 body parts was developed. The neutral temperature of each body part was adopted to give a neutral sensation reference in the local TSV prediction model. The local TSV

prediction provided a range covering around 80% of people, including mean value, lower limit, and upper limit, for the assessment of local sensation due to individual differences. 94.3% of the validation set data have an absolute value deviation smaller than 1.0. (3) Overall TSV prediction was established by the weighted average of local TSV. Distal body parts have a higher weighting coefficient than core parts. The validated data fits well with the zero-deviation line, with a high R^2 of 0.97, suggesting a satisfactory prediction result.

2. The step-up phase model development study found that (1) Significant differences in $dT_{sk,m}/dt$ were observed between different exposure periods during outdoor conditions. In the initial 0–450 s (highly-dynamic period), $dT_{sk,m}/dt$ peaked at approximately 0.006 °C/s caused by transient scenarios, while in the 450–900 s (weakly-dynamic period), it declined to about 0.001 °C/s mainly induced by natural environmental fluctuations. (2) Addressing naturally occurring thermal environmental fluctuations in outdoor settings, skin temperature data were classified into highly-dynamic and weakly-dynamic modes for model development and application. The classification is performed using an empirical critical value of $dT_{sk,i}/dt$, defined as the 75th percentile in the weakly-dynamic period. A 30 s moving window approach determines whether data belong to the highly-dynamic or weakly-dynamic mode based on the percentage of values exceeding the critical value. (3) The correlations between $dT_{sk,i}/dt$, $dT_{sk,m}/dt$, dT_{core}/dt, and $TSV_{i,dynamic}$ were analyzed. $dT_{sk,i}/dt$ and $dT_{sk,m}/dt$ exhibited stronger correlations with dynamic local TSV than dT_{core}/dt. Furthermore, weakly-dynamic period showed higher correlations between $dT_{sk,m}/dt$ and $TSV_{i,dynamic}$ than the highly-dynamic period. Since natural environmental fluctuations do not cause significant asymmetric thermal conditions, the weakly-dynamic mode utilizes $dT_{sk,m}/dt$ as the independent variable, whereas the highly-

dynamic mode primarily use $dT_{sk,i}/dt$ as independent variables, and $dT_{sk,m}/dt$ is added for calf. (4) The step-up phase of the dynamic model of each local body part during highly-dynamic and weakly-dynamic modes was developed using linear regression, with corresponding regression coefficients provided for model application. Model validation shows a satisfactory performance, with an average *Accuracy* of 74.2% for the highly-dynamic mode, and 73.8% for the weakly-dynamic mode.

3. The step-down phase model development study found that (1) The steady-state part prediction of the abdomen, foot, and neck has been rebuilt due to the wider range of skin temperature and abdomen TSV data collected in this study. Since different effects of v and T_{mrt} on TSV under high temperature conditions, a SWI correction term was added to enhance the accuracy of the steady-state part. (2) Skin temperature data were classified into the highly-dynamic mode and the weakly-dynamic mode based on the empirical critical value. Critical values, defined as the 75th percentile of $dT_{sk,i}/dt$ value of the weakly-dynamic mode, which were updated using both our previous experiment data and the data from this study. In the weakly-dynamic mode, the correlations between the $dT_{sk,i}/dt$ and dynamic local TSV are lower than those in the highly-dynamic mode, mainly attributed to that the minor negative fluctuations in environmental conditions, did not induce effective changes in skin temperature. (3) The step-up phase showed higher associations between dPETs and dTSVs than those of the step-down phase for each body part. This suggests that when people are in warm-biased conditions, the impacts of environmental changes on thermal sensation changes are more irregular during cooling than during heating. (4) The step-down phase of the dynamic model of 11 body parts during highly-dynamic and weakly-dynamic modes was developed. For the step-down phase, both highly-dynamic and weakly-dynamic modes employ $dT_{sk,i}/dt$ as the independent variable. The average *Accuracy* for the

highly-dynamic mode is 62.1%, and 69.0% for the weakly-dynamic mode. (5) The applicability of different thermal evaluation scales in outdoor spaces was assessed. For step-change outdoor environments, TSW may be more suitable than TCV and TA for thermal comfort evaluation during both the transition period (≤ 120 s) and prolonged exposure period (> 120 s), while TP would be applicable for prolonged exposure period (> 120s).

4. The exploration study of thermal alliesthesia and short-term adaptation phenomenon found that (1) Overshoot in thermal sensation persisted for at least 5 mins when the thermal environment changed. In contrast, the influence of ΔTSV on ΔTCV increased and then diminished at around the 5^{th} min, at which point short-term thermal adaptation phenomenon began to occur and such effect gradually increased. (2) The influence of dTSV on dTCV was explored in different thermal alliesthesia zones. The relation between dTSV and dTCV can be modeled by linear regression in the warm discomfort zone, and by quadratic regression in the acceptably warm zone. A 1.00 scale decrease in dTSV resulted in a 0.44 scale increase in dTCV when the preceding thermal sensation fell in the warm discomfort zone (one type of the strong alliesthesia zone). Near thermal neutrality, a proper fluctuation of thermal sensation is still encouraged. When the preceding thermal sensation fell within the acceptably warm zone (one type of moderate alliesthesia zone), a change in an environment that alters the absolute thermal sensation within about 1.00 scale could have a positive effect on thermal comfort, however, exceeding this range may negatively impact thermal comfort. (3) Skin temperatures from exposed body segments correlated better with transient TSV than those from unexposed ones. Even so, the correlation between local skin temperatures and TSV was lower than that observed in static conditions reported by other outdoor studies, especially during summer experiments. Sweat accumulation on skin and absorption by

clothing in heat-stressed conditions, and transient sweat evaporation affected by high wind speed levels are possible reasons. Also, thermal alliesthesia and short-term thermal adaptation highly influenced thermal perceptions in transient outdoor environments.

This study provides a new prospect for developing an advanced outdoor thermal sensation model. Firstly, the model development covers a relatively wide range of real outdoor environments, which enhances its applicability and accuracy. Then, the steady-state part accounts for individual differences and thermal sensation overshoot commonly occurs in outdoor thermal environments. Thirdly, natural distinct from indoor settings, the dynamic part of this model captures outdoor natural environmental fluctuations by grouping data into the highly-dynamic and weakly-dynamic modes. Most importantly, the model can predict local thermal sensation across 11 body parts, as well as overall thermal sensation, making it valuable for assessing dynamic, non-uniform thermal environments and evaluating advanced cooling strategies (e.g., mist spraying and radiant cooling panels).

The model will be integrated with thermoregulation models (e.g., JOS-3 model (Takahashi et al., 2021)) to predict thermal sensation based on environmental parameters. The completed local TSV prediction is the sum of the steady-state part and dynamic part calculation results, while the overall TSV prediction is output by the weighted average of local TSVs, which has been developed in the steady-state part. Specifically, the whole model could provide three sets of local TSVs for 11 body parts and three values of overall TSVs, including mean, the 10th percentile, and the 90^{th} percentile value. The whole model can be applied in conjunction with a multi-nodal human thermoregulation model to assess the thermal comfort condition of outdoor spaces during the design and renovation stage.

Combining the synthesis effect of thermal alliesthesia and short-term thermal adaptation, the findings suggest that dynamic thermal environments may result in a higher level of thermal comfort. Thermal variations in urban microclimate design have the potential to improve pedestrians' thermal comfort conditions. The findings in this study can give guidance for the design of more comfortable outdoor thermal environments.

7.2 Recommendations for future study

(1) Physiological and subjective responses in non-uniform thermal environments

In the context of climate change, advanced cooling strategies such as radiant cooling panels (Dharmasastha et al., 2024) and mist-spraying devices (Oh et al., 2020b), can effectively relieve thermal discomfort outdoors. However, the relationship between physiological parameters and thermal perceptions is unclear in non-uniform thermal conditions. The model developed in this study could be validated in non-uniform conditions, thereby providing guidance for the design of active cooling devices.

(2) Model applicability for different activities

The model developed in this study was initially for the design of urban recreational spaces, thus, the sitting and standing posture was first investigated. However, for walking routes, walking and running would be common activities for pedestrians. The physiological responses could be further investigated for different activities. For example, a clear trend might be possible for the core temperature change under high activity levels (e.g., higher metabolic level corresponds to higher core temperatures (Lee et al., 2010; Brown et al., 2024)), and the applicability of the current model in higher activity levels needs further investigation.

(3) Human thermoregulation under heat stress

Thermoregulation is vital to prevent heat-related health risks under high heat stress conditions. Pedestrians' thermoregulatory responses (e.g., sweat rate, sweat loss, blood flow variation, core

temperature changes) would be valuable for investigation and quantifying under heat stress, especially in hot, humid climate zones.

(4) Quantifying the impacts of outdoor thermal variations on thermal evaluations

This study investigated the effects of thermal alliesthesia and short-term thermal adaptation phenomenon on thermal perceptions. The findings suggested that dynamic microclimate conditions would result in a higher level of thermal comfort than that of unchanging conditions. The quantified impacts of thermal variation on improving pedestrians' thermal perceptions could be explored in future studies.

(5) New scales for thermal comfort evaluation in outdoor conditions

The findings in this study indicate that thermal comfort vote may not suitable for thermal evaluation in outdoor conditions. Due to the inherent difference between indoor and outdoor thermal settings, evaluation scales originally developed for indoors may not accurately capture outdoor thermal perception variations. Furthermore, the applicability of thermal evaluation scales can vary depending on specific outdoor scenarios. Future studies could explore the applicability of different thermal evaluation scales under diverse outdoor scenarios.

Appendices

Appendix A

The size of the windshield is 2.00 m (H)×3.46 m (W), including the boards with 75% void (0.18×0.18 m for each square hole), 50% void (0.15×0.15 m for each square hole), and 30% void (0.11×0.11 m for each square hole). The boards are made of clear acrylic materials to avoid deformation, and allow solar radiation to go through. Before the windshield processing, computational fluid dynamics (CFD) simulation was adopted to simulate the velocity fields behind the windshield. The simulation results of velocity fields behind the windshield are shown in Figure A2, A3. For the windshield size in the simulation case, the size of the middle-board is 1.6 m (H)×1.2 m (W), and the size of the side-board is 1.6 m (H)×0.8 m (W). The size of each hole is 0.17 m×0.17 m (75% void), and 0.15 m×0.15 m (50% void). The wind direction was perpendicular to the middle-board of the windshield, and the angle between the side-board and the middle-board of the windshield was set as 135° (Figure A2). The simulated velocity results show that the velocity field at a distance of 1.0 to 1.5 m behind the windshield is relatively uniform for the 75% and 50% void. In order to accommodate the possible postures of human subjects (including sitting and standing) during the experiment, a taller and wider windshield device was finally made (Figure A1), and a smaller void board (30% void) was also added to create lower wind speed levels. The direction of two side-boards of the windshield can be easily adjusted to block the wind blowing from the side.

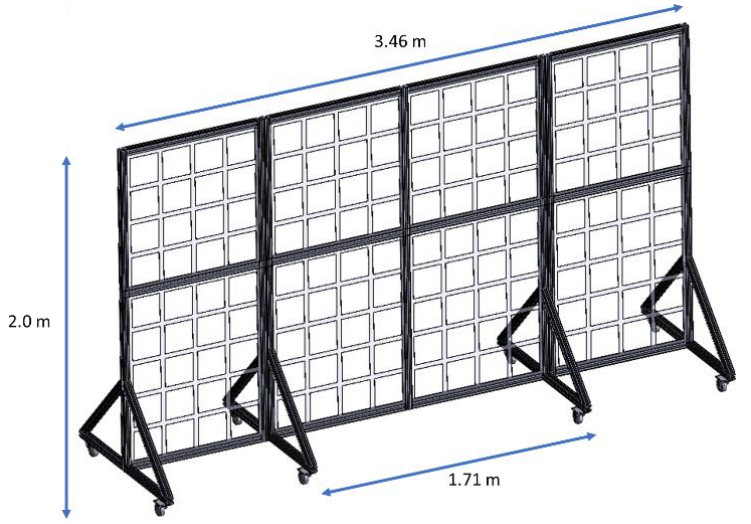

Figure A1. The sketch draft of the windshield.

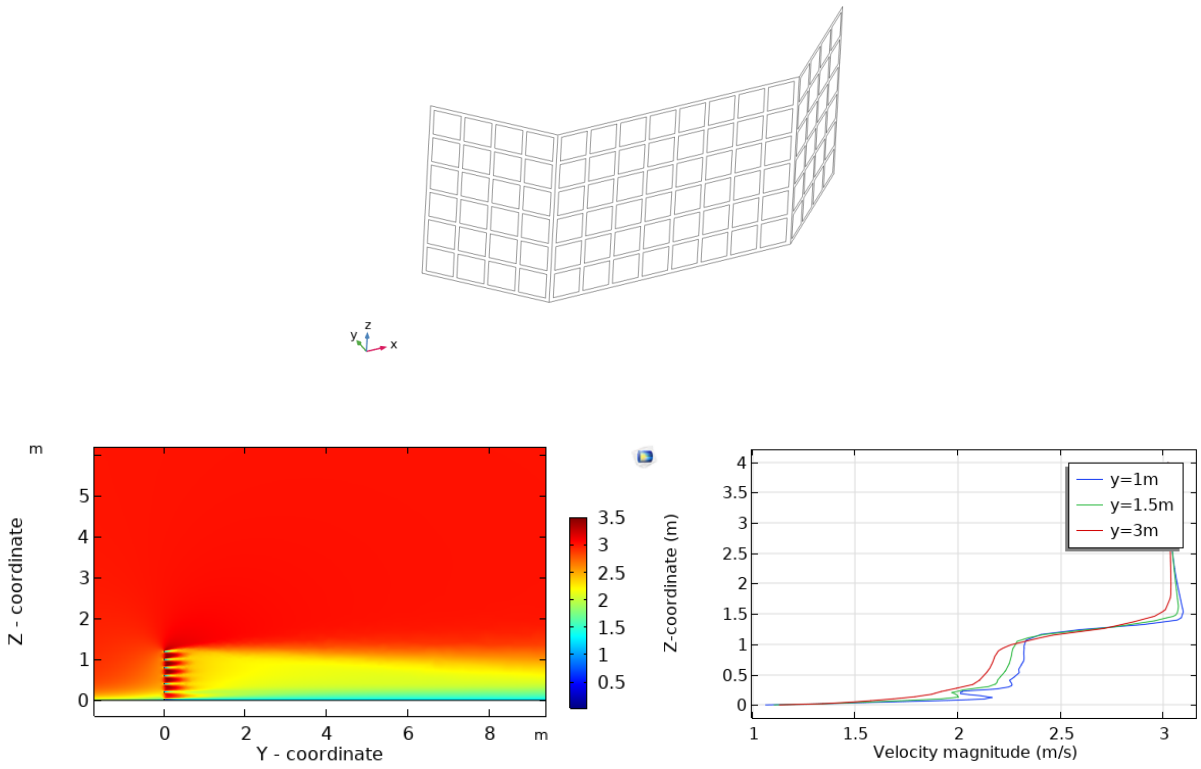

Figure A2. The simulation result of velocity fields behind the windshield when the void is 75%, with data extracted from the vertical cut through the middle board.

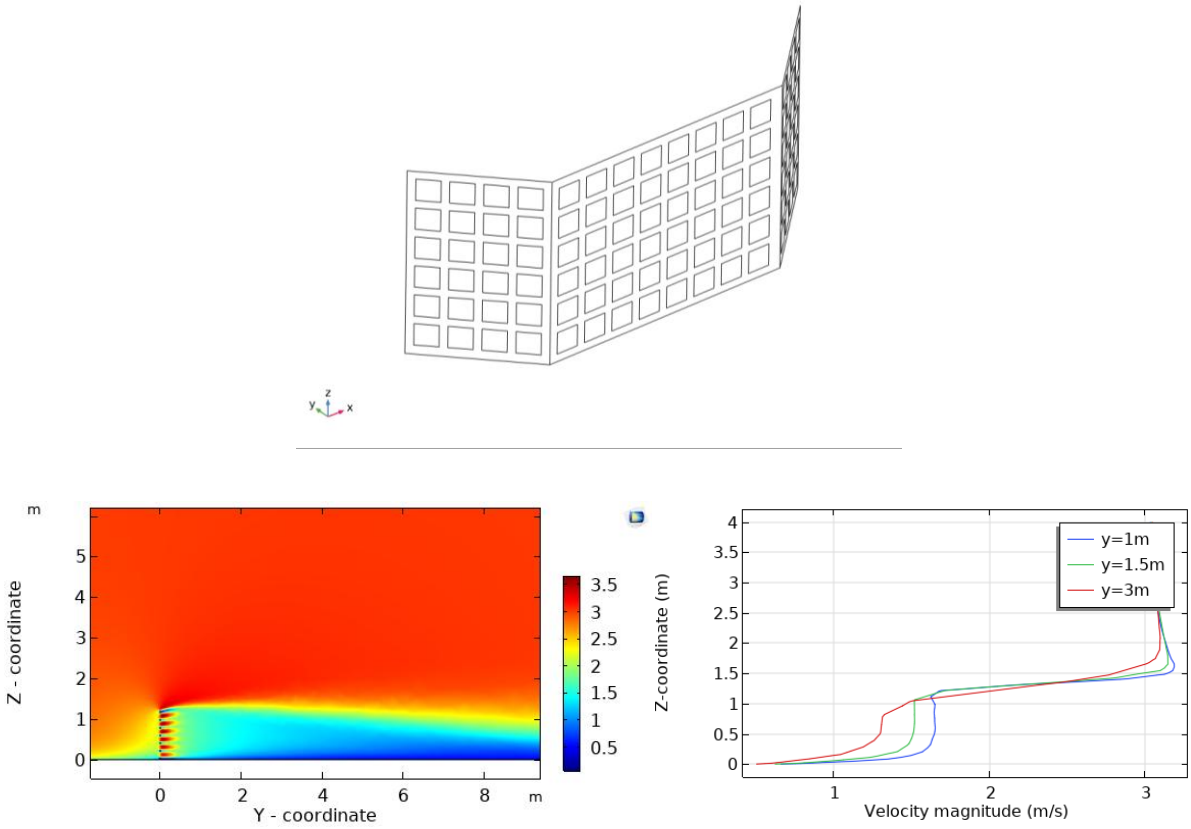

Figure A3. The simulation result of velocity fields behind the windshield when the void is 50%, with data extracted from the vertical cut through the middle board.

Appendix B

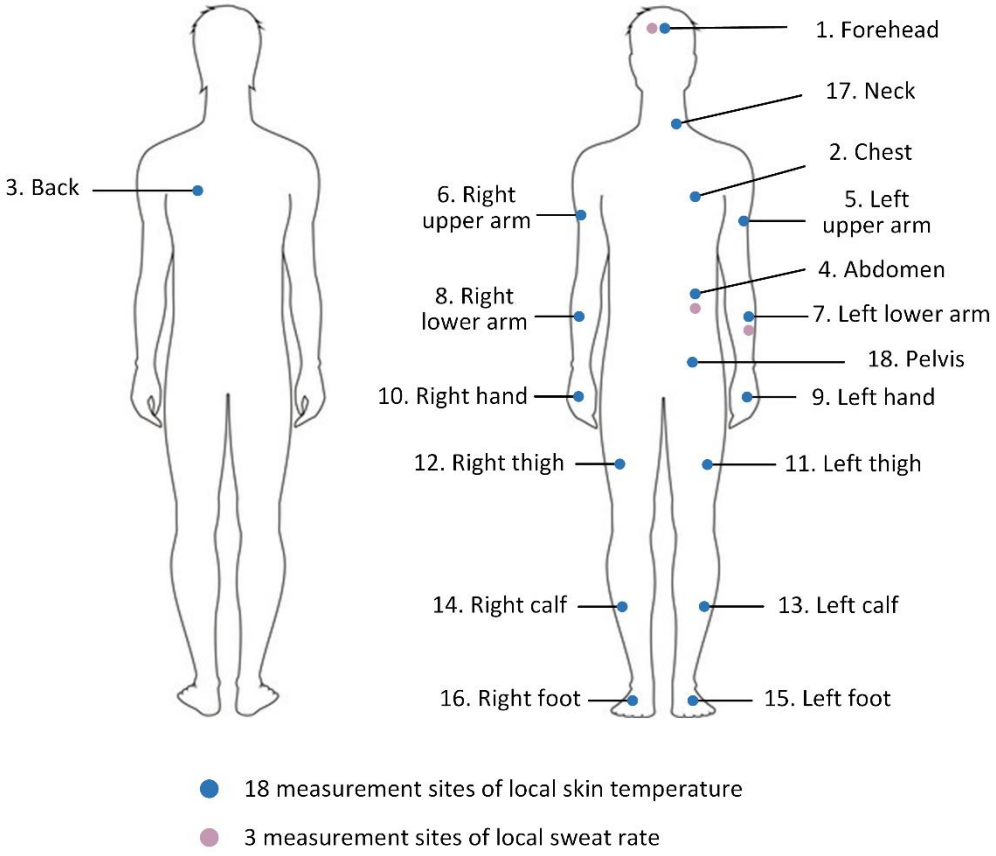

Figure B. Measurement points of local skin temperature of 18 body parts, and local sweat rate of 3 body parts.

Appendix C

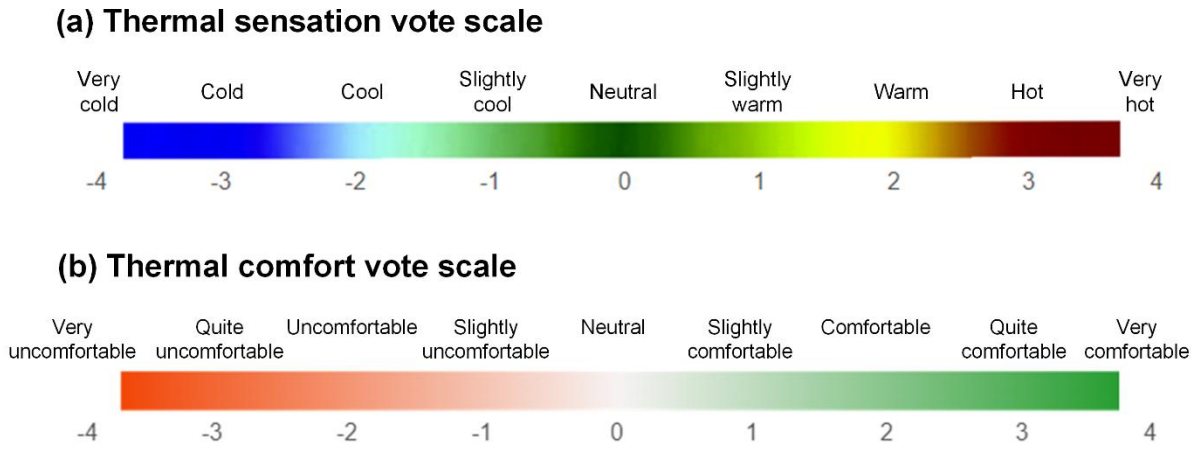

Figure C. The TSV scale and TCV scale.

Appendix D

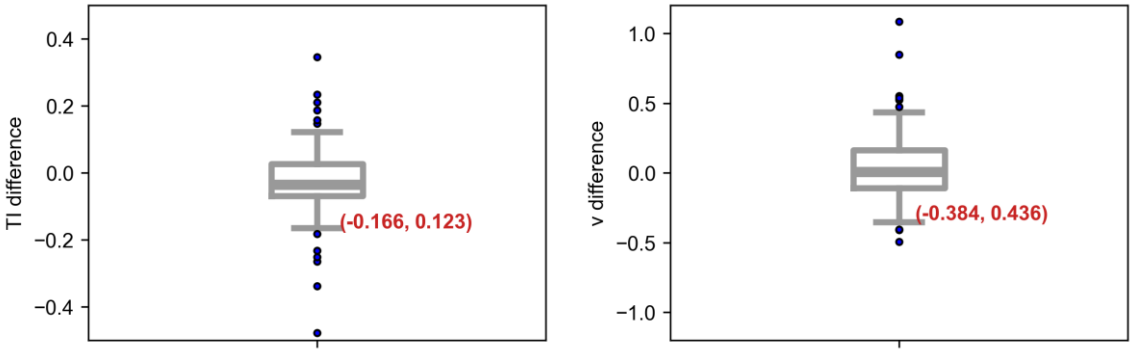

Figure D1. Boxplots of TI difference and v difference, the standard error bar was set as 1.0 QR.

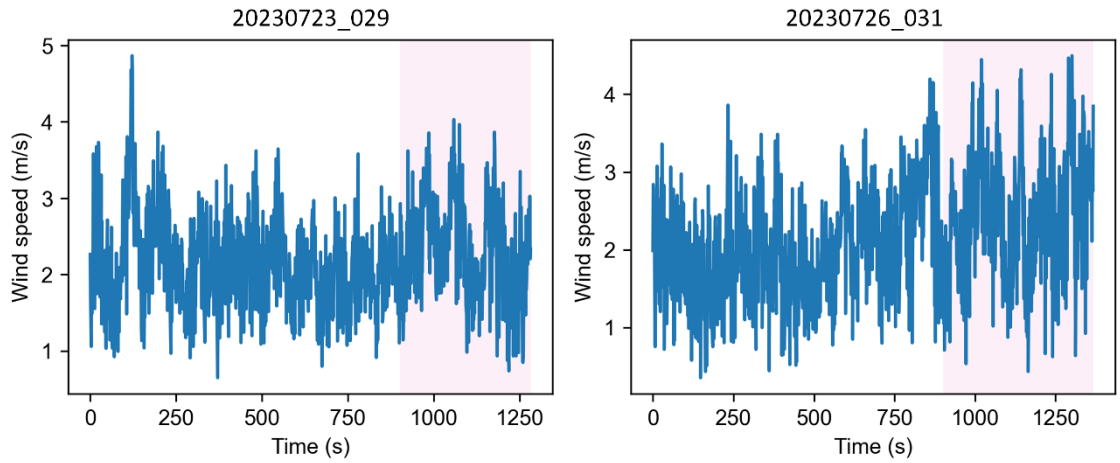

Figure D2. Samples of the wind speed data after data filtering, where the title means experiment date (year/month/day) and subject code.

Appendix E

A sample of the smoothed results for skin temperature and its derivative is shown in Figure E. Firstly, the original skin temperature data (Figure E-a, blue line) was smoothed by the Savitzky-Golay Python package (Virtanen et al., 2020), the data after smoothing is illustrated as the orange line in Figure E-a. Then, the derivative of skin temperature was calculated by the

difference between two adjacent skin temperature data (Figure E-b, blue line). The exponential weighted moving average method was further used for the data smoothing for the derivative of skin temperature, and the final smoothed result of the derivative of skin temperature is shown in Figure E-b, orange line. Similarly, the core temperature and derivative of core temperature smoothing employed the same method.

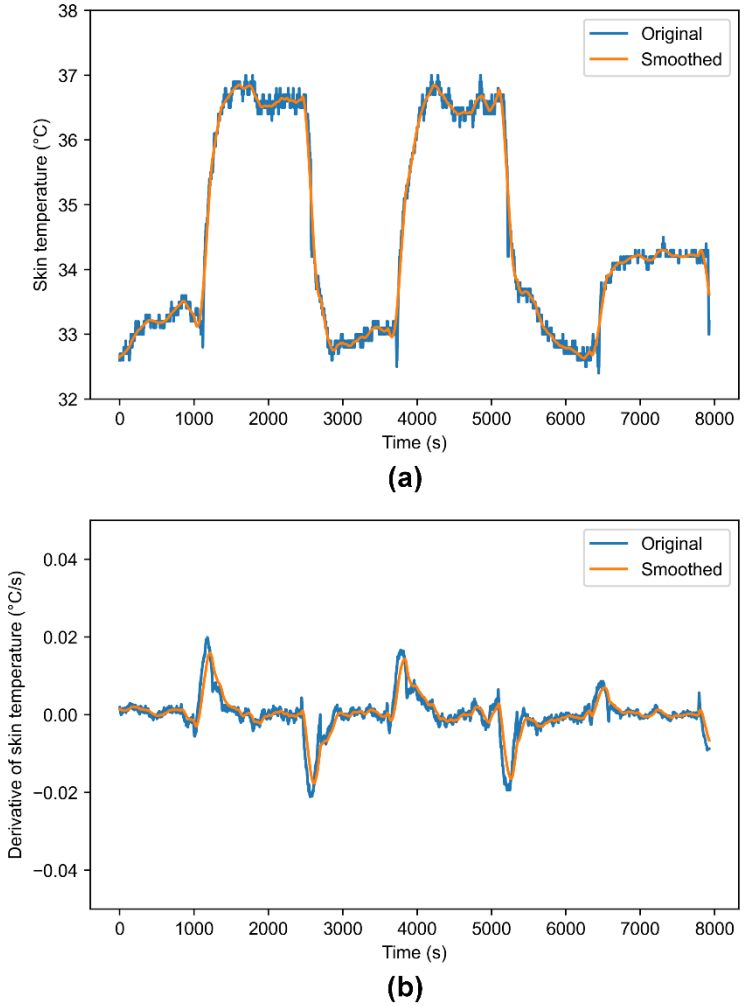

Figure E. Skin temperature smoothing sample (13072023_012, DD/MM/YYYY_subject code). (a). Skin temperature smoothing; (b). The derivative of skin temperature smoothing.

Appendix F

T_{mrt} calculated using only two-directional (ground and sky) radiation data may be overestimated under high-radiation conditions and underestimated under low-radiation conditions. Since several measurement days included only ground and sky data, a correction method was applied to improve the accuracy of T_{mrt} estimation, as shown in Figure F. Linear regression was employed to establish the relationship between the two-directional calculation (T_{mrt}_2d) and the standard six-directional calculation (T_{mrt}). A total of 11,266 data points were used, yielding a high R^2 of 0.96. The two-directional radiation data were corrected using this method.

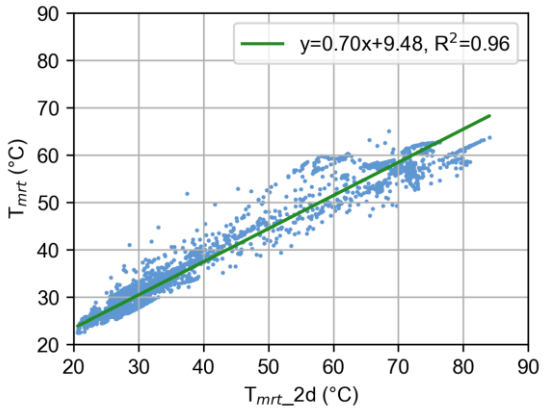

Figure F. Correction method to improve the accuracy of T_{mrt} calculation using two-directional (ground and sky) data.

Appendix G

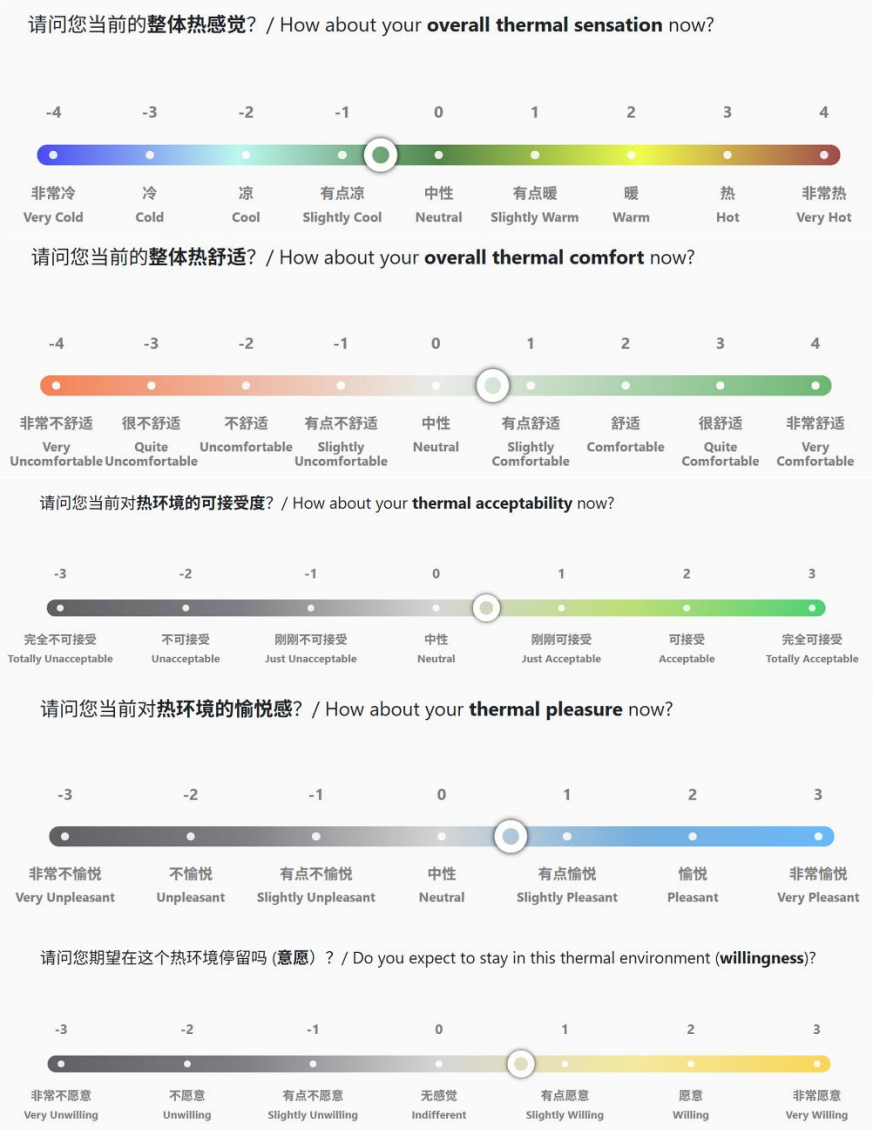

Figure G Examples of survey scales used in this study, including TSV, TCV, TA, TP, and TSW.

Appendix H

Since skin temperature variations caused by natural environmental fluctuations under the same conditions are limited, an outlier detection method was applied to the skin temperature data with exposure times exceeding 300 s. In contrast, data collected during step changes (i.e., exposure times less than 300 s) were not subjected to outlier detection. The 10th and 90th

values of $dPET/dt$, $dT_{sk,i}/dt$ are regarded as thresholds for normal fluctuations in natural thermal environments, as shown in Table H. Changes in $dPET/dt$ within the [10th, 90th] range are associated with corresponding changes in $dT_{sk,i}/dt$ within the [10th, 90th] range. Since large variations can also occur under natural environmental fluctuations, data with $dPET/dt$ values outside the [10th, 90th] range are excluded from outlier detection. Consequently, if the $dPET/dt$ falls within the [10th, 90th] range but the corresponding $dT_{sk,i}/dt$ lies outside the [10th, 90th] range, the data point is considered an outlier and removed. If the number of consecutive NaN values is less than 30, the missing data are interpolated. However, if the total number of NaN values in an entire experimental session exceeds 400, the session is discarded. Figure H shows an example of skin temperature and its derivative after outlier detection.

Table H The 10th and 90th values of $dPET/dt$ and $dT_{sk,i}/dt$

	$dPET/dt$ (°C/s)		$dT_{sk,i}/dt$ (°C/s)	
Segment	10th	90th	10th	90th
Forehead	-0.0266	0.0236	-0.0047	0.0044
Chest			-0.0020	0.0019
Abdomen			-0.0021	0.0022
Back			-0.0018	0.0018
Upper arm			-0.0023	0.0025
Forearm			-0.0028	0.0029
Hand			-0.0056	0.0055
Thigh			-0.0022	0.0020
Calf			-0.0022	0.0021
Foot			-0.0009	0.0014
Neck			-0.0062	0.0058
$T_{sk,m}$			-0.0019	0.0019

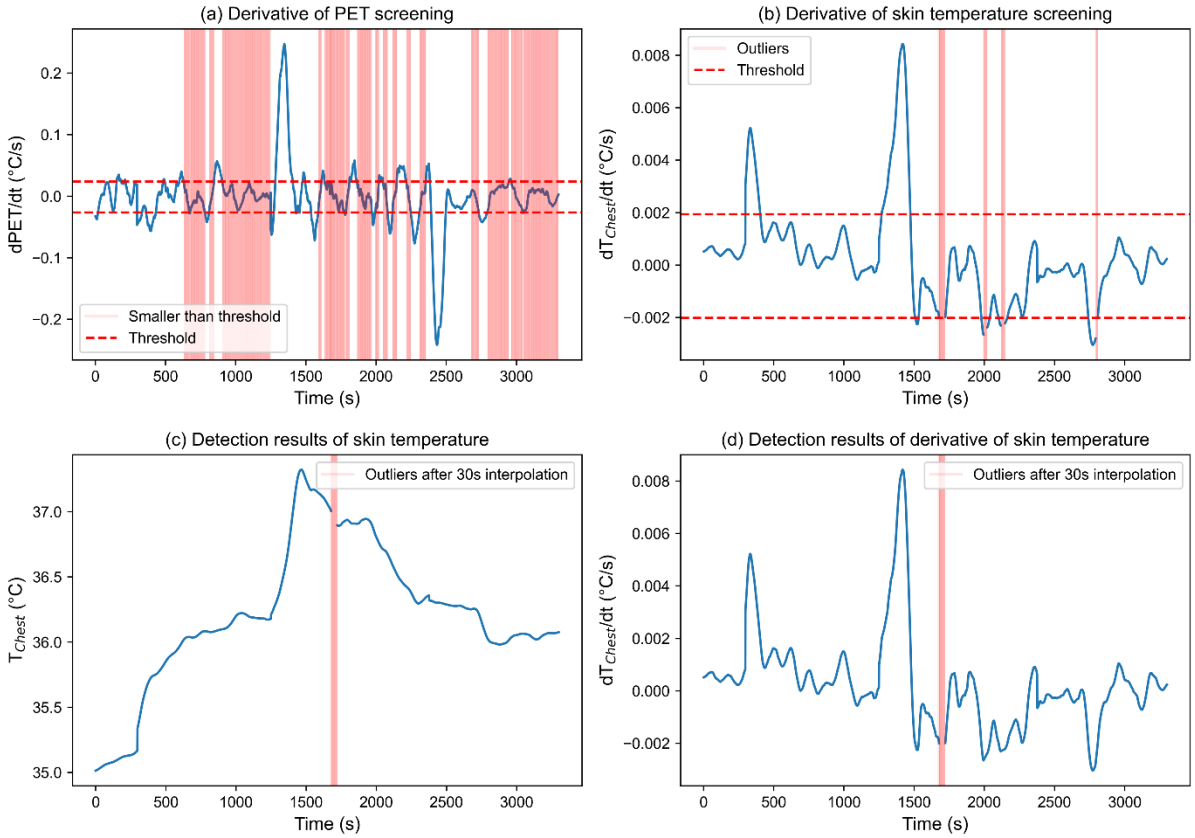

Figure H An example of skin temperature and its derivative data after outlier detection.

(a). Screening of $dPET/dt$ data (exposure time larger than 300 s), the red shaded area indicates values within the [10th, 90th] range of $dPET/dt$; (b). Screening of dT_{chest}/dt data (exposure time larger than 300 s), the red shaded area represents outliers where $dPET/dt$ is within the [10th, 90th] range but the corresponding dT_{chest}/dt lies outside the [10th, 90th] range; (c). Outlier detection results of T_{chest} after interpolation; (d). Outlier detection results of dT_{chest}/dt after interpolation.

Appendix I

Table I The coefficients for local TSV prediction model in the steady-state part (updated).

	Mean		Upper limit (the 90th percentile)		Lower limit (the 10th percentile)	
	B	C	B	C	B	C
Forehead	0.16	7.45	0.58	5.09	0.07	4.18
Chest	0.29	3.83	1.05	2.61	0.33	0.69
Abdomen	0.24	3.11	0.27	8.34	0.32	-0.74
Back	0.21	5.54	0.37	7.05	0.18	1.54
Upper arm	0.25	3.58	0.49	4.51	0.22	-0.14
Forearm	0.40	1.89	0.76	2.55	0.42	-0.48
Hand	0.34	2.34	0.50	4.75	0.51	-0.58
Thigh	0.40	1.63	0.83	1.90	0.39	-0.45
Calf	0.26	3.07	0.63	3.30	0.18	-0.43
Foot	0.36	1.49	0.47	3.80	0.38	-1.18
Neck	0.29	2.01	0.34	5.91	0.34	-1.15

Reference

Abd Elraouf, R., Elmokadem, A., Megahed, N., Eleinen, O. A., & Eltarabily, S. (2022). The impact of urban geometry on outdoor thermal comfort in a hot-humid climate. *Building and Environment*, *225*, 109632.

Abdallah, A. S. H., Hussein, S. W., & Nayel, M. (2020). The impact of outdoor shading strategies on student thermal comfort in open spaces between education building. *Sustainable Cities and Society*, *58*, 102124. https://doi.org/https://doi.org/10.1016/j.scs.2020.102124

Ahmed-Ouameur, F., & Potvin, A. (2007). Microclimates and thermal comfort in outdoor pedestrian spaces a dynamic approach assessing thermal transients and adaptability of the users. Proceedings of the solar conference,

Ali-Toudert, F., & Mayer, H. (2006). Numerical study on the effects of aspect ratio and orientation of an urban street canyon on outdoor thermal comfort in hot and dry climate [Article]. *Building and Environment*, *41*(2), 94-108. https://doi.org/10.1016/j.buildenv.2005.01.013

Altaf, M., Klabwisas, W., Thu, K. S., & Ongsakul, W. (2020, 20-22 Oct. 2020). Performance of the Outdoor Evaporative Cooling: A Case Study of Thammasat University Rangsit Campus. 2020 International Conference and Utility Exhibition on Energy, Environment and Climate Change (ICUE),

Arens, E., Zhang, H., & Huizenga, C. (2006). Partial- and whole-body thermal sensation and comfort—Part II: Non-uniform environmental conditions. *Journal of Thermal Biology*, *31*(1-2), 60-66. https://doi.org/10.1016/j.jtherbio.2005.11.027

ASHRAE. ASHRAE Standard 55-2017: Thermal Environmental Conditions for Human Occupancy. *American Society of Heating, Refrigerating and Air-Conditioning Engineers, Atlanta, GA, US, 2017*.

ASHRAE. (2021). ASHRAE Handbook - Fundamentals: Chapter 9 Thermal comfort. In: American Society of Heating, Refrigerating and Air-Conditioning Engineers.

Baker, L. B., De Chavez, P. J. D., Ungaro, C. T., Sopena, B. C., Nuccio, R. P., Reimel, A. J., & Barnes, K. A. (2019). Exercise intensity effects on total sweat electrolyte losses and regional vs. whole-body sweat [Na(+)], [Cl(-)], and [K(+)]. *Eur J Appl Physiol*, *119*(2), 361-375. https://doi.org/10.1007/s00421-018-4048-z

Binarti, F., Koerniawan, M. D., Triyadi, S., Utami, S. S., & Matzarakis, A. (2020). A review of outdoor thermal comfort indices and neutral ranges for hot-humid regions. *Urban Climate*, *31*. https://doi.org/10.1016/j.uclim.2019.100531

Brown, H. A., Topham, T. H., Clark, B., Woodward, A. P., Ioannou, L. G., Flouris, A. D., Telford, R. D., Smallcombe, J. W., Jay, O., & Periard, J. D. (2024). Thermal and cardiovascular heat adaptations in active adolescents following summer. *Temperature (Austin)*, *11*(3), 254-265. https://doi.org/10.1080/23328940.2024.2347161

Cabanac, M. (1971). Physiological Role of Pleasure: A stimulus can feel pleasant or unpleasant depending upon its usefulness as determined by internal signals. *Science*, *173*(4002), 1103-1107.

Cabanac, M. (1979). Sensory pleasure. *The quarterly review of biology*, *54*(1), 1-29.

Cabanac, M. (1992). Pleasure: the common currency. *Journal of Theoretical Biology*, *155*(2), 173-200.

Campbell, H. A., Akerman, A. P., Kissling, L. S., Prout, J. R., Gibbons, T. D., Thomas, K. N., & Cotter, J. D. (2022). Acute physiological and psychophysical responses to

different modes of heat stress. *Exp Physiol*, *107*(5), 429-440. https://doi.org/10.1113/EP089992

Cândido, C., de Dear, R., & Ohba, M. (2012). Effects of artificially induced heat acclimatization on subjects' thermal and air movement preferences. *Building and Environment*, *49*, 251-258. https://doi.org/10.1016/j.buildenv.2011.09.032

Chakraborty, S., Shah, S., Soltani, K., Swigart, A., Yang, L., & Buckingham, K. (2020). Building an automated and self-aware anomaly detection system. 2020 IEEE International Conference on Big Data (Big Data),

Charalampopoulos, I., Tsiros, I., Chronopoulou-Sereli, A., & Matzarakis, A. (2013). Analysis of thermal bioclimate in various urban configurations in Athens, Greece. *Urban Ecosystems*, *16*, 217-233.

Chen, G., Rong, L., & Zhang, G. (2021). Unsteady-state CFD simulations on the impacts of urban geometry on outdoor thermal comfort within idealized building arrays. *Sustainable Cities and Society*, *74*. https://doi.org/10.1016/j.scs.2021.103187

Chen, L., Mak, C. M., Hang, J., & Dai, Y. (2024). Influence of elevated walkways on outdoor thermal comfort in hot-humid climates based on on-site measurement and CFD modeling. *Sustainable Cities and Society*, *100*. https://doi.org/10.1016/j.scs.2023.105048

Cheng, V., Ng, E., Chan, C., & Givoni, B. (2012). Outdoor thermal comfort study in a sub-tropical climate: a longitudinal study based in Hong Kong. *International Journal of Biometeorology*, *56*(1), 43-56. https://doi.org/10.1007/s00484-010-0396-z

Cheng, Y., Liu, X., Zeng, Z., Liu, S., Wang, Z., Tang, X., & He, B.-J. (2022). Impacts of water bodies on microclimates and outdoor thermal comfort: Implications for sustainable rural revitalization. *Frontiers in Environmental Science*, *10*, 940482.

Coccolo, S., Kämpf, J., Scartezzini, J.-L., & Pearlmutter, D. (2016). Outdoor human comfort and thermal stress: A comprehensive review on models and standards. *Urban Climate*, *18*, 33-57. https://doi.org/10.1016/j.uclim.2016.08.004

Cramer, M. N., & Jay, O. (2016). Biophysical aspects of human thermoregulation during heat stress. *Autonomic Neuroscience*, *196*, 3-13. https://doi.org/https://doi.org/10.1016/j.autneu.2016.03.001

Darian-Smith, I., & Johnson, K. O. (1977). Thermal sensibility and thermoreceptors. *J Invest Dermatol*, *69*(1), 146-153. https://doi.org/10.1111/1523-1747.ep12497936

de Dear, R. J., Ring, J. W., & Fanger, P. O. (1993). Thermal Sensations Resulting From Sudden Ambient Temperature Changes [Article]. *Indoor Air*, *3*(3), 181-192. https://doi.org/10.1111/j.1600-0668.1993.t01-1-00004.x

de Quadros, B. M., & Mizgier, M. G. O. (2023). Urban green infrastructures to improve pedestrian thermal comfort: A systematic review. *Urban Forestry & Urban Greening*, *88*, 128091.

Deng, Y., Cao, B., Liu, B., & Zhu, Y. (2020). Effects of local heating on thermal comfort of standing people in extremely cold environments. *Building and Environment*, *185*, 107256. https://doi.org/10.1016/j.buildenv.2020.107256

Dhariwal, J., Manandhar, P., Bande, L., Marpu, P., Armstrong, P., & Reinhart, C. F. (2019). Evaluating the effectiveness of outdoor evaporative cooling in a hot, arid climate. *Building and Environment*, *150*, 281-288. https://doi.org/https://doi.org/10.1016/j.buildenv.2019.01.016

Dharmasastha, K., Zhong, Z., Niu, J., & Liang, H. (2023). A comprehensive review of cover-shield-assisted radiant cooling system. *Energy and Buildings*, *291*, 113121.

Dharmasastha, K., Zhong, Z., Niu, J., & Liang, H. (2024). Thermal performance investigation of membrane-assisted radiant cooling system for localised outdoor cooling hub. *Sustainable Cities and Society*, *101*. https://doi.org/10.1016/j.scs.2024.105173

Du, Q., Zhang, M., Wang, S., Che, C., Ma, R., & Ma, Z. (2019). Changes in air temperature over China in response to the recent global warming hiatus. *Journal of Geographical Sciences*, *29*(4), 496-516. https://doi.org/10.1007/s11442-019-1612-3

Du, Y., Mak, C. M., Huang, T., & Niu, J. (2017). Towards an integrated method to assess effects of lift-up design on outdoor thermal comfort in Hong Kong. *Building and Environment*, *125*, 261-272.

Dzyuban, Y., Hondula, D. M., Vanos, J. K., Middel, A., Coseo, P. J., Kuras, E. R., & Redman, C. L. (2022). Evidence of alliesthesia during a neighborhood thermal walk in a hot and dry city. *Science of the Total Environment*, *834*, 155294. https://doi.org/10.1016/j.scitotenv.2022.155294

Ebi, K. L., Capon, A., Berry, P., Broderick, C., de Dear, R., Havenith, G., Honda, Y., Kovats, R. S., Ma, W., & Malik, A. (2021). Hot weather and heat extremes: health risks. *The lancet*, *398*(10301), 698-708.

Edwards, R. R., & Fillingim, R. B. (2001). Effects of age on temporal summation and habituation of thermal pain: clinical relevance in healthy older and younger adults. *The Journal of Pain*, *2*(6), 307-317.

Elraouf, R. A., ELMokadem, A., Megahed, N., Eleinen, O. A., & Eltarabily, S. (2022). Evaluating urban outdoor thermal comfort: A validation of ENVI-met simulation through field measurement. *Journal of Building Performance Simulation*, *15*(2), 268-286.

Fang, Z., Feng, X., Liu, J., Lin, Z., Mak, C. M., Niu, J., Tse, K.-T., & Xu, X. (2019). Investigation into the differences among several outdoor thermal comfort indices

against field survey in subtropics. *Sustainable Cities and Society*, *44*, 676-690. https://doi.org/10.1016/j.scs.2018.10.022

Fang, Z., Lin, Z., Mak, C. M., Niu, J., & Tse, K.-T. (2018). Investigation into sensitivities of factors in outdoor thermal comfort indices. *Building and Environment*, *128*, 129-142. https://doi.org/10.1016/j.buildenv.2017.11.028

Fanger, P. O. (1970). Thermal comfort. Analysis and applications in environmental engineering. *Thermal comfort. Analysis and applications in environmental engineering.*, 244-pp.

Farnham, C., Emura, K., & Mizuno, T. (2015). Evaluation of cooling effects: outdoor water mist fan. *Building Research & Information*, *43*(3), 334-345.

Faul, F., Erdfelder, E., Buchner, A., & Lang, A. G. (2009). Statistical power analyses using G*Power 3.1: tests for correlation and regression analyses. *Behav Res Methods*, *41*(4), 1149-1160. https://doi.org/10.3758/BRM.41.4.1149

Fiala, D., Havenith, G., Bröde, P., Kampmann, B., & Jendritzky, G. (2011). UTCI-Fiala multi-node model of human heat transfer and temperature regulation. *International Journal of Biometeorology*, *56*(3), 429-441. https://doi.org/10.1007/s00484-011-0424-7

Fiala, D., Havenith, G., Bröde, P., Kampmann, B., & Jendritzky, G. (2012). UTCI-Fiala multi-node model of human heat transfer and temperature regulation [Article]. *International Journal of Biometeorology*, *56*(3), 429-441. https://doi.org/10.1007/s00484-011-0424-7

Fiala, D., Lomas, K. J., & Stohrer, M. (2001). Computer prediction of human thermoregulatory and temperature responses to a wide range of environmental conditions. *International Journal of Biometeorology*, *45*, 143-159.

Fiala, D., Lomas, K. J., & Stohrer, M. (2003). First principles modeling of thermal sensation responses in steady-state and transient conditions. *ASHRAE transactions*, *109*, 179.

Fiala, D., Psikuta, A., Jendritzky, G., Paulke, S., Nelson, D. A., Lichtenbelt, W. D. v. M., & Frijns, A. J. H. (2010). Physiological modeling for technical, clinical and research applications. *Frontiers in bioscience*, *2*, 939-968.

Fiorillo, E., Brilli, L., Carotenuto, F., Cremonini, L., Gioli, B., Giordano, T., & Nardino, M. (2023). Diurnal outdoor thermal comfort mapping through envi-met simulations, remotely sensed and in situ measurements. *Atmosphere*, *14*(4), 641.

Gagge, A. P., Fobelets, A., & Berglund, L. (1986). A standard predictive index of human response to the thermal environment. *ASHRAE trans*, *92*(2), 709-731.

Gagge, A. P., Stolwijk, J. A., & Nishi, Y. (1972). An effective temperature scale based on a simple model of human physiological regulatiry response. *Memoirs of the Faculty of Engineering, Hokkaido University*, *13*(Suppl), 21-36.

Galagoda, R., Jayasinghe, G., Halwatura, R., & Rupasinghe, H. (2018). The impact of urban green infrastructure as a sustainable approach towards tropical micro-climatic changes and human thermal comfort. *Urban Forestry & Urban Greening*, *34*, 1-9.

Gamero-Salinas, J., Kishnani, N., Monge-Barrio, A., López-Fidalgo, J., & Sánchez-Ostiz, A. (2021). Evaluation of thermal comfort and building form attributes in different semi-outdoor environments in a high-density tropical setting. *Building and Environment*, *205*, 108255. https://doi.org/https://doi.org/10.1016/j.buildenv.2021.108255

Givoni, B., Khedari, J., Wong, N. H., Feriadi, H., & Noguchi, M. (2006). Thermal sensation responses in hot, humid climates: effects of humidity. *Building Research & Information*, *34*(5), 496-506. https://doi.org/10.1080/09613210600861269

Haber, R. N. (1958). Discrepancy from adaptation level as a source of affect. *Journal of Experimental Psychology*, *56*(4), 370.

Hardy, J. D., Du Bois, E. F., & Soderstrom, G. (1938). The technic of measuring radiation and convection: one figure. *The Journal of Nutrition*, *15*(5), 461-475.

Harlan, S. L., Brazel, A. J., Prashad, L., Stefanov, W. L., & Larsen, L. (2006). Neighborhood microclimates and vulnerability to heat stress [Article]. *Social Science & Medicine*, *63*(11), 2847-2863. https://doi.org/10.1016/j.socscimed.2006.07.030

Havenith, G. (2002). Interaction of Clothing and Thermoregulation. *Exogenous Dermatology*, *1*(5), 221-230. https://doi.org/10.1159/000068802

He, B.-J., Ding, L., & Prasad, D. (2020). Relationships among local-scale urban morphology, urban ventilation, urban heat island and outdoor thermal comfort under sea breeze influence. *Sustainable Cities and Society*, *60*, 102289.

Hegazy, I. R., & Qurnfulah, E. M. (2020). Thermal comfort of urban spaces using simulation tools exploring street orientation influence of on the outdoor thermal comfort: a case study of Jeddah, Saudi Arabia. *International Journal of Low-Carbon Technologies*, *15*(4), 594-606.

Hodges, G. J., Kosiba, W. A., Zhao, K., & Johnson, J. M. (2009). The involvement of heating rate and vasoconstrictor nerves in the cutaneous vasodilator response to skin warming. *Am J Physiol Heart Circ Physiol*, *296*(1), H51-56. https://doi.org/10.1152/ajpheart.00919.2008

Holmer, B., Lindberg, F., & Thorsson, S. (2018). Mean radiant temperature and the shape of the standing man. 10th international conference on urban climate/14th symposium on the urban environment, New York, US,

Höppe, P. (1994). Die Wärmebilanzmodelle MEMI und IMEM zur Bewertung der thermischen Beanspruchung am Arbeitsplatz. *Verh. Dtsch. Ges. Arbeitsmed. Umweltmed*, *34*, 153-158.

Höppe, P. (1999). The physiological equivalent temperature–a universal index for the biometeorological assessment of the thermal environment. *International Journal of Biometeorology*, *43*(2), 71-75.

Höppe, P. (1999). The physiological equivalent temperature -: a universal index for the biometeorological assessment of the thermal environment [Article]. *International Journal of Biometeorology*, *43*(2), 71-75. <Go to ISI>://WOS:000083502400003

Höppe, P. (2002). Different aspects of assessing indoor and outdoor thermal comfort. *Energy and Buildings*, *34*(6), 661-665. https://doi.org/https://doi.org/10.1016/S0378-7788(02)00017-8

Huang, J., Zhou, C., Zhuo, Y., Xu, L., & Jiang, Y. (2016). Outdoor thermal environments and activities in open space: An experiment study in humid subtropical climates. *Building and Environment*, *103*, 238-249. https://doi.org/10.1016/j.buildenv.2016.03.029

Huang, T., Li, J., Xie, Y., Niu, J., & Mak, C. M. (2017). Simultaneous environmental parameter monitoring and human subject survey regarding outdoor thermal comfort and its modelling. *Building and Environment*, *125*, 502-514.

Huang, T., Niu, J., Xie, Y., Li, J., & Mak, C. M. (2020). Assessment of "lift-up" design's impact on thermal perceptions in the transition process from indoor to outdoor. *Sustainable Cities and Society*, *56*, 102081.

Huizenga, C., Hui, Z., & Arens, E. (2001). A model of human physiology and comfort for assessing complex thermal environments. *Building and Environment*, *36*(6), 691-699.

Hymczak, H., Golab, A., Mendrala, K., Plicner, D., Darocha, T., Podsiadlo, P., Hudziak, D., Gocol, R., & Kosinski, S. (2021). Core Temperature Measurement-Principles of Correct Measurement, Problems, and Complications. *Int J Environ Res Public Health*, *18*(20), 10606. https://doi.org/10.3390/ijerph182010606

Institute for Building, E., & Energy, C. (2014). *CASBEE: A Tool for Evaluating and Promoting Sustainability in the Built Environment*. IBEC.

ISO. (1998). ISO Standard, 7726. *Ergonomics of the Thermal Environment – Instruments for Measuring Physical Quantities 1998 International Standards Organization Geneva*.

ISO. (2005). 7730: 2005. *Ergonomics of the thermal environment-Analytical determination and interpretation of thermal comfort using calculation of the PMV and PPD indices and local thermal comfort criteria*.

Jay, O., Bain, A. R., Deren, T. M., Sacheli, M., & Cramer, M. N. (2011). Large differences in peak oxygen uptake do not independently alter changes in core temperature and sweating during exercise. *Am J Physiol Regul Integr Comp Physiol*, *301*(3), R832-841. https://doi.org/10.1152/ajpregu.00257.2011

Jendritzky, G., de Dear, R., & Havenith, G. (2012). UTCI-Why another thermal index? [Article]. *International Journal of Biometeorology*, *56*(3), 421-428. https://doi.org/10.1007/s00484-011-0513-7

Jepma, M., Jones, M., & Wager, T. D. (2014). The dynamics of pain: evidence for simultaneous site-specific habituation and site-nonspecific sensitization in thermal pain. *The Journal of Pain*, *15*(7), 734-746.

Ji, W., Cao, B., Geng, Y., Zhu, Y., & Lin, B. (2017). Study on human skin temperature and thermal evaluation in step change conditions: From non-neutrality to neutrality. *Energy and Buildings*, *156*, 29-39. https://doi.org/10.1016/j.enbuild.2017.09.037

Jiang, Y., Xie, Y., Liang, H., Zhang, H., Goto, T., & Niu, J. (2025). Developing a physiological-parameter-based thermal sensation model for warm-biased outdoor settings: The steady-state part. *Sustainable Cities and Society*, *118*, 106020. https://doi.org/10.1016/j.scs.2024.106020

Jiang, Y., Xie, Y., & Niu, J. (2024). Short-term dynamic thermal perception and physiological response to step changes between real-life indoor and outdoor environments. *Building and Environment*, *251*, 111223. https://doi.org/10.1016/j.buildenv.2024.111223

Kenny, N. A., Warland, J. S., Brown, R. D., & Gillespie, T. G. (2009a). Part A: Assessing the performance of the COMFA outdoor thermal comfort model on subjects performing physical activity. *International Journal of Biometeorology*, *53*(5), 415-428. https://doi.org/10.1007/s00484-009-0226-3

Kenny, N. A., Warland, J. S., Brown, R. D., & Gillespie, T. G. (2009b). Part B: Revisions to the COMFA outdoor thermal comfort model for application to subjects performing physical activity. *International Journal of Biometeorology*, *53*(5), 429-441. https://doi.org/10.1007/s00484-009-0227-2

Kim, S. W., & Brown, R. D. (2022). Pedestrians' behavior based on outdoor thermal comfort and micro-scale thermal environments, Austin, TX. *Science of the Total Environment*, *808*, 152143.

Kircher, K., Eriksson, O., Forsman, Å., Vadeby, A., & Ahlstrom, C. (2017). Design and analysis of semi-controlled studies. *Transportation Research Part F: Traffic Psychology and Behaviour*, *46*, 404-412. https://doi.org/10.1016/j.trf.2016.06.016

Kotharkar, R., Dongarsane, P., & Ghosh, A. (2024). Quantification of summertime thermal stress and PET range in a tropical Indian city. *Urban Climate*, *53*, 101758. https://doi.org/10.1016/j.uclim.2023.101758

Lai, D., & Chen, Q. (2016). A two-dimensional model for calculating heat transfer in the human body in a transient and non-uniform thermal environment. *Energy and Buildings*, *118*, 114-122. https://doi.org/10.1016/j.enbuild.2016.02.051

Lai, D., Guo, D., Hou, Y., Lin, C., & Chen, Q. (2014). Studies of outdoor thermal comfort in northern China. *Building and Environment*, *77*, 110-118. https://doi.org/https://doi.org/10.1016/j.buildenv.2014.03.026

Lai, D., Lian, Z., Liu, W., Guo, C., Liu, W., Liu, K., & Chen, Q. (2020). A comprehensive review of thermal comfort studies in urban open spaces. *Science of the Total Environment*, *742*, 140092. https://doi.org/10.1016/j.scitotenv.2020.140092

Lai, D., Zhou, C., Huang, J., Jiang, Y., Long, Z., & Chen, Q. (2014). Outdoor space quality: A field study in an urban residential community in central China. *Energy and Buildings*, *68*, 713-720. https://doi.org/10.1016/j.enbuild.2013.02.051

Lai, D., Zhou, X., & Chen, Q. (2017a). Measurements and predictions of the skin temperature of human subjects on outdoor environment. *Energy and Buildings*, *151*, 476-486. https://doi.org/10.1016/j.enbuild.2017.07.009

Lai, D., Zhou, X., & Chen, Q. (2017b). Modelling dynamic thermal sensation of human subjects in outdoor environments. *Energy and Buildings*, *149*, 16-25. https://doi.org/10.1016/j.enbuild.2017.05.028

Lai, D. Y., Liu, W. Y., Gan, T. T., Liu, K. X., & Chen, Q. Y. (2019). A review of mitigating strategies to improve the thermal environment and thermal comfort in urban outdoor spaces [Review]. *Science of the Total Environment*, *661*, 337-353. https://doi.org/10.1016/j.scitotenv.2019.01.062

Lan, L., & Lian, Z. (2010). Application of statistical power analysis – How to determine the right sample size in human health, comfort and productivity research. *Building and Environment*, *45*(5), 1202-1213. https://doi.org/https://doi.org/10.1016/j.buildenv.2009.11.002

Lau, K. K.-L., Shi, Y., & Ng, E. Y.-Y. (2019). Dynamic response of pedestrian thermal comfort under outdoor transient conditions. *International Journal of Biometeorology*, *63*, 979-989.

Lawson, T., & AD, P. (1977). The effects of wind on people in the vicinity of buildings.

Lee, J. K., Nio, A. Q., Lim, C. L., Teo, E. Y., & Byrne, C. (2010). Thermoregulation, pacing and fluid balance during mass participation distance running in a warm and humid environment. *European Journal of Applied Physiology*, *109*, 887-898.

Lee, K. Y., & Mak, C. M. (2022). Effects of different wind directions on ventilation of surrounding areas of two generic building configurations in Hong Kong. *Indoor and Built Environment*, *31*(2), 414-434.

Li, J., Niu, J., Huang, T., & Mak, C. M. (2022). Dynamic effects of frequent step changes in outdoor microclimate environments on thermal sensation and dissatisfaction of pedestrian during summer. *Sustainable Cities and Society*, *79*, 103670. https://doi.org/https://doi.org/10.1016/j.scs.2022.103670

Li, J., Niu, J., & Mak, C. M. (2022). Study of pedestrians' mixed thermal responses when experiencing rapid and simultaneous variations in sun and wind conditions in urban continuums. *Sustainable Cities and Society*, *87*. https://doi.org/10.1016/j.scs.2022.104169

Li, J., Niu, J., & Mak, C. M. (2023). Influences of variable thermal exposures on walking thermal comfort in hot summer - Physio-psychological responses. *Building and Environment*, *239*, 110346. https://doi.org/10.1016/j.buildenv.2023.110346

Li, J., Niu, J., Mak, C. M., Huang, T., & Xie, Y. (2018). Assessment of outdoor thermal comfort in Hong Kong based on the individual desirability and acceptability of sun and wind conditions. *Building and Environment*, *145*, 50-61. https://doi.org/10.1016/j.buildenv.2018.08.059

Li, J., Niu, J., Mak, C. M., Huang, T., & Xie, Y. (2020). Exploration of applicability of UTCI and thermally comfortable sun and wind conditions outdoors in a subtropical city of Hong Kong. *Sustainable Cities and Society*, *52*. https://doi.org/10.1016/j.scs.2019.101793

Li, W., Mak, C. M., Fu, Y., Cai, C., Tse, K. T., & Niu, J. (2024). The impact of twisted wind on pedestrian comfort around two non-identical-height buildings in tandem arrangement: a wind tunnel study. *Building and Environment*, *262*, 111847. https://doi.org/https://doi.org/10.1016/j.buildenv.2024.111847

Li, Y., Hong, B., Wang, Y., Bai, H., & Chen, H. (2022). Assessing heat stress relief measures to enhance outdoor thermal comfort: A field study in China's cold region. *Sustainable Cities and Society*, *80*, 103813. https://doi.org/https://doi.org/10.1016/j.scs.2022.103813

Li, Y., Li, L., Wang, W., Kong, H., Chen, L., & Yang, L. (2024). How to enhance thermal comfort in greenway walking? An exploration of the physical environment, walking status, and emotional perspectives. *Urban Climate*, *56*, 102053.

Liang, Y., Yang, J., Zhong, Z., Xie, Y., Dharmasastha, K., & Niu, J.-L. (2024). Thermal performance and energy efficacy of membrane-assisted radiant cooling outdoors. *Sustainable Cities and Society*, *114*, 105787.

Libert, J., Candas, V., & Vogt, J. (1979). Effect of rate of change in skin temperature on local sweating rate. *Journal of applied physiology*, *47*(2), 306-311.

Lin, T.-P., Matzarakis, A., & Hwang, R.-L. (2010). Shading effect on long-term outdoor thermal comfort. *Building and Environment*, *45*(1), 213-221.

Lin, T.-P., Yang, S.-R., Chen, Y.-C., & Matzarakis, A. (2018). The potential of a modified physiologically equivalent temperature (mPET) based on local thermal comfort perception in hot and humid regions. *Theoretical and Applied Climatology*, *135*(3-4), 873-876. https://doi.org/10.1007/s00704-018-2419-3

Lin, T. P. (2009). Thermal perception, adaptation and attendance in a public square in hot and humid regions [Article]. *Building and Environment*, *44*(10), 2017-2026. https://doi.org/10.1016/j.buildenv.2009.02.004

Lin, T. P., De Dear, R., & Hwang, R. L. (2011). Effect of thermal adaptation on seasonal outdoor thermal comfort. *International Journal of Climatology*, *31*(2), 302-312.

Liu, J., Niu, J., & Xia, Q. (2016). Combining measured thermal parameters and simulated wind velocity to predict outdoor thermal comfort. *Building and Environment*, *105*, 185-197. https://doi.org/https://doi.org/10.1016/j.buildenv.2016.05.038

Liu, K., Nie, T., Liu, W., Liu, Y., & Lai, D. (2020). A machine learning approach to predict outdoor thermal comfort using local skin temperatures. *Sustainable Cities and Society*, *59*. https://doi.org/10.1016/j.scs.2020.102216

Liu, S., Nazarian, N., Hart, M. A., Niu, J., Xie, Y., & de Dear, R. (2021). Dynamic thermal pleasure in outdoor environments - temporal alliesthesia. *Science of the Total Environment*, *771*, 144910. https://doi.org/10.1016/j.scitotenv.2020.144910

Liu, S., Nazarian, N., Niu, J., Hart, M. A., & de Dear, R. (2020). From thermal sensation to thermal affect: A multi-dimensional semantic space to assess outdoor thermal comfort. *Building and Environment*, *182*, 107112. https://doi.org/https://doi.org/10.1016/j.buildenv.2020.107112

Liu, W., Zhang, Y., & Deng, Q. (2016). The effects of urban microclimate on outdoor thermal sensation and neutral temperature in hot-summer and cold-winter climate. *Energy and Buildings*, *128*, 190-197. https://doi.org/10.1016/j.enbuild.2016.06.086

Mahmoud, A. H. A. (2011). Analysis of the microclimatic and human comfort conditions in an urban park in hot and arid regions. *Building and Environment*, *46*(12), 2641-2656. https://doi.org/https://doi.org/10.1016/j.buildenv.2011.06.025

Mahmoud, R. M. A., & Abdallah, A. S. H. (2022). Assessment of outdoor shading strategies to improve outdoor thermal comfort in school courtyards in hot and arid climates. *Sustainable Cities and Society*, *86*, 104147.

Matthews, T. K., Wilby, R. L., & Murphy, C. (2017). Communicating the deadly consequences of global warming for human heat stress. *Proc Natl Acad Sci U S A*, *114*(15), 3861-3866. https://doi.org/10.1073/pnas.1617526114

Matzarakis, A., & Amelung, B. (2008). Physiological equivalent temperature as indicator for impacts of climate change on thermal comfort of humans. In *Seasonal forecasts, climatic change and human health: health and climate* (pp. 161-172). Springer.

Matzarakis, A., Mayer, H., & Iziomon, M. G. (1999). Applications of a universal thermal index: physiological equivalent temperature. *International Journal of Biometeorology*, *43*(2), 76-84. https://doi.org/10.1007/s004840050119

Melnikov, V., Krzhizhanovskaya, V. V., Lees, M. H., & Sloot, P. M. A. (2018). System dynamics of human body thermal regulation in outdoor environments. *Building and Environment*, *143*, 760-769. https://doi.org/10.1016/j.buildenv.2018.07.024

Miao, C., He, X., Gao, Z., Chen, W., & He, B.-J. (2023). Assessing the vertical synergies between outdoor thermal comfort and air quality in an urban street canyon based on field measurements. *Building and Environment*, *227*, 109810.

Morakinyo, T. E., Dahanayake, K. W. D. K. C., Adegun, O. B., & Balogun, A. A. (2016). Modelling the effect of tree-shading on summer indoor and outdoor thermal condition of two similar buildings in a Nigerian university. *Energy and Buildings*, *130*, 721-732. https://doi.org/10.1016/j.enbuild.2016.08.087

Nadel, E. R., Bullard, R. W., & Stolwijk, J. (1971). Importance of skin temperature in the regulation of sweating. *Journal of applied physiology*, *31*(1), 80-87.

Nakayoshi, M., Kanda, M., Shi, R., & de Dear, R. (2015). Outdoor thermal physiology along human pathways: a study using a wearable measurement system. *International Journal of Biometeorology*, *59*(5), 503-515. https://doi.org/10.1007/s00484-014-0864-y

Ng, E. (2009). *Urban Climatic Map and Standards for Wind Environment – Feasibility Study Technical Guide*. The Chinese University of Hong Kong.

Ng, E., Chen, L., Wang, Y. N., & Yuan, C. (2012). A study on the cooling effects of greening in a high-density city: An experience from Hong Kong [Article]. *Building and Environment*, *47*, 256-271. https://doi.org/10.1016/j.buildenv.2011.07.014

Nikolopoulou, M., Baker, N., & Steemers, K. (2001). Thermal comfort in outdoor urban spaces: understanding the human parameter. *Solar Energy*, *70*(3), 227-235.

Nikolopoulou, M., & Lykoudis, S. (2006). Thermal comfort in outdoor urban spaces: Analysis across different European countries [Article]. *Building and Environment*, *41*(11), 1455-1470. https://doi.org/10.1016/j.buildenv.2005.05.031

Nikolopoulou, M., Lykoudis, S., & Kikira, M. (2003). Thermal comfort in outdoor spaces: field studies in Greece. Proceedings of the fifth international conference on urban climate, Lodz,

Nikolopoulou, M., & Steemers, K. (2003). Thermal comfort and psychological adaptation as a guide for designing urban spaces. *Energy and Buildings*, *35*(1), 95-101. https://doi.org/https://doi.org/10.1016/S0378-7788(02)00084-1

Niu, J., Liu, J., Lee, T.-c., Lin, Z., Mak, C., Tse, K.-T., Tang, B.-s., & Kwok, K. C. S. (2015). A new method to assess spatial variations of outdoor thermal comfort: Onsite monitoring results and implications for precinct planning. *Building and Environment*, *91*, 263-270. https://doi.org/10.1016/j.buildenv.2015.02.017

Norton, B. A., Coutts, A. M., Livesley, S. J., Harris, R. J., Hunter, A. M., & Williams, N. S. G. (2015). Planning for cooler cities: A framework to prioritise green infrastructure to mitigate high temperatures in urban landscapes [Article]. *Landscape and Urban Planning*, *134*, 127-138. https://doi.org/10.1016/j.landurbplan.2014.10.018

Obermeyer, Z., Samra, J. K., & Mullainathan, S. (2017). Individual differences in normal body temperature: longitudinal big data analysis of patient records. *BMJ*, *359*, j5468. https://doi.org/10.1136/bmj.j5468

Obradovich, N., & Fowler, J. H. (2017). Climate change may alter human physical activity patterns. *Nature Human Behaviour*, *1*(5), 0097. https://doi.org/10.1038/s41562-017-0097

Oh, W., Ooka, R., Nakano, J., Kikumoto, H., & Ogawa, O. (2019). Environmental index for evaluating thermal sensations in a mist spraying environment. *Building and Environment*, *161*, 106219.

Oh, W., Ooka, R., Nakano, J., Kikumoto, H., & Ogawa, O. (2020a). Evaluation of mist-spraying environment on thermal sensations, thermal environment, and skin temperature under different operation modes. *Building and Environment*, *168*, 106484. https://doi.org/https://doi.org/10.1016/j.buildenv.2019.106484

Oh, W., Ooka, R., Nakano, J., Kikumoto, H., & Ogawa, O. (2020b). Evaluation of mist-spraying environment on thermal sensations, thermal environment, and skin temperature under different operation modes. *Building and Environment*, *168*. https://doi.org/10.1016/j.buildenv.2019.106484

Olesen, B. W. (1982). *Thermal comfort* (Vol. 2). Bruel & Kjaer.

Oleson, K. W., Monaghan, A., Wilhelmi, O., Barlage, M., Brunsell, N., Feddema, J., Hu, L., & Steinhoff, D. F. (2013). Interactions between urbanization, heat stress, and climate change. *Climatic Change*, *129*(3-4), 525-541. https://doi.org/10.1007/s10584-013-0936-8

Otani, H., Takayuki, G., Heita, G., & and Shirato, M. (2017). Time-of-day effects of exposure to solar radiation on thermoregulation during outdoor exercise in the heat. *Chronobiology International*, *34*(9), 1224-1238. https://doi.org/10.1080/07420528.2017.1358735

Ouyang, W., Morakinyo, T. E., Lee, Y., Tan, Z., Ren, C., & Ng, E. (2023). How to quantify the cooling effects of green infrastructure strategies from a spatio-temporal perspective: Experience from a parametric study. *Landscape and Urban Planning*, *237*, 104808.

Parkinson, T., & de Dear, R. (2014). Thermal pleasure in built environments: physiology of alliesthesia. *Building Research & Information*, *43*(3), 288-301. https://doi.org/10.1080/09613218.2015.989662

Parkinson, T., & de Dear, R. (2015). Thermal pleasure in built environments: spatial alliesthesia from contact heating. *Building Research & Information*, *44*(3), 248-262. https://doi.org/10.1080/09613218.2015.1082334

Parkinson, T., & de Dear, R. (2016). Thermal pleasure in built environments: spatial alliesthesia from air movement. *Building Research & Information*, *45*(3), 320-335. https://doi.org/10.1080/09613218.2016.1140932

Parkinson, T., de Dear, R., & Candido, C. (2016). Thermal pleasure in built environments: alliesthesia in different thermoregulatory zones. *Building Research & Information*, *44*(1), 20-33.

Peel, M. C., Finlayson, B. L., & McMahon, T. A. (2007). Updated world map of the Köppen-Geiger climate classification. *Hydrology and earth system sciences*, *11*(5), 1633-1644.

Peng, Z., Bardhan, R., Ellard, C., & Steemers, K. (2022). Urban climate walk: A stop-and-go assessment of the dynamic thermal sensation and perception in two waterfront districts in Rome, Italy. *Building and Environment*, *221*. https://doi.org/10.1016/j.buildenv.2022.109267

Pennes, H. H. (1948). Analysis of tissue and arterial blood temperatures in the resting human forearm. *Journal of applied physiology*, *1*(2), 93-122.

Periard, J. D., Eijsvogels, T. M. H., & Daanen, H. A. M. (2021). Exercise under heat stress: thermoregulation, hydration, performance implications, and mitigation strategies. *Physiol Rev*, *101*(4), 1873-1979. https://doi.org/10.1152/physrev.00038.2020

Pickup, J., & de Dear, R. (2000). An outdoor thermal comfort index (OUT_SET*)-part I-the model and its assumptions. Biometeorology and urban climatology at the turn of the millenium. Selected papers from the Conference ICB-ICUC,

Potchter, O., Cohen, P., Lin, T. P., & Matzarakis, A. (2018). Outdoor human thermal perception in various climates: A comprehensive review of approaches, methods and quantification. *Science of the Total Environment*, *631-632*, 390-406. https://doi.org/10.1016/j.scitotenv.2018.02.276

Pouri, S., Saadatjoo, P., & Rahimi, L. (2025). Exploring the effect of building form and arrangement on outdoor thermal comfort in residential complexes (case study: Tabriz city). *Environment, Development and Sustainability*, *27*(3), 7817-7842.

Ren, Z., Fu, Y., Dong, Y., Zhang, P., & He, X. (2022). Rapid urbanization and climate change significantly contribute to worsening urban human thermal comfort: A national 183-city, 26-year study in China. *Urban Climate*, *43*. https://doi.org/10.1016/j.uclim.2022.101154

Ring, J. W., & Dear, R. (1991). Temperature Transients: A Model for Heat Diffusion through the Skin, Thermoreceptor Response and Thermal Sensation. *Indoor Air*, *1*(4), 448-456. https://doi.org/10.1111/j.1600-0668.1991.00009.x

Rupp, R. F., Vásquez, N. G., & Lamberts, R. (2015). A review of human thermal comfort in the built environment [Review]. *Energy and Buildings*, *105*, 178-205. https://doi.org/10.1016/j.enbuild.2015.07.047

Salata, F., Golasi, I., de Lieto Vollaro, R., & de Lieto Vollaro, A. (2016a). Outdoor thermal comfort in the Mediterranean area. A transversal study in Rome, Italy. *Building and Environment*, *96*, 46-61. https://doi.org/10.1016/j.buildenv.2015.11.023

Salata, F., Golasi, I., de Lieto Vollaro, R., & de Lieto Vollaro, A. (2016b). Urban microclimate and outdoor thermal comfort. A proper procedure to fit ENVI-met simulation outputs to experimental data. *Sustainable Cities and Society*, *26*, 318-343.

Schibuola, L., & Tambani, C. (2022). A monthly performance comparison of green infrastructures enhancing urban outdoor thermal comfort. *Energy and Buildings*, *273*, 112368.

Schulze, E., Daanen, H. A., Levels, K., Casadio, J. R., Plews, D. J., Kilding, A. E., Siegel, R., & Laursen, P. B. (2015). Effect of thermal state and thermal comfort on cycling

performance in the heat. *Int J Sports Physiol Perform*, *10*(5), 655-663. https://doi.org/10.1123/ijspp.2014-0281

Schweiker, M., Schakib-Ekbatan, K., Fuchs, X., & Becker, S. (2020). A seasonal approach to alliesthesia. Is there a conflict with thermal adaptation? *Energy and Buildings*, *212*. https://doi.org/10.1016/j.enbuild.2019.109745

Solomon, S. G., & Kohn, A. (2014). Moving sensory adaptation beyond suppressive effects in single neurons. *Current Biology*, *24*(20), R1012-1022. https://doi.org/10.1016/j.cub.2014.09.001

Song, W., Lu, Y., Liu, Y., Yang, Y., & Jiang, X. (2020). Effect of partial-body heating on thermal comfort and sleep quality of young female adults in a cold indoor environment. *Building and Environment*, *169*, 106585. https://doi.org/10.1016/j.buildenv.2019.106585

Spagnolo, J., & de Dear, R. (2003). A field study of thermal comfort in outdoor and semi-outdoor environments in subtropical Sydney Australia [Article]. *Building and Environment*, *38*(5), 721-738. https://doi.org/10.1016/s0360-1323(02)00209-3

Stolwijk, J. A. (1971). *A mathematical model of physiological temperature regulation in man*.

Su, M., Hong, B., Su, X., Liu, A., & Chang, J. (2022). How the nozzle density and height of mist spraying affect pedestrian outdoor thermal comfort: A field study. *Building and Environment*, *215*, 108968.

Su, X., Wang, Z., Xu, Y., & Liu, N. (2020). Thermal comfort under asymmetric cold radiant environment at different exposure distances. *Building and Environment*, *178*. https://doi.org/10.1016/j.buildenv.2020.106961

Sudprasert, S. (2021). Utilization of an evaporative air cooler to achieve thermal comfort in Thailand. *Building Research & Information*, *49*(3), 325-335.

Sun, R., Liu, J., Lai, D., & Liu, W. (2023). Building form and outdoor thermal comfort: Inverse design the microclimate of outdoor space for a kindergarten. *Energy and Buildings*, *284*, 112824. https://doi.org/https://doi.org/10.1016/j.enbuild.2023.112824

Takada, S., Matsumoto, S., & Matsushita, T. (2013). Prediction of whole-body thermal sensation in the non-steady state based on skin temperature. *Building and Environment*, *68*, 123-133. https://doi.org/10.1016/j.buildenv.2013.06.004

Takahashi, Y., Nomoto, A., Yoda, S., Hisayama, R., Ogata, M., Ozeki, Y., & Tanabe, S.-i. (2021). Thermoregulation model JOS-3 with new open source code. *Energy and Buildings*, *231*, 110575. https://doi.org/10.1016/j.enbuild.2020.110575

Taleghani, M., Kleerekoper, L., Tenpierik, M., & van den Dobbelsteen, A. (2015). Outdoor thermal comfort within five different urban forms in the Netherlands. *Building and Environment*, *83*, 65-78. https://doi.org/https://doi.org/10.1016/j.buildenv.2014.03.014

Tan, C. L., Wong, N. H., & Jusuf, S. K. (2013). Outdoor mean radiant temperature estimation in the tropical urban environment. *Building and Environment*, *64*, 118-129.

Tanabe, S.-i., Kobayashi, K., Nakano, J., Ozeki, Y., & Konishi, M. (2002). Evaluation of thermal comfort using combined multi-node thermoregulation (65MN) and radiation models and computational fluid dynamics (CFD). *Energy and Buildings*, *34*(6), 637-646. https://doi.org/https://doi.org/10.1016/S0378-7788(02)00014-2

Tartarini, F., & Schiavon, S. (2020). pythermalcomfort: A Python package for thermal comfort research. *SoftwareX*, *12*, 100578. https://doi.org/10.1016/j.softx.2020.100578

Taylor, N. A. S. (2006). Ethnic differences in thermoregulation: Genotypic versus phenotypic heat adaptation. *Journal of Thermal Biology*, *31*(1), 90-104. https://doi.org/https://doi.org/10.1016/j.jtherbio.2005.11.007

Taylor, N. A. S., Tipton, M. J., & Kenny, G. P. (2014). Considerations for the measurement of core, skin and mean body temperatures. *Journal of Thermal Biology*, *46*, 72-101. https://doi.org/https://doi.org/10.1016/j.jtherbio.2014.10.006

Teshnehdel, S., Gatto, E., Li, D., & Brown, R. D. (2022). Improving outdoor thermal comfort in a steppe climate: Effect of water and trees in an urban park. *Land*, *11*(3), 431.

Theeuwes, N. E., Solcerova, A., & Steeneveld, G. J. (2013). Modeling the influence of open water surfaces on the summertime temperature and thermal comfort in the city. *Journal of Geophysical Research: Atmospheres*, *118*(16), 8881-8896.

Thorsson, S., Lindberg, F., Eliasson, I., & Holmer, B. (2007). Different methods for estimating the mean radiant temperature in an outdoor urban setting [Article; Proceedings Paper]. *International Journal of Climatology*, *27*(14), 1983-1993. https://doi.org/10.1002/joc.1537

Tsitoura, M., Tsoutsos, T., & Daras, T. (2014). Evaluation of comfort conditions in urban open spaces. Application in the island of Crete. *Energy Conversion and Management*, *86*, 250-258. https://doi.org/https://doi.org/10.1016/j.enconman.2014.04.059

Vasilikou, C., & Nikolopoulou, M. (2020). Outdoor thermal comfort for pedestrians in movement: thermal walks in complex urban morphology. *International Journal of Biometeorology*, *64*, 277-291.

VDI 3787-1. (2015). Environmental Meteorology – Climate and Air Quality Maps for Cities and Regions – Part 1: Climate. In *VDI 3787-1*. Düsseldorf: Beuth Verlag.

Vellei, M. (2024). Derivation and validation of a whole-body dynamic mean thermal sensation model. *Building and Environment*, *256*, 111469. https://doi.org/10.1016/j.buildenv.2024.111469

Vellei, M., de Dear, R., Inard, C., & Jay, O. (2021). Dynamic thermal perception: A review and agenda for future experimental research. *Building and Environment*, *205*. https://doi.org/10.1016/j.buildenv.2021.108269

Virtanen, P., Gommers, R., Oliphant, T. E., Haberland, M., Reddy, T., Cournapeau, D., Burovski, E., Peterson, P., Weckesser, W., & Bright, J. (2020). SciPy 1.0: fundamental algorithms for scientific computing in Python. *Nature methods*, *17*(3), 261-272.

Wai, K.-M., Yuan, C., Lai, A., & Yu, P. K. (2020). Relationship between pedestrian-level outdoor thermal comfort and building morphology in a high-density city. *Science of the Total Environment*, *708*, 134516.

Walther, E., & Goestchel, Q. (2018). The P.E.T. comfort index: Questioning the model. *Building and Environment*, *137*, 1-10. https://doi.org/10.1016/j.buildenv.2018.03.054

Wang, Y., Berardi, U., & Akbari, H. (2016). Comparing the effects of urban heat island mitigation strategies for Toronto, Canada. *Energy and Buildings*, *114*, 2-19.

Wang, Z., de Dear, R., Luo, M., Lin, B., He, Y., Ghahramani, A., & Zhu, Y. (2018). Individual difference in thermal comfort: A literature review. *Building and Environment*, *138*, 181-193. https://doi.org/10.1016/j.buildenv.2018.04.040

Watanabe, H., Sugi, T., Saito, K., & Nagashima, K. (2024). Mechanism underlying the influence of humidity on thermal comfort and stress under mimicked working conditions. *Physiol Behav*, *285*, 114653. https://doi.org/10.1016/j.physbeh.2024.114653

Watanabe, S., Nagano, K., Ishii, J., & Horikoshi, T. (2014). Evaluation of outdoor thermal comfort in sunlight, building shade, and pergola shade during summer in a humid subtropical region. *Building and Environment*, *82*, 556-565.

White, M. P., Alcock, I., Grellier, J., Wheeler, B. W., Hartig, T., Warber, S. L., Bone, A., Depledge, M. H., & Fleming, L. E. (2019). Spending at least 120 minutes a week in nature is associated with good health and wellbeing. *Sci Rep*, *9*(1), 7730. https://doi.org/10.1038/s41598-019-44097-3

Xi, T., Li, Q., Mochida, A., & Meng, Q. (2012). Study on the outdoor thermal environment and thermal comfort around campus clusters in subtropical urban areas. *Building and Environment*, *52*, 162-170. https://doi.org/10.1016/j.buildenv.2011.11.006

Xi, T., Wang, M., Cao, E., Li, J., Wang, Y., Lu, L., & Zhang, X. (2024). A preliminary study of multidimensional semantic evaluation of outdoor thermal comfort in Chinese. *Architectural Intelligence*, *3*(1). https://doi.org/10.1007/s44223-024-00051-6

Xia, Q., Liu, X., Niu, J., & Kwok, K. C. (2017). Effects of building lift-up design on the wind environment for pedestrians. *Indoor and Built Environment*, *26*(9), 1214-1231.

Xie, Y., Liu, J., Huang, T., Li, J., Niu, J., Mak, C. M., & Lee, T.-c. (2019). Outdoor thermal sensation and logistic regression analysis of comfort range of meteorological parameters in Hong Kong. *Building and Environment*, *155*, 175-186. https://doi.org/https://doi.org/10.1016/j.buildenv.2019.03.035

Xie, Y., Niu, J., Zhang, H., Liu, S., Liu, J., Huang, T., Li, J., & Mak, C. M. (2020). Development of a multi-nodal thermal regulation and comfort model for the outdoor environment assessment. *Building and Environment*, *176*. https://doi.org/10.1016/j.buildenv.2020.106809

Xie, Y., Wang, X., Wen, J., Geng, Y., Yan, L., Liu, S., Zhang, D., & Lin, B. (2022). Experimental study and theoretical discussion of dynamic outdoor thermal comfort in

walking spaces: Effect of short-term thermal history. *Building and Environment*, *216*, 109039. https://doi.org/10.1016/j.buildenv.2022.109039

Xie, Y. X., Huang, T. Y., Li, J. N., Liu, J. L., Niu, J. L., Mak, C. M., & Lin, Z. (2018). Evaluation of a multi-nodal thermal regulation model for assessment of outdoor thermal comfort: Sensitivity to wind speed and solar radiation. *Building and Environment*, *132*, 45-56. https://doi.org/10.1016/j.buildenv.2018.01.025

Xiong, J., Zhou, X., Lian, Z., You, J., & Lin, Y. (2016). Thermal perception and skin temperature in different transient thermal environments in summer. *Energy and Buildings*, *128*, 155-163. https://doi.org/10.1016/j.enbuild.2016.06.085

Xu, J., Wei, Q., Huang, X., Zhu, X., & Li, G. (2010). Evaluation of human thermal comfort near urban waterbody during summer. *Building and Environment*, *45*(4), 1072-1080.

Xu, T., Yao, R., Du, C., & Huang, X. (2022). A method of predicting the dynamic thermal sensation under varying outdoor heat stress conditions in summer. *Building and Environment*, *223*, 109454. https://doi.org/10.1016/j.buildenv.2022.109454

Xu, X., Li, S., Yang, Y., & Lian, Z. (2023). Effects of thermal environment on body temperature rhythm and thermal sensation before and after getting into bed: A laboratory study in Shanghai, China. *Energy and Buildings*, *301*, 113748. https://doi.org/10.1016/j.enbuild.2023.113748

Yang, J., Fan, Y., Wu, Z., Luo, X., Gao, N., Fang, Z., & Wu, P. (2025). Investigation of the outdoor workers' thermal comfort and improving technology. *Energy and Buildings*, 115332.

Yang, J., Liang, Y., Zhong, Z., Dharmasastha, K., Xie, Y., & Niu, J.-L. (2024). Thermal comfort investigation of membrane-assisted radiant cooling in outdoor settings. *Sustainable Cities and Society*, *113*, 105634.

Yang, Y., Lyu, J., Lian, Z., Xie, Y., Jiang, Y., Lin, J., & Niu, J. (2024). Subjective information in thermal comfort evaluation methods: A critical review. *Energy and Buildings*, *325*. https://doi.org/10.1016/j.enbuild.2024.115019

Yao, J., Yang, F., Zhuang, Z., Shao, Y., & Yuan, P. F. (2018). The effect of personal and microclimatic variables on outdoor thermal comfort: A field study in a cold season in Lujiazui CBD, Shanghai. *Sustainable Cities and Society*, *39*, 181-188. https://doi.org/10.1016/j.scs.2018.02.025

Yilmaz, S., Külekçi, E. A., Mutlu, B. E., & Sezen, I. (2021). Analysis of winter thermal comfort conditions: street scenarios using ENVI-met model. *Environmental Science and Pollution Research*, *28*, 63837-63859.

Yu, Y., Liu, J., Chauhan, K., de Dear, R., & Niu, J. (2020). Experimental study on convective heat transfer coefficients for the human body exposed to turbulent wind conditions. *Building and Environment*, *169*. https://doi.org/10.1016/j.buildenv.2019.106533

Yuan, J., Masuko, S., Shimazaki, Y., Yamanaka, T., & Kobayashi, T. (2022). Evaluation of outdoor thermal comfort under different building external-wall-surface with different reflective directional properties using CFD analysis and model experiment. *Building and Environment*, *207*, 108478.

Yuen, H. K., & Jenkins, G. R. (2020). Factors associated with changes in subjective well-being immediately after urban park visit. *Int J Environ Health Res*, *30*(2), 134-145. https://doi.org/10.1080/09603123.2019.1577368

Zhai, Y., Zhao, S., Yang, L., Wei, N., Xu, Q., Zhang, H., & Arens, E. (2019). Transient human thermophysiological and comfort responses indoors after simulated summer commutes. *Building and Environment*, *157*, 257-267. https://doi.org/10.1016/j.buildenv.2019.04.023

Zhang, F., de Dear, R., & Candido, C. (2016). Thermal comfort during temperature cycles induced by direct load control strategies of peak electricity demand management. *Building and Environment*, *103*, 9-20. https://doi.org/10.1016/j.buildenv.2016.03.020

Zhang, H. (2003). *Human thermal sensation and comfort in transient and non-uniform thermal environments* University of California, Berkeley].

Zhang, H., Arens, E., Huizenga, C., & Han, T. (2010a). Thermal sensation and comfort models for non-uniform and transient environments, part II: Local comfort of individual body parts. *Building and Environment*, *45*(2), 389-398.

Zhang, H., Arens, E., Huizenga, C., & Han, T. (2010b). Thermal sensation and comfort models for non-uniform and transient environments, part III: Whole-body sensation and comfort. *Building and Environment*, *45*(2), 399-410.

Zhang, H., Arens, E., Huizenga, C., & Han, T. (2010c). Thermal sensation and comfort models for non-uniform and transient environments: Part I: Local sensation of individual body parts. *Building and Environment*, *45*(2), 380-388.

Zhang, S., Zhang, X., Niu, D., Fang, Z., Chang, H., & Lin, Z. (2023). Physiological equivalent temperature-based and universal thermal climate index-based adaptive-rational outdoor thermal comfort models. *Building and Environment*, *228*. https://doi.org/10.1016/j.buildenv.2022.109900

Zhang, Y., Zheng, Z., Zhang, S., Fang, Z., & Lin, Z. (2024). Exploring thermal comfort and pleasure in outdoor shaded spaces: Inspiration for improving thermal index models. *Building and Environment*, *265*. https://doi.org/10.1016/j.buildenv.2024.111933

Zhang, Y., Zhou, X., Zheng, Z., Oladokun, M. O., & Fang, Z. (2020). Experimental investigation into the effects of different metabolic rates of body movement on

thermal comfort. *Building and Environment*, *168*. https://doi.org/10.1016/j.buildenv.2019.106489

Zhang, Z., Zhang, Y., & Ding, E. (2017). Acceptable temperature steps for transitional spaces in the hot-humid area of China. *Building and Environment*, *121*, 190-199. https://doi.org/10.1016/j.buildenv.2017.05.026

Zhao, H., Zhao, L., Zhai, Y., Jin, L., Meng, Q., Yan, J., Wu, R., & Brown, R. D. (2024). The impact of dynamic thermal experiences on pedestrian thermal comfort: A whole-trip perspective from laboratory studies. *Building and Environment*, *258*, 111599.

Zhao, Y., Zhao, K., Zhang, X., Zhang, Y., & Du, Z. (2024). Assessment of combined passive cooling strategies for improving outdoor thermal comfort in a school courtyard. *Building and Environment*, *252*, 111247. https://doi.org/https://doi.org/10.1016/j.buildenv.2024.111247

Zhong, B., Jiang, K., Wang, L., & Shen, G. (2022). Wearable Sweat Loss Measuring Devices: From the Role of Sweat Loss to Advanced Mechanisms and Designs. *Adv Sci (Weinh)*, *9*(1), e2103257. https://doi.org/10.1002/advs.202103257

Zhong, J., Liu, J., Xu, Y., & Liang, G. (2022). Pedestrian-level gust wind flow and comfort around a building array–Influencing assessment on the pocket park. *Sustainable Cities and Society*, *83*. https://doi.org/10.1016/j.scs.2022.103953

Zhong, Z., Niu, J., Ma, W., Yao, S., Yang, M., & Wang, Z. (2021). Condensation performance of superhydrophobic aluminium surface material used for cooled ceiling panels under highly humid indoor conditions. Journal of Physics: Conference Series,

Zhu, X., Liu, H., He, M., Wu, Y., Xiong, F., & Li, B. (2025). Comparing the improvement of occupant thermal comfort with local heating devices in cold environments. *Building and Environment*, *268*. https://doi.org/10.1016/j.buildenv.2024.112350

Zölch, T., Rahman, M. A., Pfleiderer, E., Wagner, G., & Pauleit, S. (2019). Designing public squares with green infrastructure to optimize human thermal comfort. *Building and Environment*, *149*, 640-654.